

NOTE TO USERS

This reproduction is the best copy available.

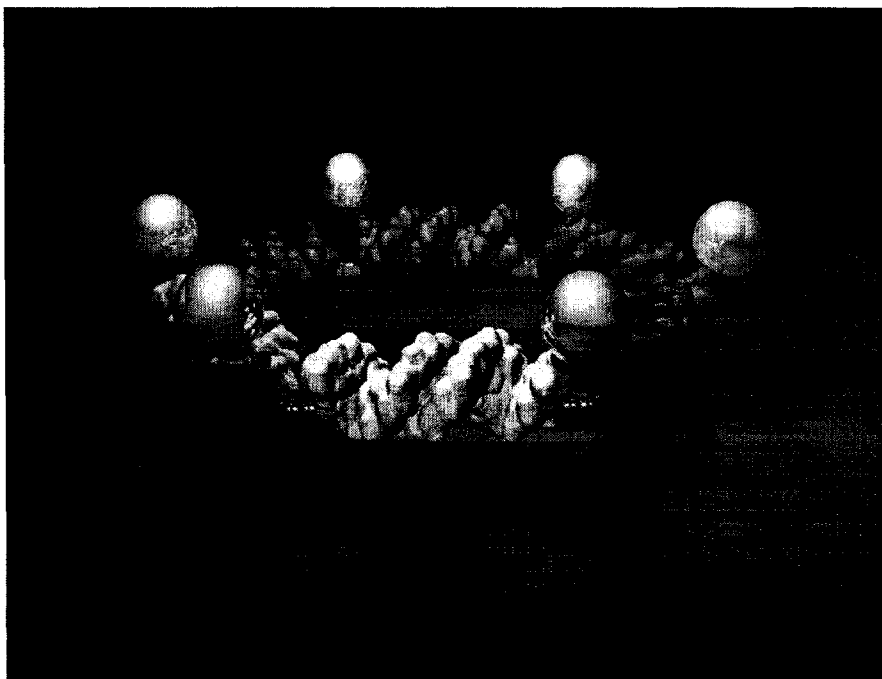
UMI[®]

Supramolecular DNA nanotechnology: Discrete nanoparticle organization, three-dimensional DNA construction, and molecule templated DNA assembly

Faisal A. Aldaye

Department of Chemistry, McGill University

A thesis submitted to McGill University in partial fulfillment of the requirements of the degree
Doctorate of Philosophy. August 2008.



© Faisal A. Aldaye. All rights reserved.



Library and Archives
Canada

Published Heritage
Branch

395 Wellington Street
Ottawa ON K1A 0N4
Canada

Bibliothèque et
Archives Canada

Direction du
Patrimoine de l'édition

395, rue Wellington
Ottawa ON K1A 0N4
Canada

Your file Votre référence
ISBN: 978-0-494-66278-6
Our file Notre référence
ISBN: 978-0-494-66278-6

NOTICE:

The author has granted a non-exclusive license allowing Library and Archives Canada to reproduce, publish, archive, preserve, conserve, communicate to the public by telecommunication or on the Internet, loan, distribute and sell theses worldwide, for commercial or non-commercial purposes, in microform, paper, electronic and/or any other formats.

The author retains copyright ownership and moral rights in this thesis. Neither the thesis nor substantial extracts from it may be printed or otherwise reproduced without the author's permission.

AVIS:

L'auteur a accordé une licence non exclusive permettant à la Bibliothèque et Archives Canada de reproduire, publier, archiver, sauvegarder, conserver, transmettre au public par télécommunication ou par l'Internet, prêter, distribuer et vendre des thèses partout dans le monde, à des fins commerciales ou autres, sur support microforme, papier, électronique et/ou autres formats.

L'auteur conserve la propriété du droit d'auteur et des droits moraux qui protègent cette thèse. Ni la thèse ni des extraits substantiels de celle-ci ne doivent être imprimés ou autrement reproduits sans son autorisation.

In compliance with the Canadian Privacy Act some supporting forms may have been removed from this thesis.

While these forms may be included in the document page count, their removal does not represent any loss of content from the thesis.

Conformément à la loi canadienne sur la protection de la vie privée, quelques formulaires secondaires ont été enlevés de cette thèse.

Bien que ces formulaires aient inclus dans la pagination, il n'y aura aucun contenu manquant.


Canada

I dedicate this thesis to my mother **Ghada A. Soubra**, and to the memory of my father **Assaad M. Aldaye**. I only hope to one day become the kind of person that my mom has always been to me, and to my brothers, **Mamdouh, Ahmed, and Fahed**.

Abstract

The field of structural DNA nanotechnology utilizes DNA's powerful base-pairing molecular recognition criteria to help solve real challenges facing researchers in material science and nanotechnology, some of which include synthesis, sensing, catalysis, delivery, storage, optics, electronics, and scaffolding. In it, DNA is stripped away from any of its preconceived biological roles, and is treated as a powerful synthetic polymer. A subarea of research that our group has recently termed supramolecular DNA nanotechnology is emerging, and is proving to be a powerful complement to some of the already established rules of structural DNA nanotechnology. The work within this thesis falls under the umbrella of supramolecular DNA nanotechnology, and can conceptually be divided into three parts. (1) The first deals with the problem of discrete nanoparticle organization. In it we present an approach for the facile and economical access to libraries of discrete nanoparticle assemblies that are addressable and switchable post-assembly. (2) The second deals with the synthesis of three-dimensional DNA assemblies. In it we present an approach for the facile construction of discrete three-dimensional DNA cages that can be structurally oscillated between pre-defined lengths, and adapt this approach to generate geometrically well-defined DNA columns of modular stiffness. (3) The last part deals with the use of small molecules to reprogram the assembly behavior of DNA. In it we use molecules to address the issue of error-correction, during and after the assembly process, and to facilitate the synthesis of "higher-order" DNA helices composed of more than two DNA strands. This work collectively offers a set of simple solutions to some of the bigger challenges currently facing researchers in DNA nanotechnology, and provides a snapshot of what is to be expected from the emerging discipline that is supramolecular DNA nanotechnology.

Résumé

Le domaine des nanotechnologies de structure de l'ADN utilise les règles de complémentarité des bases de l'ADN afin de résoudre les défis auxquels les chercheurs en sciences des matériaux et des technologies doivent faire face. Ces difficultés incluent la synthèse, le dépistage, la catalyse, le transport, le stockage, l'optique, l'électronique et l'échafaudage. Dans ces cas-ci, l'ADN s'éloigne de ses rôles biologiques préconçus et est plutôt traité comme un puissant polymère synthétique. Une sous-section de recherche appelée nanotechnologie supramoléculaire de l'ADN est présentement en émergence et s'avère être un complément important au niveau des règles de la nanotechnologie structurale de l'ADN déjà établies. Le travail réalisé dans cette thèse tient du domaine de la nanotechnologie supramoléculaire de l'ADN et peut être divisé conceptuellement en trois parties. La première partie traite du problème d'organisation de nanoparticules discrètes. Nous présentons dans ce cas une approche qui facilite et économise l'accès aux bibliothèques d'assemblage des nanoparticules discrètes, qui sont adressables et interchangeables après l'assemblage. La seconde partie traite de la synthèse d'assemblage d'ADN tridimensionnelle. Nous y présentons une approche qui consiste en la construction de cages discrètes et tridimensionnelles d'ADN dont les structures peuvent osciller parmi un certain nombre de tailles prédéfinies. Nous adaptons aussi cette approche pour générer des formes géométriques triangulaires et carrées bien définies de nanotubes d'ADN qui peuvent s'ouvrir et se fermer. La dernière partie traite de l'utilisation de petites molécules pour reprogrammer le comportement d'assemblage de l'ADN. Dans ce cas, nous utilisons des molécules pour résoudre le problème de correction d'erreur pendant et après le processus d'assemblage et pour faciliter la synthèse d'hélices d'ADN d'ordre supérieur composées de plus de deux brins. Ce travail offre une collection de solutions simples à certains des plus importants défis de la nanotechnologie de l'ADN et fournit également un aperçu des possibilités de la nanotechnologie supramoléculaire.

Translated by **Annie Dorris**

Acknowledgments

A privilege that one gets when completing a Doctorate is this opportunity to thank the people who helped along the way. First and foremost, I would like to express my most sincere and humble gratitude to my supervisor, Professor Hanadi Sleiman. Her leadership, superb level of creativity, devotion to science, and endless attention to detail, have collectively shown me what it is to be a true scholar; her positive impact on my development as a scientist and as a person is monumental. Professor Masad Damha is our Director of Graduate Studies, and for a year was my surrogate supervisor; I am eternally grateful for the constant encouragement and support that he has given me throughout my entire stay here at McGill University. I have had the privilege of working with Professor David Harpp, on and off over the past few years, and thank him for showing me the importance of doing what one loves for a living. Professor Peter Grütter welcomed me into his department with open arms, teaching me the value of collaboration, and for this I am grateful. During my time at McGill University, I attended classes by Professors Ashok Kakkar, Bruce Arndtsen, George Just, Hanadi Sleiman, Karine Auclair, Masad Damha, and Patrick Farrell (alphabetical, first name); to all these brilliant people, thank you.

Professor Antonella Badia and Patricia Moraille taught me everything I know about AFM. Professor Hojatolla Vali, Dr. Kelly Sears, and Jeannie Mui taught me everything I know about TEM. Kimberly Metera, An Thien Ngo, and Pierre Karam taught me everything I know about fluorescence spectroscopy. Antisar Hlil and Nadim Saade *never* turned me away when I needed to have a sample analyzed using MALDI-TOF MS or ESI MS. Alison Palmer helped prepare some of the manuscripts, Dr. Kevin Yager and James Hedberg helped prepare some of the illustrations used in the figures and schemes, while Annie Dorris translated the abstract; thank you all. A special thank you goes out to A. Hlil and C. McLaughlin for helping me submit this thesis, and for taking care of the details.

Since I joined this lab, I trained a number of students. They are: Alison Palmer, Dr. Bingzhi Chen, Christopher McLaughlin, Hua Yang, Karina Carneiro, Mohamed Slim, Pik Kwan (Peggy) Lo, Rachel Nassif, Dr. Sankaran Nedumbamanabrahmadatan, and Yoshihiro Ishihara (alphabetical, first name). Thank you all for giving me your trust.

I thank McGill University, and especially the Department of Chemistry (including its amazing staff, e.g., Chantal Marotte and Sandra Aerssen), for their continual support throughout my entire graduate studies, and I would like to take this opportunity to thank Professor Bruce

Lennox for his endless selfless devotion to both the department and to all of its students. I am truly honored to become an Alma Mater of this department, and only hope to one day make you as proud of me as I am of you.

Professor Luba Zuk and Professor Alexander Solopov, you mean the world to me; you know why. A truly great man once said: "There's nothing remarkable about it, all one has to do is hit the right keys at the right time and the instrument plays itself."



Perhaps *J. S. Bach* was right, but I know I would have hit many fewer "right keys" these past few years without the help of those mentioned above, as well as the help of many others who I did not get to mention here by name. Thank you.

Sincerely,

Faisal A. Aldaye

Author contributions

Chapter 5 **Pik Kwan Lo** helped prepare the gels in Figures 5.3, 5.4 and 5.6. **Christopher K. McLaughlin** contributed to project design.

Chapter 7 **Pik Kwan Lo** helped synthesize the polyadenine DNA strands A_5 , A_6 , A_8 , A_{10} , A_{15} and A_{20} .

Table of contents

Chapter 1	Background	1
1.1	DNA	2
1.2	DNA in nanotechnology	3
1.3	Structural DNA nanotechnology	6
	1.3.1 Developments	7
	1.3.2.1 Applications: Protein organization	9
	1.3.2.2 Applications: Nanoparticle organization	12
	1.3.2.3 Applications: DNA computation and DNA nanomachines	13
1.4	Supramolecular DNA nanotechnology	15
	1.4.1 Molecules that provide structural and functional benefits to DNA nanotechnology	15
	1.4.2 Molecules that refine the assembly process in DNA nanotechnology	17
Chapter 2	Sequential self-assembly of a DNA hexagon as a template for the organization of gold nanoparticles	19
2.1	Synthesis	21
2.2	Results and discussion	24
2.3	Conclusions	28
2.4	Experimental	28
Chapter 3	Dynamic DNA templates for discrete gold nanoparticle assemblies: Control of geometry, modularity, write/erase, and structural switching	33
3.1	Synthesis	35
3.2	Results and discussion	42
3.3	Conclusions	47

3.4	Experimental	48
Chapter 4	Modular access to structurally switchable three-dimensional discrete DNA assemblies	52
4.1	Synthesis	54
4.2	Results and discussion	56
4.3	Conclusions	61
4.4	Coda	61
4.5	Experimental	61
Chapter 5	Modular construction of DNA nanotubes with readily tunable geometry, rigidity, and single- or double-stranded character	66
5.1	Synthesis	69
5.2	Results and discussion	71
5.3	Conclusions	76
5.4	Experimental	77
Chapter 6	Guest-mediated access to a single DNA nanostructure from a library of multiple assemblies	81
6.1	Synthesis	84
6.2	Results and discussion	87
6.3	Conclusions	96
6.4	Experimental	97
Chapter 7	Small molecule templated synthesis of higher-order DNA Assemblies	103
7.1	Results and discussion	106
7.2	Conclusions	113
7.3	Experimental	114

Chapter 8	Summary	117
8.1	Contributions to knowledge	117
8.2	Future work	121
8.3	Publications	122
8.4	Patents	124
8.5	Selected conference presentations	124
Chapter 9	References	127

Background

Faisal A. Aldaye, Alison L. Palmer, Hanadi F. Sleiman, *Science* **2008**, 321, 1795-1799.

In 1865, Mendel observed that traits are inherited according to specific laws,¹ and a year later, Haeckel proposed that the factors responsible for the transmission of such traits are to be found in the nucleus.² Today, it is common knowledge that deoxyribonucleic acid (DNA) is the molecule responsible for the storage and transmission of genetic information – making it one of the most, if not the most, important molecules discovered to date. But is that enough? Can we ask more of DNA? Researchers in nanotechnology are starting to use DNA to solve a number of problems, and they are succeeding. The revolution that is DNA nanotechnology was started by Seeman and co-workers in the 1980's, and a great deal of biologists, chemists, physicists, computer scientists, and engineers are currently contributing to its evolution. This field promises to solve a number of challenging problems facing researchers in nanotechnology, some of which include synthesis, sensing, catalysis, delivery, storage, optics, electronics, and scaffolding. A subarea of research that our group has recently termed *supramolecular DNA nanotechnology* is emerging, and is proving to be a powerful complement to some of the already established rules of structural DNA nanotechnology. The work within this thesis falls under the umbrella of supramolecular DNA nanotechnology, and addresses a number of important research topics.

In chapter 2 we present the first example of a *well-defined* DNA-mediated *discrete nanoparticle assembly*, and in chapter 3 we refine this approach to allow for the *facile access* to a large number of well-defined discrete nanoparticle constructs that can also be *structurally and functionally addressed* in response to external stimuli in real-time. Gold nanoparticle assemblies have recently emerged as a promising class of materials with novel optical, electronic, catalytic and sensing applications.³⁻⁶ Our ability to systematically organize them into discrete and well-defined model systems will be a necessary requirement for their full potential to be explored and realized.^{4,7}

In chapter 4 we present a *modular approach to quantitatively generate a large number* of different and complex discrete three-dimensional DNA assemblies, and present the first example in which one of these capsules can be *structurally oscillated* between a number of different predetermined dimensions. Three-dimensional DNA nanostructures have tremendous potential to

encapsulate and release drugs, regulate the folding and activity of encapsulated proteins, selectively encage nanomaterials, and assemble three-dimensional DNA networks for catalysis and biomolecule crystallization.⁸⁻¹² Additionally, in chapter 5 we extend this unique method to construct *geometrically well-defined DNA nanotubes* that are triangular and square-shaped, and also construct the first example of DNA nanotube assemblies that can exist in both double- or single-stranded forms. The later opens the door to the possibility of using these nanotubes in their more accessible single-stranded form for loading materials, biomolecules or drugs, followed by their subsequent closure to ensure encapsulation.

In chapter 6 we apply the well-established supramolecular rules of host/guest chemistry to DNA nanotechnology, and *template the selective synthesis* of a “correct” DNA nanostructure from a library of many other “incorrect” members, and further *convert each already formed incorrect member* into the same correct assembly. The former is a solution to error prevention within DNA nanotechnology, while the latter is a solution to error correction – major bottleneck facing researchers in DNA nanotechnology.¹³

In chapter 8 we use small molecules that contain all the necessary structural and functional information to *reprogram the assembly behavior of unmodified DNA*, and use this approach to rationally construct DNA triplexes from strands that otherwise assemble into duplexes. Higher-order DNA assemblies composed of more than two DNA strands provide an untapped wealth of potentially unique structural, physical, and chemical properties. Many areas of research will benefit from our ability to easily generate a large number of such higher-order helices, including materials science and biology.^{14,15}

Collectively, this body of work provides a set of simple solutions to a number of challenges currently facing researchers in DNA nanotechnology, and offers a snapshot of what is to be expected from the symbiosis that is supramolecular DNA nanotechnology.

1.1 DNA

DNA is a masterpiece of engineering. Structurally, DNA is a long polymer made up of simple units joined together by a backbone of sugar and phosphate groups. The sugar in DNA is deoxyribose. Attached to each sugar is one of four nitrogenous bases, adenine (A), cytosine (C), guanine (G) or thymine (T). Double-stranded DNA is constructed from two anti-parallel single strands that hydrogen-bond and π -stack according to specific base-pair recognition criteria, that is, A with T and C with G. Adenine possesses a donor-acceptor hydrogen-bonding face

complementary to the acceptor-donor face of thymine, while cytosine possesses a donor-acceptor-donor face complementary to the acceptor-donor-acceptor face of guanine. This set of hydrogen-bonding motifs is known as Watson-Crick, and is usually preferred because it tends to generate a double-helix that is thermodynamically more stable than other structures – due to base-stacking, hydrogen-bonding and minimal helix distortion.¹⁶ This base-pair recognition requirement is what makes DNA such a superbly programmable molecule. Additionally, B-DNA, the most common form, has a diameter of ~ 2 nm, a pitch of ~ 10.5 bases, a persistence length of ~ 50 nm, and a potentially addressable bit density of ~ 0.34 nm.¹⁶ This, coupled with the fact that nature provides us with a toolbox of enzymes to selectively manipulate this molecule, makes DNA structurally, chemically, and functionally superb for use in material science and nanotechnology.

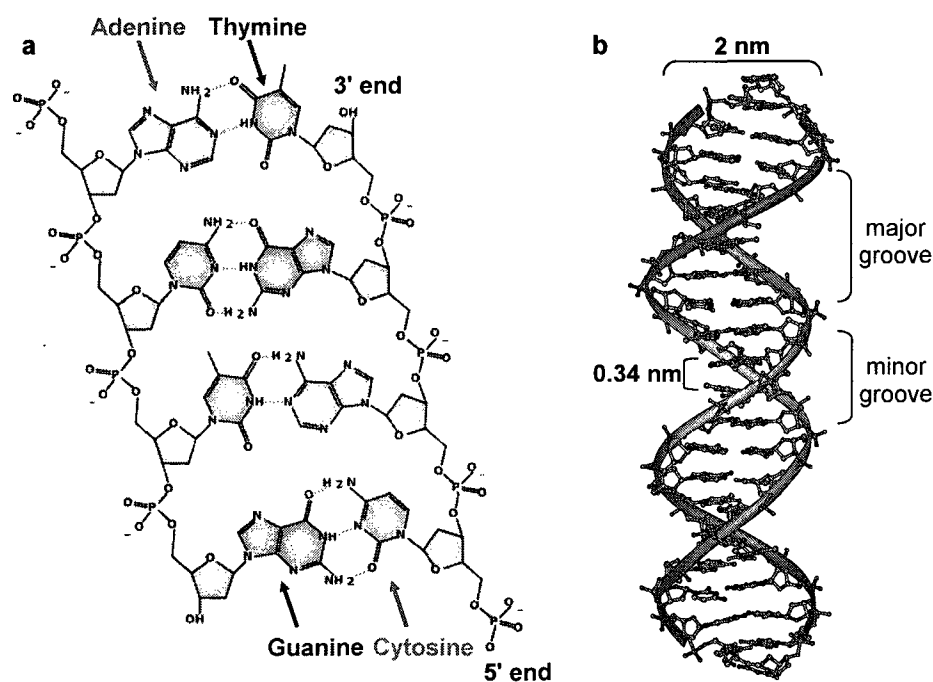


Figure 1.1 DNA double helix. (a) Typically, two DNA strands hybridize to each other in an antiparallel fashion according to specific base pairing rules, that is, A with T and C with G. The resulting double-stranded helix contains an inner core of bases and an outer backbone of sugar phosphates. (b) Typically, DNA has a diameter of ~ 2 nm, a pitch of ~ 10.5 nm, a distance of ~ 0.34 nm between each base, and a persistence length of ~ 50 nm. [Adapted from Wikipedia].

1.2 DNA in nanotechnology

DNA can be used to template material growth. Pioneering work by Braun and co-workers provided the first example of a DNA templated metallic nanowire.¹⁷ The group positioned a 16

μm long strand of λ -DNA between two gold electrodes, electrostatically localized silver ions onto the DNA's backbone, reduced the ions to generate silver aggregates, and developed these aggregates to form 100 nm thick silver wires. DNA templated gold, platinum, copper, and palladium wires have also been reported.¹⁸ Braun and co-workers later developed an approach to metallize sequence-specific regions of DNA (Figure 1.2).¹⁹ Using glutaraldehyde functionalized DNA that localizes metal ions, and RecA proteins that bind sequence-specific regions of the DNA's backbone, the group synthesized conductive gold nanowires separated by pre-designed gaps of specific length and location. Other materials have also been grown on DNA. Sargeant and co-workers reported the synthesis of DNA templated semiconducting nanocrystals with excellent quantum efficiencies retained in the solid-state,²⁰ He and co-workers reported the synthesis of conjugated oligomers by the enzymatic polymerization of aniline monomers electrostatically bound to the DNA's backbone (Figure 1.3),²¹ while Schuster and co-workers covalently attached aniline monomers onto specific DNA bases and reported the sequence-specific synthesis of "conjoined" oligoaniline nanowires.²² In a recent development, Eaton and co-workers applied the rules of *in vitro* selection to evolve a library of ribonucleic acid (RNA) molecules towards the best binders of palladium ions, and then selected the best of these RNA candidates to template the growth of a new class of palladium nanoparticles.²³ The three-dimensional structure of the RNA molecules is what dictated the resulting size and shape of the nanoparticle synthesized; this could, in principle, be adapted to three-dimensional DNA assemblies.

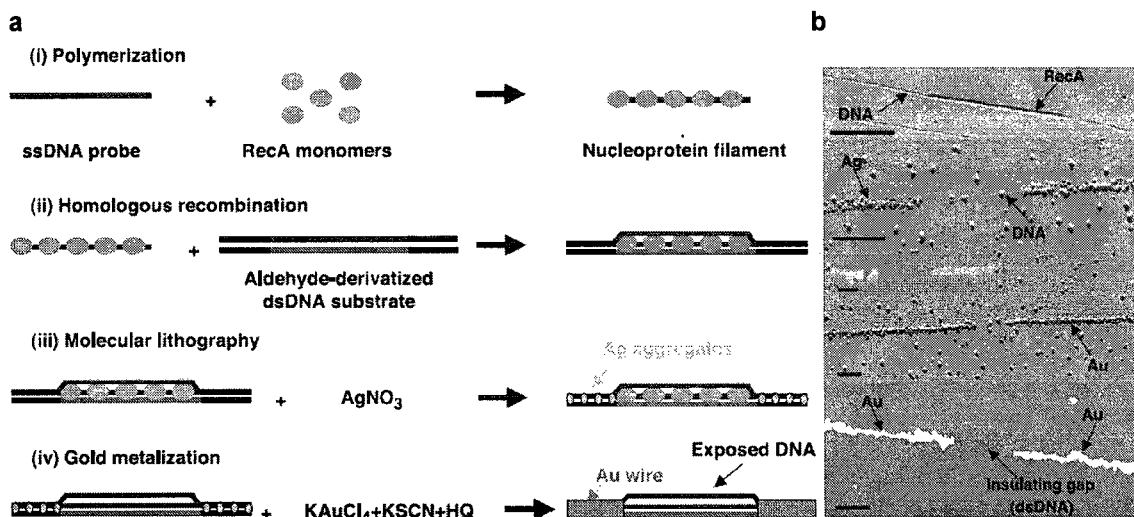


Figure 1.2 Site selective DNA templated molecular lithography. (a) (i) RecA monomers bind a single-stranded DNA probe to form a filament that then (ii) binds a double-stranded substrate DNA molecule at a specific homologous sequence. (iii) Addition of AgNO_3 results in the formation of silver aggregates along the regions unprotected by RecA, (iv) which then serve as catalytic sites for the specific deposition of gold to convert the unprotected regions to conductive gold wires. (b) This process can be monitored in real time using AFM and SEM. From top to bottom: Double-stranded DNA protected by RecA, silver deposition, gold growth (AFM), gold growth (SEM). [Adapted from reference 19].

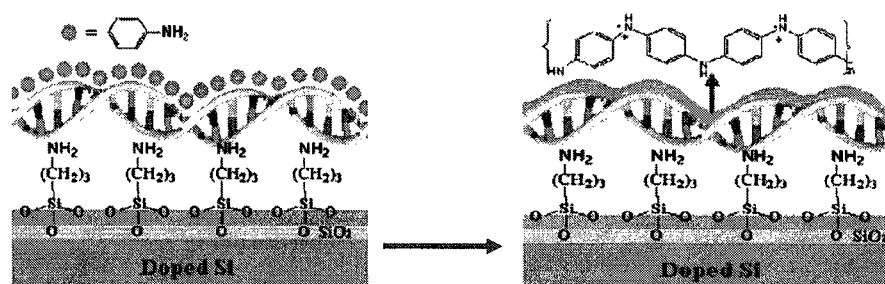


Figure 1.3 DNA templated polyaniline wires. Double-stranded DNA is stretched on a silicon surface, and is used as a template to polymerize non-covalently bound aniline monomers into polyaniline nanowires. [Adapted from reference 21].

DNA can also be used as a template for material organization. Electrostatic interactions have been used to organize positively charged nanoparticles onto DNA via its backbone,²⁴⁻²⁸ while intercalation interactions have been used to localize modified metallic nanoparticles onto DNA via its bases.²⁹⁻³¹ The true power of this molecule, however, lies in its sequence addressability. Materials modified with single-stranded DNA molecules can be targeted to assemble onto specific regions within a complementary DNA template. This approach provides exquisite control over the level of organization. In 1996, Alivisatos and co-workers modified gold nanoparticles with unique DNA sequences, and organized them into head-to-head and a head-to-tail dimers (Figure 1.4a).³² The group later used this approach to organize two gold nanoparticles of different sizes into dimers and trimers, with complete control over combination (Figure 1.4b).³³ In a separate contribution, Mao and co-workers used the principle of rolling circle amplification (RCA) to synthesize 4 μm long DNA templates, with many repeating units, and organized gold nanoparticles modified with the complementary sequence into extended one-dimensional nanoparticle assemblies (Figure 1.4c).³⁴ Niemeyer and co-workers modified proteins with DNA molecules, and presented the first example of DNA templated protein organization. This was later adapted to construct an artificial two-enzyme complex in which the spatial proximity of the enzymes was found to be beneficial for their overall bioactivity. The group also used the biotin-streptavidin interaction as a “universal linker” to organize a number of different materials, including antibodies, enzymes, gold nanoparticles, and fluorescent molecules.³⁵

The above examples are selected to illustrate the potential of DNA in nanotechnology. If the full promise of this molecule is to be exploited, however, then rational access to non-natural two- and three-dimensional DNA assemblies will need to be realized. This area of research is referred to as structural DNA nanotechnology.

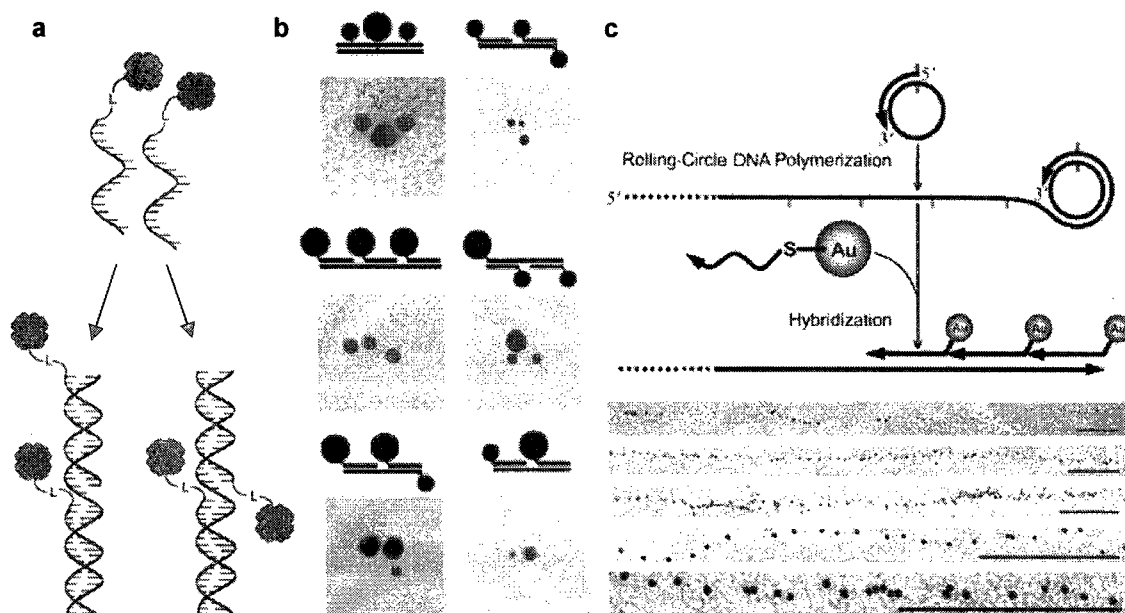


Figure 1.4 DNA templated sequence-specific nanoparticle organization. (a) Two nanoparticle modified with unique single strands of DNA are organized into head-to-head and head-to-tail dimers using a complementary DNA template. (b) The same approach is used to generate discrete nanoparticle trimers, of all possible combinations. (c) Rolling circle amplification generates an “extremely long” DNA template with a repeating region, which is used to organize gold nanoparticles tagged with the complementary sequence into one-dimensional linear assemblies. [Adapted from references 32-34].

1.3 Structural DNA nanotechnology

The field of structural DNA nanotechnology utilizes DNA’s powerful base-pair molecular recognition requirement to help solve a number of challenges facing researchers in material science and nanotechnology. In it, DNA is stripped away from any of its preconceived biological roles and is treated as a powerful synthetic polymer. The initial challenge within this field was to generate a branched DNA motif. If realized, then access to two- and three-dimensional DNA assemblies would be feasible. In the early

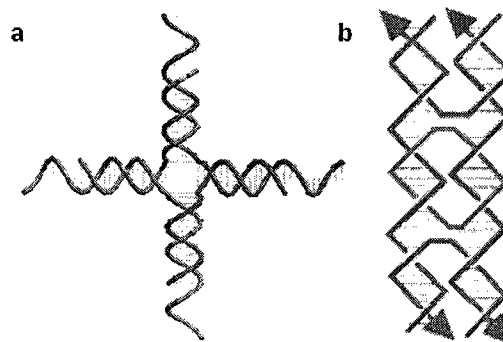


Figure 1.5 First set of DNA building blocks. (a) Four DNA strands are programmed to assemble into a four-way branched DNA building block with sticky ends at its periphery, that could, in principle, be used to construct two- and three-dimensional DNA assemblies. (b) Two duplexes are locked into position using a number of crossovers to generate a structurally well-defined tile with four sticky ends (arrow head). The different colors denote different strands. [Adapted from reference 38].

1980's, Seeman and co-workers took initial inspiration from the naturally occurring branched Holliday junction, and assembled four synthetic DNA strands into a four-way branched molecule (Figure 1.5a).³⁶ By incorporating addressable sticky ends at the periphery of this four-armed building block, the group developed the first example of a rationally designed artificial DNA unit capable of constructing higher-order assemblies. However, this initial design produced flexible junctions that did not assemble into real-space structures, but that rather generated topological constructs. The level of flexibility within the branching points needs to be controlled if access to *well-defined* two- and three-dimensional DNA systems is to be achieved. The second challenge within this field, therefore, was to generate well-defined DNA building blocks. By joining two double helices with a single strand exchange process, Seeman and co-workers constructed a double crossover (DX) tile with addressable sticky ends at the edges (Figure 1.5b).³⁷ The group used this tile to generate well-defined two-dimensional crystalline lattices, with complete control over the size and shape of its periodicity. It is the sum of this initial work that laid the foundations for the development of structural DNA nanotechnology. These relatively simple principles of construction have since been used, adapted, and developed to generate systems with exquisite control over design and function.

1.3.1 Developments. In addition to the four-way Holliday Junction and the double crossover tile discussed above, a number of other branching building blocks have since been generated; see reference 38 for a recent review. Most of these can be classified as being a planar tile, a branched junction, a discrete building block, or a helix bundle. Planar tiles are constructed from a number of helices joined together by inter-strand crossovers, and currently come in a number of different flavors; the number and sense (i.e. polarity) of crossovers is what determines the type of tile produced. Double crossovers are constructed by joining together two helices with two crossovers, while triple crossovers are formed when three DNA helices are connected using four crossovers motifs (Figure 1.6a, left). Four, eight, and even twelve helix tiles (Figure 1.6a, left) have also been constructed. These planar tiles have been assembled into linear arrays, two-dimensional lattices (Figure 1a, right), and into DNA nanotubes.³⁸ Branched junctions are constructed from multiple helices that branch from a central core, and almost always contain a number of cross-over motifs to increase rigidity (Figure 1.6b). Three, four, six, eight, and twelve-arm branched DNA junctions are synthesized using this approach, and have been used to assemble two-dimensional arrays with square, hexagonal, and compound cavities.^{38,39} Discrete building blocks are constructed from a number of DNA strands that assemble into a well-defined module, with addressable sticky-ends for its further assembly (Figure 1.6c). Examples include

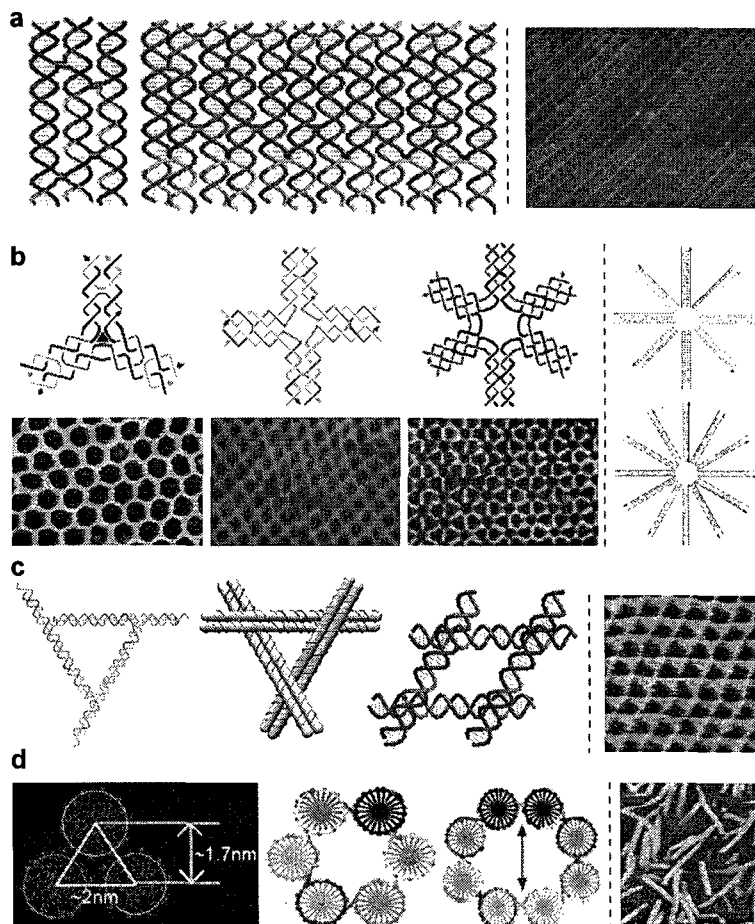


Figure 1.6 DNA nanotechnology developments. (a) (*left*) A triple crossover tile and a twelve-helix crossover tile. (*right*) An example of a two-dimensional DNA assembly generated from a double crossover tile; lines represent hairpins programmed to protrude from each tile to aid in their visual detection using AFM. (b) (*left*) A three-, four- and six-arm branched junctions used to generate two-dimensional hexagonal, square, and compound lattices, respectively. (*right*) Simple eight and twelve-arm branched DNA junctions. (c) (*left*) Triangular and square-shaped discrete DNA building blocks, with sticky end overhangs. (*right*) A triangular shaped DNA lattice generated from a triangular DNA building block (central object in left panel). (d) (*left*) Three-, six-, and eight-membered helix bundles. (*right*) A nanocolumn assembly generated from the three helix bundle (left object in left panel). [Adapted from references 38,39].

parallelogram and triangular-shaped tiles that assemble into two-dimensional arrays with square, hexagonal or rhombic cavities.³⁸ Helix bundles are constructed from a number of parallel DNA double strands that are linked via crossovers (Figure 1.6d). Three, six, and eight-helix bundles have been generated. These can be assembled into extended one-dimensional nanotube or two-dimensional periodic arrays.^{38,39}

In a recent advancement, Rothemund developed a new approach to assembling DNA nanostructures. In *DNA origami*, a single continuous single-stranded DNA template is systematically folded into a number of different arbitrary shapes with the help of smaller

“stapling” strands that pin-together the assembly via strand-exchange crossovers.⁴⁰ The long strand traverses the shape of the final construct, from side to side, and participates in each helix formed from each stapling strand. Using this approach, Rothemund folded the same strand of genomic DNA into squares, rectangles, stars, smiley faces, triangles with rectangular domains, and sharp triangles with trapezoidal domains and bridges between them. And because each stapling strand is unique, the assemblies generated are also selectively addressable with a spatial resolution of ~ 6 nm. A number of applications utilizing DNA origami have already appeared. Yan and co-workers constructed an origami-based array for the label-free detection of RNA molecules,⁴¹ and in a separate contribution used an origami array to study the distance-dependence binding of ligands and proteins.⁴² Shih, Chou, Douglas and co-workers used the approach of DNA origami to weave a long strand into a discrete six-helix nanotube, which they use to align transmembrane proteins for NMR structural analysis.⁴³

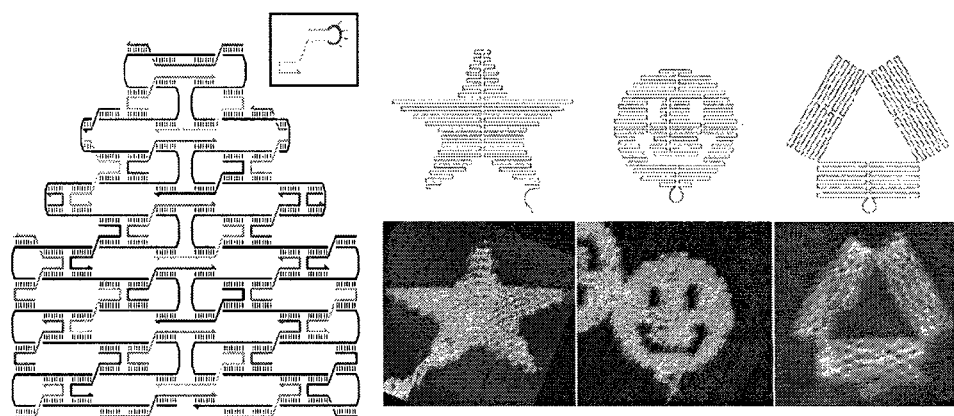


Figure 1.7 DNA origami. (*left*) In DNA origami, a long DNA strand is folded into the desired structure, and is held into shape using many “stapling” strands (colored). Inset: Illustrates how each stapling strand could be selectively addressed, in this case using a hairpin. (*right*) This approach is used to construct a number of different two-dimensional architectures, including a star, a smiley face, and a triangle. [Adapted from reference 40].

1.3.2.1 Applications: Protein organization. Proteins are functional molecules with applications in biosynthesis, sensing, and catalysis. Control over their organization in one- and two-dimensions is a requirement if their full potential in DNA nanotechnology is to be exploited. Yan and co-workers demonstrated the feasibility of using the principles of DNA nanotechnology for the *one*-dimensional organization of proteins. The group constructed a triple cross-over rectangular tile capable of assembling into a one-dimensional array, and modified each of these tiles with either one or two biotin molecules.⁴⁴ Because biotin binds the protein strepavidin selectively, it can be used as a tether to direct the positional organization of this protein. Tiles

modified with a single biotin molecule generate a linear array of Streptavidin proteins, while tiles modified with two biotin molecules produce a two-line double linear protein array. In a separate contribution, the same group used a similar triple cross-over tile modified with DNA aptamers to direct the organization of thrombin proteins into one-dimensional linear arrays.⁴⁵ DNA aptamers can be engineered to selectively bind a number of different target proteins, using systematic evolution of ligands by exponential enrichment (SELEX), which makes this later contribution of particular interest.^{46,47}

The first example of a *two*-dimensional protein array was presented by Yan, LaBean, and co-workers in 2003.⁴⁸ The group first constructed a four-way branched DNA tile capable of assembling into extended two-dimensional square networks. By modifying the junctions of each of these tiles with a biotin molecule, Yan and co-workers organized streptavidin proteins into periodic two-dimensional square assemblies. In a subsequent contribution, the same group demonstrated control over periodicity.⁴⁹ By generating the same two-dimensional square array from two alternating tiles, instead of a single tile, Yan and co-workers controlled the periodicity of biotin molecules within the DNA assembly and constructed two-dimensional streptavidin arrays of either continuous or alternating assemblies (Figure 1.8a). In 2006, Mao and co-workers modified the inner core of this same four-arm branched tile with fluorescein antigens, instead of biotin molecules, and produced two-dimensional periodic arrays of the fluorescein antibody

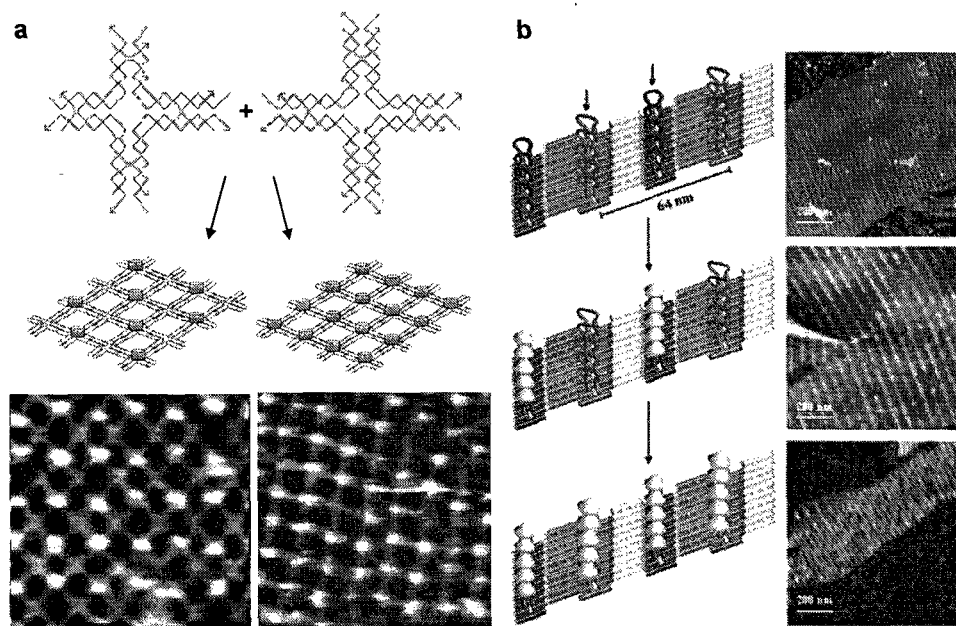


Figure 1.8 Two-dimensional protein organization. (a) Two branched DNA junctions assemble to generate a square-shaped array. If one of these tiles is modified with biotin, then an alternating array of streptavidin proteins is generated (*left*), but if both tiles are modified, then a continuous protein array is produced (*right*). (b) Four tiles are assembled into an array with two unique aptamers (red and green) that organize two different proteins into alternating lines. [Adapted from references 49,51].

protein.⁵⁰ The antibody-antigen interaction is of interest to researchers in proteomics, drug discovery, and immunodiagnostic medicine, making this first example of a rationally designed antibody array of interest. Planar tiles can also be used to generate two-dimensional protein. Four different double cross-over tiles can be programmed to assemble into an alternating array of four unique rows. Each of these rows has the potential of being selectively addressed. By modifying one of these tiles (i.e. rows) with the *myc*-peptide, Yan, Chaput, and co-workers utilized the protein-protein interaction between the *myc*-peptide and the anti-*myc* antibody to produce rows of antibodies, with a 64 nm spacing.⁵¹ In a separate contribution, Yan and co-workers modified two such tiles with two different aptamers, one specific to thrombin and the other specific to platelet derived growth factors, and produced alternating rows of two different proteins with no unwanted cross-talk between them (Figure 1.8b).⁵²

Unmodified two-dimensional DNA arrays can also template the organization of proteins. Dervan and co-workers developed a class of pyrrole-imidazole polyamides that sequence-specifically bind the minor groove of double-stranded DNA at specific sites. The group utilized this selectivity to direct the organization of proteins onto specific regions within an unmodified pre-assembled DNA array.⁵³ Specifically, an array from four different planar tiles is constructed, each of which could be selectively addressed using a specific biotin-modified polyamide strand, and is used to subsequently organize streptavidin with complete control over periodicity (Figure 1.9a). Turberfield and co-workers organized the protein RuvA into extended two-dimensional

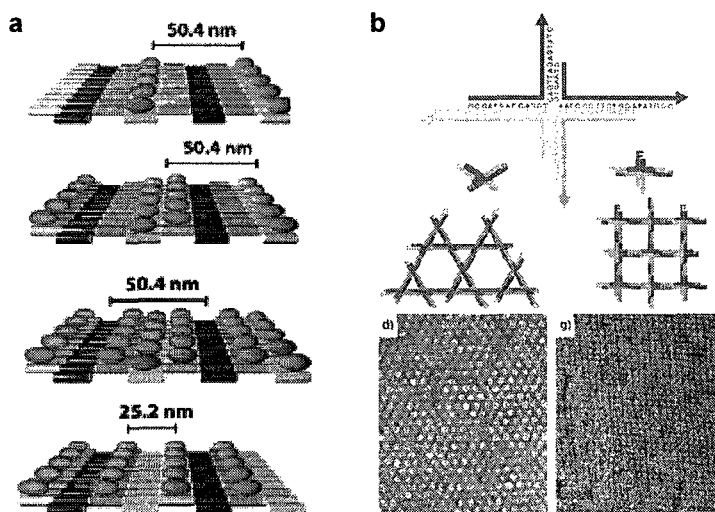


Figure 1.9 Two-dimensional protein organization, using unmodified DNA arrays. (a) Polyamides that sequence selectively bind specific tiles can be used to position proteins onto targeted lanes within an assembled two-dimensional DNA array, of different combinations. (b) A four-way branched junction that typically assembles into a hexagonal-type array (*left*) can be made to assemble into a square-shaped array upon binding to the protein RuvA (*right*). [Adapted from references 53, 54].

arrays using unmodified DNA junctions.⁵⁴ RuvA is a DNA binding protein. The group used this interaction to bind four-armed Holliday junctions, now structurally oriented at a 90° angle, and assembled them into a well-defined square-planar array, simultaneously organizing RuvA (Figure 1.9b). The assembly process occurred with a high enough fidelity to allow for the protein's crystal structure to be determined with a resolution of 3.5 Å.

1.3.2.2 Applications: Nanoparticle organization. Nanoparticle assemblies hold great promise in nanoelectronics, sensing, catalysis, and nanophotonics. Their collective properties strongly depend on their relative arrangement within these assemblies. Our ability to organize them into well-defined systems is of great importance. In 2004, Seeman and co-workers presented the first example of a DNA templated two-dimensional gold nanoparticle array.⁵⁵ Five nanometer gold nanoparticles functionalized with multiple DNA strands were organized into lines on an array constructed from four unique planar tiles, one of which contained a protruding DNA capture probe complementary to the DNA sequence conjugated to the particles. By modifying a second tile with a different DNA capture probe, the group was able to later organize two different sizes of gold nanoparticles into alternating lines (Figure 1.10a).⁵⁶ Yan and co-workers constructed a two-dimensional DNA array from two four-arm branched junctions, and used it to organize five

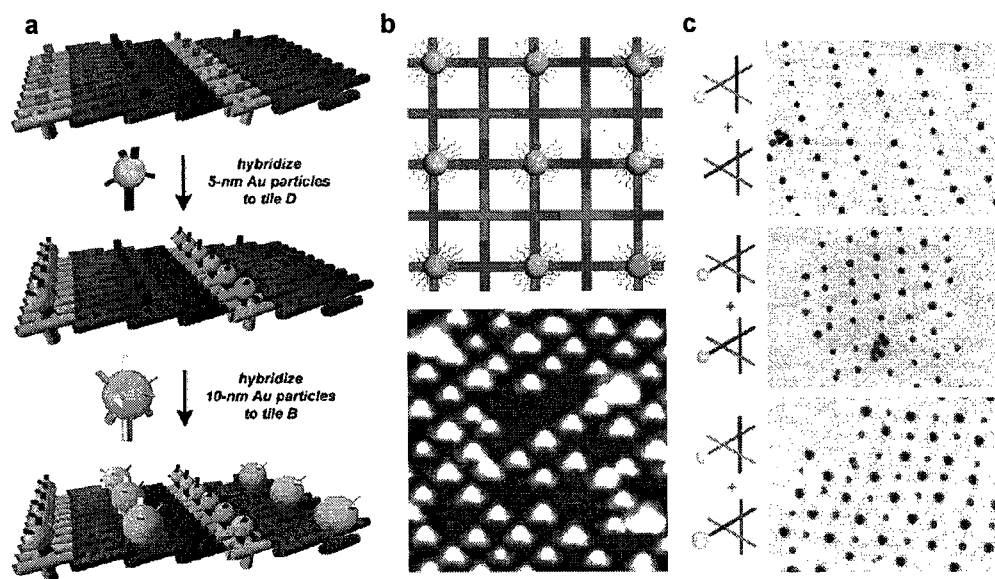


Figure 1.10 Two-dimensional gold nanoparticle organization. (a) Four DX tiles assemble into an array with two alternating protruding capture probes. Gold nanoparticles modified with the complementary sequences are instructed to assemble into alternating lines. (b) Modifying the inner core of a single junction with a protruding DNA sequence results in an assembly that organizes gold particles into an alternating square array. (b) The modification of triangular DNA building blocks with gold nanoparticles results in a gold assembly of normal or alternating periodicity. [Adapted from references 56, 57, 59].

nanometer gold nanoparticles into an alternating square arrangement (Figure 1.10b).⁵⁷ The approach involved modifying the core of one of these tiles with a protruding DNA capture probe complementary to the DNA strands coating the gold nanoparticles. In a second contribution, the same group directly conjugated the core of one of these tiles with a gold particle, and used a second unmodified tile to generate a number of different gold assemblies with control over periodicity and cavity size.⁵⁸ Exquisite control over the two-dimensional organization of discrete nanoparticles was demonstrated by Seeman and co-workers.⁵⁹ The group constructed two double cross-over triangular tiles capable of assembling into an extended rhombic lattice, which they used to organize two different sizes of gold nanoparticles into an alternating assembly (Figure 1.10c). This approach involved mono-functionalizing each respective gold nanoparticle with a single DNA strand, and subsequent incorporation of this conjugate into the triangular tile prior to its use in array formation.

Although a number of well-defined two-dimensional nanoparticle arrays have been constructed, little has been achieved in the area of well-defined discrete nanoparticle organization. The problem lies in the fact that branched DNA junctions are inherently flexible, and that the cross-over approaches developed to rigidify them typically need to be part of an extended motif to maintain their overall structural robustness.

1.3.2.3 Applications: DNA computation and DNA nanomachines. A full summary of all other applications of DNA nanotechnology is beyond the scope of this section, however, the fields of DNA computation and DNA nanomachines merit mention. Adelman and co-workers presented a breakthrough in the area of DNA computing when they developed a simple DNA-based system capable of solving the seven point “Hamiltonian path” problem.⁶⁰ DNA computing promises to address some of the limitations that our current silicon-based technology is starting to face with respect to miniaturization. Shapiro and co-workers engineered the first actual DNA computer with an input, computation, and output modules.⁶¹ They developed a system capable of analyzing input mRNA molecules to release a single-stranded DNA molecule that acts as a drug. Winfree and co-workers designed a set of DNA building blocks that represent Wang tiles.⁶² Conceptually, Wang tiles contain a single color on each of their four sides, and assemble so that the adjacent sides of each square are of the same color. This requirement necessarily means that each tile can only fit in a specific way within the assembly. Winfree and co-workers adapted this methodology to rectangular-shaped DNA tiles with four addressable sticky ends at each side, and demonstrated the feasibility of this algorithmic assembly using a number of arrays.⁶² Since all

mathematical algorithms can be translated into Wang tiles, this work is of particular value to researchers in DNA computing.

Seeman and co-workers constructed a DNA based nanomechanical device capable of undergoing a structural transition. This machine consists of two DX molecules connected by a double helix that undergoes a B-DNA to Z-DNA structural conversion, at high ionic strengths, and induces a nanomechanical movement of the DX tiles (Figure 1.12a).⁶³ DNA nanomachines are of interest because they promise to create new technologies for use in molecular sensing, intelligent drug delivery, and in programmable chemical synthesis. The disadvantage of using an unspecific molecule to activate motion, such as the use

of salt ions in the case of B-Z systems, is that a number of embedded devices would all respond simultaneously. Strand-displacement based devices, however, offer a sequence-dependant mechanism for actuation and allow for the selective control of different parts within the same device. Yurke and co-

workers constructed a pair of DNA tweezers with two rigid double-stranded arms connected at one end by a flexible single-stranded hinge, and sequence selectively cycled it between a closed and an open state using “fuel” and “antifuel” DNA strands (Figure 1.12b).⁶⁴ Turberfield, Yan, Reif, and co-workers applied the same principles of strand-displacement to construct a DNA based nanomachine with a unidirectional autonomous motor capable of “walking” across a DNA scaffold.⁶⁵ Turberfield and co-workers recently reviewed this fertile area of research.⁶⁶

In structural DNA nanotechnology, DNA is used in all parts of the assembly. A number of recent publications have shown that small molecules can also be incorporated into DNA nanostructures, and that they additionally instill structural and functional advantages to the system that DNA alone cannot. Cram, Lehn, and Pedersen received the 1987 Nobel Prize for their work in Supramolecular chemistry. This area of research deals with the study and application of non-covalent molecular interactions, such as hydrogen bonding, metal coordination, hydrophobic

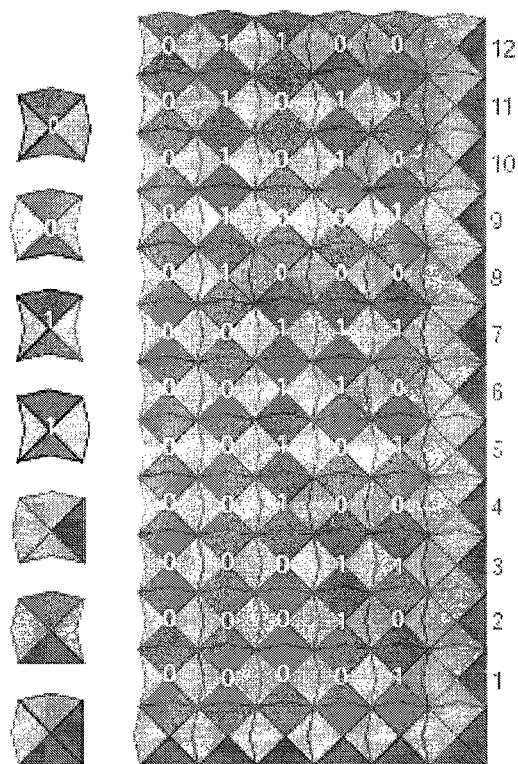


Figure 1.11 Computing with DNA. In this example, seven tiles are used to count from 1 to 12. Each of these tiles represents a DNA tile with four addressable sticky ends. The bottom three tiles form the borders, while the remaining four tiles are used to represent the integers 0 or 1. This assembly counts from 1 (bottom row) to 12 (top row). [Adapted from reference 62].

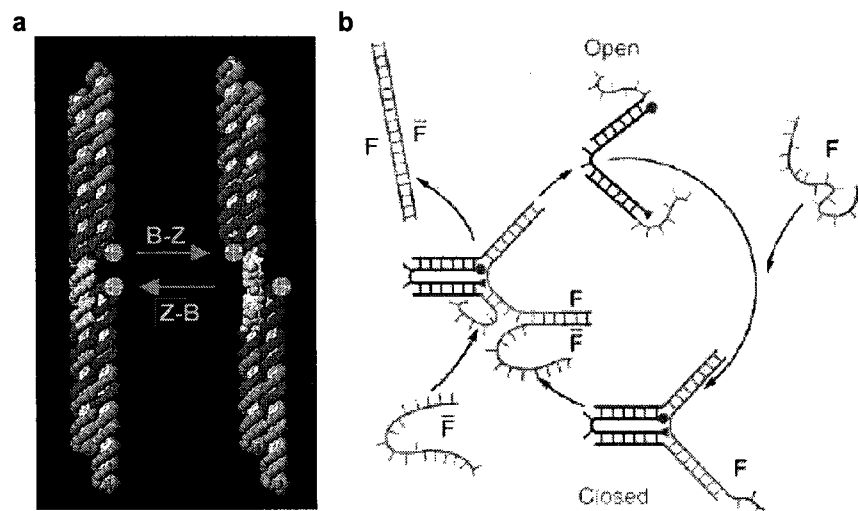


Figure 1.12 DNA nanomachines. (a) The B-Z DNA structural transition is monitored using FRET, and can in principle be used as a two-state switch. (b) Sequence-dependant actuation is demonstrated using a DNA systems that contains two overhangs. In the open state, the two strands are free, addition of a fuel molecule locks the assembly into a well-defined construct, while addition of an anti-fuel molecule reopens the system. [Adapted from references 63, 64].

effects, π - π interactions, and electrostatic forces. These rules are now being used to empower the field of DNA nanotechnology, and are resulting in an emerging subarea of research that our group has recently termed supramolecular DNA nanotechnology.

1.4 Supramolecular DNA nanotechnology

Molecules have structure and function. These can be exploited by DNA, and can also be used to exploit DNA.

1.4.1 Molecules that provide structural and functional benefits to DNA nanotechnology.

In DNA nanotechnology, the entire structures are made up of DNA. In *supramolecular* DNA nanotechnology, molecules can be used to replace parts of these structures. Small molecules possess a number of different branching points, angles, and are relatively small; this means that they can be seamlessly incorporated into DNA. For example, organic aliphatic molecules can be used to construct branched DNA building blocks with an organic core. Von Kiedrowski and co-workers synthesized a three-arm DNA building block radiating from a single aliphatic three-arm linker.⁶⁷ The group assembled these building blocks into discrete dimers, tetramer, and higher-order structures. Shchepinov and co-workers used a polyglycol-based core, constructed on the solid-support, to synthesize DNA building blocks with two, three, six, nine, and twenty seven

arms.⁶⁸ Steric considerations make it difficult to access a small twenty seven armed DNA building block using just DNA; the biggest being a twelve arm branching point, recently reported by Seeman and co-workers (Figure 1.13a).³⁹ Organic aromatic molecules can also be incorporated. Bergstrom and co-workers synthesized a self-complementary two arm branched DNA building block with an aromatic *p*-(2-hydroxyethyl)phenylethynylphenyl spacers that are attached to a single tetrahedral carbon atom, as the vertex, and assembled it into discrete structures containing two, four, five, etc units (Figure 1.13b).⁶⁹

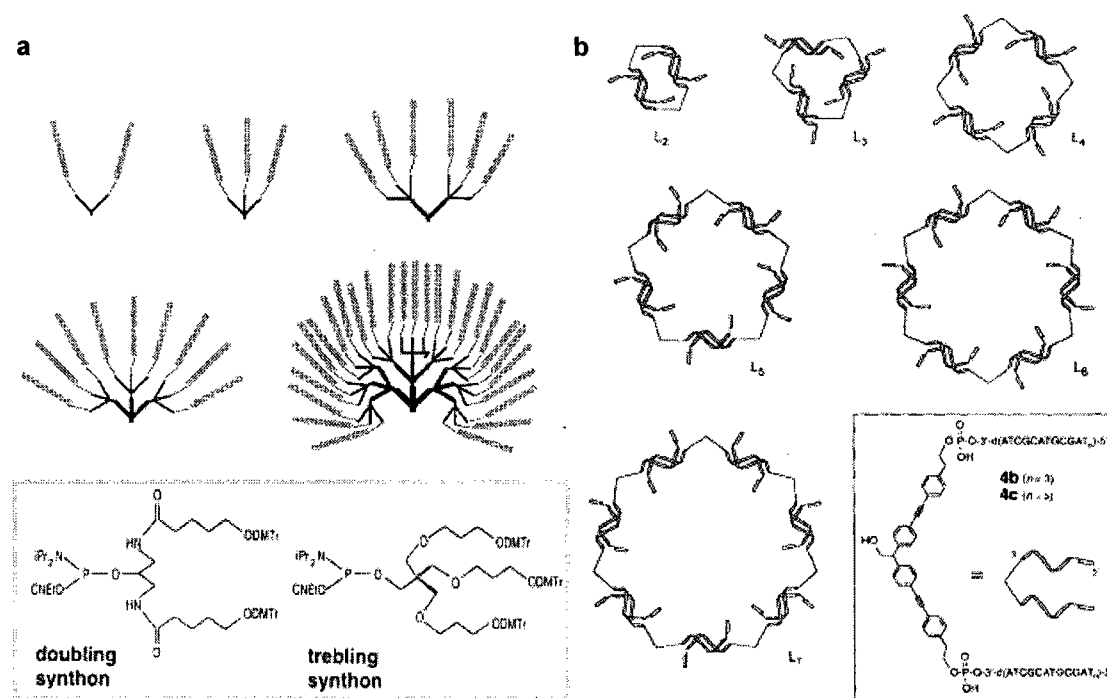


Figure 1.13 Organic DNA building blocks. (a) Branched DNA building blocks in which a number of DNA arms radiate from a central aliphatic core are constructed using two- and three-arm branching synthons (inset below). (b) A symmetrically branched DNA building block in which two arms radiate from a central aromatic core assembles into discrete assemblies of two, three, etc building blocks. [Adapted from references 68, 69].

Inorganic molecules are of particular interest because in addition to structural features, they can also impart functional electronic, catalytic, and optical properties to DNA. Bunz and co-workers synthesized a two-arm branched DNA building block containing a cobalt tetraphenylcyclobutadiene(cyclopentadienyl) vertex, and modularly assembled it into linear tapes using branched DNA building blocks with a phenyleneethynylene aromatic core.⁷⁰ Sleiman and co-workers synthesized a two-arm branched DNA building block with a ruthenium tris(bipyridine) core, which they assembled into the first example of a cyclic metal DNA nanostructure (Figure 1.14a).^{71,72} McLaughlin and co-workers synthesized a two-arm ruthenium bis(terpyridine) DNA

building block,⁷³ and later presented the synthesis of a four-arm nickel cyclam⁷⁴ and a six-arm ruthenium tris(bipyridyl) branched complexes (Figure 1.14b).⁷⁵ Access to inorganic branched DNA building blocks can be synthetically limited as a consequence of the conditions used in standard automated DNA synthesis. Sleiman and Yang recently developed a synthetic approach that synergistically stabilizes both the metal environment and the DNA duplex to access metallated DNA building blocks that would otherwise be difficult to synthesize (Figure 1.14c).⁷⁶

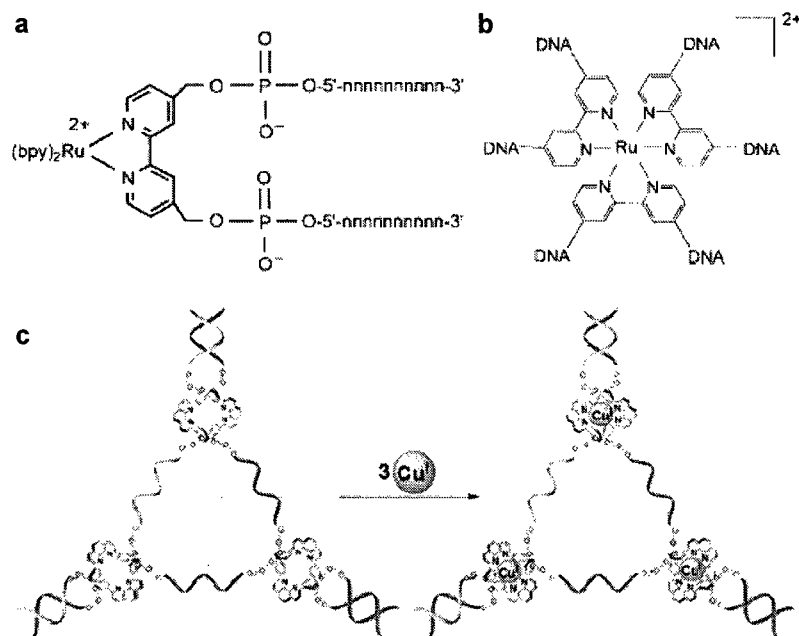


Figure 1.14 Inorganic DNA building blocks. (a) A two-arm branched DNA building block with an inorganic ruthenium core. (b) A six-arm branched DNA building block with an inorganic ruthenium core. (c) In this approach to accessing inorganic DNA assemblies, a construct with containing metal binding ligands is first synthesized and assembled, this is then used as a template to position metals to generate stable inorganic DNA assemblies. [Adapted from references 71, 75, 76].

1.4.2 Molecules that refine the assembly process in DNA nanotechnology. In supramolecular chemistry, the interplay between hydrogen-bonding, metal coordination, π - π stacking, and hydrophobic interactions is what determines the assembly outcome. In structural DNA nanotechnology, the assembly outcome is essentially dictated by the sequence of each strand; this is the power of DNA. However, by modifying DNA with supramolecular building blocks, the assembly process can now be fine-tuned as a function of both sequence and supramolecular interactions. For example, Kramer and co-workers modified the ends of a single molecule of DNA with metal binding terpyridine ligands, and used zinc to induce cyclization and override duplex formation (Figure 1.15a).⁷⁷ Li and co-workers incorporated π -conjugated molecules into

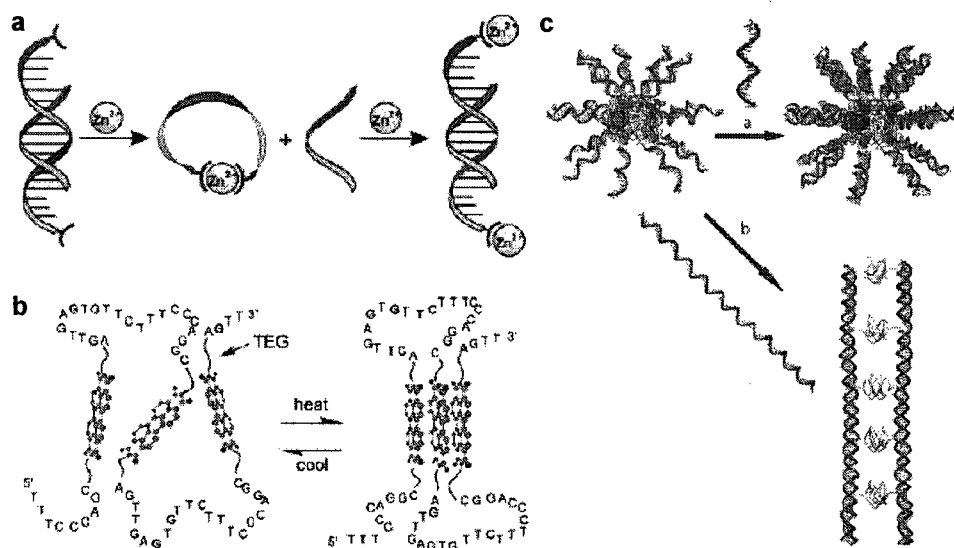


Figure 1.15 Supramolecular DNA nanotechnology. (a) DNA strands that are end modified with metal coordinating ligands can be used to bind zinc, and override DNA duplex formation, and can be allowed to rehybridize to the complementary DNA strand up addition of excess zinc. (b) Extended aromatic molecules can be inserted into DNA to create folded structures through π -stacking interactions. (c) DNA strands (blue) attached to polymers (green) result in block copolymers that assemble into micelles through microphase separation of the incompatible blocks. Addition of a complementary strand of DNA (red short) does not affect the overall morphology, while addition of a longer complementary strand of DNA (red long) results in a change of the overall morphology. [Adapted from references 77-79].

DNA that assemble into π -stabilized stacks, and generated thermophilic foldable oligo-polymers in which the π -conjugated stacks contributed to the final assembly process (Figure 1.15b).⁷⁸ Berger, Herrmann, and co-workers generated a class of DNA-polypropyleneoxide polymers – with a hydrophilic DNA region and a hydrophobic polymeric region – that microphase separate into spherical micelles, and further demonstrated that these assemblies can be inter-converted into rod-like micelles using an external DNA template strand with a repeating complementary repeating region (Figure 1.15c).⁷⁹

Sequential self-assembly of a DNA hexagon as a template for the organization of gold nanoparticles

Faisal A. Aldaye and Hanadi F. Sleiman, *Angew. Chem. Int. Ed.* **2006**, *45*, 2204-2209.

Nanoparticle assemblies hold great promise as new materials for biodetection, catalysis, and for nanoelectronics and photonic applications.³⁻⁹ Many of these properties, however, are strongly dependent on the relative arrangement of the individual nanoparticles within each assembly.⁶⁻⁹ The lack of current approaches to systematically generate well-defined discrete model systems has hampered the understanding of these properties. In here, we present a unique method for the modular and programmable construction of nanoparticle assemblies of well-defined structure.

As discussed in Chapter 1, some of the earliest work on the use of DNA in nanotechnology was on discrete nanoparticle assemblies that essentially established the feasibility of using DNA to template the organization of nanoparticles. Since then, Kornberg and co-workers synthesized glutathione coated 46-atom gold clusters mono-functionalized with a single DNA strand, and assembled them into discrete dimers.⁸⁰ Alivisatos and co-workers functionalized CdSe/ZnS core/shell quantum dots (QD) with a discrete number of DNA strands, and mono-functionalized gold nanoparticles with the complementary sequence to generate discrete gold/QD assemblies of single quantum dots surrounded by one, two, three, or four gold nanoparticles (Figure 2.1a).⁸¹ The same group later used a three-arm branched DNA template to generate a number of discrete branched gold nanoparticle groupings (Figure 2.1b).⁸² However, because of nicks present within the DNA assemblies, or because of the flexibility inherent to the branching points used, all discrete systems to date resulted in nanoparticle assemblies that are flexible. If we are to truly tap into the structure/function relationship of these nanoparticle systems, we will need to be able to access nanoparticle assemblies that are positionally well-

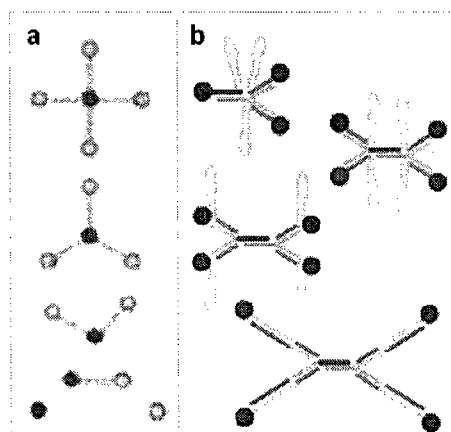


Figure 2.1 Discrete nanoparticle grouping. (a) Discrete nanoparticle assemblies of quantum dots (red) and gold nanoparticles (yellow). The lines connecting the nanoparticles represents double-stranded DNA. (b) Assemblies of an internal hairpin trimer, internal hairpin tetramer, external hairpin tetramer, and an extended tetramer of gold nanoparticles. [Adapted from references 81, 82].

defined. To do so, it will be necessary to eliminate nicks within the backbone of the DNA scaffolds – necessary for maintaining rigidity along a single dimension – and to generate well-defined branched architectures – necessary for maintaining rigidity along multiple dimensions.

In an attempt to eliminate nicks present within discrete nanoparticle assemblies, Alivisatos and co-workers developed a post-assembly enzymatic ligation approach.⁸³ As seen in Figure 2.2a, gold nanoparticles are assembled into dimers, using a fully complementary DNA strand, and are then enzymatically ligated to form a fully linked discrete dimer that can be purified. The group uses this methodology to link dimers and trimers of gold nanoparticles, which they assemble into discrete gold tetramers and hexamers. Li and co-workers developed a method to immobilize gold nanoparticles onto fully double-stranded DNA templates that are already assembled, and could in principle adapt this approach to generate nanoparticle assemblies that are inherently nick-free (Figure 2.2b).⁸⁴

The group immobilized gold nano-

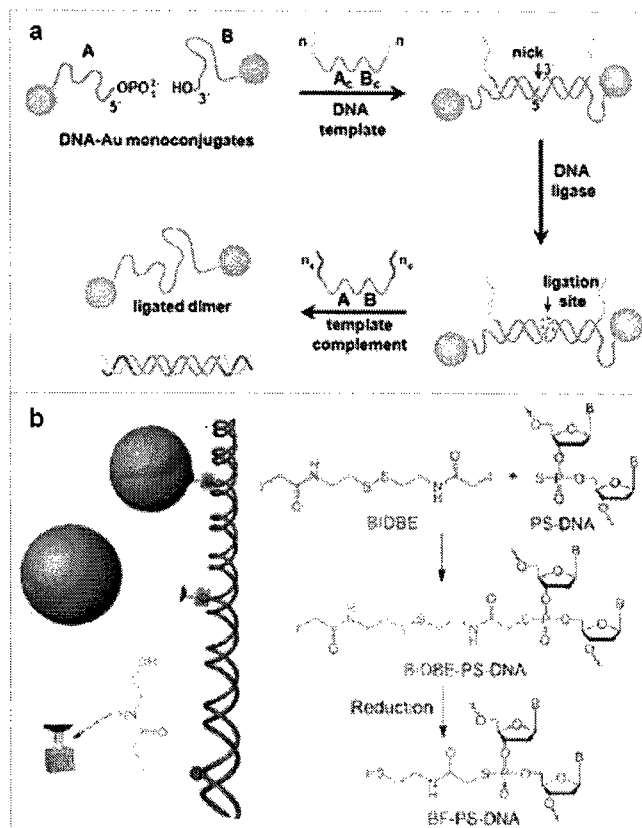


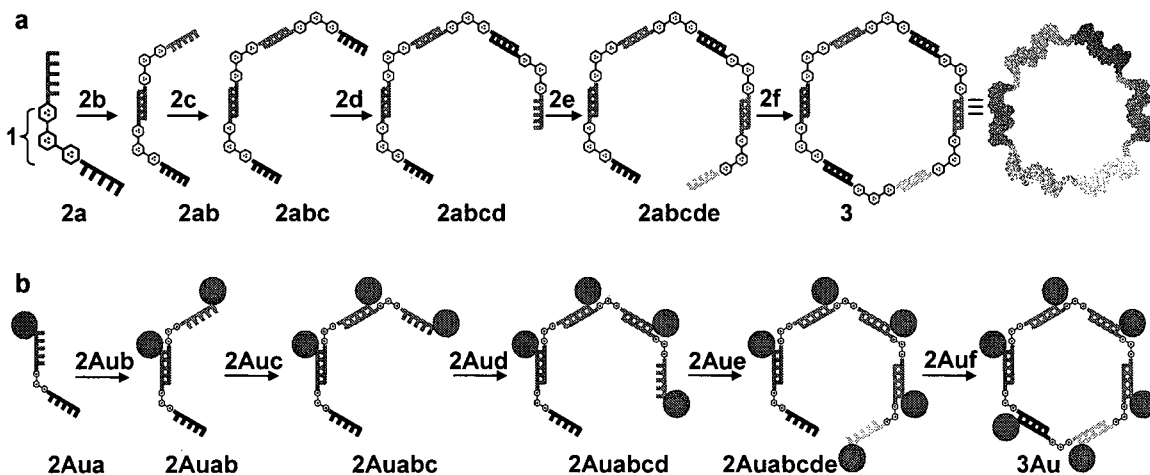
Figure 2.2 Discrete DNA assemblies that are free of nicks. (a) Nicks that might result during the construction process can be removed using enzymatic ligation. (b) Gold nanoparticles assemble onto a double-stranded DNA template using an iodo/thio bifunctional fastener (BF) that directly tethers gold nanoparticles onto incorporated phosphorothioate groups. [Adapted from references 83, 84].

particles onto specific regions of a linear double-stranded DNA template using an iodo/thio bifunctional fastener that conjugates gold nanoparticles onto selectively incorporated phosphorothioate bases. Extending this methodology onto the second dimension will necessarily require the use of branching junctions. DNA branching points are, however, inherently flexible. A number of crossover approaches have been developed to rigidify them, but these typically need to be part of an extended system to maintain their robustness. This is why a large number of well-defined two-dimensional nanoparticle arrays have been constructed, but relatively little has been achieved in the area of DNA templated, well-defined, discrete nanoparticle organization. Here we present the first example of a *well-defined two-dimensional discrete* gold nanoparticle

assembly, and organize six gold nanoparticle into a discrete hexagon. This work provides a modular approach to generate discrete nanoparticle assemblies for the systematic study of their catalytic, electronic, photonic, and plasmonic properties, and will contribute to the bottom-up design of nanoscale circuitry that accomplishes complex functions.

A hexameric assembly will necessarily contain six well-defined sides that are linear, and six well-defined corner units that are held at an angle of 120° . In our approach, sides are made up of fully double-stranded DNA, while corner units are made up of rigid organic molecules (Scheme 2.1). We use DNA building blocks, which contain rigid organic vertices, to insure formation of a well-defined DNA template, and to also simultaneously dictate the position of each nanoparticle within the final construct. Specifically, we synthesize six DNA molecules **2a-2f** with two different DNA arms that radiate from the rigid organic 120° vertex **1**, and assemble them into a discrete hexagonal DNA nanostructure **3** with a cyclic arrangement of six DNA duplexes and six rigid vertices (Scheme 2.1a). Labeling each of these molecules with a single gold nanoparticle then allows us to generate the discrete hexameric gold nanoparticle assembly **3Au** (Scheme 2.1b).

Scheme 2.1 Sequential addition of **2a-2f** to generate **3**, and of **2Aua-2Auf** to generate **3Au**.



2.1 Synthesis

Initial efforts are directed towards the synthesis of the six DNA building blocks **2a-2f**; each constructed from two 17-mer DNA arms held together by the rigid organic vertex **1**. DNA sequences of **2a-2f** are designed so that a single arm of each building is complementary to a single arm of the next building block, with the remaining arms of **2a** and **2f** being complementary to one another. Solid-phase automated synthesis of **2a-2f** is accomplished by the initial synthesis

of the first DNA arm, incorporation of the phosphoramidite derivative of vertex 1, 5, subsequent synthesis of the second arm, and by the incorporation of an amino-phosphoramidite molecule. The amine is introduced at the 5' end of each building block to facilitate its subsequent conjugation to gold nanoparticles. Purification of **2a-2f** is performed using denaturing polyacrylamide gel electrophoresis (PAGE; Figure 2.3).

With building blocks **2a-2f** in hand, we proceeded to label each unit with a single gold nanoparticle. 1.4 nm gold nanoparticles monofunctionalized with a succinimidyl ester moiety are incubated with each of the amino-modified building blocks **2a-2f**. Unreacted gold is removed by size exclusion filtration, while unreacted DNA is separated using agarose gel electrophoresis. The bands corresponding to gold/DNA **2Aua-2Auf** are purified and characterized using gels stained with ethidium bromide to detect DNA, and silver-enhanced to detect gold (Figure 2.4).

An experiment is conducted to confirm the specificity of silver-enhancement as a detection tool for gold nanoparticles, and not DNA. A gel containing **2ab** and **2Aua** is stained with ethidium bromide and silver-enhanced at different time intervals. The band corresponding to **2ab** contains only DNA, and should only be detected by ethidium bromide, while the band corresponding to **2Aua** contains both DNA and gold, and should thus be detected using both ethidium bromide and silver-enhancement. As seen in Figure 2.5, silver-enhancement detects the gold-containing band **2Aua** in just 30 seconds, while the band corresponding to **2ab** is not silver-enhanced even after an over-exposure period of 300 seconds.

The 1:1 molar ratio of gold to DNA in strands **2Aua-f** is confirmed using UV/vis analysis and agarose gel titration experiments. UV/vis spectroscopy is used to quantify the relative ratio of gold to DNA because the observed absorbance at 420 nm is due to gold only. Given that $\epsilon_{\text{DNA},260}$

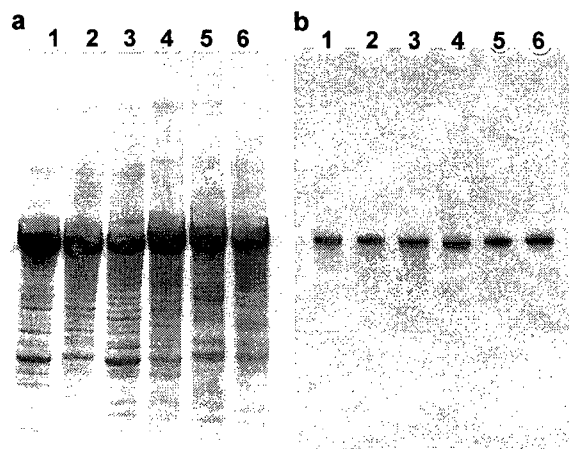


Figure 2.3 Building blocks 2a-2f. 24% denaturing polyacrylamide gels of (a) crude **2a-2f** (lanes 1-6, respectively), and of (b) purified **2a-2f** (lanes 1-6, respectively).

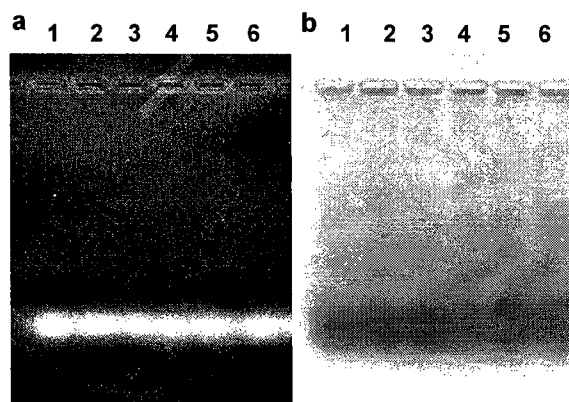


Figure 2.4 Building blocks 2Aua-2Af. 3% agarose gel of purified **2Aua-2Af** (lanes 1-6, respectively) visualized by (a) ethidium bromide elumination, and (b) silver-enhancement staining.

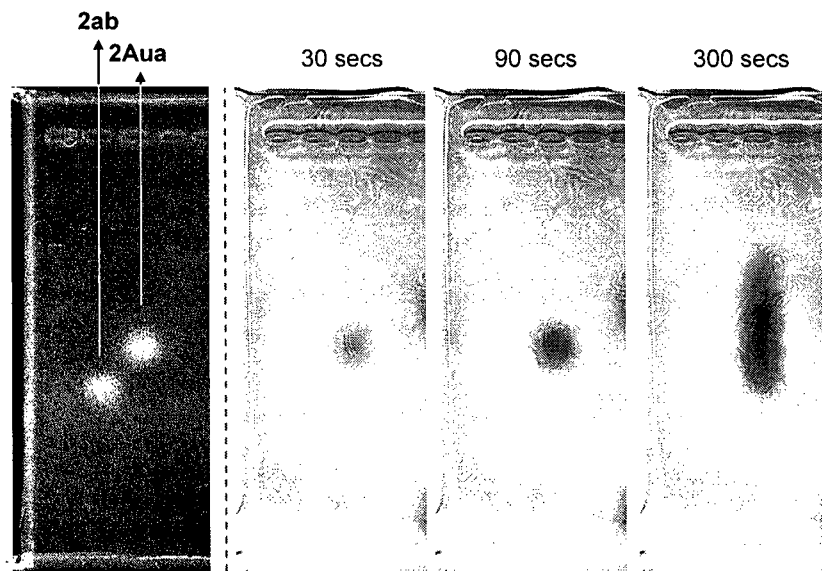


Figure 2.5 Selectivity of silver-enhancement to gold. An assembly containing DNA **2ab**, and an assembly containing both DNA and gold **2Aua**, are subjected to ethidium bromide staining (*left*) and silver-enhancement, for different time intervals (*right*).

$= 5.5 \times 10^5 \text{ L mol}^{-1} \text{ cm}^{-1}$, $\epsilon_{\text{gold},260} = 3.1 \times 10^5 \text{ L mol}^{-1} \text{ cm}^{-1}$, and $\epsilon_{\text{gold},420} = 1.1 \times 10^5 \text{ L mol}^{-1} \text{ cm}^{-1}$, and given an absorbance at 260 nm of 0.2010 and an absorbance at 420 nm of 0.0258, for **2Aua**, the calculated gold-DNA molar ratio in **2Aua** is 1.0:1.1 (Figure 2.6a). This ratio is further confirmed using titration experiments of gold/DNA constructs with their complementary partners (Figure 2.6b). Using **2Aua:2Aub**, as an example, addition of **2Aub** to **2Aua** at a 1:0.5, 1:1, or a 1:3 molar ratio results in the formation of a single band of lower electrophoretic mobility, assigned to duplex **2Auab**, and to no other bands of lower mobility.

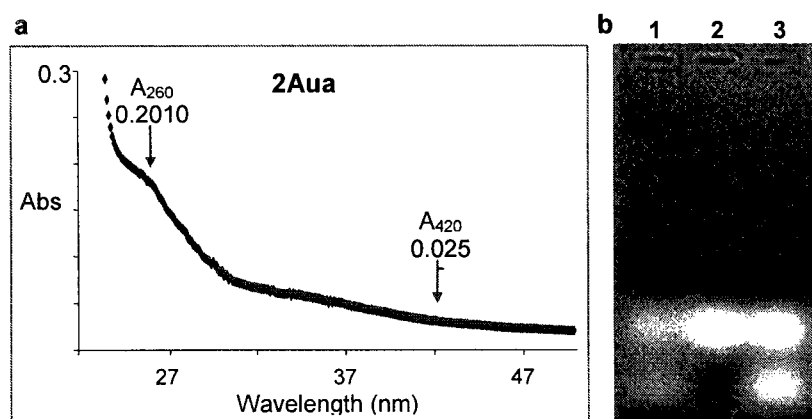


Figure 2.6 Characterization of the 1:1 molar ratio of gold/DNA. (a) UV/Vis absorbance spectrum of **2Aua** verifies the 1:1 molar ratio between gold and DNA. (b) Hybridizations of **2Aua** with **2Aub** in the varying ratios of 1:0/5, 1:1, and 1:3 (lanes 1-3, respectively) also confirm the 1:1 gold to DNA ratio.

2.2 Results and discussion

With building blocks **2a-f** in hand, we proceed to examine their ability to undergo sequential self-assembly into the desired DNA hexagonal structure **3**. As seen in Figure 2.7, **2a** alone shows a band of relatively high mobility when characterized by native PAGE (lane 1). The assembly of two (**2ab**), three (**2abc**), four (**2abcd**) and five (**2abcde**) building blocks results in single bands of steadily decreasing mobility that correlate well with the 10 base pair linear DNA ladder in lane 8 (lanes 2-5, respectively). Addition of the sixth building block **2f** to **2abcde** results in cyclization to generate the hexameric DNA assembly **3**, and concomitant formation of higher-order oligomeric species (lane 6). Although **3** is calculated to have 102 base pairs, it is found to move as a 200-mer when compared to the molecular weight marker, which is consistent with the fact that cyclic structures travel anomalously in gel electrophoresis when compared to their linear counterparts.⁸⁵ DNA hexamer **3** is purified by electroelution (lane 7).

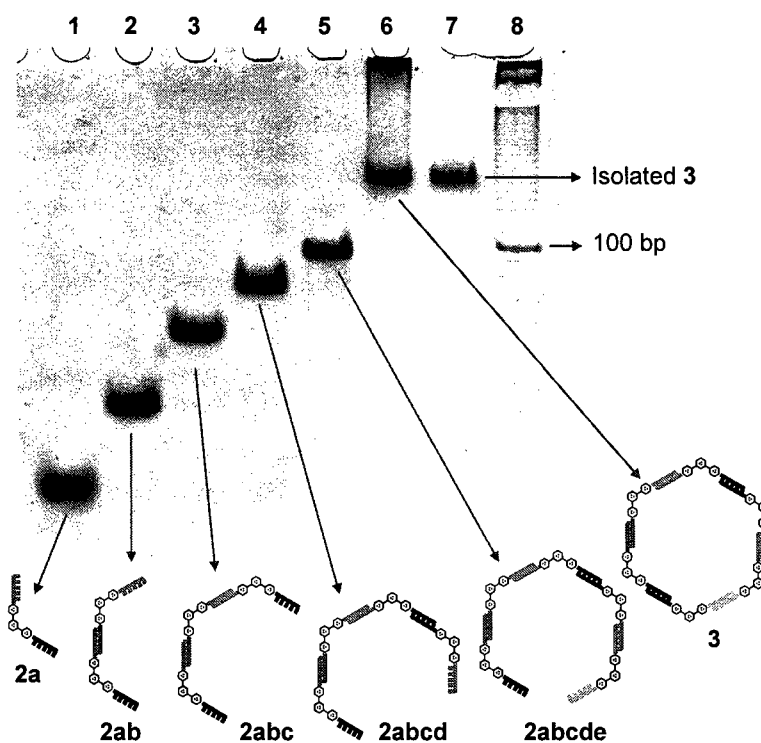


Figure 2.7 Sequential assembly of **3**. Native polyacrylamide gel of the sequential addition of **2a-2f**, forming **2ab**, **2abc**, **2abcd**, **2abcde**, and **3** (lanes 1 to 6, respectively), and of the isolated hexameric assembly **3** (lane 7). 10 bp molecular weight marker (lane 8).

The relative ratio of the discrete DNA assembly **3** to oligomers can be optimized as a function of temperature and time. Figure 2.8 illustrates a study in which a sample containing **2a-**

2f is cycled 1, 5, 25, and 99 times between 20 and 90°C, at a rate of 0.1°C/s. Analysis of the resulting systems show an increase in the relative ratio of **3** to oligomers as the number of such cycles increases from 0 to 1, 5, and 25. This observation is consistent with the significant stability of **3**, and suggests that the higher-order oligomers might be kinetic products.

The cyclic nature of **3** is essential for its use as an effective template. A number of studies are conducted to ascertain that **3** is indeed cyclic. In a first experiment, we subjected purified **3** to digestion assays using the enzyme Mung Bean Nuclease (MBN). Under optimized conditions, this enzyme is selective for the digestion of single-stranded DNA over that of double-stranded DNA.^{86,87} MBN is thus expected to degrade linear, open structures containing single-stranded DNA, but is not expected to degrade cyclic closed structures containing only double-stranded DNA. See section 2.4 for the optimization of MBN digestions towards our **2a-2f** DNA molecules.

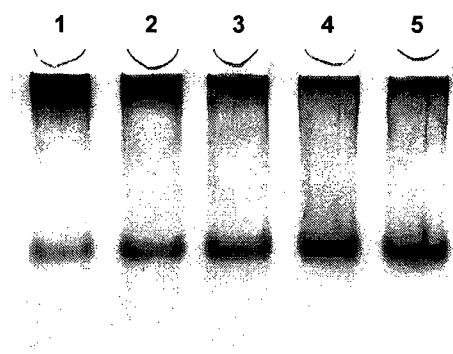


Figure 2.8 Thermocycling of **3** and oligomers. The assembled mixture generated from **2a-2f** is cycled between 90 and 20°C a total of 0, 1, 5, 25, and 99 times (lanes 1-5, respectively).

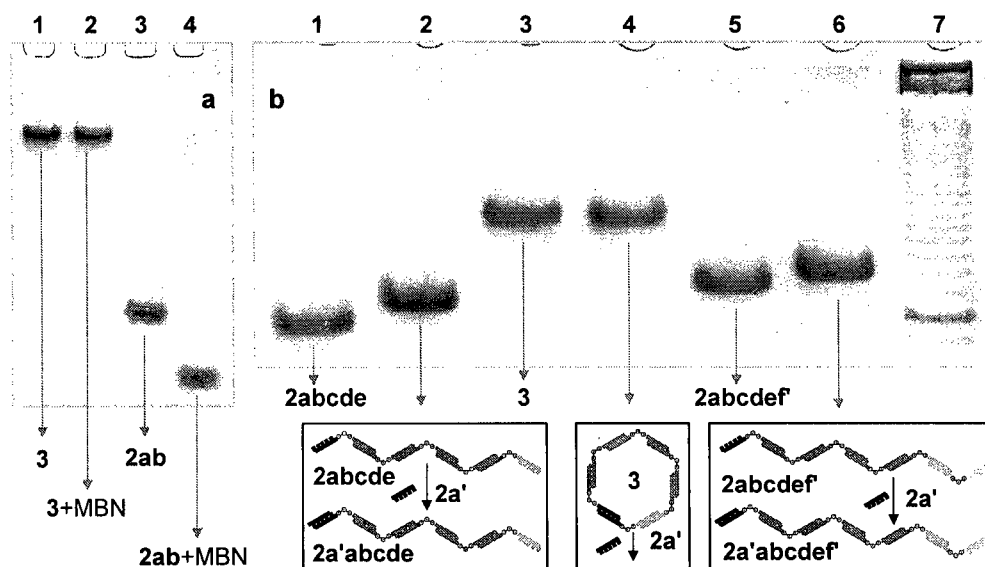


Figure 2.9 cyclic nature of **3**. (a) MBN enzymatic digestion of **3** (lane 1) results in no detectable shift in band mobility (lane 2). Control **2ab** containing double and single-stranded DNA (lane 3) is degraded using MBN (lane 4). (b) Linear pentamer **2abcde** (lane 1). **2abcde** and single-arm complement **2a'** show reduced mobility due to hybridization (lane 2). DNA hexamer **3** (lane 3). DNA hexamer **3** and **2a'** show no change in band mobility (lane 4). Deliberately synthesized linear hexamer **2abcdef'** (lane 5). Linear hexamer **2abcdef'** and **2a'** show reduced mobility due to hybridization. 10 bp DNA ladder (lane 7).

As seen in Figure 2.9a, subjecting purified **3** to MBN treatment results in no detectable shift in band mobility for hexamer **3**. In a second experiment, we deliberately synthesized a linear hexamer **2abcdef'** incapable of cyclizing, which interestingly, unlike hexamer **3**, now correlates well with the linear base-pair DNA ladder (Figure 2.9b, lane 5). When a single arm complement is added to the linear pentamer **2abcde**, linear hexamer **2abcdef'**, and to purified **3**, bands of reduced mobility are observed in the case of pentamer **2abcde** and hexamer **2abcdef'** only (Figure 2.9b). This is consistent with the cyclic nature of **3** in which all of its arms are sequestered and double-stranded.

Finally, Ferguson-plot analysis reveals a steadily increasing gel retardation coefficients for the linear structures **2ab**, **2abc**, **2abcd**, **2abcde**, and **2abcdef'**, and an anomalously higher retardation coefficient for the cyclic hexamer **3**, when compared to its linear counterpart **2abcdef'** (Figure 2.10). The experimentally obtained retardation coefficients for **2ab**, **2abc**, **2abcd**, **2abcde**, **2abcdef'** and **3** are 0.056,

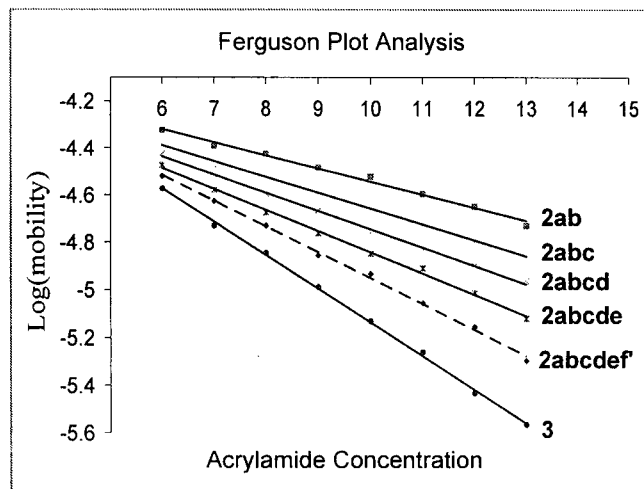


Figure 2.10 Ferguson plot analysis of **2ab**, **2abc**, **2abcd**, **2abcde**, **2abcdef'** and **3**.

0.067, 0.077, 0.089, 0.109, and 0.141, respectively. These experiments collectively establish hexamer **3** to be a fully double-stranded cyclic DNA assembly, with six well-defined double-stranded DNA sides and six rigid organic vertices.

Can this well-defined DNA template be used to organize six gold nanoparticles into a well-defined hexamer? The assembly process of these gold modified DNA building blocks **2Aua**-**2Auf** is monitored sequentially using agarose gels visualized using ethidium bromide, to detect DNA, and silver-enhanced, to detect gold. As seen in Figure 2.11, the linear gold assemblies **2Aua**, **2Auab**, **2Auabc**, **2Auabcd** and **2Auabcde** – corresponding to linear gold groupings of two, three, four, and five gold nanoparticles – result in single bands of relatively decreasing electrophoretic mobility (lanes 1-5). As expected, addition of the sixth building block **2Auf** to pentamer **2Auabcde** results in both cyclization of the gold hexamer **3Au** and formation of oligomeric species (lane 6). The hexameric assembly of six gold nanoparticles **3Au** is purified using electroelution (lane 7). To confirm the cyclic nature of **3Au**, similar gel-shift mobility assays are conducted. First, a linear hexameric assembly of six gold nanoparticles **2Auabcdef'** incapable of cyclizing is synthesized; also found to have a greater electrophoretic mobility when

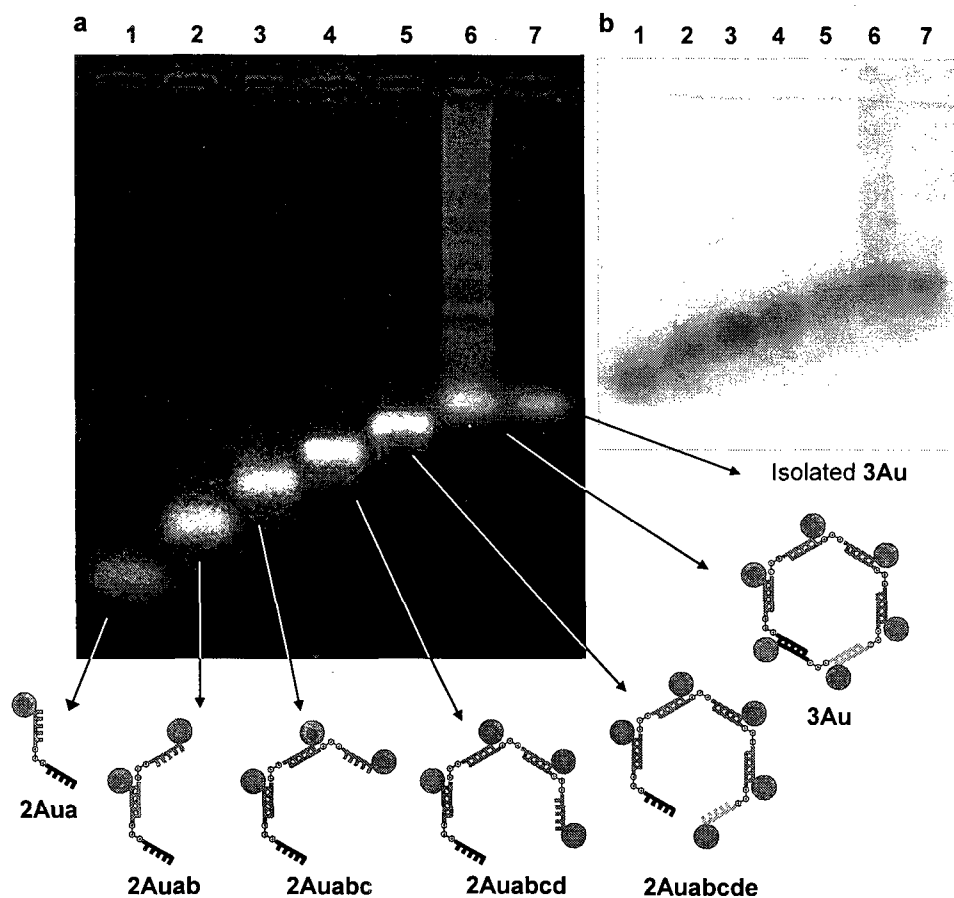


Figure 2.11 Assembly of 3Au from 2Aua-2Auf. Sequential assembly of gold conjugated building blocks 2Aua-2Auf (lanes 1-6) and the isolation of 3Au (lane 7), as visualized by (a) ethidium bromide, and by (b) silver-enhancement staining.

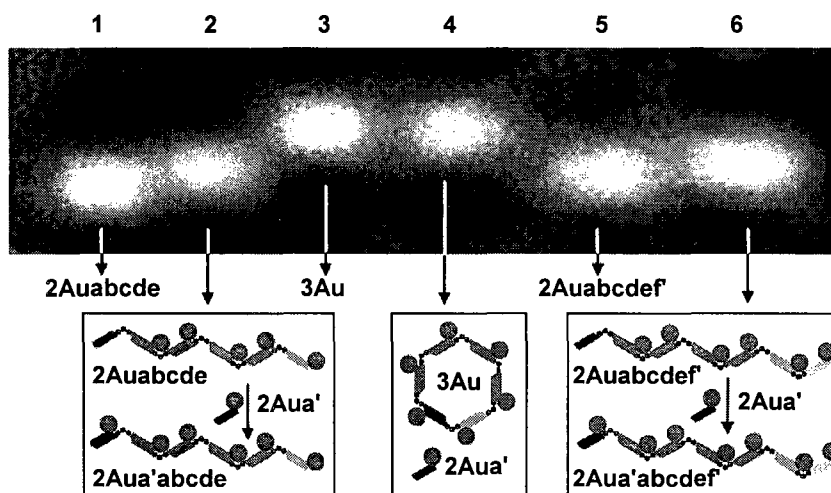


Figure 2.12 Cyclic nature of 3Au. Linear pentamer of gold nanoparticles 2Auabcde (lane 1). 2Auabcde and gold labeled single-arm complement 2Aua' (lane 2), showing a reduction in band mobility. DNA-templated gold hexamer 3Au (lane 3). 3Au and 2Aua' (lane 4), showing no change in band mobility. Deliberately synthesized linear hexamer of gold nanoparticles 2Auabcdef' (lane 5). 2Auabcdef' and 2a' (lane 6), showing a reduction in band mobility due to hybridization.

compared to its cyclic counterpart **3Au** (Figure 2.12, lane 5). Second, addition of the single-arm gold conjugate **2Aua'** (i.e. the gold analogue of **2a'**) to linear pentamer **2Auabcde**, linear hexamer **2Auabcdef**, and cyclic hexamer **3Au**, results in retardation of only the linear assemblies **2Auabcde** and **2Auabcdef** (Figure 2.12). These experiments collectively confirm the cyclic nature of **3Au**, in which six gold nanoparticles are organized into a well-defined hexagon.

2.3 Conclusions

We have demonstrated the organization of six gold nanoparticles into a discrete, well-defined, two-dimensional hexamer using a cyclic scaffold that contains both rigid organic vertices and double-stranded DNA arms. Our approach may be generalized for the construction of any discrete assembly of nanoparticles in which it is a requirement to spatially position the particles in a well-defined organized pattern. Because of the sequential nature of this method, different types of nanoparticles can be appended on each of the building blocks, thus potentially resulting in hetero-assemblies of precisely positioned nanoparticles. By varying the length of the DNA arms and the type of vertices, one can envisage the construction of a plethora of scaffolds of different sizes on which nanoparticles may be organized (i.e. triangles, squares, pentagons, etc). Finally, the use of vertices that contain three or more DNA arms can extend this organizational control into the third dimension.

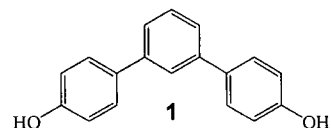
2.4 Experimental

General. 4-Bromoanisole, *m*-dibromobenzene, trityl chloride, magnesium turnings, dibromoethane, pyridine, HCl, triethylamine, diisopropylethylamine, dimethylaminopyridine, ethylenediaminetetracetic acid, MgCl₂·6H₂O, StainsAll[®], ethidium bromide, acetic acid, tris(hydroxymethyl)-aminomethane (Tris), formamide, and GeneElute[™] minus EtBr spin columns are used as purchased from Aldrich. Palladium tetrakis(triphenylphosphine) is purchased from Strem Chemicals. 2-Cyanoethyl diisopropylchlorophosphoramidite, guanidine derivatized 1000Å LCAA-CPG support with a loading density of 32 μmol/g, 5-ethylthiotetrazole, and reagents used for automated DNA synthesis, are purchased from ChemGenes. Sephadex G-25 (super fine, DNA grade), and Mung Bean Nuclease (source: Mung Bean Sprouts) are purchased from Amersham Biosciences. 10 bp Molecular weight DNA ladder (1.0 μg/μL) is purchased from Invitrogen Life Technologies. Sulfo-N-hydroxysuccinimido gold nanoparticles

(S-NHS-Nanogold[®]) and silver-enhancement reagent kits are used as received from NanoProbes. Microcon[®] size-exclusion centrifugal filter devices were purchased from Millipore.

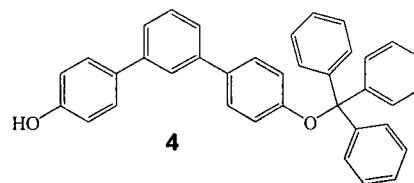
Instrumentation. ¹H-NMR is obtained using a Mercury 400MHz NMR spectrometer. ¹³C-NMR is obtained using a Mercury 300MHz NMR spectrometer. ³¹P-NMR spectra is obtained using a Gemini 200MHz NMR spectrometer. Matrix assisted laser desorption time-of-flight spectra are obtained using a KOMPACT MALDI III mass spectrometer. Standard automated oligonucleotide solid-phase syntheses are performed on a Perspective Biosystems Expedite 8900 DNA synthesizer. UV/vis experiments are conducted on a Varian Cary 300 biospectrophotometer. Temperature cycling experiments are performed on a Flexigene Techno 60 well thermocycler. Gel electrophoresis experiments are carried out on an acrylamide 20 X 20 cm vertical Hoefer 600 electrophoresis unit, and an agarose 7 X 8 cm horizontal Owl separation minigel system. Electroelutions are performed using a Centrilutor[®] electroeluter from Millipore. Ethidium bromide gels are visualized on a Fischer Scientific variable wavelength transilluminator.

Synthesis of 1,3-bis-(4-hydroxyphenyl)benzene (1). **1** is prepared in an overall synthetic yield of 71.2% according to a procedure reported by Nye and co-workers.⁸⁸ ¹H-NMR (CDCl₃, 400MHz):



δ7.69 (m, 1H, ArH), 7.55 (d, 4H, ArH, J=8.8Hz), 7.43-7.47 (m, 3H, ArH), 6.97 (d, 4H, ArH) ppm; ¹³C-NMR (CDCl₃, 400MHz): δ159.31, 141.48, 133.97, 129.33, 128.47, 125.54, 125.37, 114.44 ppm.

Synthesis of the mono-protected trityl derivative of 1 (4). **4** is prepared in a 58% synthetic yield according to a procedure reported by Nayale and co-workers.⁸⁹ Briefly, **1** (600 mg, 2.29 mol), dimethylaminopyridine (56.1 mg, 0.46 mol), and trityl chloride (638 mg, 2.29 mol) are dissolved in 500 mL of dry CH₂Cl₂. To this solution, diisopropylethylamine (0.519 mL, 2.98 mol) is added dropwise over a period of 30 minutes,



and the mixture is left stirring for an additional 16 hours. **4** is purified from a yellowish crude precipitate on a silica gel column by elution with dichloromethane:hexanes:triethylamine (80:16:4) (R_f 0.58). ¹H-NMR (CDCl₃, 400MHz): δ7.64 (s, 1H, ArH), 7.54 (d, 6H, ArH, J=7.0Hz), 7.49-7.27 (m, 20H, ArH), 6.86 (d, 2H, ArH, J=9.0Hz) ppm; ¹³C-NMR (CDCl₃, 300MHz): δ157.88, 156.01, 144.25, 141.68, 140.99, 134.15, 131.83, 129.18, 129.01, 128.32,

[illegible]

are characterized using matrix assisted laser desorption time-of-flight (MALDI-TOF; Table 2.1) mass spectrometry according to a procedure by Distler and co-workers.⁹¹

Table 2.1 Sequences and molar masses of DNA building blocks 2a-2f.

	Sequence (5'-3')	Molar Masses (mol/g)	
		Calc.	Experimental
2a	H ₂ N-CGATCTTGTGGCATTAG-1-CATTAGCTCGCAGGACG	10942.84	10943.86
2b	H ₂ N-CTAATGCCACAAGATCG-1-CTGGTTCTCTCAAGTAG	10870.85	10895.21 [M+Mg ²⁺]
2c	H ₂ N-GACACCTAGTGCACACG-1-CTACTTGAGAGAACCAG	10898.88	10898.51
2d	H ₂ N-CGTGTGCACTAGGTGTC-1-CTAACCGATACTCGTTG	10893.83	10895.21
2e	H ₂ N-CTCAGTTGTGACTTATG-1-CAACGAGTATCGGTTAG	10956.85	10974.12 [M+K ⁺]
2f	H ₂ N-CATAAGTCACAAGTCTGAG-1-CGTCCTGCGAGCTAATG	10904.89	10903.45

Synthesis of 2Aua, 2Aub, 2Auc, 2Aud, 2Aue and 2Auf. Mono-functionalized sulfo-N-hydroxysuccinimido gold nanoparticles with a diameter of 1.4 nm are used as purchased from NanoProbes. Generally, 6 nmol of gold is incubated with 12 nmol of each respective DNA building block (10 μ L HEPES buffer, pH 7.5; 16 hrs, 25°C). Excess unreacted gold nanoparticles are removed using Microcon[®] YM-100 filters, while excess unreacted DNA is removed using 3% agarose gel electrophoresis. The extracted gold-DNA conjugates are purified using GeneElute[™] minus EtBr spin columns.

Synthesis of 2f', 2a', 2Auf', and 2Aua'. The respective sequences of **2f'** and **2a'** are H₂N-CATAAGTCACAAGTCTGAG-1-CTTATCGTACAGACTCG and H₂N-CGTCCTGCGAGCTAATG. Synthesis and purification of **2f'/2a'** and **2Auf'/2Aua'** is analogous to the synthesis and purification of **2a-f** and **2Aua-f**, respectively. The theoretically calculated and experimentally obtained molecular weights of **2f'** and **2a'** are 10863.86/10861.46 and 5334.93/5353.86 [M+K⁺], respectively.

Hybridizations. Generally, 1.2×10^{-10} moles of each building block is initially dissolved in 5 μ L of TAEmg buffer (40 mM Tris, 20 mM acetic acid, 2 mM EDTA·2Na·2H₂O, 12.5 mM MgCl₂·6H₂O). These are then sequentially hybridized to each other in 20 minute time intervals. For example, **2abc** is assembled by combining **2b** (5 μ L) to **2a** (5 μ L), incubating for 20 minutes to form **2ab** (now in 10 μ L), and by adding **2c** (5 μ L) to the newly formed **2ab**, followed by an incubation period of 20 minutes to form **2abc** (now in 15 μ L). Assemblies are characterized

using 16% native polyacrylamide gels (18 hrs, 4°C), and are visualized using StainsAll® (2 hrs; 12.5 mg StainsAll®, 125 mL distilled water, 125 mL formamide).

Munge Bean Nuclease Digestions. In an attempt to confirm the enzyme's activity on DNA building blocks containing "our" synthetic organic vertices, and to determine the conditions under which the enzyme digests single-stranded DNA preferentially over that of double-stranded DNA, a study is conducted in which **2ab** is subjected to varying amounts of MBN. Digestions are performed on 1.2×10^{-10} moles of **2ab** (10 μ L TAE buffer), in an ice bath, and for a period of 3 hours. Under these conditions, 36 units of MBN results in the selective and complete digestion of the single-stranded portions of **2ab**.

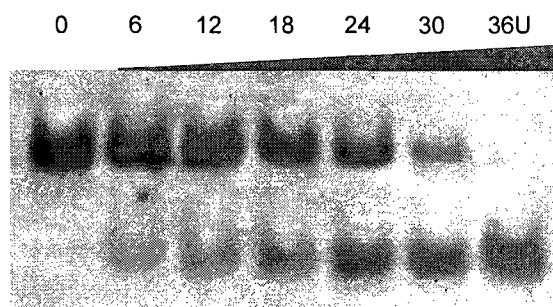


Figure 2.12 Optimization of MBN digestions assays. Complete degradation of the single-stranded arms of **2ab** is achieved using 36 U of MBN (0°C, 3 hrs).

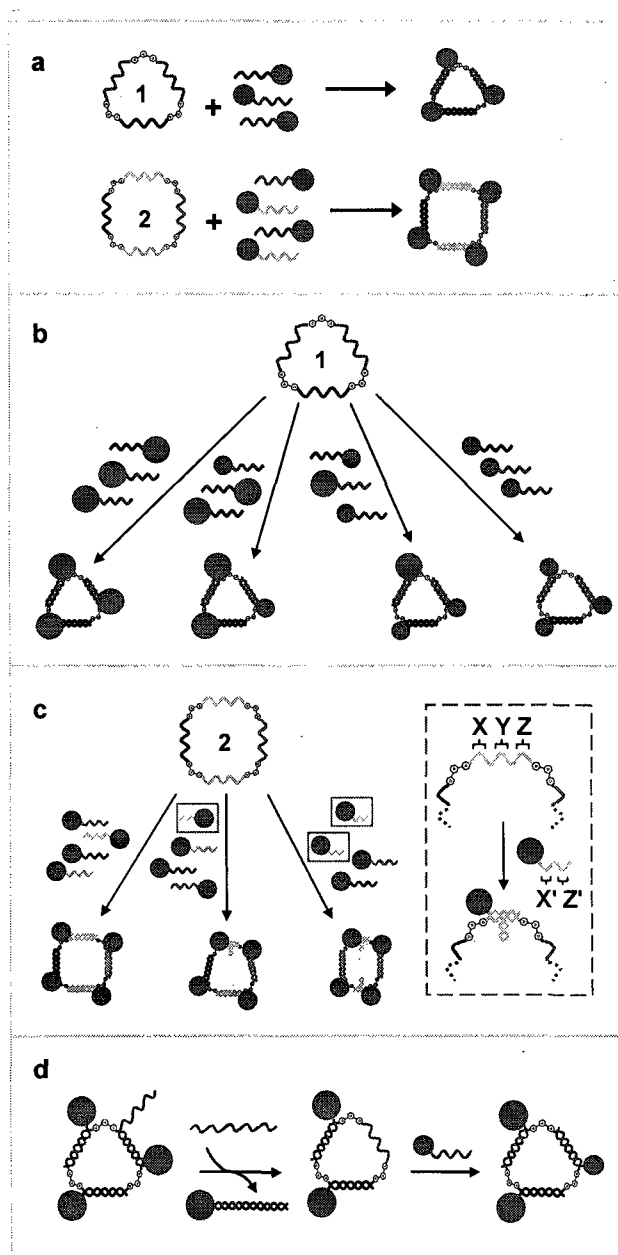
Dynamic DNA templates for discrete gold nanoparticle assemblies: Control of geometry, modularity, write/erase, and structural switching

Faisal A. Aldaye and Hanadi F. Sleiman, *J. Am. Chem. Soc.* **2007**, *129*, 4130-4131.

One of the central challenges of nanoscience is the ability to organize nanoparticles according to a deliberately designed pattern, *and* the ability to structurally and functionally control these assemblies at will.³⁻⁹ Molecular responsive assemblies provide control over the electronic and optical transport properties of nanoparticle assemblies, and will contribute to the bottom-up design of nanoscale circuitry capable of performing complex functions.⁶⁻⁹ In chapter 2 of this thesis we presented the first example of a well-defined, two-dimensional, discrete nanoparticle assembly. The approach involved weaving together gold nanoparticles modified with DNA building blocks that contain rigid organic vertices. In this chapter, we present a second generation system for the facile *modular construction* of a large number of nanoparticle assemblies, of *different geometries*, that can also be *structurally switched* and *addressed* in real-time.

Cyclic and single-stranded DNA templates embedded with rigid organic molecules that are fully functional and independent from the nanoparticles being organized, and that are embedded with rigid organic vertices, are used. Specifically, DNA templates triangle **1** and square **2** are synthesized (Scheme 3.1). Triangle **1** contains three molecules of the well-defined rigid organic vertex, as its corner units, while square **2** contains four. Gold nanoparticles modified with complementary strands of DNA, of the appropriate sequence, can then be organized into triangular and square assemblies using **1** and **2**, respectively (Scheme 3.1a). The modularity of our approach is demonstrated by assembling two different sizes of gold nanoparticles into all possible triangular combinations using template **1** (Scheme 3.1b). The structural switching capability of these assemblies is demonstrated by the use of the same square DNA template **2** to construct square, trapezoidal and rectangular assemblies (Scheme 3.1c). While the overall addressability of these assemblies is demonstrated by generating a triangular construct of three gold nanoparticles, selectively removing one of these particles from within the assembly, and the “writing” of a gold particle with a different size (Scheme 3.1d). The same template thus provides selective access to a large number of nanoparticle groupings, all of which are addressable and switchable post-assembly. This approach provides the field of photonics and nanoelectronics

Scheme 3.1 Single-stranded and cyclic DNA templates for the ready access to dynamic nanoparticle assemblies.



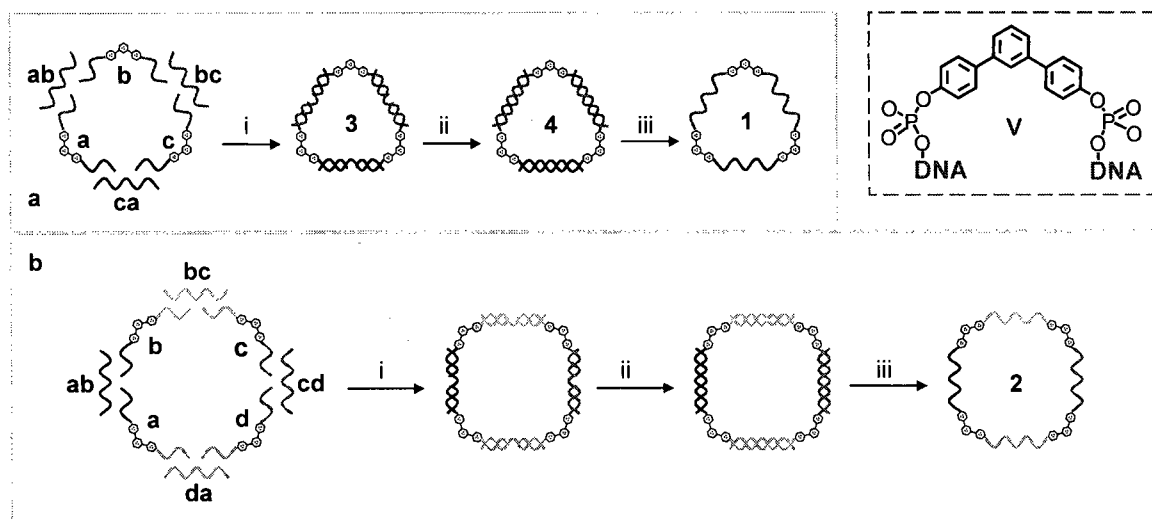
(a) Templates 1 and 2 organize gold nanoparticles mono-functionalized with DNA into triangles and squares, respectively. (b) The same template 1 is used to access all possible triangular combinations from two gold nanoparticles of different sizes (i.e. three larger; two larger / one smaller; one larger/ two smaller; three smaller particles). (c) The same square template 2 is used to access square, trapezoidal and rectangular assemblies of four gold nanoparticles; inset shows how the incorporation of an internal loop can be used to shorten a template's side. (d) Post-assembly addressability is demonstrated by a write/erase experiment in which three gold nano-particles of a single size are assembled into a triangular arrangement, a specific particle is erased using an external eraser strand, and the empty position is re-written with a smaller sized particle.

with a set of tools to readily access a large number of well-defined nanoparticle assemblies with which to investigate fundamental phenomena such as single electron transport and plasmonic coupling, and empowers them with the ability to probe and modify these systems in real-time.

3.1 Synthesis

Initial efforts are directed towards synthesis of the cyclic and single-stranded DNA templates **1** and **2**. The approach is illustrated in Scheme 3.2. In both cases, DNA building blocks – composed of two twenty base long DNA arms branching from a rigid organic vertex **V** – are assembled into the appropriate geometry using complementary linking strands, enzymatically ligated to generate a fully cyclized double-stranded intermediate, and purified to obtain the respective single-stranded DNA template. The linear triangular **3** and square **4** analogues are synthesized for control experiments. See section 3.4 for the synthesis of strands **a-d**, **ab**, **bc**, **cd**, **da**, and **ca**.

Scheme 3.2 Synthesis of templates **1** and **2**.



(i) Self-assembly into a fully double-stranded cyclic intermediate; (ii) ligation using T4 DNA ligase to generate a fully cyclized assembly; (iii) purification using denaturing PAGE to isolate the respective single-stranded and cyclic DNA template. Inset: Connectivity of vertex **V** within DNA.

The assembly of templates **1** and **2** is monitored sequentially using native polyacrylamide gel electrophoresis (PAGE; Figure 3.1). For triangle **1**, building block **a** alone results in a single band of relatively high electrophoretic mobility (lane 1). Assembly of the linear constructs of two **a^{ab}b** and three building blocks **a^{ab}b^{bc}c** show well-defined single bands of steadily decreasing

mobility (lanes 2 and 3, respectively). The assignment of all three linear species correlates well with the 10 base-pair linear DNA ladder. Addition of linker strand **ca** to the linear assembly $a^{ab}b^{bc}c$ results in both duplex formation and cyclization. A single band of reduced mobility relative to that of $a^{ab}b^{bc}c$ is observed (lane 4) and is assigned to the triangular construct $a^{ab}b^{bc}c^{ca}$. The cyclized triangular assembly $a^{ab}b^{bc}c^{ca}$ contains sixty base pairs, but is found to move as a 185-mer when compared to the linear base pair marker, which is consistent with the fact that cyclic structures travel anomalously on polyacrylamide gels when compared to their linear counterparts.⁸⁵ A second band of extremely low electrophoretic mobility is also detected in lane 4, suggesting the concomitant formation of higher-order oligomeric species. Pure cyclic triangle 1 is obtained by direct isolation using electroelution (lane 5).

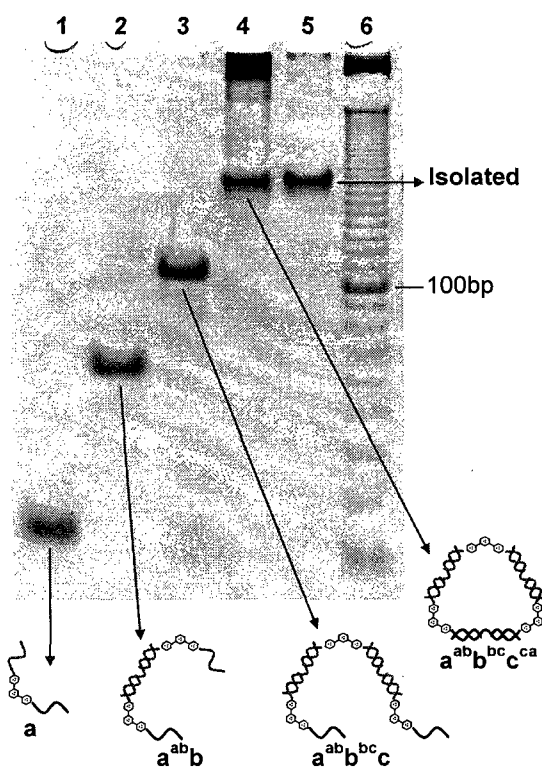


Figure 3.1 Sequential self-assembly of triangle $a^{ab}b^{bc}c^{ca}$. 10% Native polyacrylamide gel of the sequential self-assembly of the triangular construct via the step-wise addition of linker strands **ab**, **bc**, **ca** to building blocks **a**, **b**, **c**, forming **a**, **a^{ab}b**, **a^{ab}b^{bc}c**, **a^{ab}b^{bc}c^{ca}** (lanes 1-4, respectively). The triangular assembly $a^{ab}b^{bc}c^{ca}$ is directly isolated using electroelution and is characterized in lane 5. 10 bp DNA ladder (lane 6).

The cyclic nature of isolated triangle assembly $a^{ab}b^{bc}c^{ca}$ is confirmed using enzymatic digestion assays with Mung Bean nuclease (MBN). Under optimized conditions, MBN degrades linear open structures containing single-stranded DNA, but not cyclic closed structures containing only double-stranded DNA.^{86,87} See section 3.4 for the optimization of MBN digestions towards our

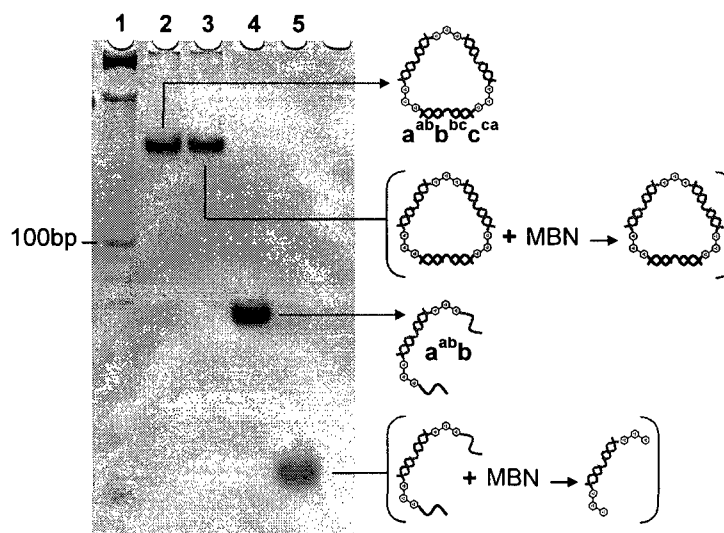


Figure 3.2 Enzymatic digestion assay of $a^{ab}b^{bc}c^{ca}$. MBN enzymatic digestion confirms the double-stranded cyclic nature of the isolated triangle $a^{ab}b^{bc}c^{ca}$. Lanes 2 and 3, contain isolated $a^{ab}b^{bc}c^{ca}$ before and after treatment with MBN, while lanes 4 and 5 contain the single and double-stranded control $a^{ab}b$ before and after treatment with MBN 10 bp DNA ladder (lane 1).

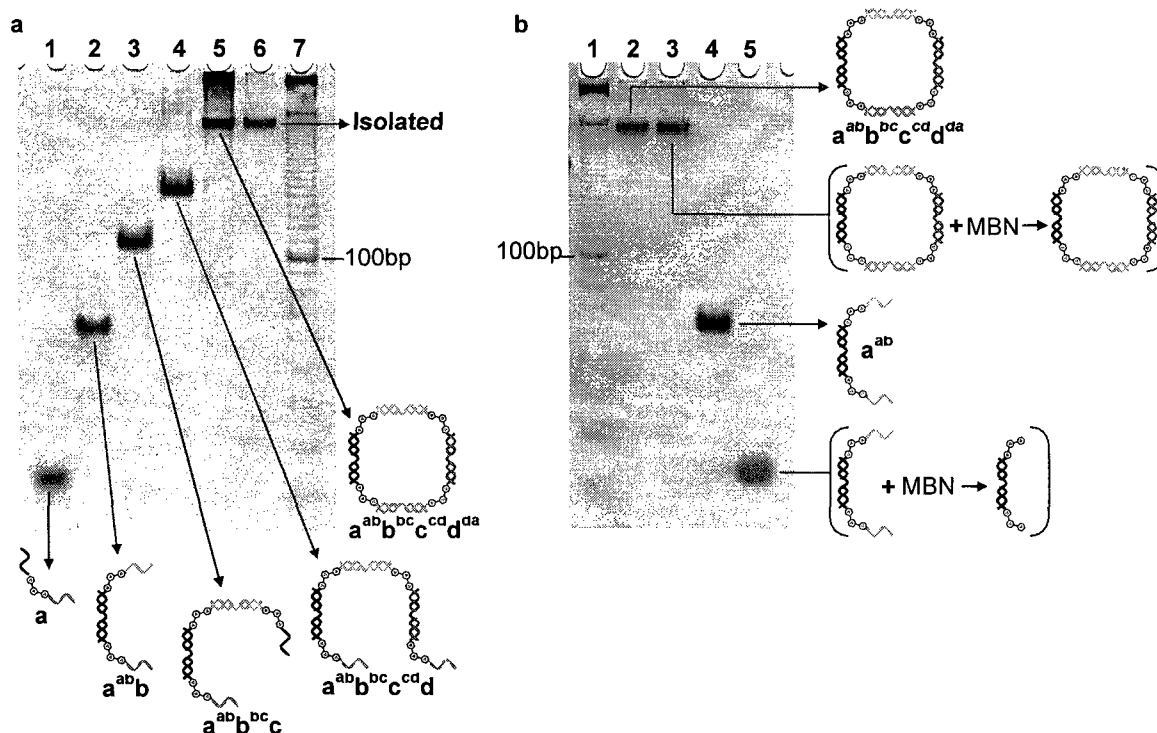


Figure 3.3 Sequential self-assembly and enzymatic digestion of isolated square $a^{ab}b^{bc}c^{cd}d^{da}$. (a) Sequential self-assembly of square $a^{ab}b^{bc}c^{cd}d^{da}$ via the step-wise addition of linker strands ab , bc , cd , da , to building blocks a , b , c , d , forming a , a^{ab} , $a^{ab}b^{bc}$, $a^{ab}b^{bc}c^{cd}$, $a^{ab}b^{bc}c^{cd}d^{da}$ (lanes 1-5, respectively), and of isolated $a^{ab}b^{bc}c^{cd}d^{da}$ (lane 6). 10 bp ladder (lane 7). (b) Native polyacrylamide gel of isolated $a^{ab}b^{bc}c^{cd}d^{da}$ before and after MBN enzymatic digestion (lanes 2 and 3, respectively) and of single and double stranded control assembly a^{ab} before and after MBN digestion (lanes 4 and 5, respectively). 10 bp ladder (lane 1).

DNA molecules. As seen in Figure 3.2, treatment of the purified triangular assembly with MBN results in no detectable shift in band mobility for the cyclic double-stranded triangle $a^{ab}b^{bc}c^{ca}$. The sequential assembly of the square intermediate $a^{ab}b^{bc}c^{cd}d^{da}$ is similarly monitored using native PAGE, and its cyclic nature is similarly confirmed using MBN digestion assays (Figure 3.3).

We proceeded to ligate the sides of triangle $a^{ab}b^{bc}c^{ca}$ and square $a^{ab}b^{bc}c^{cd}d^{da}$ with the enzyme T4 DNA ligase^{92,93} to generate templates **1** and **2**, respectively (Figure 3.4a and 3.4b, respectively); see section 3.4 for details. Lanes 1 in both gels contain single-stranded internal markers constructed from the ligated linear assemblies of two $a^{ab}b$, three $a^{ab}b^{bc}c$ and four $a^{ab}b^{bc}c^{cd}d$ building blocks (i.e. **ab-ligated**, **3**, **4**). The ligation products in lanes 2 of Figures 3.4a and 3.4b contain single bands assigned to single-stranded triangle **1** and square **2**, respectively. As expected, the fully cyclized triangular and square templates are slightly retarded in mobility when compared to their respective linear counterparts. Both the linear and cyclic analogous of the single-stranded grouping of three building blocks (i.e. linear **3** and cyclic triangle **1**) and of four building blocks (i.e. linear **4** and cyclic square **2**) are purified via electroelution and quantified using UV/vis analysis.

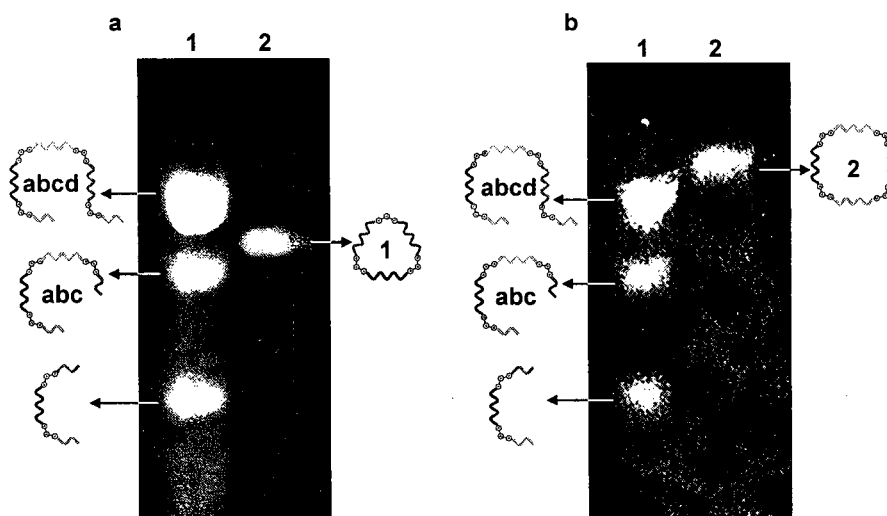


Figure 3.4 Enzymatic ligation of triangular and square assemblies for the synthesis of triangle **1** and square **2**. Enzymatic ligation of triangle **1** (lane 2 in left panel), of square **2** (lane 2 in right panel), and of the linear assemblies of two (**ab**), three (**abc**) and four (**abcd**) building blocks (lane 1 of both panels).

1, **2**, **3**, and **4**, are further characterized using experiments in which each building block is sequentially titrated with complementary DNA strands, as seen in Figures 3.5a and 3.5b for linear trimer **3** and cyclic triangle **1**, respectively. As expected, the mobility of the ligated trimer **3** hybridized to two linker strands (Figure 3.5a lane 3) is very similar to that of the unligated

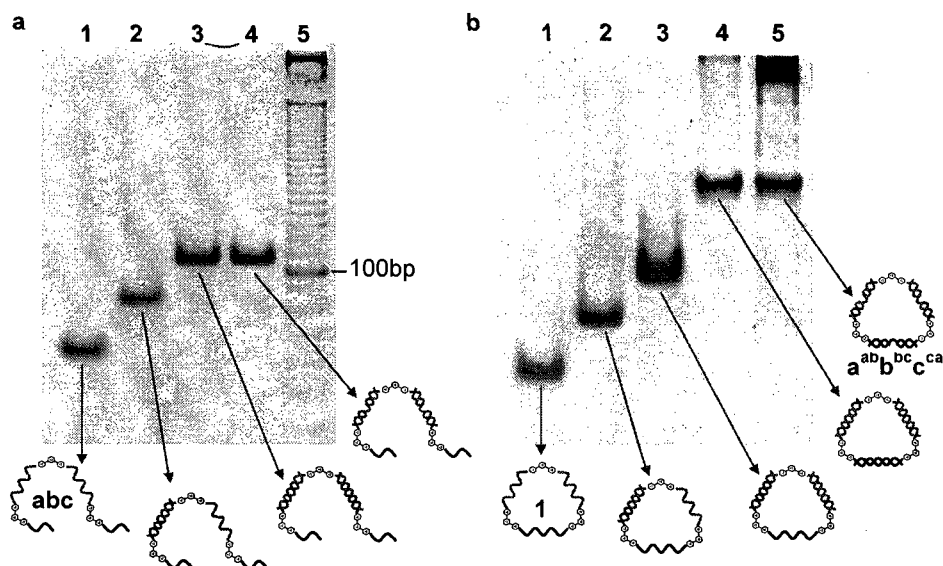


Figure 3.5 Titration of single-stranded *abc* and *1* with complementary strands of DNA. (a) Sequential titration of isolated single-stranded trimer *abc* (lane 1) with complementary linker strands *ab* (lane 2) and *ab, bc* (lane 3). Linear trimer *a^{ab}b^{bc}c* (lane 4). 10 bp DNA ladder (lane 5). (b) Titration of isolated triangle *1* (lane 1) with complementary linker strands *ab* (lane 2), *ab, bc* (lane 3) and *ab, bc, ca* (lane 4). Assembly of triangle *a^{ab}b^{bc}c^{ca}* (lane 5).

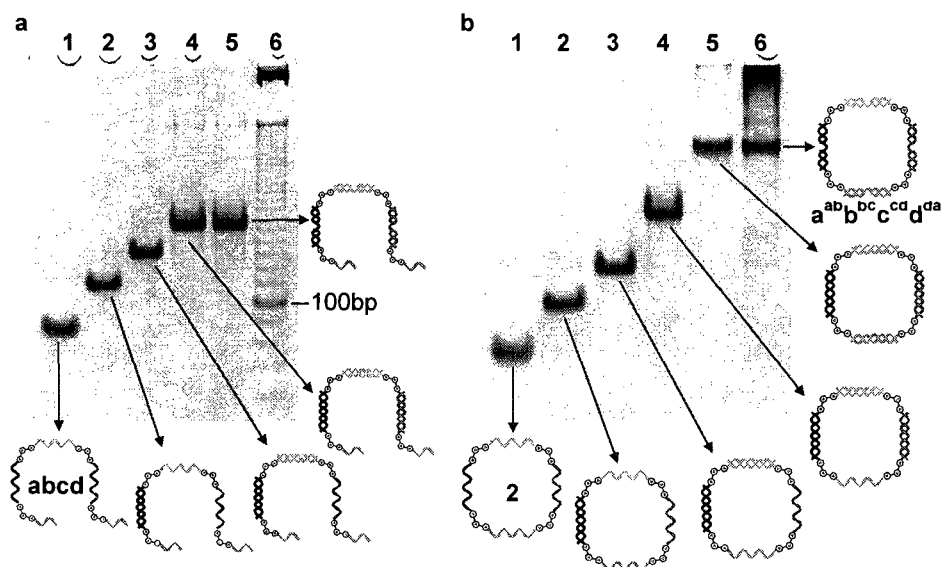
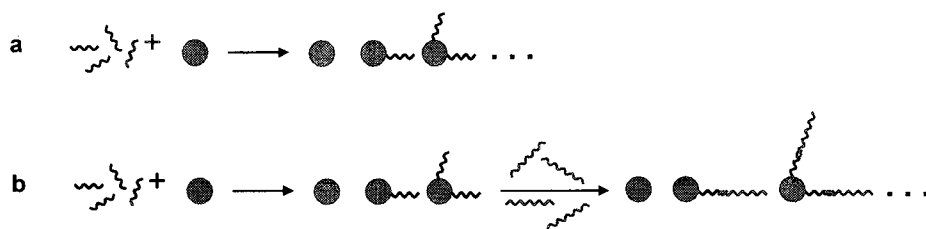


Figure 3.6 Titration of single-stranded *abcd* and *2* with complementary strands of DNA. (a) Sequential titration of the single-stranded tetramer *abcd* (lane 1) with linker strands *ab* (lane 2), *ab, bc* (lane 3) and *ab, bc, cd* (lane 4). Linear tetramer *a^{ab}b^{bc}c^{cd}d* (lane 5), 10 bp DNA ladder (lane 6). (b) Titration of the square *2* (lane 1) with linker strands *ab* (lane 2), *ab, bc* (lane 3), *ab, bc, ca* (lane 4) and *ab, bc, cd, da* (lane 5). Assembly of square *a^{ab}b^{bc}c^{cd}d^{da}* (lane 6).

double-stranded $a^{ab}b^{bc}c$ (lane 4), and the mobility of the fully titrated cyclic triangle **1** hybridized to linker strands **ab**, **bc**, **ca** (Figure 3.5b lane 4) is essentially identical to that of the triangular assembly $a^{ab}b^{bc}c^{ca}$ (lane 5). Isolated linear tetramer **4** and cyclic square **2** are similarly characterized (Figure 3.6).

With single-stranded DNA templates **1** and **2** in hand, work was then directed towards synthesis of 5 and 10 nm gold nanoparticles mono-functionalized with complementary strands of DNA, of appropriate sequence. Conjugation is typically carried out by the incubation of each gold nanoparticle with freshly-reduced thiolated DNA, to generate a mixture of adducts (Scheme 3.3a), followed by separation and purification of the mono-functionalized gold/DNA species using agarose gel electrophoresis.^{82,94}

Scheme 3.3 Conjugation of thiolated DNA to gold nanoparticles.



(a) Incubation of forty-base DNA strands with five nm gold nanoparticles. (b) Non-covalent extension of the DNA strands within the same mixture by a seventy base run of thymines provides adequate mass/charge ratio for separation using agarose gel electrophoresis.

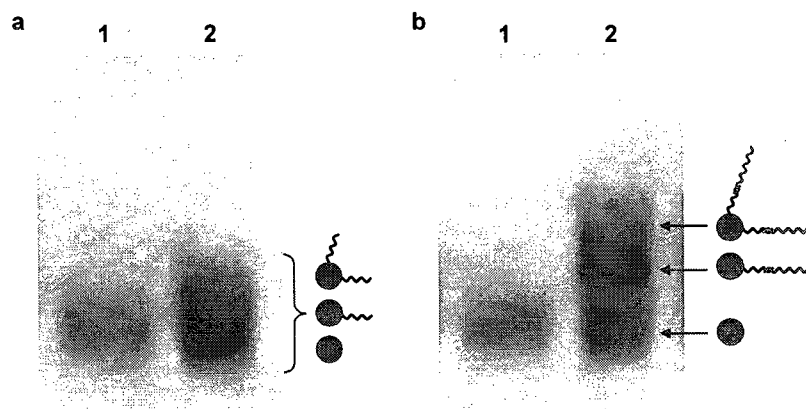


Figure 3.7 Analysis of gold/DNA mixtures with and without extension strands. (a) When the mixture from the incubation of **ab** to 5 nm Au particles is analyzed using 2% agarose gel electrophoresis, separation between the conjugates is not observed (lane 2). (b) However, when the DNA strands within the same mixture are lengthened by 70 bases using **ab**-extension, adequate separation is obtained (lane 2). Lane 1 contains 5 nm Au particles as a control.

Interestingly, when the resulting mixtures are characterized using agarose gel electrophoresis, adequate separation between the different gold/DNA conjugates is not observed (Figure 3.7a). Previous studies have shown a forty-base DNA sequence (i.e. the length of our thiolated linker strands) to not be long enough to achieve functional separation between conjugates, when 5 nm gold nanoparticles are used, and certainly not long enough for larger nanoparticles.⁹⁴

To overcome this problem, we developed a synthetic methodology that allows for the purification of both 5 and 10 nm gold nanoparticle modified with such “shorter” DNA strands. The approach involves the use of extension strands that effectively lengthen the DNA, and that provide the adequate charge-to-mass ratio for separation using agarose electrophoresis (Scheme 3.3b). Each extension strand contains a unique fifteen base region, complementary to the last fifteen bases of the thiolated DNA strand to be extended, and a common seventy base run of thymines that serves to reversibly lengthen each forty base DNA sequence into a 110-mer. As seen in Figure 3.7b, the use of extension strands provides the necessary separation for the gold/DNA conjugates, and allows for the purification of the mono-conjugated gold/DNA adducts.

Extension strands are not expected to interfere with the hybridization of the isolated mono-functionalized gold/DNA adduct with any of the templates. This is because the hybridization of all forty bases of the template strand is expected to occur preferentially over that of the fifteen bases within the extension strand. This is confirmed using native PAGE experiments (Figure 3.8). An experiment is conducted in which the forty base long thiolated DNA strand **ab-ligated** (lane 1) is hybridized to its respective extension strand (lane 2), via fifteen bases, to yield an assembly that is 110 bases long (lane 3). When the ligated dimer template **ab-ligated**, which contains the fully complementary 40 base sequence to **ab**, is added, the extension strand is quantitatively displaced (lane 4).

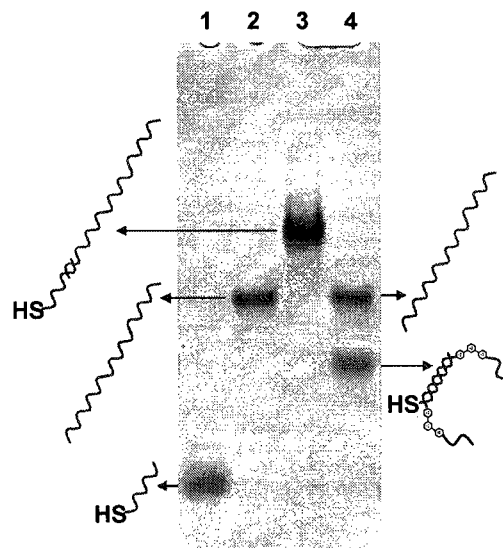


Figure 3.8 Quantitative displacement of extension strands. 10% Native polyacryl-amide gel confirming the quantitative hybridization of an extender strand (lane 2) to the partially complementary linker strand **ab** (lane 1) yields a single assembly (lane 3). Quantitative displacement of the extender strand in the presence of a template (lane 4).

3.2 Results and discussion

With single-stranded triangle **1**, square **2**, and monofunctionalized gold-DNA adducts in hand, we proceeded to test the ability of these templates to yield nanoparticle groupings with geometrical control. Template **1** codes for the organization of three gold nanoparticles into a triangle, while template **2** codes for the assembly of four gold particles into a square. When **1** is incubated with three 15 nm gold/DNA monoconjugates, each complementary to one of the template's arms, well-defined triangles of gold nanoparticle assemblies are observed using transmission electron microscopy (TEM; Figure 3.9a). In contrast, incubation of the same gold-DNA monoconjugates with the linear analogue **3** yields linear gold trimers with many more degrees of freedom (Figure 3.9b). Similarly, incubation of **2** with the four complementary gold-DNA monoconjugates results in a well-defined gold particle squares, while template **4** results in linear tetramers (Figures 3.9c and 3.9d, respectively). Cyclic templates **1** and **2** thus result in the selective assembly of gold nanoparticle triangles and squares.

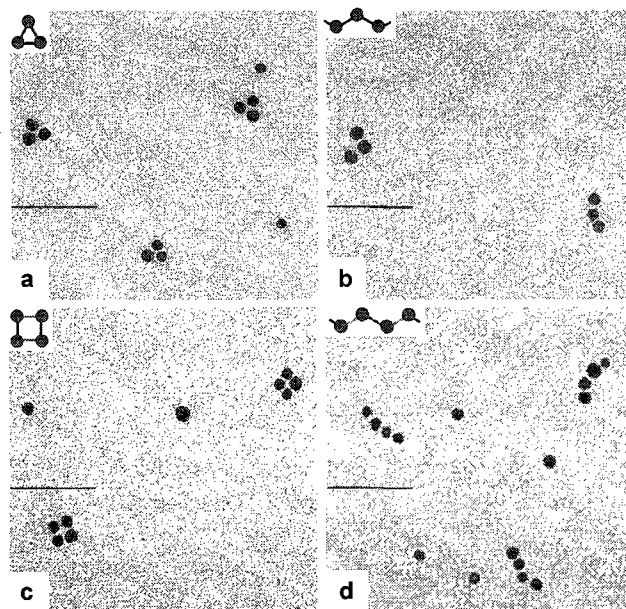


Figure 3.9 Gold assemblies using **1**, **2**, **3**, and **4**. (a) Triangle template **1** is used to organize three gold nanoparticles into a triangle, (b) while the linear trimer **5** generates open linear assemblies of three gold nanoparticles. Similarly, (c) square template **2** mediates the organization of four gold nanoparticles into a square assembly, (d) while the linear tetramer **6** results in open linear assemblies of four gold particles. Bar corresponds to 50 nm.

The modular nature of this system is examined to test whether different nanoparticles can in fact be instructed to assemble on their targeted location within the same template. Using triangle **1**, “larger” 15 nm gold nanoparticles and “smaller” 5 nm gold particle are assembled into all the

possible triangular combinations. Triangles with three larger gold particles, two larger / one smaller, one larger / two smaller, and three smaller nanoparticles are created selectively using the same DNA template 1 (Figure 3.10).

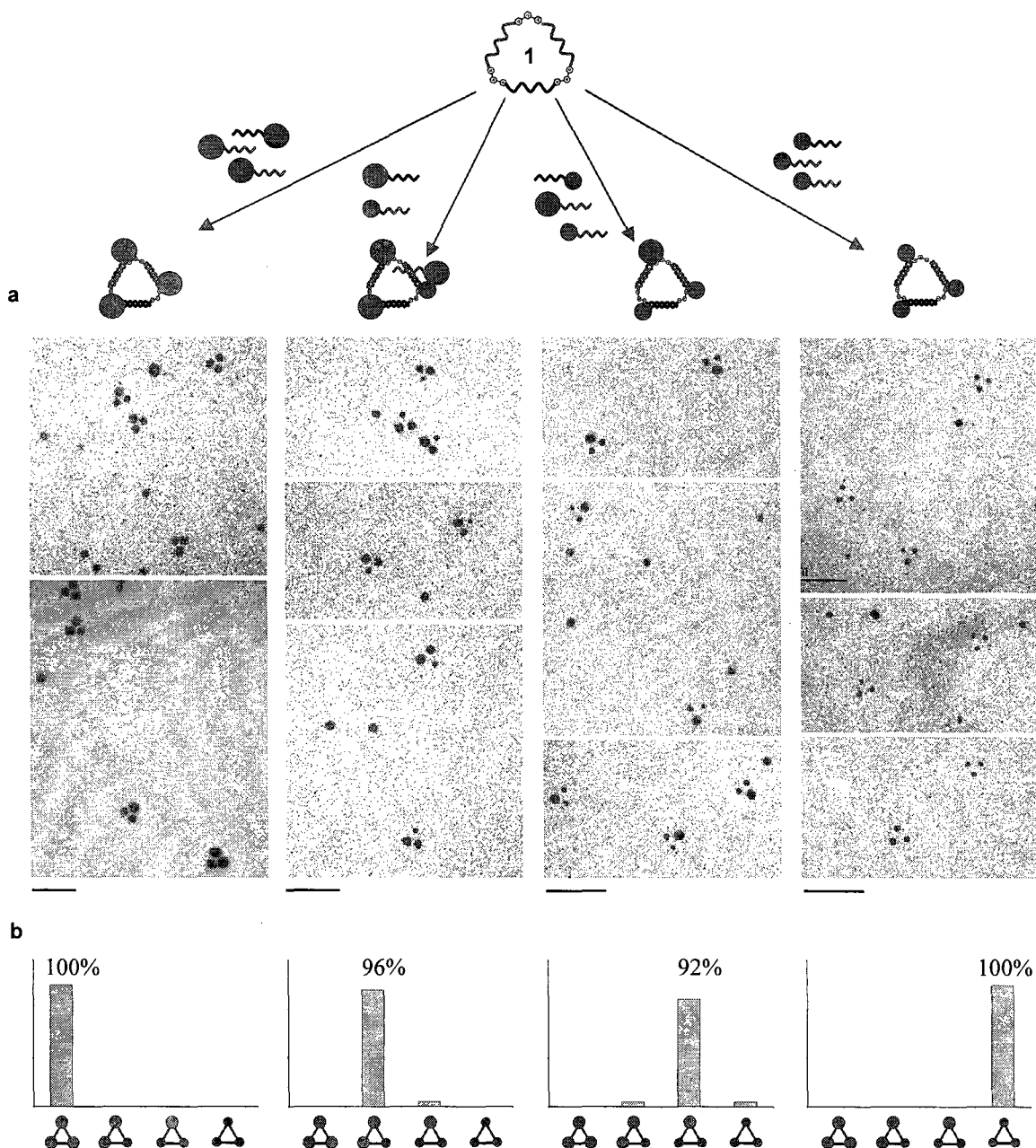


Figure 3.10 Nanoparticle assemblies generated using triangle 1. (a) 1 is used to generate all the possible combinatorial combinations that two gold nanoparticles of different sizes may be organized in. This is achieved by the simple tagging of each respective gold nanoparticle with a sequence of DNA that serves to dictate its final location within the construct. (b) When these assemblies are further analyzed to determine the percentage in which the desired grouping is formed, the templates were found to mediate the assembly of the desired combination in over 90% yield. Bar corresponds to 50 nm.

The statistical distribution of all triangular groupings produced within each system are compared and contrasted to truly measure the ability of template **1** to program the organization of gold nanoparticle assemblies. For example, when attempting to construct assemblies of two larger / one smaller gold nanoparticles, what percentage of the observed triangular assemblies is in fact two larger / one smaller? What percentage is three larger, one larger / two smaller, and three smaller? As seen in Figure 3.10b, when all the triangular assemblies within each case are analyzed for formation of the desired construct, the yield is found to essentially be quantitative.

It should be noted, however, that statistical analysis of the *overall* observed yield of the desired assembly within each system is in fact $\sim 25\%$. The instability of the thiol linkage between the gold nanoparticles and the DNA strands is expected to contribute to the overall lowering of the observed synthetic yields. This is because the isolated mono-functionalized gold/DNA adducts are expected to undergo reequilibration upon purification.^{95,96} An electrophoresis experiment is conducted in which a mono-functionalized gold/DNA adduct is isolated, allowed to sit at room temperature (in our buffer conditions), and is then re-analyzed for the type of conjugates in solution (Figure 3.11). Within fifteen minutes, the isolated mono-functionalized gold/DNA adduct undergoes re-equilibration into a mixture that contains gold nanoparticle conjugates with zero, one, two and three DNA strands. The future development of mono-functionalized gold/DNA conjugates that possess long-term stability is expected to improve the overall observed synthetic yield of any of our assemblies. This is a general problem in the current attempts to generate mono-functionalized gold/DNA adducts, and is a separate problem from the specificity of our approach to generate particle assemblies with control over combination and geometry, which statistical analysis shows to be high.

Unlike other approaches in DNA nanotechnology, in which the DNA templates used for organization are double-stranded and rigid, our method uses single-stranded and cyclic DNA templates that are, in principle, amenable to structural modulation. Internal loops can be incor-

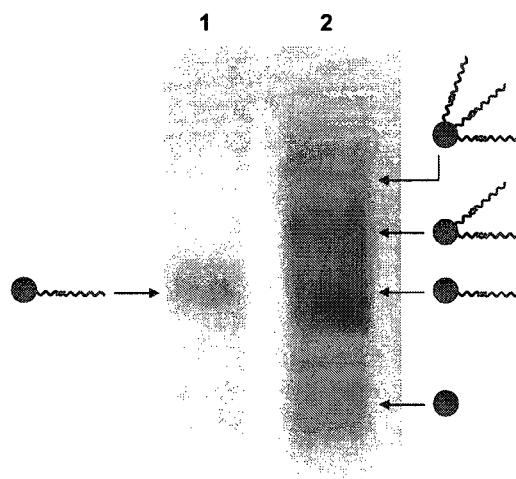


Figure 3.11 Stability of freshly isolated mono-functionalized gold/DNA conjugates. Mono-functionalized gold/DNA conjugates (using **ab** and **ab-extension**) are characterized using 2% gel electrophoresis within fifteen seconds (lane 1) and fifteen minutes (lane 2) of isolation.

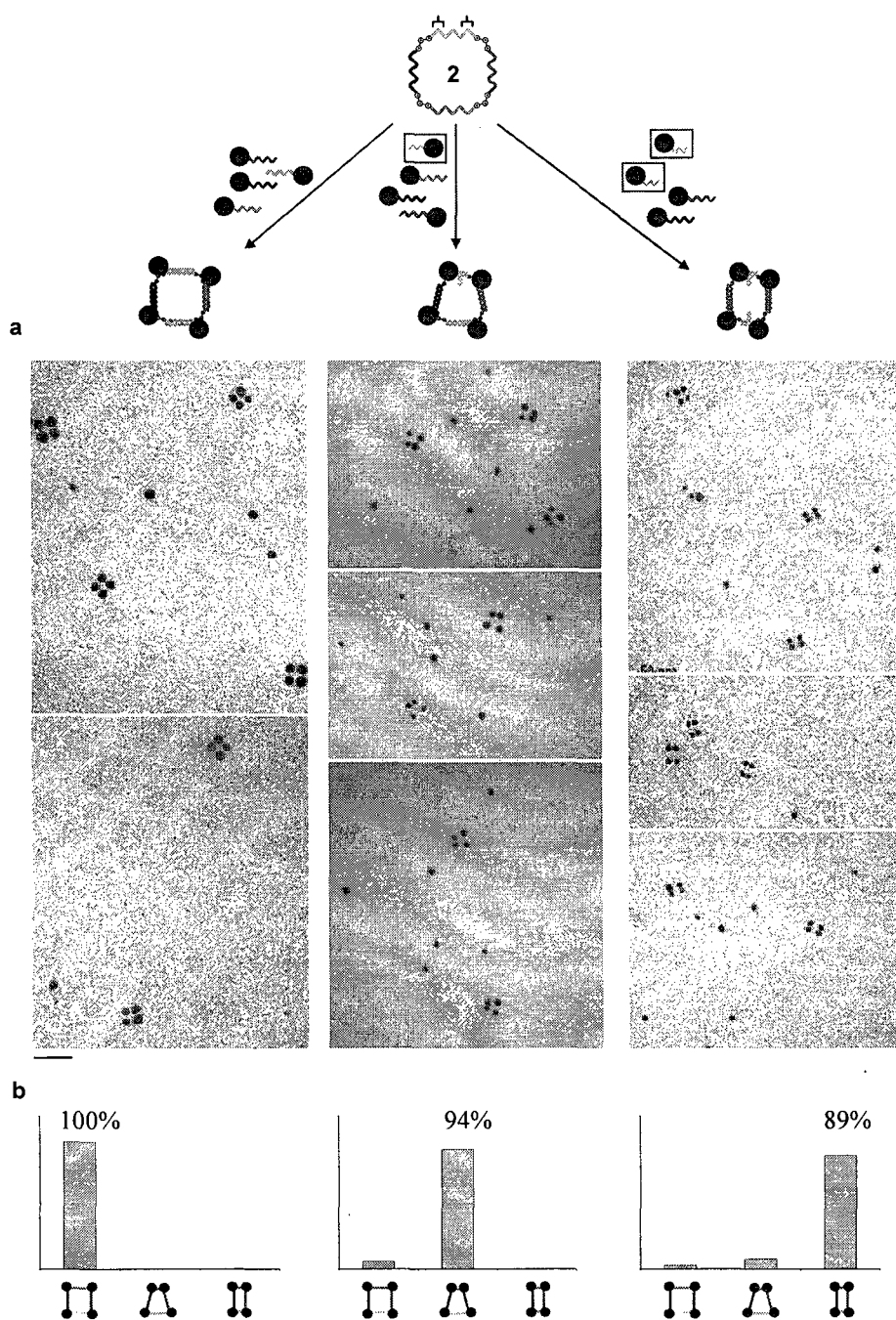


Figure 3.12 Statistical analysis on the types of quadrilaterals formed using templates 2. (a) Template 2 is used to assemble four gold nanoparticles into three geometrically distinct quadrilaterals. (b) Statistical analysis on the type of quadrilaterals formed using template 2 reveal the ability of our single stranded cyclic template to mediate the assembly of the three different assemblies in ~90% yield. Bar corresponds to 50 nm.

porated to shorten the length of each respective arm within a template (Scheme 1c). To achieve this, gold nanoparticles are mono-functionalized with a short twenty base DNA strand complementary to the two outer ten base regions of a specific arm within **2**. **2** is a square template. However, if one of the gold nanoparticles is mono-functionalized with such a DNA strand, then the same template now codes for the assembly of a trapezoidal grouping of four gold nanoparticles (Figure 3.12a). When two such shorter gold conjugates are selectively placed on two parallel arms of **2**, square template **2** now codes for the assembly of rectangular grouping of four gold particles (Figure 3.12a). Analysis shows that the expected trapezoidal and rectangular geometries, of the gold nanoparticle tetramers, to be observed in a >90% yield (Figure 3.12b).

The use of cyclic templates allows for the real-time addressability of each nanoparticle within the assembly with no fear of affecting the connectivity between the remaining particles. The nanoparticle to be erased is designed to contain a twenty base overhang to facilitate its specific re-

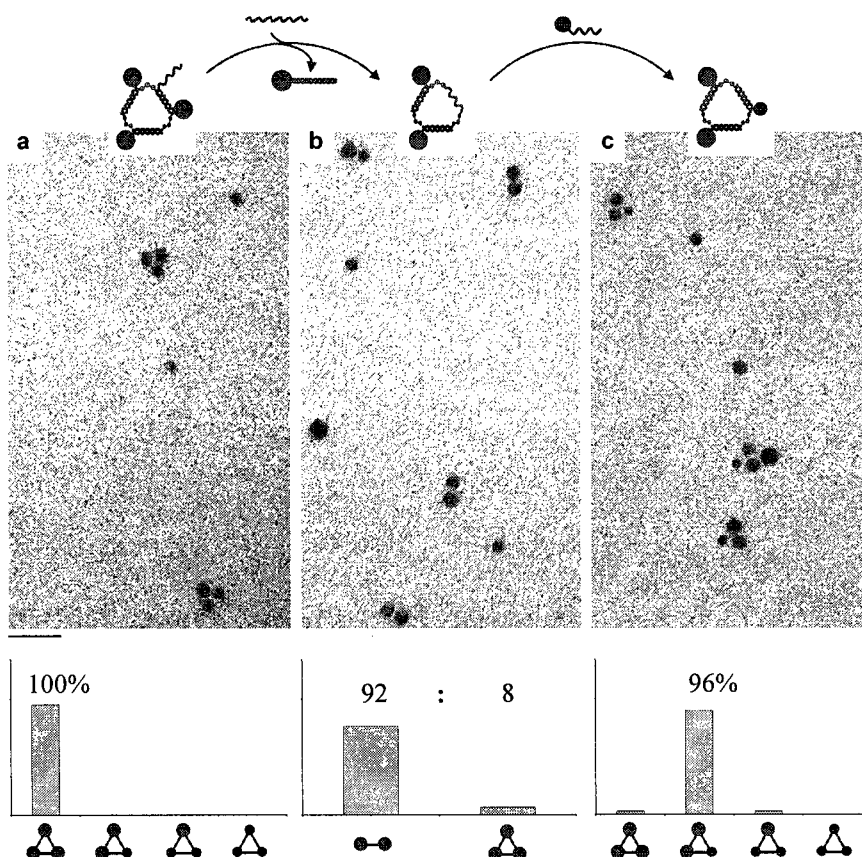


Figure 3.13 Statistical analysis on the type of triangular groupings observed during a write/erase experiment. (a) Three fifteen nm gold nanoparticles are assembled into a triangle. (b) A specific particle is removed using a DNA eraser strand, and (c) the empty position is replaced with a five nm gold nanoparticle. Bar corresponds to 40 nm.

removal upon hybridization to a fully complementary “eraser” DNA strand. Three larger sized gold nanoparticles are assembled into a triangle (Figure 3.13a). The specific particle containing the twenty base overhang is removed using a fully complementary eraser strand (Figure 3.13b), and is replaced with a smaller sized gold nanoparticle mono-functionalized with the appropriate sequence (Figure 3.13c). Statistical analysis shows the specific formation of the expected assembly with near quantitative selectivity at all three stages of the experiment. The ability to write and erase information into nanoparticle assemblies could give rise to dynamic circuitry, whose properties may be switched in real time and in response to external stimuli.

To confirm the fidelity of this process, a write / erase experiment is conducted in which the eraser step is omitted. As expected, none of the larger sized gold nanoparticles within the assembly are replaced by the smaller-sized gold nanoparticles (Figure 3.14).

3.3 Conclusions

We have thus constructed DNA templates for the dynamic and modular assembly of discrete gold nanoparticle groupings. This approach not only provides the ability to finely control the geometry of the assembly and the precise position of each nanoparticle, but also allows for the modification and tuning of these structural features post-assembly. In principle, any DNA-labeled nanocomponent can be assembled with these templates, and thus, this represents a highly economical method to organize materials using DNA. Access to libraries of precisely positioned nanoparticle groupings will allow for the systematic examination of their optical, electronic, and catalytic properties, as a function of structure and will lead to advances in the use of these particles as components of nanoelectronic/photonic circuitry, as plasmonic tools, and as surface-enhanced Raman scattering substrates.

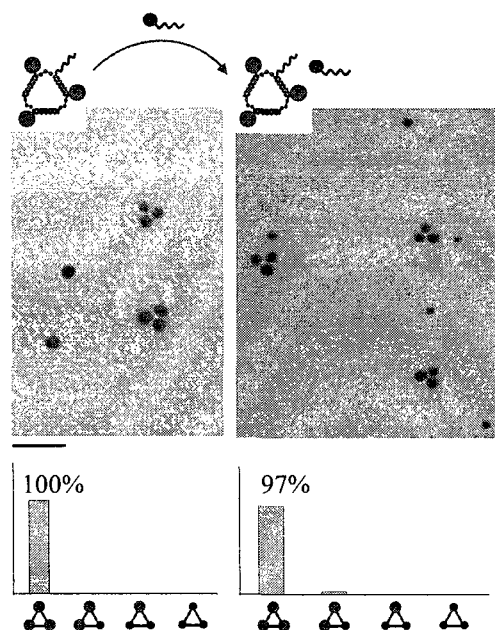


Figure 3.14 Write/erase experiment in which the intermediate eraser step is omitted. Addition of mono-functionalized five nm gold nanoparticles to the triangular assembly of fifteen nm gold nanoparticles, without an intermediate eraser step, does not result in replacement of either of the nanoparticles on the assembly. Bar corresponds to 40 nm.

3.4 Experimental

General. Tris(hydroxymethyl)-aminomethane (Tris), boric acid, acetic acid, ethylenediamine-tetraacetic acid, NaCl, $\text{MgCl}_2 \cdot 6\text{H}_2\text{O}$, DL-dithiothreitol (DTT), StainsAll[®], formamide, and ethidium bromide are used as purchased from Aldrich. 5' phosphate modification reagent 2-[2-(4,4'-dimethoxytrityloxy)ethylsulfonyl] ethylcyanoethyl-(N,N'-diisopropyl)-phosphoramidite, 5' thiol modification reagent dimethoxy trityl protected amidite derivative of bis(6-hydroxyhexyl)disulfide, guanidine derivatized 1000Å LCAA-CPG solid-support with a loading density of 28 $\mu\text{mol/g}$, 5-ethylthiotetrazole, and reagents used for automated DNA synthesis are purchased from ChemGenes. Sephadex G-25 (super fine DNA grade), T4 DNA ligase (source: recombinant), and Mung Bean Nuclease (source: Mung Bean Sprouts) are purchased from Amersham Biosciences. Molecular weight DNA ladder (1.0 $\mu\text{g}/\mu\text{L}$) is purchased from Invitrogen Life Technologies. Microcon[®] size-exclusion centrifugal filter devices are purchased from Millipore. Citrate coated gold nanoparticles are either made in-house or purchased from Ted Pella. The ligand bis(*p*-sulfonatophenyl)phenylphosphine dihydrate dipotassium salt is purchased from Strem Chemicals. 400 mesh carbon coated copper grids for transmission electron microscopy imaging are purchased from Electron Microscopy Sciences.

Instrumentation. Standard automated oligonucleotide solid-phase syntheses are performed on a Perspective Biosystems Expedite 8900 DNA synthesizer. UV/vis experiments are conducted on a Varian Cary 300 biospectrophotometer. Gel electrophoresis experiments are carried out on an acrylamide 20 X 20 cm vertical Hoefer 600 electrophoresis unit, and an agarose 7 X 8 cm horizontal Owl separation minigel system. Electroelutions are performed using a Centrilutor[®] electroeluter from Millipore. Ethidium bromide gels are visualized on a Fischer Scientific variable wavelength transilluminator. Matrix assisted laser desorption time-of-flight spectra are obtained using a KOMPACT MALDI III mass spectrometer. Transmission electron microscopy images are obtained using a JOEL 2000FX electron microscope.

Synthesis of a, b, c, d, ab, bc, cd, da, and ca. The synthesis of building blocks **a**, **b**, **c**, and **d** is performed on 1000Å LCAA-CPG solid-support with a loading density of 28 $\mu\text{mol/g}$. For each respective building block, the first DNA arm is grown using standard automated oligonucleotide synthetic protocols, followed by incorporation of the trityl protected amidite derivative of 1,3-bis(4-hydroxyphenyl)benzene (coupling/deprotection 10/2 mins), synthesis of the second DNA arm of appropriate sequence, and termination using the phosphate reagent 2-[2-(4,4'-

dimethoxytrityloxy)ethylsulfonyl]ethyl-(2-cyanoethyl)-(N,N'-diisopropyl)-phosphoramidite. The 5' phosphate is chemically incorporated to facilitate enzymatic ligation. Synthesis of vertex **1** is previously reported,⁹⁷ and is described in section 2.4. The building blocks are cleaved and deprotected in concentrated ammonium hydroxide (12 hrs, 55°C), and are purified from 24% 7M urea polyacrylamide gels. The desired bands are excised, extracted into 3 mL of water (16 hrs, 37°C), and purified using Sephadex G-25 column chromatography. Quantification is carried by UV/vis analysis using Beer's law ($A_{\text{total}} = A_{\text{vertex}} + A_{\text{DNA}}$), in which the extinction coefficient of the vertex at 260 nm is calculated to be $2.30 \times 10^5 \text{ L mol}^{-1} \text{ cm}^{-1}$. Table 3.1 summarizes the sequences of building blocks **a**, **b**, **c**, **d** along with their expected and experimentally obtained molecular masses (MM). Matrix assisted laser desorption time-of-flight mass spectrometry (MALDI-TOF MS) is performed according to a procedure reported by Allison and co-workers.⁹¹

Table 3.1 Building blocks a, b, c, d: Sequences and calculated/obtained MM.

	Sequence (5' → 3')	MW (g/mol)	
		Calc.	Obtained
a	Phosphate -TTTGCTAACTGGTAGAGTTC-V-GACCAATAACACAAATCGGG	12,740.13	12,764.47 [M+ Na ⁺]
b	Phosphate -GCAATACTATTTGATCTGG-V-ACATGGTAGAAGGAGGAAAG	12,869.16	12,869.74
c	Phosphate -CCTGCTCATACTGCAATCTG-V-CCAGAATGACATCACCTTGG	12,540.07	12,537.30
d	Phosphate -ACGCCCAAACCTTTCAACTT-V-CCCAGCCTTTGACATCTCG	12,444.06	12,445.40

Linker strands **ab**, **bc**, **cd**, **da** and **ca** are also synthesized on 1000Å LCAA-CPG solid-support with a loading density of 28 $\mu\text{mol/g}$. The strands are end-functionalized with the dimethoxy trityl protected amidite derivative of bis(6-hydroxyhexyl)disulfide (coupling/deprotection 10/2 mins). This 5' thiol modifying reagent is incorporated to facilitate subsequent conjugation of these DNA strands to gold nanoparticles. Cleavage, deprotection, and the simultaneous reduction of the 5' disulfide is performed in a 0.05 M solution of DTT in concentrated ammonium hydroxide (16 hrs, 55°C). The desired products are isolated from 24% 7M urea polyacrylamide gels, purified using Sephadex G-25 column chromatography, quantified using UV/vis analysis, and are characterized using MALDI-TOF MS. Table 3.2 summarizes the sequence of linker strands **ab**, **bc**, **cd**, **da**, and **ca**, along with their calculated and experimentally obtained molecular masses.

Table 3.2 Strands ab, bc, cd, ca, da: Sequences and calculated/obtained MM

	Sequence (5' → 3')	MW (g/mol)	
		Calc.	Obtained
ab	HS-CCAGATCGAAATAGTATTGCCCGATTTGTGTTATTGGTC	12,482.08	12,505.23 [M+ Na ⁺]
bc	HS-CAGATTGCAGTATGAGCAGGCTTCTCCTTCTACCATGT	12,405.07	12,401.05
cd	HS-AGGTTGAAAGGTTTGGGCGTCCAAGGTGATGTCAGGCTGG	12,718.12	12,719.47
ca	HS-GAACTCTACCAAGTTAGCAACCAAGGTGATGTCAGGCTGG	12,544.13	12,543.75
da	HS-GAACTCTACCAAGTTAGCAACGAGATGTCGAAAGGCTGGG	12,593.15	12,626.17 [M+ Na ⁺]

Synthesis of the DNA strands used in the trapezoidal/rectangular assemblies, and in the write/erase experiments. The two shortening sequences **ab-short** (5' HS-CCAGATCGAAGTTATTGGTC) and **cd-short** (5' HS-AGGTTGAAAGGTCAGGCTGG) are synthesized in a manner similar to that of **ab** and **cd**, and are found to have respective calculated/observed molecular masses of 6,325.09/6,324.25 and 6,822.19/3,822.97. Write/erase experiments are conducted using the thiolated strand **ab-write** (5' HS-CCAGATCGAAATAGTATTGCCCGATTTGTGTTATTGGTCTTGGTTTTTGTGTTTTGGTTTTT), and its full complement **ab-eraser** (5'-AAAACCAAAAACAAAACCAAGACCAATAACACAAATCGGGGCAATACTATTTCGATCTGG). The respective calculated/observed molecular masses of purified **ab-write** and **ab-eraser** are found to be 18,688.03/18,902.74 [M + Na⁺] and 18,432.20/18,432.60.

Mung Bean Nuclease digestions. The linear assembly **a^{ab}b** is subjected to digestions using varying amounts of MBN to ensure that the enzyme is still active on “our” DNA molecules, and to optimize conditions for the digestion of single-stranded DNA. As seen in Figure 3.15, the addition of 36 units of MBN (1.2×10^{-10} moles; 10 μ L TAE buffer; 3 hrs, 0°C) results in the selective and complete digestion of the single-stranded portion of **a^{ab}b**.

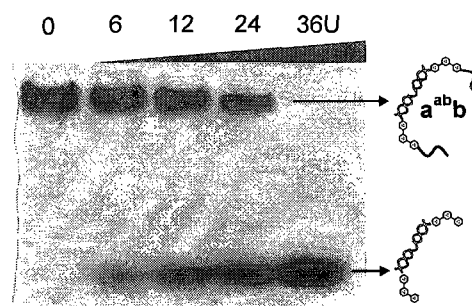


Figure 3.15 Protocol for the selective digestion of single-stranded DNA. 36 U of MBN at 0°C and 3 hours is selective digests single-strand DNA.

Gold nanoparticle synthesis and conjugation to DNA. Gold nanoparticles are either prepared in-house using the citrate/tannic acid method, or directly obtained from Ted Pella. In either case, the citrate-coated gold nanoparticles are not stable enough at the salt concentrations required to conjugate DNA, and are thus first exchanged with a negatively charged phosphine shell using the

reagent bis(*p*-sulfonatophenyl)phenylphosphine dehydrate dipotassium salt as per Alivisatos and co-workers.^{81,94} Solutions of freshly-reduced thiolated DNA and phosphine-coated gold nanoparticles are mixed in a 1:1 molar ratio (200 mM NaCl, 2 hrs, 25°C), and the resulting mono-functionalized gold-DNA conjugates are purified from agarose gels using our developed extension strategy described in section 3.1. Table 3.3 summarizes the sequence of the extension strands, along with their calculated and experimentally obtained molecular masses.

Table 3.3 Strands ab-extension, bc-extension, cd-extension, ca-extension, da-extension: Sequences and calculated/ obtained MM.

	Sequence (5' → 3')	MW (g/mol)	
		Calc.	Obtained
ab-extension	(T) ₇₀ GACCAATAACACAAA	25,828.07	25,854.14 [M + Na ⁺]
bc-extension	(T) ₇₀ ACATGGTAGAAGGAG	25,971.07	25,974.32
cd-extension	(T) ₇₀ CCAGCCTGACATCAC	25,763.07	25,764.18
ca-extension	Same as cd-extension	”	”
da-extension	(T) ₇₀ CCCAGCCTTTCGACA	25,754.01	25,796.55 [M + K ⁺]

TEM sample preparation. Freshly isolated mono-functionalized gold-DNA conjugates are added to each respective template in a 1.2:1 molar ratio, and are left incubating at room temperature for less than 5 minutes before deposition on the TEM grids. Deposition involves the addition of the assembled mixture onto the grid (10 µL), an adsorption period of fifteen minutes, removal of the excess solution using a filter paper, and a single wash step with Milli-Q water. When possible, analysis is performed within 48 hours to minimize sample degradation.

Modular access to structurally switchable three-dimensional discrete DNA assemblies

Faisal A. Aldaye and Hanadi F. Sleiman, *J. Am. Chem. Soc.* **2007**, *129*, 13376-13377.

DNA polyhedra present tremendous potential to encapsulate and release drugs, regulate protein folding and activity, and assemble three-dimensional (3D) networks for catalysis and biomolecule crystallization.⁹⁸ Easy access to discrete three-dimensional DNA assemblies, however, is not trivial. Seeman and co-workers constructed the first 3D-DNA object in 1991, a cube.⁹⁹ In his approach, two quadrilaterals are ligated to form a belt-like molecule, which is then purified, reconstituted, cyclized, and ligated to produce an assembly of six interconnected cyclic DNA strands with the topology of a cube, in less than 1% yield (Figure 4.1a). The same group later adapted this methodology for the solid-phase synthesis of a truncated DNA octahedron with fourteen interconnected cyclic DNA strands.¹⁰⁰ Despite this initial work, the field of 3D-DNA construction only recently gained momentum. Turberfield and co-workers synthesized a DNA tetrahedron¹⁰¹ (Figure 4.1b) and a trigonal bipyramid.¹⁰² His approach involved (1) programming single strands of DNA so that they would assemble into the target construct, (2) incorporating unhybridized bases into the corners units to alleviate strain, and (3) consistently using triangular edges to insure the overall structural integrity of the final assembly. This group later encapsulated the protein cytochrome *c* into a DNA tetrahedron by chemically conjugating it to

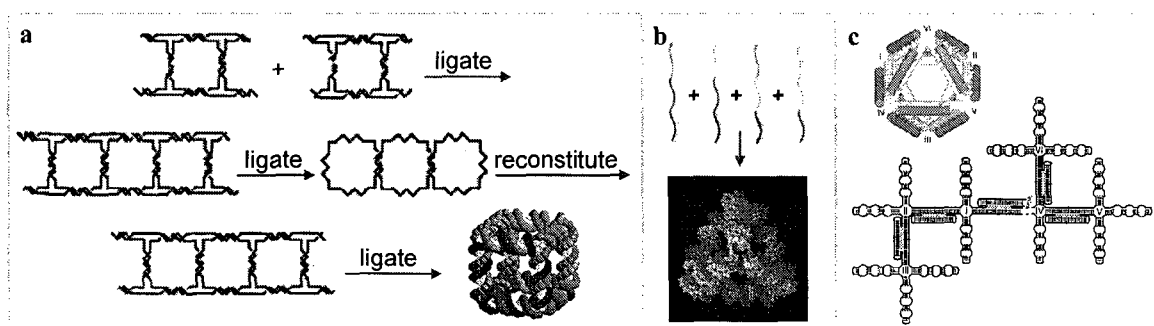
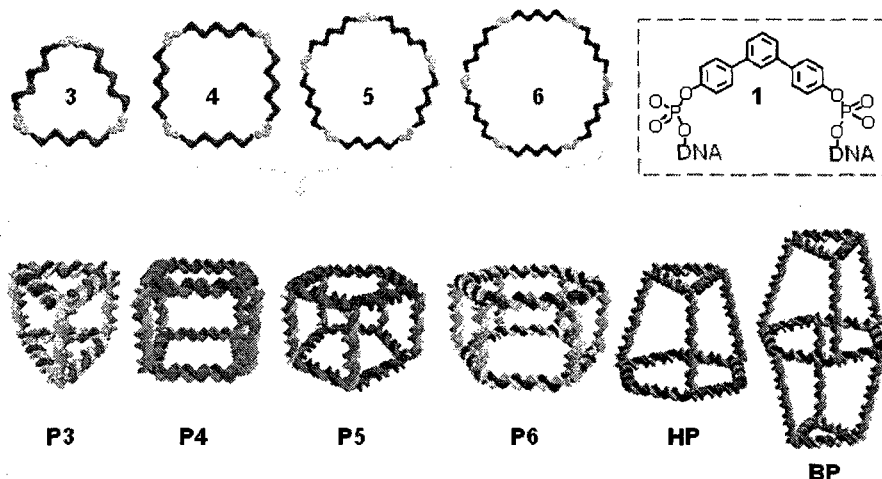


Figure 4.1 Discrete three-dimensional DNA assemblies. (a) Two quadrilaterals are ligated to form a belt-like molecule, which is then denature, reconstituted, cyclized, ligate again to form an assembly with the topology of a DNA cube. (b) Four unique single strands are programmed to assemble into a DNA tetrahedron. (c) A single synthetic DNA strand is folded using five DX motifs (colored in cyan) and seven PX motifs (rainbow colors) to form a DNA octahedron. [Figures adapted from references 99, 101, 103]

the inner-surface of the cage,⁹⁸ which is of interest since the functional properties of proteins can in principle be modulated when encapsulated. In a separate approach, Joyce and co-workers assembled a 3D-DNA object, an octahedron, by folding a long synthetic DNA template with the help of five smaller DNA strands (Figure 4.1c).¹⁰³

As seen from the above examples, this field suffers from the lack of synthetic accessibility. Since the DNA cube in 1991, only four more reports on three-dimensional discrete DNA construction have emerged, and more importantly, none of these contributions presented a modular approach to construction. If the true potential of 3D-DNA assemblies is to be exploited, synthetic access to such systems will need to be facile and economical. In this chapter we present a *modular method* for the quantitative generation of a large number of different and complex three-dimensional DNA objects, and present the first example in which one of these capsules is *structurally oscillated* between three well-defined dimensions. We noticed that almost all platonic and non-platonic solids are composed of simple triangular, square, pentagonal, or hexagonal faces, and that a small set of geometrically simple DNA building blocks (i.e. a DNA triangle, square, pentagon and hexagon) could in principle be used to modularly construct any of these objects. Using this approach, we synthesized a set of well-defined DNA templates made up of single-stranded DNA sides and rigid organic corner units, and used them to modularly construct a number of different three-dimensional DNA objects. As seen in Scheme 4.1, triangle **3**, square **4**, pentagon **5** and hexagon **6** are used to generate a triangular prism, a cube, a pentameric prism, a hexameric prism, and even a heteroprism and biprism. Moreover, because our approach involves the use of single-stranded DNA building blocks, the three-dimensional assemblies generated are amenable to structural modulation. We construct a well-defined dynamic triangular prism capable of structural oscillation between three predefined lengths. In principle,

Scheme 4.2 Modular access to three-dimensional DNA assemblies.

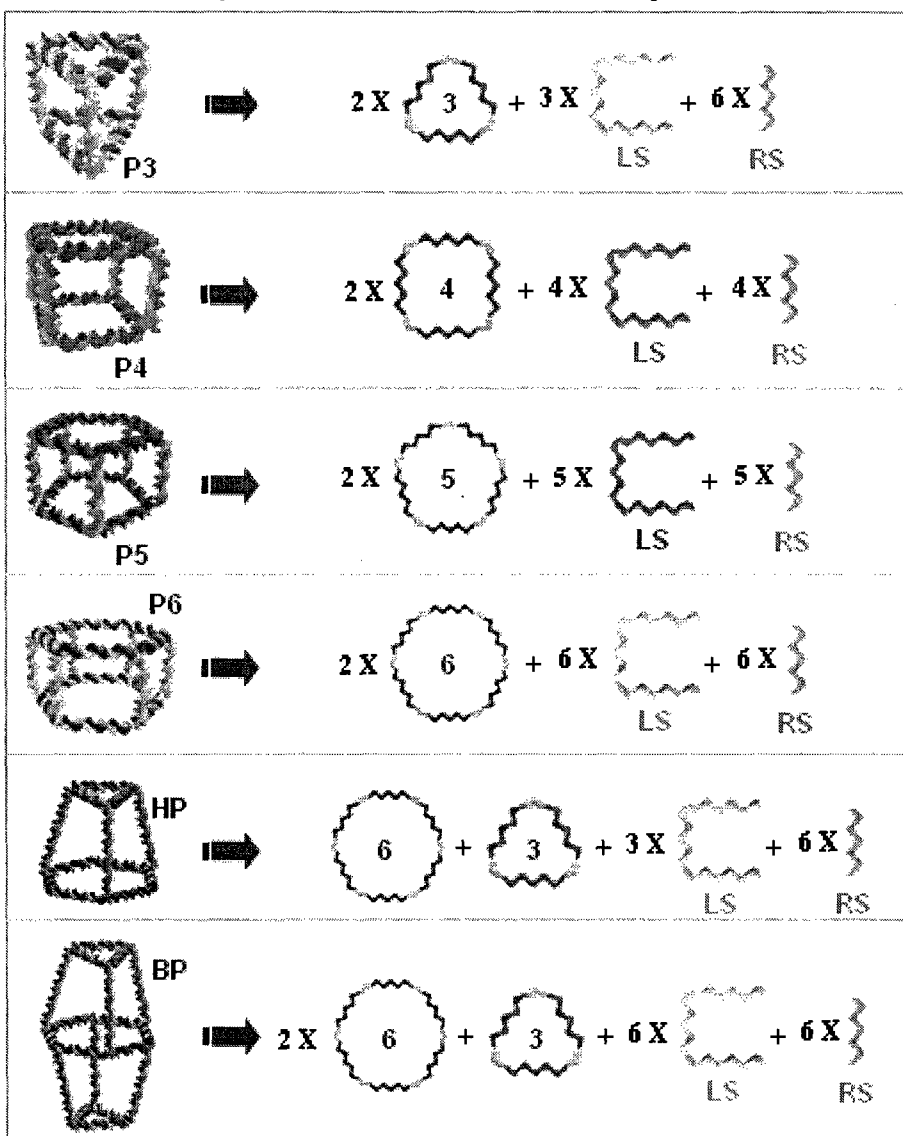


any discrete assembly that can be retrosynthetically broken down into our set of building blocks can also be generated, and thus this approach represents a highly straightforward and economical way to access libraries of discrete and structurally dynamic three-dimensional DNA assemblies.

4.1 Synthesis

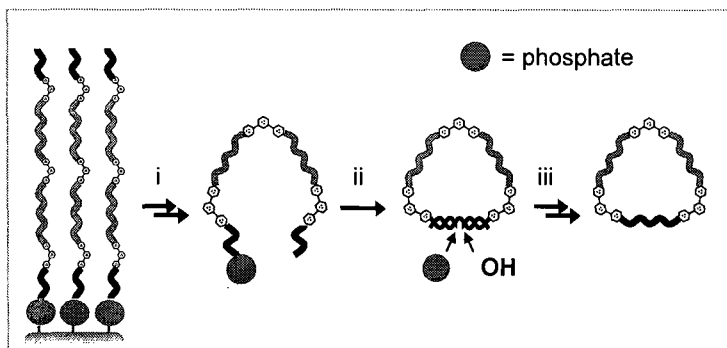
The first step in our approach is to retro-synthetically break down the target three-dimensional DNA objects into our set of DNA building blocks triangle 3, square 4, pentagon 5 and hexagon 6. For example, a triangular prism contains two triangular faces, and would therefore be constructed from two units of triangle 3 linked together by three “linking” strands, to generate a single-

Scheme 4.3 Retrosynthesis of three-dimensional DNA objects.



stranded intermediate, and with three “rigidifying” strands to generate the double-stranded prism (Scheme 4.3). Similarly, cube **P4**, pentameric prism **P5**, hexameric prism **P6**, heteroprism **HP**, and biprism **BP** are retro-synthetically broken down into two units of **4**, two units of **5**, two units of **6**, one unit of **3** and **6**, and to two units of **3** and one unit of **6**, respectively (Scheme 4.3).

Scheme 4.4 Synthesis of the cyclic and single-stranded triangle **3**.



DNA of the appropriate length, sequence, and number of vertex **1** molecules is (i) synthesized on phosphate-CPG to afford the *linear analogue* of triangle **3**. (ii) These strands are then cyclized using a complementary template strand, and (iii) are chemically ligated to yield the final single-stranded and cyclic triangle **3**, following purification from denaturing polyacrylamide gel electrophoresis.

Work was thus directed towards the generation of our toolbox of fully cyclized single-stranded DNA building blocks triangle **3**, square **4**, pentagon **5** and hexagon **6**. In general, this involves synthesis of continuous DNA strands, embedded with the appropriate number of vertex **1** molecules (i.e. three for triangle **3**, four for square **4**, etc), and its subsequent cyclization and chemical ligation (Scheme 4.4). Synthesis is conducted using phosphate-CPG that incorporates a 3' phosphate into the linear templates to facilitate chemical ligation. The clean isolation of the linear analogues of triangle **3**, square **4**, pentamer **5** and hexamer **6** is demonstrated using denaturing polyacrylamide gel electrophoresis (PAGE; Figure 4.2).

The linear analogues of **3-6** are cyclized and chemically ligated using cyanogen bromide.¹⁰⁴ In all cases, analysis using PAGE reveals formation of a single product possessing a

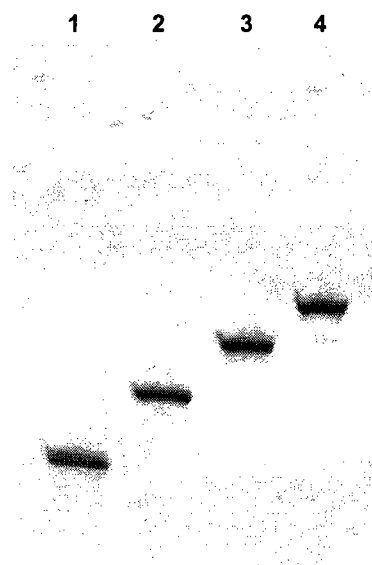


Figure 4.2 linear analogues of **3**, **4**, **5**, and **6**. 24% denaturing polyacrylamide gel characterization of the purified linear analogues of **3**, **4**, **5** and **6** (lanes 1, 2, 3 and 4).

relatively lower electrophoretic mobility compared to the unligated starting material, which is assigned to triangle **3**, square **4**, pentagon **5** or hexagon **6**, respectively (Figure 4.3a). The cyclic and single-stranded nature of **3-6** is confirmed using enzymatic digestion assays with ExoVII (Figure 4.3b).

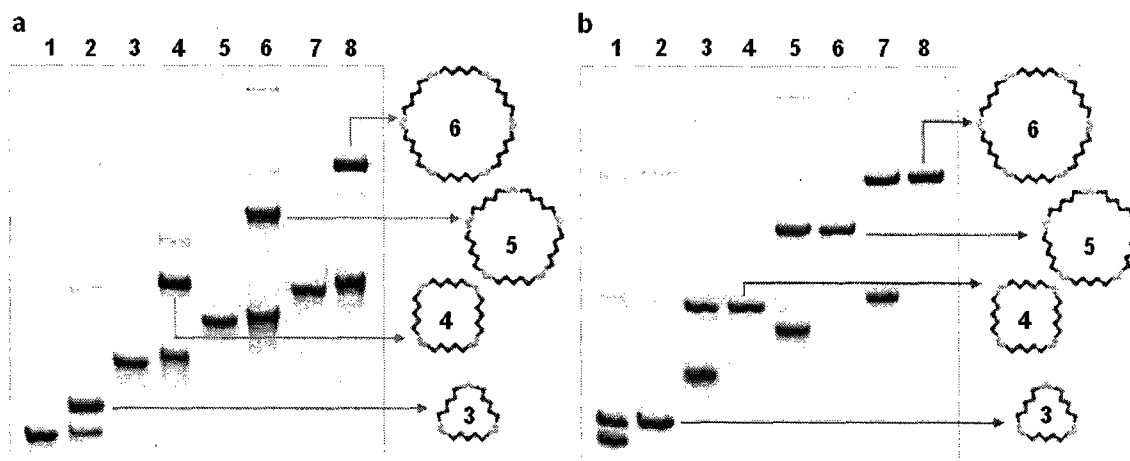


Figure 4.3 Construction of **3, **4**, **5**, and **6**.** (a) Ligation of the linear analogues of **3**, **4**, **5** and **6** (lanes 1, 3, 5 and 7, respectively) results in a single other product is, assigned to triangle **3**, square **4**, pentamer **5** and hexamer **6** (lanes 2, 4, 6 and 8, respectively). (b) ExoVII digestion assays of **3**, **4**, **5** and **6** (lanes 1, 3, 5 and 7, respectively) confirms the band assignment of cyclic triangle **3**, square **4**, pentagon **5** and hexagon **6** (lanes 2, 4, 6 and 8, respectively).

4.2 Results and discussion

With the single-stranded and cyclic DNA building blocks triangle **3**, square **4**, pentagon **5** and hexagon **6** in hand, we proceeded to examine their self-assembly potential to generate 3D-DNA objects. The assembly process of the triangular prism **P3** is sequentially monitored using native PAGE. Figure 4.4a reveals the clean generation of all intermediates leading to the formation of the single-stranded triangular prism **P3ss**, and the subsequent quantitative synthesis of the fully double-stranded **P3**. To confirm the connectivity within **P3**, enzymatic digestion assay using Mung Bean Nuclease (MBN) and ExoVII are conducted. MBN will digest any portion of DNA within the assembly that is single-stranded, while ExoVII will only digest open uncyclized single-stranded regions of DNA. As expected, prism **P3** is unaffected by either MBN or ExoVII, the single-stranded analogue **P3** is digested by just MBN, while the uncapped single-stranded intermediate **P3** is fully degraded by both enzymes (Figure 4.4b). To further characterize the structural connectivity of **P3**, fluorescence resonance energy transfer studies (FRET) are conducted. One of the linking strands is end-labeled with the fluorophore ROX and the quencher

BHQ-2 (Figure 4.4c). The observed fluorescence of the single-stranded triangular prism **P3ss** is 15% of the fully unquenched double-stranded probe, and translates into a calculated FRET distance of 4.4 nm. Importantly, the fluorescence of the double-stranded prism **P3** is 40% of the unquenched probe, revealing that the well-defined triangular prism **P3** is 5.2 nm long.

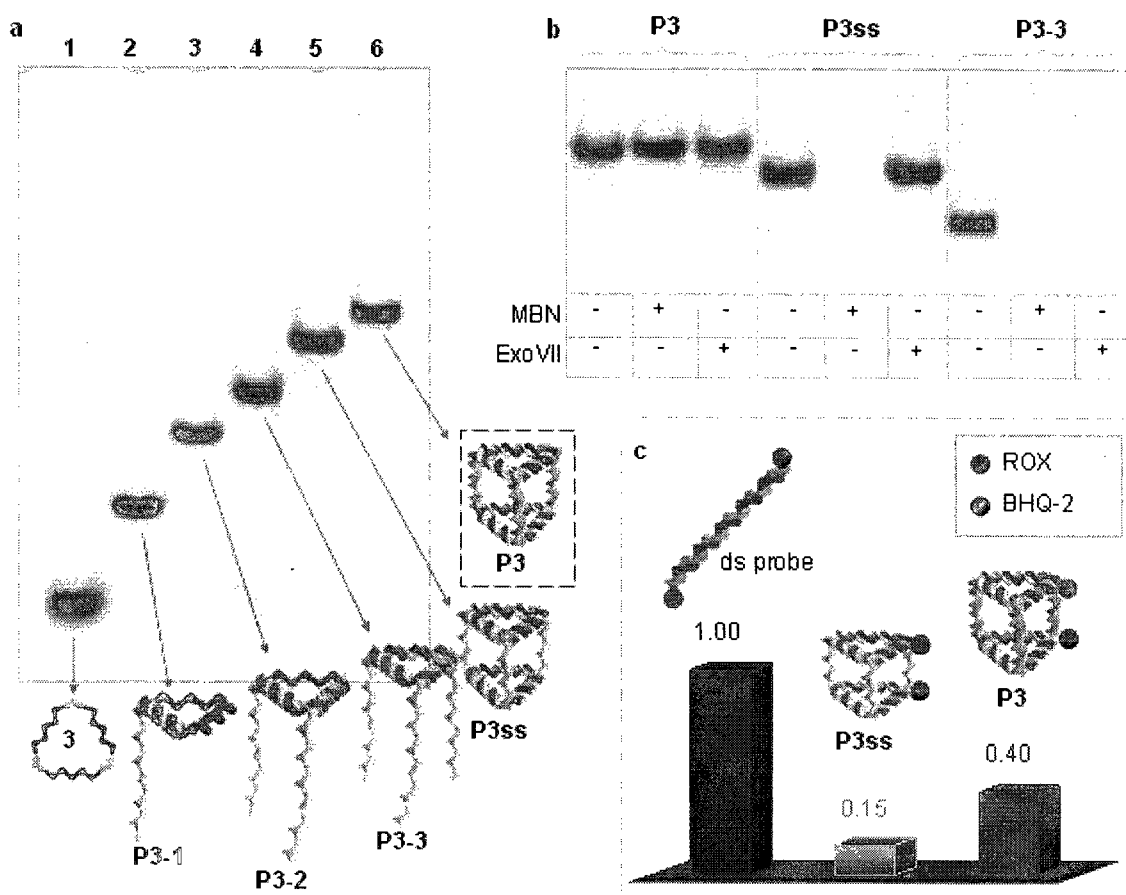


Figure 4.4 Characterization of the construction of the well-defined triangular prism **P3**. (a) Analysis of triangle **3** (lane 1), all the possible intermediates leading to construction of **P3** (lanes 2-5), and of the assembly **P3** (lane 6). (b) **P3** is unaffected by either MBN or ExoVII, **P3ss** is only degraded by MBN, while **P3-3** is digested by both MBN and ExoVII. (c) FRET analysis of the formation of **P3** from **P3ss**.

To demonstrate the generality of this approach to access a large number of three-dimensional DNA assemblies, five more different three-dimensional DNA objects are constructed. Access to cube **P4**, pentameric prism **P5**, hexameric prism **P6**, heteroprism **HP**, biprism **BP** is conducted in a manner similar to that of **P3**; Scheme 4.2 outlines the type and number of DNA building blocks used to construct each of these objects. Electrophoresis analysis is used to confirm the quantitative synthesis of cube **P5**, pentameric prism **P5**, and hexameric prism **P6** (Figure 4.5a), and to monitor the sequential assembly of the intermediates leading to the quantitative formation of heteroprism **HP** (Figure 4.5b) and biprism **BP** (Figure 4.5c). The connectivity between each of

these objects is also confirmed using enzymatic digestions with MBN and ExoVII (Figure 4.6). The assembly of **BP** is monitored using FRET studies, in which two linking strands are end modified with ROX and BHQ-2. As expected, the rigidification of the single-stranded intermediate of **BP** increases the overall observed fluorescence (Figure 4.7). Our approach of using a small number of presynthesized single-stranded cyclic DNA building blocks, as the sides

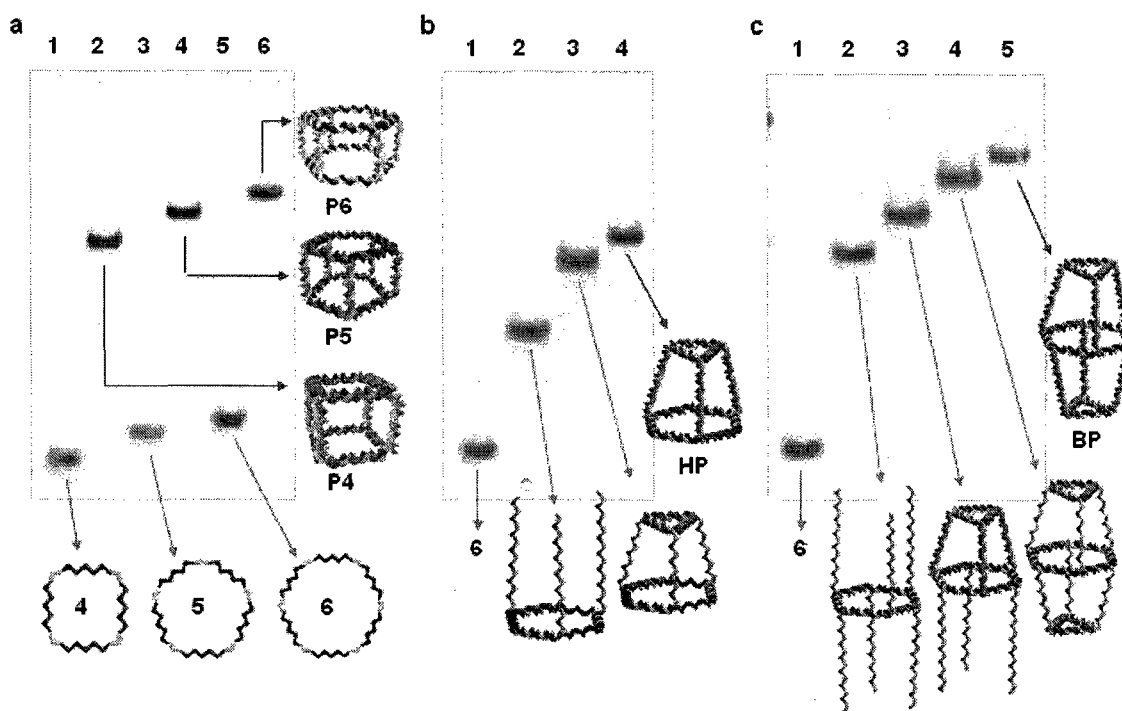


Figure 4.5 Assemblies of three-dimensional DNA cages. (a) Square **P4**, pentagon **P5** and hexagon **P6** (lanes 1, 3, 5) quantitatively generate cubic **P4**, pentagonal **P5** and hexagonal **P6** prisms (lanes 2, 4, 6). (b-left) hexagon **P6** (lane 1), assembly intermediates leading to construction of **HP** (lanes 2, 3), quantitative assembly of **HP** (lane 4). (b-right) **P6** (lane 1), intermediates leading to **BP** (lanes 2-4), quantitative assembly of **BP** (lane 5).

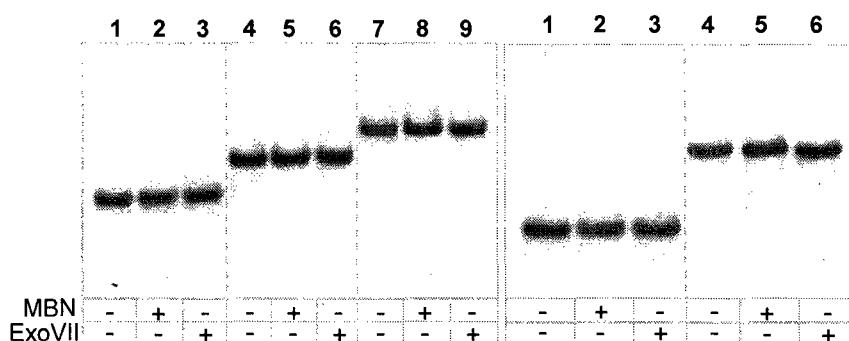


Figure 4.6 Enzymatic digestion assays of HP and BP. (Left panel) Square **P4** (lane 1), pentameric **P5** (lane 4) and hexameric prism **P6** (lane 7) were unaffected by enzymatic digestions with either MBN or ExoVII (lanes 2 and 3, lanes 5 and 6, and lanes 8 and 9, respectively). (Right panel) Both heteroprism **HP** (lane 1) and biprism **BP** (lane 4) were unaffected by enzymatic digestion with either MBN or ExoVII (lanes 2 and 3, and lanes 5 and 6, respectively).

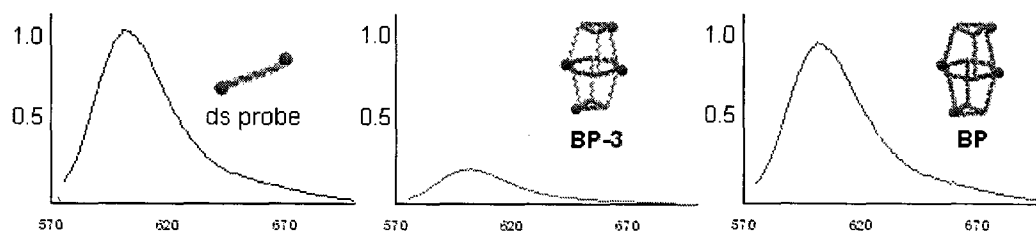


Figure 4.7 FRET analysis of BP. Normalized fluorescence measurements obtained from the double-stranded analogue of dually the end-labeled probe **LS7** (left), single-stranded intermediate of the biprism **BP-3** (middle), and of the fully double-stranded prism **BP** (right).

or planes of discrete DNA objects, provides for a facile method for generating a large number of relatively complex 3D discrete assemblies.

DNA building blocks that are cyclic can maintain their structural integrity in their single-stranded form, and thus, their use provides for an opportunity to generate structurally dynamic addressable assemblies. To demonstrate this, we constructed a triangular prism **dynP** that contains single-stranded regions separating both triangular faces. This synthetic intermediate is used to generate the three well-defined triangular prisms of different lengths **dynP10**, **dynP14** and **dynP20** (Figure 4.8). Assembly of each prism is achieved using strands 7-9, capable of introducing internal loops within **dynP** of different lengths, while real-time oscillation between each structure is conducted using eraser strands 10-12. One of the linking strands was end-labelled with ROX/BHQ-2, so that in addition to PAGE the resulting assemblies could also be probed using FRET analysis. Starting with **dynP**, addition of 7 generates a triangular prism **dynP10** with 10 base internal loops and a calculated FRET length of 5.2 nm. **dynP10** is converted into prism **dynP14** (calculated length of 6.9 nm) following addition of 10, to regenerate **dynP**, and 8, to incorporate 6 base internal loops within the assembled triangular prism **dynP14**. This assembly is similarly converted into a triangular prism assembly **dynP20** (calculated length of 8.9 nm) using strands 9 and 11. Strand 12 regenerates the initially constructed **dynP** and completes this structural cycle (Figure 4.8). Many applications can be anticipated for these switchable capsules, including molecule-triggered drug delivery and dynamic 3D DNA crystals.

It is of interest to note that a difference in electrophoretic mobility between the 10, 14 and 20 bases long DNA prisms is expected. And that it was not possible to run the samples in the gel of Figure 3b any longer to observe such a difference without over-running the lower bands corresponding to the double stranded 20-mers, 24-mers and 30-mers past the front line of the gel. Therefore, a separate experiment is conducted in which the gel is run longer in order to allow for a truly representative analysis of the differences in mobility between the three prismatic species

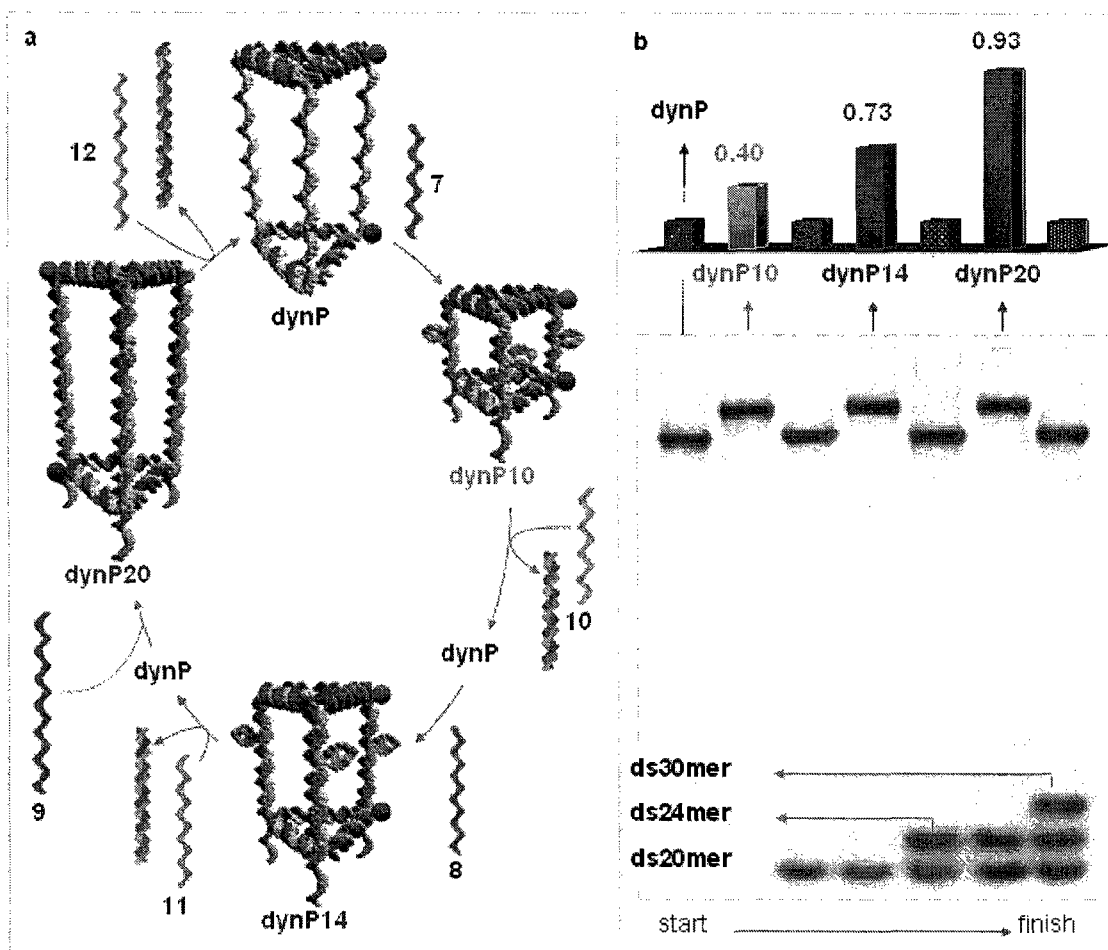


Figure 4.8 Dynamic triangular prism capable of oscillation between predefined dimensions. (a) Addition of **RS 7** incorporates a 10 base internal loop into **dynP**, and generates the well-defined triangular prism **dynP10**. The length of this prism is switched to that of **dynP14** following removal of the **RS 7** with fully complementary **ES 10**, and addition of **RS 8** to incorporate 6 base internal loops. The length of triangular prism **dynP14** is similarly modulated to that of **dynP20** using **11** and **9**. Removal of the **RS 9** using **ES 12** regenerates **dynP** and completes the structural cycle. (b) Real-time structural switching between **dynP10**, **dynP14** and **dynP20** is also monitored using PAGE and FRET studies.

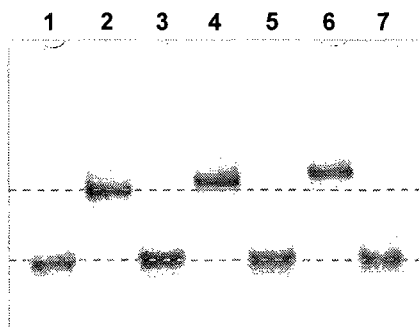


Figure 4.9 Gel-shift mobility analysis of **dynP10**, **dynP14** and **dynP20**. Lanes 1, 3, 5 and 7 contain the single-stranded intermediates, while lanes 2, 4 and 6 contain prism **dynP** with lengths corresponding to 10, 14 and 20 bases.

dynP10, **dynP4** and **dynP20** (120 V, 17 hrs, 0°C). As expected, **dynP14** is slightly retarded in mobility when compared to **dynP10**, and **dynP20** is retarded even more so (Figure 4.9). This is the first example of a dynamic 3D discrete DNA object that is controllably oscillated between three predetermined dimensions.

4.3 Conclusions

We have thus presented a new method that allows for the facile and quantitative construction of a library of discrete three-dimensional DNA structures from a small set of DNA building blocks. Moreover, reversible structural switching of these three-dimensional DNA objects in response to external agents was demonstrated. The approach involves the use of building blocks that are cyclic and single-stranded, as the faces or sides of the target three-dimensional DNA object, and in principle, any structure that can be retrosynthetically broken down into such DNA cycles can be readily obtained. This approach represents a highly economical method to access a large number of dynamic three-dimensional DNA objects and is expected to significantly expand the applications of three-dimensional DNA construction.

4.4 Coda

Since the publication of this work in late 2007, two more reports on three-dimensional DNA construction have emerged. Mao and co-workers synthesized a DNA tetrahedron, dodecahedron, and a buckminsterfullerene shaped object from a sequence-symmetric DNA junction,¹⁰⁵ while von Kiedrowski and co-workers synthesized a DNA dodecahedron from a set of branched DNA building blocks containing an organic core.¹⁰⁶

4.5 Experimental

General. Acetic acid, boric acid, cyanogen bromide (5M in acetonitrile), ethylenediamine-tetracetic acid, formamide, 4-morpholineethanesulfonic acid (MES), MgCl₂, StainsAll®, and tris(hydroxymethyl)-aminomethane (Tris) are used as purchased from Aldrich. 1000Å base derivatized LCAA-CPG solid support with a loading density of 32 µmol/g for general DNA synthesis, 2000Å phosphate-CPG with a loading density of 15 µmol/g, 5-ethylthiotetrazole, and reagents for automated DNA synthesis are used as purchased from ChemGenes. Sephadex G-25 (super fine DNA grade), Mung Bean Nuclease (MBN, source: Mung Bean Sprouts), and Exo-

nuclease VII (ExoVII, source: recombinant) are used as purchased from Amersham Biosciences. Microcon[®] size-exclusion centrifugal filter devices were purchased from Millipore. 5-carboxy-X-rhodamine (ROX) and 4'-(4-nitrophenyldiazo)-2'-methoxy-5'-methoxyazobenzene (BHQ-2) end-labeled DNA strands are used as purchased from Sigma-Genosys (HPLC purified).

Instrumentation. Standard automated oligonucleotide solid-phase syntheses are performed on a Perspective Biosystems Expedite 8900 DNA synthesizer. UV/vis measurements are conducted on a Varian Cary 300 biospectrophotometer. Gel electrophoresis experiments are carried out on an acrylamide 20 X 20 cm vertical Hoefer 600 electrophoresis unit. Electroelutions are performed using a Centrilutor[®] electroeluter from Millipore. Matrix assisted laser desorption time-of-flight spectra are obtained using a KOMPACT MALDI III mass spectrometer. Fluorescence experiments are conducted using a Photon Technology International TimeMaster spectrofluorimeter (model C-720F).

Synthesis of triangle 3, square 4, pentagon 5 and hexagon 6. Synthesis of the linear analogues of 3-6 is conducted on phosphate-CPG (2000Å, 15 µmol/g) using standard oligonucleotide synthetic protocols. The synthesis of the amidite derivative of vertex 1 (i.e. 2) is previously reported,^{97,107} and briefly described in section 2.4. The strands are cleaved and deprotected from the solid-support in a solution of ammonium hydroxide (55°C, 12 hrs), purified using 24% 7M urea PAGE, extracted into 3 mL of water (16 hrs, 37°C), and desalted using Sephadex G-25 column chromatography. Quantification is carried by UV/vis analysis using Beer's law ($A_{\text{total}} = A_{\text{vertex}} + A_{\text{DNA}}$), in which the extinction coefficient of the vertex at 260 nm is calculated to be $2.30 \times 10^5 \text{ L mol}^{-1} \text{ cm}^{-1}$. Table 4.1 summarizes the expected and experimentally obtained molecular masses (MM) of the linear analogues of 3-6, used within these assemblies. Matrix assisted laser desorption time-of-flight (MALDI-TOF) mass spectrometry is conducted according to a protocol by Allison and co-workers.⁹¹

Table 4.1 Calculated/ experimental molar masses of 3-6.

	MM	
	Calculated	Experimental
3a	10335.9	1,0360.0 [M + Na ⁺]
3b	10,351.00	13,449.00
4a	13,795.35	13,831.6 [M + K ⁺]
4b	15,707.70	15,707.00
5a	17,224.70	17,249.0 [M + Na ⁺]
5b	17,233.80	17,258.7 [M + Na ⁺]
6a	21,049.39	21,086.3 [M + K ⁺]
6b	20,649.10	20,649.90

We proceeded to cyclize and chemically ligate the linear templates 3-6. The ligation of these assemblies using cyanogen bromide is conducted according to a procedure reported by Damha and co-workers.¹⁰⁴ To confirm the potential and efficiency of this approach for ligating a 5'

hydroxyl strand to a 3' phosphate strand, studies are conducted on a control system composed of three linear strands (Figure 4.10a). 10 μ L of cyanogen

Table 4.2 MM of cyclic 3-6. Calculated and obtained molecular masses of cyclic single-stranded triangle 3, square 4, pentamer 5 and hexamer 6.

	Calc./Exper. (MM)		Calc./Exper. (MM)
3a	10,317.0 / 10,310.0	3b	10,333.0 / 10,350.1 [M + Na ⁺]
4a	13,777.4 / 13,794.5 [M + Na ⁺]	4b	15,689.7 / 15,694.0
5a	17,206.7 / 17,232.1 [M + Na ⁺]	5b	17,215.8 / 17,217.2 [M + K ⁺]
6a	21,031.4 / 21,033.7	6b	20,631.1 / 20,636.7

bromide (5 M in acetonitrile) is added to this simple DNA system (30 μ L MES buffer; 250 mM MES, 20 mM MgCl₂, pH 7.6) and is left incubating at 0°C for 15 minutes. The DNA is recovered by precipitation using 2% LiClO₄ in acetone (350 μ L; dry ice 15 mins), centrifugation at 13,000 rpm (3 mins), decanting, and lyophilization of the residual solution. As seen in the 24% denaturing polyacrylamide gel in Figure 4.10b, chemical ligation using cyanogen bromide occurs with a +80% yield. Cyclized 3-6 are thus chemically ligated using 10 μ L of cyanogen bromide (30 μ L MES buffer; 0°C. 15 mins). Table 4.2 summarizes their MALDI-TOFF mass spectrometry obtained molar masses.

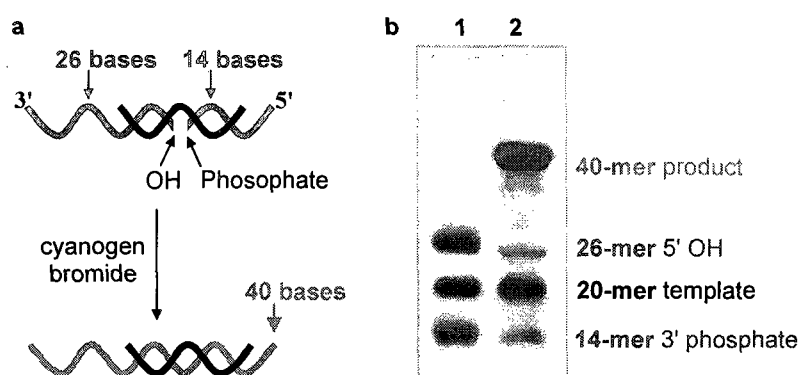


Figure 4.10 Chemical ligations using cyanogen bromide. (a) When a 26mer 5'-OH and a 14mer 3'-phosphate strand, templated by a 20mer strand, are chemically ligated using cyanogen bromide a 40mer strand of DNA is generated. (b) This is indeed confirmed using a 24% denaturing polyacrylamide gel (lane 1 pre-ligation, lane 2 post-ligation).

Hybridizations. Hybridizations are typically conducted by combining all of the DNA strands in the correct molar ratios to generate an assembly that is 3×10^{-10} moles (10 μ L TAE mg buffer), and are slowly cooled from 95°C to room temperature over a period of 15 hours.

Enzymatic digestions. Conditions for the digestion of “our” DNA building block using the enzyme MBN have been previously reported,¹⁰⁷ and are briefly described. To determine the optimal conditions under which single-stranded uncyclized DNA is digested using the enzyme ExoVII, the linear analogue of triangle **3** is subjected to varying amounts of ExoVII (37°C, 22 mins). In all these cases, 1.2×10^{-10} moles of DNA (10 μ L TAE buffer; 40 mM Tris, 20 mM acetic acid, 2 mM EDTA, 12.5 mM $MgCl_2$) is subjected to 0.5, 1, 3 and 5 units of ExoVII. As seen in Figure 4.11, addition of 5 units of the enzyme results in the complete degradation of the single-stranded species. Triangle **3**, square **4**, pentagon **5** and hexagon **6** are purified via electroelution, and characterized using MALDI-TOF MS.

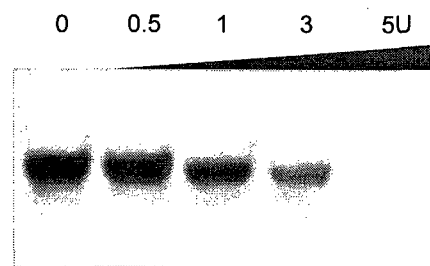


Figure 4.11 ExoVII optimization. The use of 5 units of ExoVII (37°C, 22 minutes) results in complete degradation of single-stranded DNA.

Fluorescence resonance energy transfer.

Given that the fluorophore ROX has a quantum yield Φ of 0.7, and given the respective emission and absorption spectra of ROX and BHQ-2 (Figure 4.12), an overlap integral $J(\lambda)$ of $3.89289 \times 10^{-13} M^{-1} cm^3$ and a Förster distance R_0 of 5.89 nm is calculated. Measurements are conducted on 2×10^{-10} moles of material (75 μ L of TAE buffer; 0°C), excited at 570 nm and monitored at 602 nm. Measurements conducted on just the double-stranded probe

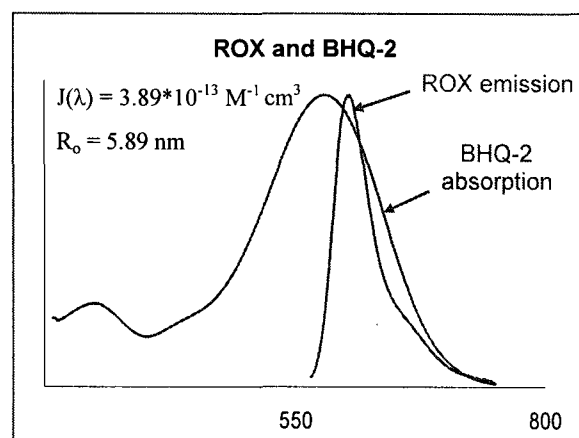


Figure 4.12 Fluorescence and absorption spectra of ROX/BHQ-2. An overlap integral $J(\lambda)$ of $3.89289 \times 10^{-13} M^{-1} cm^3$ and Förster distance R_0 of 5.89 nm is calculated.

are performed to determine the fluorescence magnitude of totally unquenched ROX, which is doable because the length of a double-stranded 30-mer is more than twice of the Förster distance.

Sequences. The sequences of the strands used to construct **P3**, **P4**, **P5**, **P6**, **HP**, and **BP**, and the sequences used for the structural oscillation of **dynP** are: **3a** TTGTG-1-TTATTGGTCA-1-TTAGGTTGAA-1-CCGAT-P; **3b** TGTCA-1-GAGTATGAGC-1-AGCCAACCAA-1-GGTGA-P; **4a** TGTCA-1-GAGTATGAGC-1-AGCCAACCAA-1-GGTGA-P; **4a** TTGTG-1-TTATTGGTCA-1-TTAGGTTGAA-1-AGGTTTGCTG-1-CCGAT-P; **4b** TGTCA-1-AGCCAGATTT-1-

GAGTATGAGC-1-AGCCAACCAA-1-GGTGA-P; **5a** TTGTG-1-TTATTGGTCA-1-TTAGGT
 TGAA-1-AGGTTTGCTG-1-GGAACTCTTG-1-CCGAT-P; **5b** TGTCA-1-AGGTGATGTC-1-
 AGCCAGATTT-1-GAGTATGAGC-1-AGCCAACCAA-1-GGTGA-P; **6a** TTGTG-1-TTAT
 TGGTCA-1-TTAGGTTGAA-1-AGGTTTGCTG-1-GGAACTCTTG-1-AAGGTAGGAA-1-CC
 GAT-P; **6b** TGTCA-1-CGGGCGTCCA-1-AGGTGATGTC-1-AGCCAGATTT-1-GAGT
 ATGAGC-1-AGCCAACCAA-1-GGTGA-P; **6c** TTGAC-1-CAAGATAACA-1-CAGATA
 GACA-1-GGTGACCTCC-1-ACACTCGACC-1-CCTAACAATC-1-GACCT-P; **Ta** CACA
 AATCGG; **Tb** TGACATCACC; **Tc** GTCAAAGGTC; **LS1** TGACATCACCACGACATCTCCA
 CAAATCGG; **LS2** TTGGTTGGCTACGACATCTCTGACCAATAA ; **LS3** GCTCATACT
 CACGACATCTCTTCAACCTAA; **LS4** GACATCACCTACGACATCTCCAAGAGTTCC;
LS5 AAATCTGGCTACGACATCTCCAGCAAACCT; **LS6** TTCAACCTAAATGCCGATCGA
 TAGCTAGCTATCTGTGTTA; **LS7** TGGACGCCCCGACGACATCTCTTCCTACCTT; **LS8**
 TGACCAATAAATGCCGATCGATAGCTAGCTAGTGTGGAGG; **LS9** CACAAATCGGAT
 GCCGATCGATAGCTAGCTCAATCGACCT; **LS10** TTGGTTGGCTATGCCGATCGATAG
 CTAGCTTCACCTGTCT; **LS11** GCTCATACTCATGCCGATCGATAGCTAGCTTTAG
 GGGTCG; **LS12** TGACATCACCATGCCGATCGATAGCTAGCTTCTTGGTCAA; **RS1**
 GAGATGTCGT; **RS2** AGCTAGCTATCGATCGGCAT; **RS3** TCTTGGTCAA; **RS4**
 TCACCTGTCT; **RS5** TTAGGGGTCG; **LS13** TGACATCACCATGCCGATCGATAGCT
 AGCTCACAAATCGG; **LS14** TTGGTTGGCTATGCCGATCGATAGCTAGCTTGACC
 AATAA; **LS15** GCTCATACTCATGCCGATCGATAGCTAGCTTTCAACCTAA; **RS6 (20-**
mer) ATGCCGATCGATAGCTAGCTACGCATCTC; **RS6-erase** GAGATGTCGTAGCTAGC
 TATCGATCGGCAT; **RS7 (24-mer)** ATGCCGAGCTAGCTACGACATCTC; **RS7-erase**
 GAGATGTCGTAGCTAGCTCGGCAT; **RS8 (30-mer)** ATGCCTAGCTACGACATCTC; **RS8-**
erase GAGATGTCGTAGCTAGGCAT.

Modular construction of DNA nanotubes with readily tunable geometry, rigidity, and single- or double-stranded character

Faisal A. Aldaye, Pik Kwan Lo, Christopher K. McLaughlin, and Hanadi F. Sleiman,
Nature Nanotechnology, submitted August 8, 2008.

DNA nanotubes hold great promise in applications ranging from material nanofabrication to fundamental biophysical research. For example, they can template the growth of nanowires,⁴⁸ orient transmembrane proteins for structural NMR determination,⁴³ and potentially act as stiff interconnects, tracks for molecular motors, and as drug nanocarriers.¹⁰⁸ DNA nanotubes are currently synthesized using one of two approaches. The first involves rolling and cyclizing a two-dimensional DNA array with complementary sticky ends at its periphery. Arrays can be induced to cyclize by rationally programming a specific nonzero degree of curvature within each tile (Figure 5.1a). Although the resulting tubes would have a preferred size, a mixture with a certain amount of variation around an optimum is typically generated. Rothemund and co-workers synthesized two such DX tiles that tessellate into a curved array, and used it to synthesize nanotubes ranging in diameter from seven to twenty nanometers,¹⁰⁹ while Turberfield and co-workers used a similar approach, and folded a DNA sheet into nanotubes with alternating rings, and nanotubes that are chiral with nested helices (Figure 5.1b).¹¹⁰

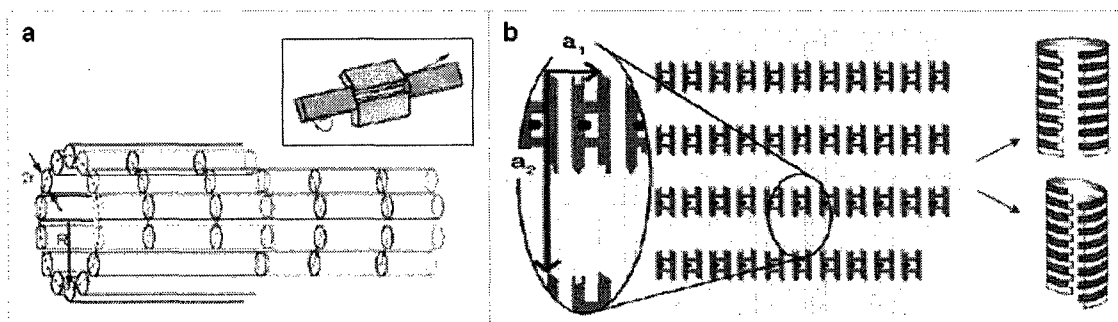


Figure 5.1 DNA nanotube construction: First approach. (a) A non-zero degree of curvature is incorporated into rectangular DX tile assemblies (see inset), so that the generated two-dimensional array would fold upon itself and close to generate a DNA nanotube. (b) This has been used to generate symmetrical and chiral DNA nanotubes with nested helices. [Adapted from references 109, 110].

The second approach involves programming the sequence of different DNA double-strands so that they would necessarily assemble into a helix-bundle with a fixed number of helices within

its cross-section.¹¹¹ Yan, LaBean, and co-workers linked together three DNA helices into a discrete column, and used it to construct one-dimensional DNA columnar assemblies (Figure 5.2a),³⁹ while Seeman and co-workers programmed a number of DNA strands to assemble into well-defined DNA nanotubes of six and eight helices (Figure 5.2b).^{112,113}

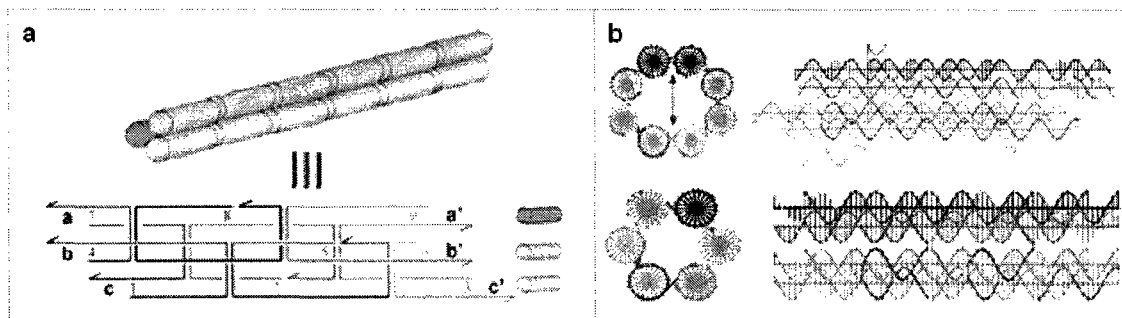
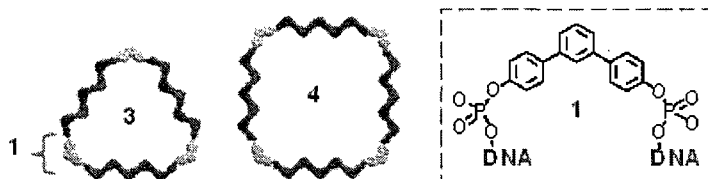


Figure 5.2 DNA nanotube construction: Second approach. (a) Nine different DNA strands are programmed to assemble into a three-helix bundle containing six crossover motifs. These units are then assembled into long one-dimensional DNA columns. (b) The same approach is used to generate six and eight helix DNA nanotubes. [Adapted from references 39, 112, 113].

From these selected examples, it is evident that the current approaches to DNA nanotube construction always result in cylindrical assemblies that are symmetrical and fully double-stranded. Our ability to control the surface topology of nanotubes provides a new parameter that could be used to fine-tune their resulting physical and chemical properties, which is, however, a general challenge common to all nanotube construction, including polymeric and carbon nanotubes. Here we present a unique approach to DNA nanotube synthesis that provides access to nanotubes of any pre-determined geometry, and report the first example of triangular and square-shaped DNA nanotubes. We also show how this approach is readily amendable to the construction of DNA nanotubes that can be fully double-stranded and “closed”, or partially single-stranded and “open”. This method provides a new set of parameters to tune DNA nanotube construction, such as geometry, stiffness, double and single-stranded character, and promises to facilitate access to designer DNA nanotubes with applications for the growth of

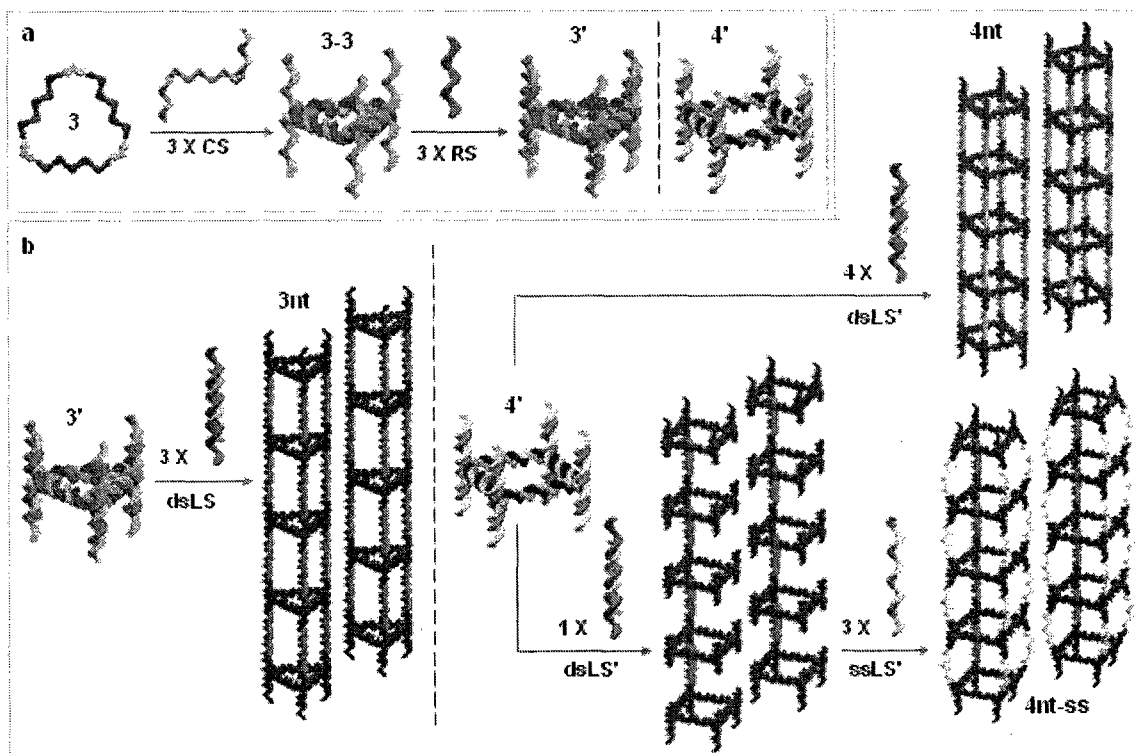
Scheme 5.1 DNA templates 3 and 4.



nanowires of controlled shape, the loading and release of cargo, and the real-time modulation of stiffness and persistence length in interconnects.

To construct a triangular DNA nanotube **3nt**, for example, a single-stranded triangular template **3** (Scheme 5.1) is used as a scaffold to first generate a well-defined triangular building block **3'**. This is achieved by hybridizing **3** to three complementary DNA strands (**CS**), which contain six sticky-end overhang cohesions, to form **3-3**, followed by the addition of three rigidifying strands (**RS**) to spatially orient each of these sticky-ends above and below the plane of triangle **3'** (Scheme 5.2a). Three double-stranded linking strands (**dsLS**) of appropriate sequence then assemble the set of building blocks **3'** into the well-defined triangular DNA nanotubes **3nt** (Scheme 5.2b). Considering the ease with which geometrically unique cyclic and single-stranded DNA templates such as triangles, squares, pentagons, and hexagons have been previously synthesized (see Chapter 4 of this thesis),¹¹⁴ this approach can in fact be used to generate nanotubes of any arbitrary shape and size. This method similarly enabled the synthesis of fully double-stranded square-shaped DNA nanotubes **4nt**, and partially single-stranded square DNA nanotubes **4nt-ss**, from the cyclic and single-stranded square template **4** (Schemes 5.1 and 5.2).

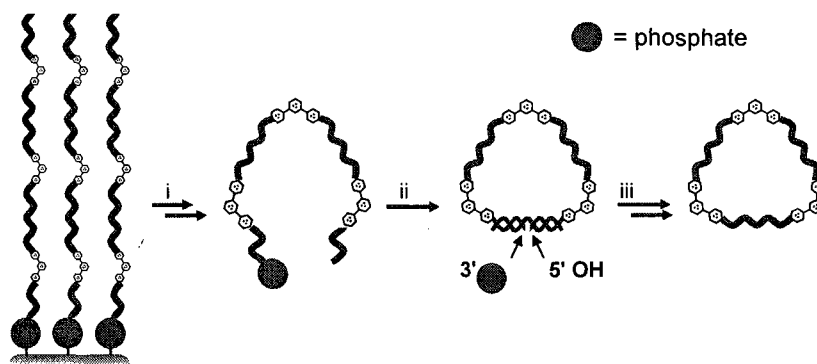
Scheme 5.2 Construction of the triangular and square DNA nanotubes **3nt** and **4nt**, and of the single-stranded square DNA nanotube **4nt-ss**.



5.1 Synthesis

Initial efforts are directed towards construction of the triangular **3'** and square **4'** modules from the single-stranded and cyclic DNA templates triangle **3** and square **4**, respectively. To do so, it is first necessary to synthesize the DNA templates **3** and **4**. This involves construction of a single continuous DNA strand (Scheme 5.3i), embedded with the appropriate number of rigid organic vertex molecules **1** (i.e. three for triangle **3** and four for square **4**), and its subsequent DNA templated cyclization (Scheme 5.3ii), and chemical ligation to produce the cyclic building blocks **3** or **4** (Scheme 5.3iii).

Scheme 5.3 Synthesis of templates **3** and **4**.



The clean isolation of the linear analogues of triangle **3**, square **4** and the template strand is demonstrated using 24% polyacrylamide gel electrophoresis (PAGE; Figure 5.3). The templated cyclization of linear **3** and linear **4** is monitored using 10% native PAGE, and is found to occur quantitatively for both **3** and **4** (Figure 5.4a). The subsequent ligation of these self-assembled mixtures is conducted using cyanogen bromide according to a previously reported procedure by Damha and co-workers,¹⁰⁴ and in all cases resulted in a single other band of relatively slower electrophoretic mobility assigned to the fully cyclic triangle **3** and square **4**, respectively (Figure 5.4b).

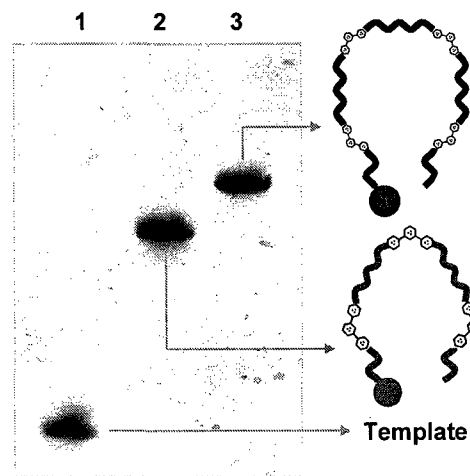


Figure 5.3 Template strand, and the linear analogues of **3** and **4**. Denaturing PAGE analysis of the linear analogues of **3** (lane 2) and **4** (lanes 3), and of the template strand used to cyclize them (lane 1).

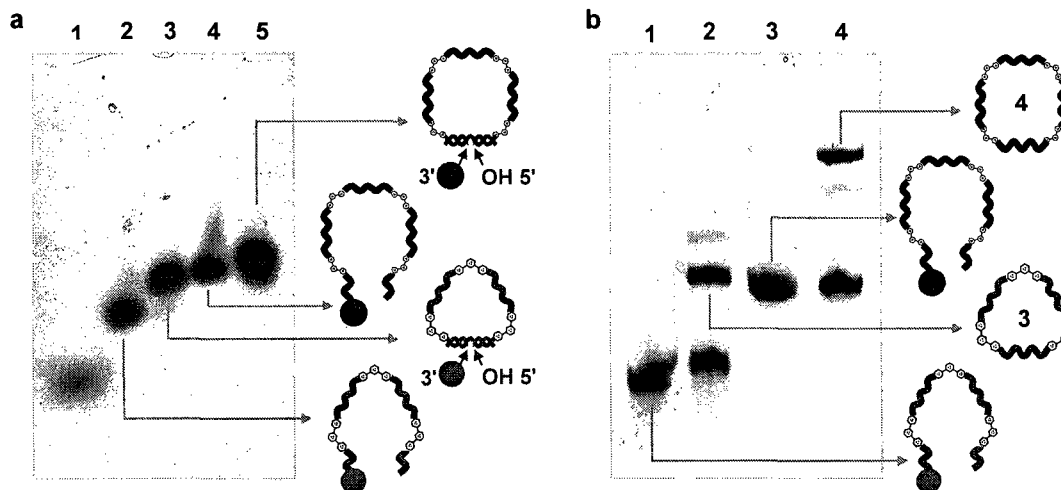


Figure 5.4 Assembly and ligation of cyclic 3 and 4 from the linear analogues of 3 and 4, respectively. (a) Native PAGE reveals the clean templated cyclization of 3 (lane 3) and 4 (lanes 5), using their respective linear analogues (lanes 2 and 4, respectively) and the complementary template strand (lane 1). (b) Denaturing PAGE reveals the generation of a single other band of relatively retarded electrophoretic mobility when the cyclic assemblies of 3 (lane 1) and 4 (lane 3) are chemically ligated using cyanogen bromide (lanes 2 and 4, respectively). These single other bands are respectively assigned to the cyclic templates 3 and 4.

The cyclic nature of triangle 3 and square 4 is confirmed using enzymatic digestion assays with ExoVII.¹¹⁴ This enzyme is selective for the digestion of open single-stranded DNA, and will not digest single-stranded DNA that is cyclized. The digestion of the mixtures generated from the ligation of 3 and 4 indeed results in the complete degradation of the linear analogues of 3 and 4, and does not affect the bands assigned to cyclic 3 and 4 (Figure 5.5).

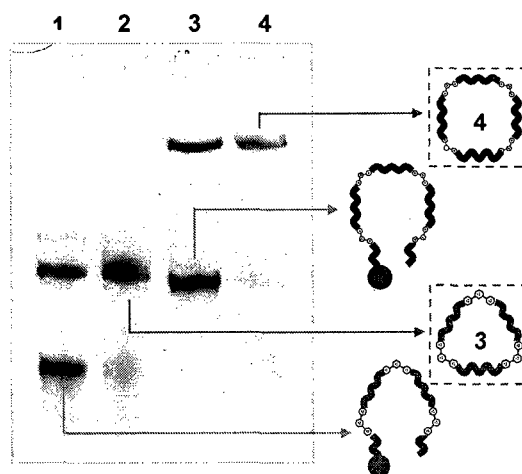


Figure 5.5 Enzymatic digestions of 3 and 4. The crude mixtures generated from the cyclization of 3 (lane 1) and 4 (lane 3) are enzymatically digested using ExoVII (lanes 2 and 4, respectively), which confirm the cyclic nature of the bands assigned to the single-stranded and cyclic DNA templates 3 and 4.

With single-stranded and cyclic DNA templates **3** and **4** in hand, we proceeded to construct the triangular and square modules **3'** and **4'**, from complementary and rigidifying strands (Scheme 5.2a). **3'**, for example, is constructed from one unit of the triangular template **3**, three complementary strands containing sticky-end overhang cohesions **CS1-CS3**, and from three rigidifying strands that orient each of these sticky-ends into one of two lateral directions **RS1-RS3**. The assembly process is monitored sequentially using native PAGE, and is found to occur quantitatively at each step leading to, and including, the construction of the well-defined triangular and square rungs **3'** and **4'** (Figures 5.6a and 5.6b, respectively).

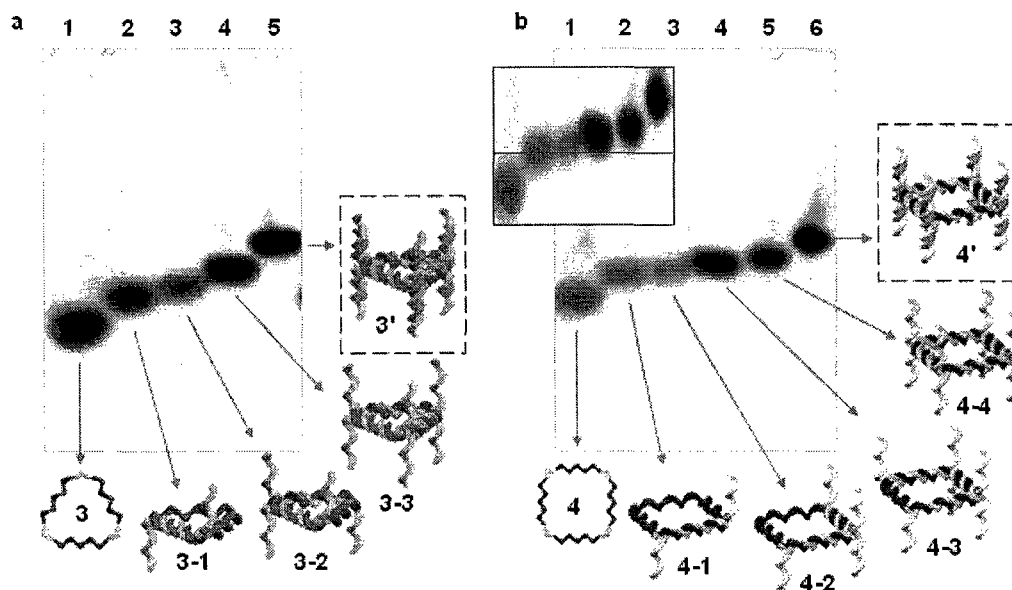


Figure 5.6 Assembly of **3'** and **4'**. (a) The single-stranded triangle **3** (lane 1) is sequentially titrated with the complementary strands **CS1-CS3** (lanes 2-4, respectively), and with the rigidifying strands **RS1-RS3** to quantitatively generate a fully assembled triangular rung **3'** (lane 5). (b) **4** (lane 1) is similarly titrated with **CS1-CS4** (lanes 2-5, respectively), and with **RS1-RS4** to quantitatively generate **4'** (lane 6). Inset: An expanded view of the gel is incorporated to better illustrate the difference in band mobility for each intermediate assemblies.

5.2 Results and discussion

With the triangular **3'** and square **4'** modules in hand, we proceeded to examine their self-assembly potential to generate well-defined triangular and square-shaped DNA nanotubes, respectively. A hierarchical approach is found necessary to insure the overall fidelity of the assembly process.¹¹⁵ In the case of **3'**, one of the sides contains sticky-end overhangs that are seven bases long, while the remaining two sides contain overhangs that are only five bases. Therefore, as the mixture is slowly cooled, the longer sticky-ends cohere first to generate aligned

linear assemblies of **3'** molecules, followed by the favorable cohesion of the remaining pre-organized shorter sides to generate the final triangular DNA nanotube **3nt** in high yields. An analysis of the resulting assemblies using atomic force microscopy (AFM) reveals that well-defined DNA nanotubes, extending over tens of microns, indeed form (Figure 5.7a).

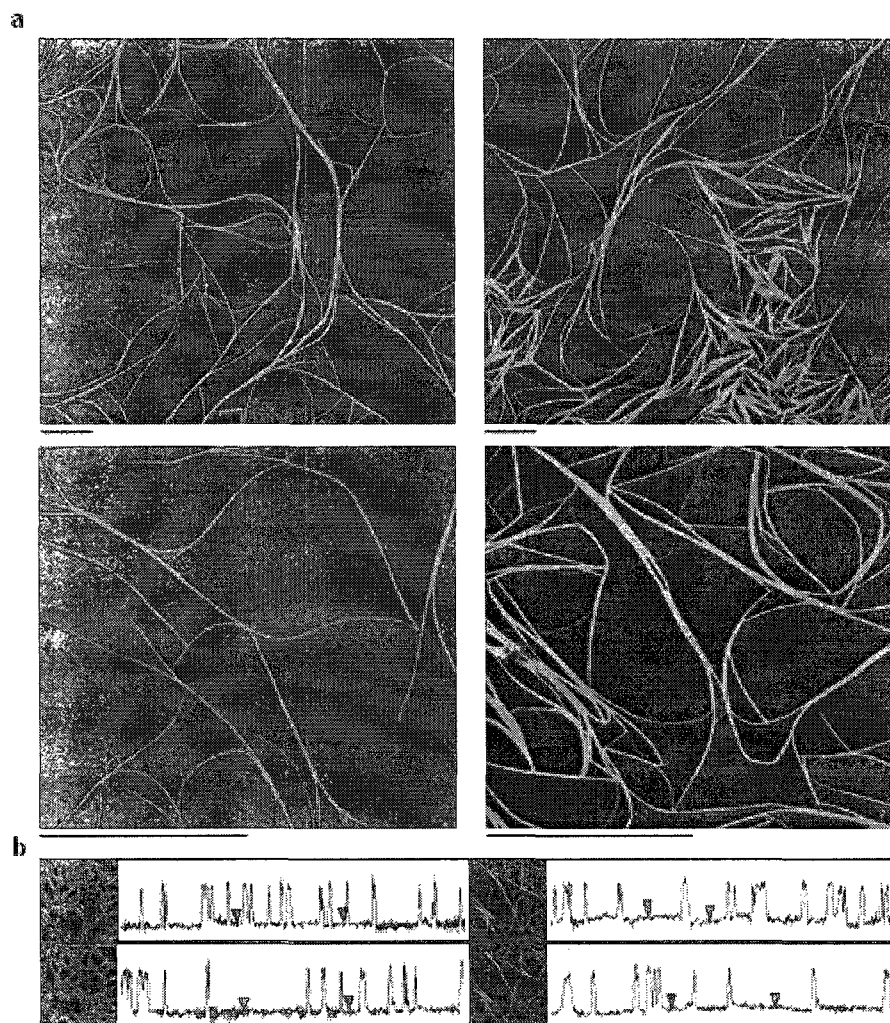


Figure 5.7 AFM characterization of **3nt**. (a) AFM analysis of **3nt** reveals the formation of extended one-dimensional DNA nanotube assemblies. Bar is 2.5 μm . (b) Cross-sectional analysis shows them all to be of the same size.

These nanotubes are characterized along both their lateral and longitudinal axes. Lateral cross-sectional analysis shows them all to be of the same height (Figure 5.7b), which is consistent with a well-defined DNA nanotube assembly of a single size. Longitudinal analysis is conducted on the rungs within each DNA nanotube, and is performed using rungs that modified with protruding hairpins to provide a visual probe detectable by AFM. Hairpins are incorporated into each corner unit of **3'-hp** by the use of rigidifying strands with hairpins (**RS-hp**; Figure 5.8a).

The distance between each rung is estimated to be ~ 15 nm. A remarkably uniform 1D-array of hairpins with a periodicity of 45 nm – exactly three times that of 15 nm – is observed (Figure 5.8a). This is consistent with a 40° rotation of each triangular rung, with respect to the next one, and a realignment of the hairpins every fourth rung. The triangular DNA nanotube assembly **3nt-hp** thus possesses a helical screw axis with nine rungs for each full turn (Figure 5.8b).

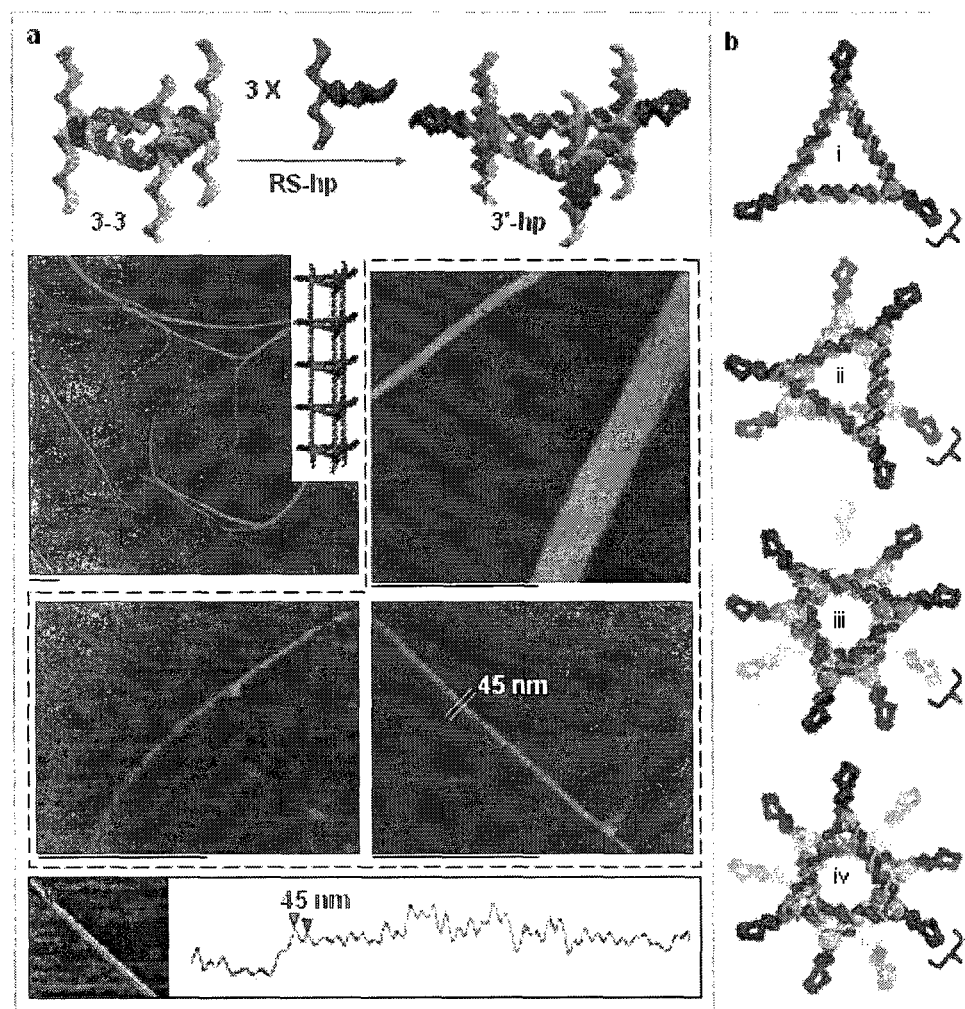


Figure 5.8 AFM characterization of 3nt-hp. (a) Protruding hairpins incorporated into the corner units of each triangular rung **3'-hp**, using rigidifying strands **RS-hp**, assemble into triangular-shaped DNA nanotubes **3nt-hp** with hairpins radially protruding from each of its corner units. Cross-sectional AFM analysis reveals a spacing between each consecutive hairpin of 45 nm – exactly three times the distance that is between two consecutive rungs – in which each rung is rotated by an angle of 40° . Bar is 1 μ m. (b) To better illustrate the helicity within **3nt-hp**, a top-view sectional analysis is conducted. (i) A single hypothetical hairpin is selected within rung 1. (ii) Superimposition of rung 2, separated from rung 1 by a distance of 15 nm and rotated by an angle of 40° , does not result in the alignment of any of its hairpins onto any of those within rung 1. (iii) Rung 3, now separated from rung 1 by a distance of 30 nm and rotated with respect to rung 1 by an angle of 80° , still does not align. (iv) Rung 4, however, which is now separated from rung 1 by a distance of 45 nm and is rotated with respect to rung 1 by an angle of 120° , is superimposed onto the hairpins being monitored within rung 1.

DNA nanotubes that are laterally constructed one rung at a time can be easily modulated with respect to size and shape. Thus, in addition to triangular DNA tubes **3nt**, geometrically well-defined square DNA nanotubes can be readily accessed by starting with the square-shaped DNA template **4**. Assembly of **4** into **4'** (as with **3'** above) equips this template with cohesive DNA strands above and below its plane (Schemes 5.1 and 5.2). Addition of double-stranded linking strands **dsLS'** generates square DNA nanotubes **4nt**. AFM analysis confirms the construction of highly uniform nanotubes, and their extension over tens of microns, and shows them to be of a uniform size (Figure 5.9). In principle, this approach can be seamlessly adapted to construct a new class of designer DNA nanotubes, with programmable control over the size and shape of each rung.

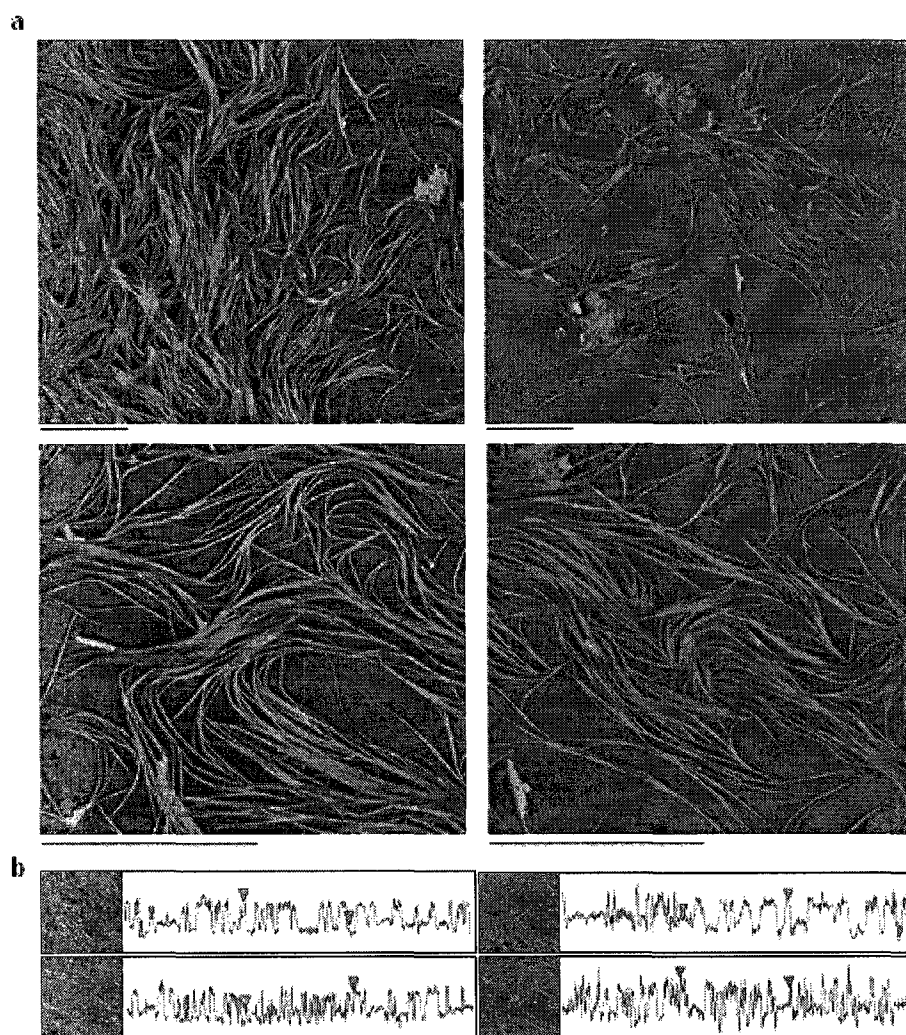


Figure 5.9 AFM characterization of **4nt**. (a) AFM analysis of **4nt** reveals the formation of extended one-dimensional DNA nanotube assemblies. Bar is 5 μm . (b) Cross-sectional analysis shows them all to be of the same size.

It is of interest to note that sample preparation of the DNA nanotubes for imaging using AFM resulted in nanotube assemblies that are always somewhat embedded on the mica surface. Cross-sectional analysis of **3nt** and **4nt** is therefore conducted on the phase images, and can only be used to confirm that all of the DNA nanotube assemblies are of the same size. Although it is difficult to obtain an accurate value for the diameter of either **3nt** or **4nt** using height images in which the DNA assemblies are somewhat embedded, the relative ratio of the observed dimensions can be used to better ascertain the formation of triangular and square-shaped DNA nanotube assemblies of the expected size. The theoretically calculated diameter of **3nt** is 8.9 nm, while that of **4nt** is 11 nm. Therefore, the relative diameter ratio of **3nt** to **4nt** is theoretically expected to be 0.81. The experimentally obtained cross-sectional height analysis of the **3nt** and **4nt** using the height images is consistently found to be 2.95 nm and 3.56 nm for all nanotubes measured, which translates into a diameter ratio of **3nt** to **4nt** of 0.83 (Figure 5.10). This value is in good agreement with the theoretically calculated value of 0.81, and can be used to indirectly confirm the formation of triangular and square-shaped DNA nanotubes of the expected size.

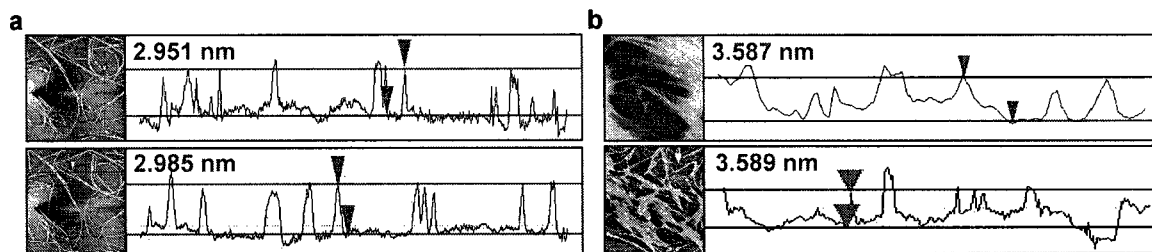


Figure 5.10 Height analysis of **3nt** and **4nt**. Cross-sectional height analysis on **3nt** and **4nt** reveals a consistent height of (a) 2.95 nm for triangle **3nt**, and of (b) 3.56 nm for square **4nt**, which translates into a height ratio between **3nt** and **4nt** of 0.83.

Our approach constructs DNA nanotubes that can be completely double-stranded and rigid, or single-stranded and more flexible and permeable. If the linking strands that join the square rungs **4'** are double stranded, well-defined DNA nanotubes **4nt** that are fully double-stranded are obtained (as described above). The average length of each nanotube over which it behaves as a rigid rod (i.e. before it starts bending) is measured to be $\sim 1 \mu\text{m}$ from AFM analysis, ~ 100 times stiffer than double-stranded DNA (rigid over ~ 10 nm). However, if three of the four linking strands used within this system are single-stranded, DNA nanotubes **4nt-ss** with single-stranded regions are generated (Scheme 2). These nanotubes now possess one double-stranded side and three single-stranded sides and are thus predicted to be less rigid. When characterized by AFM analysis, **4nt-ss** nanotube assemblies are found to be significantly more flexible, with shorter distances ($\sim 0.5 \mu\text{m}$) between bent regions (Figure 5.11). To our knowledge, this is the first

example a DNA single-stranded nanotube. This approach thus allows deliberate control of the stiffness, persistence length and permeability of these materials. It also opens the door to the possibility of using these nanotubes in their more accessible single-stranded form to allow loading of materials, biomolecules or drugs, and subsequently closing these nanotubes to their double-stranded form to ensure encapsulation.

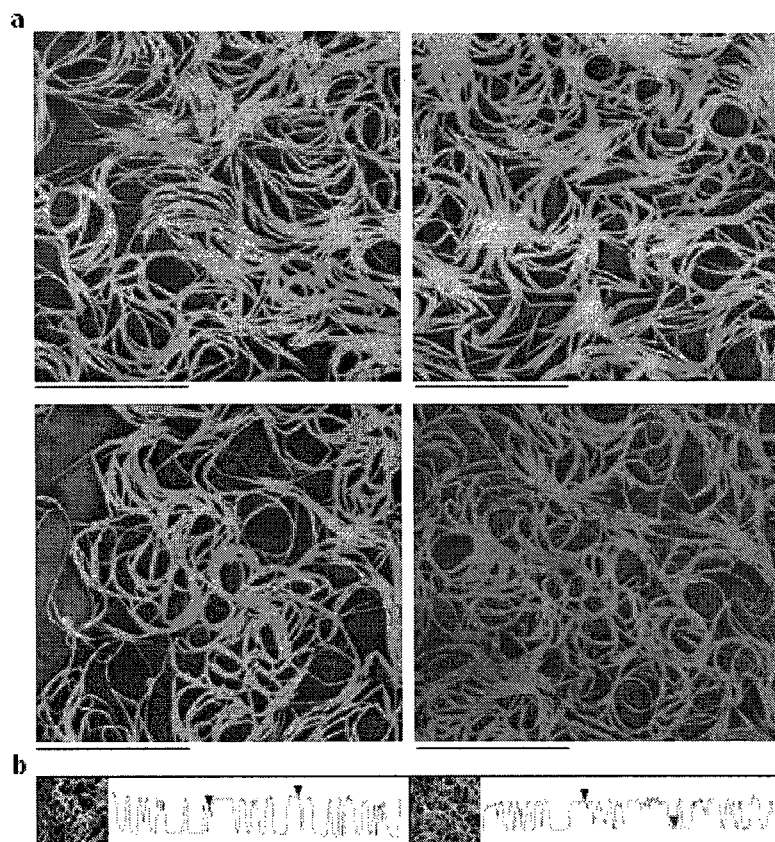


Figure 5.11 AFM characterization of 4nt-ss. (a) AFM analysis of 4nt-ss reveals the formation of extended DNA nanotubes that are relatively more flexible than their fully double-stranded analogous 4nt. (b) Cross-sectional analysis of these assemblies shows them all to be of the same size. Bar is 5 μm.

5.3 Conclusions

This work has shown a modular approach to DNA nanotube construction that offers new elements of structural control in the assembly process of these materials. Geometry, size, stiffness, double or single-stranded character and possibly as well permeability can all be tuned and modified, thus providing ready access to deliberately designed nanotube architectures. The method uses single-stranded and cyclic DNA templates to generate “rungs” of well-defined geometries, and assembles these units longitudinally to produce nanotubes with pre-designed

structures. Triangular and square DNA nanotubes can be readily accessed in their single-stranded and double-stranded forms. These assemblies are highly uniform, both longitudinally and laterally, and are 100 times stiffer than double-stranded DNA. Numerous applications of these well-defined nanostructures can be envisaged, such as in the growth of metallic or semiconductor nanowires of tunable size and geometry, encapsulation of proteins or nanoparticles in their double-stranded form, and possible release in their single-stranded form, and as interconnects with switchable persistence lengths, among others.

5.4 Experimental

General. Acetic acid, boric acid, cyanogen bromide (5M in acetonitrile), formamide, 4-morpholineethanesulfonic acid (MES), $\text{MgCl}_2 \cdot 6\text{H}_2\text{O}$, StainsAll[®], and tris(hydroxymethyl)-aminomethane (Tris) are used as purchased from Aldrich. 5-Ethylthiotetrazole, 2000Å phosphate-CPG with a loading density of 5.4 $\mu\text{mol/g}$, and reagents used for automated DNA synthesis are purchased from ChemGenes. Exonuclease VII (ExoVII; source: recombinant), and sephadex G-25 (super fine DNA grade) are used as purchased from Amersham Biosciences. Microcon[®] size-exclusion centrifugal filter devices (YM10) are purchased from Millipore. RubyRed mica sheets for AFM are purchased from Electron Microscopy Sciences. Etched silicon cantilevers (OMCL-AC160TS) for AFM imaging are used as purchased from Olympus.

Instrumentation. Standard automated oligonucleotide solid-phase syntheses are performed on a Perspective Biosystems Expedite 8900 DNA synthesizer. UV/vis quantifications are conducted on a Varian Cary 300 biospectrophotometer. Gel electrophoresis experiments are carried out on an acrylamide 20 X 20 cm vertical Hoefer 600 electrophoresis unit. Electroelutions are performed using a Centrilutor[®] electroeluter from Millipore. Temperature controlled hybridizations are conducted using a Flexigene Techné 60 well thermocycler. AFM images are either acquired on a Digital Instruments "Dimension 3100" or on an E-scope microscope (Santa Barbara, CA).

Synthesis of single-stranded and cyclic triangle 3 and square 4. Synthesis of the linear analogous of 3 and 4 is conducted on 2000Å phosphate-CPG with a loading density of 15 $\mu\text{mol/g}$ using standard oligonucleotide synthetic protocols. The phosphate group is synthetically incorporated to facilitate subsequent chemical ligation. The coupling of vertex 1 is conducted using a trityl protected amidite derivative (i.e. 2), with an extended coupling and deprotection times of 15 and

2 minutes. **2** is prepared according to a previously reported method by Sleiman and co-workers.^{107,114} In the case of triangle **3**, for example, sixty bases of the appropriate sequence are synthesized and are embedded with three units of vertex **2** at positions 10, 30, and 50. The DNA strands are cleaved and deprotected from the solid-support in a concentrated solution of ammonium hydroxide (55°C, 12 hrs), purified using 24% 7M urea polyacrylamide gels, extracted into 3 mL of water (16 hrs, 37°C), and desalted using Sephadex G-25 column chromatography. Quantification is carried by UV/vis analysis using Beer's law ($A_{\text{total}} = A_{\text{vertex}} + A_{\text{DNA}}$), in which the extinction coefficient of the vertex at 260 nm is calculated to be $2.30 \times 10^5 \text{ L mol}^{-1} \text{ cm}^{-1}$. Table 5.1 summarizes the sequences of the linear templates **3** and **4**, and of the template strand used to cyclize them.

Table 5.1 Sequences of **3**, **4**, and template strand.

	Sequences (5' - 3')
Linear 3	TATTGGTTTG-1-TGACCAATAACACAAATCGG-1- TCAGTAATCTCTTGAAGGTA-1-GGAAACGACA-phosphate
Linear 4	TATTGGTTTG-1-TGACCAATAACACAAATCGG-1-AAAGCTTGAAGG GGGGAATC-1-TCAGTAATCTCTTGAAGGTA-1-GGAAACGACA-phosphate
Template	CAAACCAATATGTCGTTTCC

The templated cyclization of the linear triangle **3** and the linear square **4** is generally conducted by combining 1.2×10^{-10} moles of either of the linear strands and 1.2×10^{-10} moles of the template strand, in 10 μL of TAmg buffer (40 mM Tris, 20 mM acetic acid, 12.5 mM $\text{MgCl}_2 \cdot 6\text{H}_2\text{O}$; pH 7.8), and are left incubating at 0°C for 10 minutes. Ligations using cyanogen bromide are conducted according to a procedure by Damha and co-workers,¹⁰⁴ and involve the addition of 10 μL of cyanogen bromide (5 M in acetonitrile) to the pre-cyclized template, in 30 μL of the ligation buffer MES (250 mM MES, 20 mM MgCl_2 , pH 7.6), followed by an incubation period of 15 minutes at 0°C. The resulting structures are purified using Microcon[®] size-exclusion centrifugal filter devices (YM10). Enzymatic digestions using ExoVII involves the use of 5 units of the enzyme, and an incubation period of 22 minutes at 37°C. **3** and **4** are purified via electroelution.

Assembly of the well-defined triangular 3' and square 4' modules. Assemblies are typically conducted by combining all DNA strands in the correct molar ratios (final assembly 1.2×10^{-10} moles; 30 μL TAmg buffer), and by incubating at 95°C for 10 minutes followed by slowly

cooling to 5°C over a period of 16 hours. Table 5.2 summarizes the sequences of the strands used to construct **3'** and **4'** from **3** and **4**, respectively.

Table 5.2 Sequences of CS1-CS4 and RS1-RS4.

	Sequences (5' - 3')		
CS1	GCTGGGAAGGTTTGCTGCCTTTGCTGTATAACCAACATAGTATTGCCACCA		
CS2	AAAAAGGAACCTCTTGACTGGTTATTGTGTTTAGCCAAGGTAGGAATAGGA		
CS3	TGAAAGCGACATCTCAGTCATTAGAGAACTTCCATTTAGGTTGAAAACTCTG		
RS1	TTCAACCTAACAGCAAACCT	RS3	TTCCTACCTTGAGATGTCGT
RS2	GCAATACTATCAAGAGTTCC		
CS1'	Same as CS1		
CS2'	AAAAAGGAACCTTGACTGGTTATTGTGTTAGCCCCAGATCGAAACGAC		
CS3'	ATCTCGAAAGGCTGGTTTCGAACCTCCCCCTTAGAAGGTAGGAATAGGA		
CS4'	Same as CS3		
RS1'	Same as RS1	RS2'	Same as RS2
RS3'	TTCGATCTGGCCAGCCTTTC	RS4'	Same as RS3

Assemblies of DNA nanotubes

3nt, 3nt-hp, 4nt, 4nt-ss.

Assemblies are typically conducted in 30 µL of TAMg buffer, and involve addition of the double-stranded linking strands to the already assembled rungs **3'**, **4'**, or **3'-hp** at 40°C, for 10 minutes, followed by the slow cooling to 5°C over a period of 16 hours. The linking strands are mixed with their respective rungs, in the correct molar

Table 5.3 Sequences of LS and dsLS.

Sequences (5' - 3')	
LS1	TCCAGCACATCACCTTGGTTGGCTGCTCATACCAAGAGTT
LS2	TTTTTTGACATCACCTTGGTTGGCTGCTCATACTCTGGGT
LS3	CTTCATGACATCACCTTGGTTGGCTGCTCATACTCTCCTA
dsLS1	GTATGAGCAGCCAACCAAGGTGATGT
dsLS23	GAGTATGAGCAGCCAACCAAGGTGATGTCA
LS1'	Same as LS1
LS2'	Same as LS2
LS3'	GAGATTGACATCACCTTGGTTGGCTGCTCATACTCTGTCGT
LS4'	Same as LS3
dsLS1'	Same as dsLS1
dsLS234'	Same as dsLS23

ratio, to generate an assembly with a final concentration of 4.0×10^{-6} mol L⁻¹. Table 5.3 summarizes the sequences of the strands used to construct **3nt** and **4nt** from **3'** and **4'**, respectively.

Atomic force microscopy analysis. AFM sample preparation typically involves the deposition of 10 μL of the self-assembled mixture (concentration of 10 μM) onto freshly cleaved mica (dimensions 2 X 2 cm), followed by adequate evaporation to achieve complete dryness (typically 30 mins in a fumehood). Whenever possible, imaging is conducted within 24 hours in order to minimize time-dependant sample degradation. AFM images are acquired in air, and at room temperature. "Tapping mode" (i.e. intermittent contact imaging) is performed at a scan rate of 1 Hz using etched silicon cantilevers with a resonance frequency of ~ 300 kHz, a spring constant of ~ 42 N/m, and a tip radius of < 10 nm. All images are acquired with medium tip oscillation damping (20-30%).

$$\text{N.B. \% oscillation damping} = \frac{(\text{free air amplitude} - \text{imaging setpoint amplitude})}{\text{free air amplitude}} \times 100$$

Guest-mediated access to a single DNA nanostructure from a library of multiple assemblies

Faisal A. Aldaye and Hanadi F. Sleiman, *J. Am. Chem. Soc.* 2007, **129**, 10070-10071.

As it becomes necessary to design larger and more complex DNA assemblies, it inevitably becomes necessary to also incorporate degenerate DNA sequences that may assemble into a number of undesirable products. This is currently a major bottleneck facing researchers in DNA nanotechnology.¹¹⁶ Errors during the self-assembly process typically occur when a DNA sequence hybridizes to an "incorrect" strand at an energetically sub-optimal configuration. One approach to address this issue would be to reduce the number of unique sequences that are used. For example, even though a four-way branched junction is structurally symmetric, it is typically constructed from nine sequence unique strands that assemble into four unique arms (Figure 6.1a, *top*). Mao and co-workers judiciously incorporated symmetry into the structurally symmetric regions of this building block, and constructed a functional four-way junction from three strands

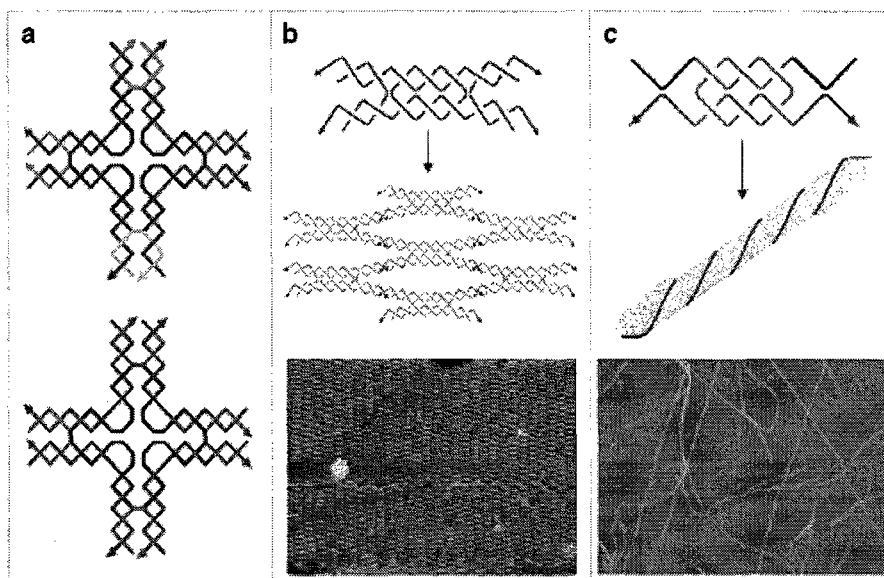


Figure 6.1 Sequence symmetry within DNA tiles. (a) An asymmetric four-arm branched junction is typically constructed from nine unique strands (*top*). A symmetric four-arm branched motif is however constructed from three DNA strands, with judiciously programmed sequence symmetry (*bottom*), and assembles into extended two-dimensional square DNA arrays. (b) A double crossover DNA tile can be constructed from only two strands, and assembles into a well-defined periodic two-dimensional DNA array. (c) A single DNA strand can be assembled into a symmetric DNA tile capable of further generated an extended one-dimensional DNA nanotube. Different colors represent different sequences. [Adapted from references 117-119].

instead of nine (Figure 6.1a, *bottom*).¹¹⁷ The same group later synthesized a DX tile from two strands instead of four (Figure 6.1b),¹¹⁸ and even assembled a DNA column from a single DNA strand (Figure 6.1c).¹¹⁹ Yan and co-workers applied the rules of symmetry to reduce the number of unique tiles within a DNA array of finite sizes.¹²⁰

Another approach to reduce the number of necessary sequences incorporated into a DNA assembly, is hierarchical self-assembly. In principle, if the assembly process could be conducted sequentially, then some of the sequestered sticky-end sequences could be reused with no fear of crosstalk. Dwyer, LaBean, and co-workers used this approach to assemble a sixteen tile nanoarray in four steps from four unique sticky-end sequences (Figure 6.2).¹¹⁵

Although symmetry considerations and hierarchical self-assembly provide mechanisms to minimize the number of sequences incorporated, it is not always feasible to use a small enough sequence-set to completely eliminate the probability of error formation. What to do when errors occur? Since mismatches are typically hybridized at an energetically sub-optimal configuration, in principle, if the system is allowed to equilibrate, then the energy landscape would be thoroughly sampled and the “correct” interactions would be favored on the bases of their thermodynamic stability. The field of DNA computation is very sensitive to imperfections that might occur during the assembly process, and has developed a number of algorithmic approaches to deal with potential mistakes. For example, Winfree and co-workers developed a system based on a two-dimensional tile array that proof-reads errors and corrects for them.¹²¹ The tiles are programmed to stop growing when a mistake occurs unless another is made, and since the chances of another mistake occurring is relatively small, assembly halts. This pause provides the correct tile enough time to seek out and replace the thermodynamically less stable mismatched tile. Pierce and co-workers generated a number of metastable folded DNA intermediates that systematically interact with each other to assemble into a single product (Figure 6.3a).¹²² By programming the biochemical pathway leading to a final assembly, Pierce’s approach can be used to better direct the assembly process, and is in fact an example of error prevention. Lu and co-workers presented an enzymatic approach to proofreading and correcting for errors.¹²³ A DNAzyme capable of cleaving DNA is used to select for errors and delete them (Figure 6.3b). In

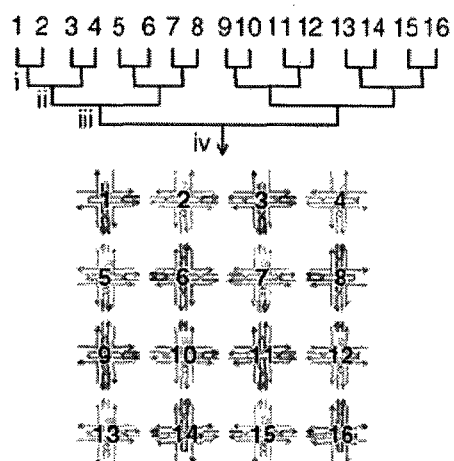


Figure 6.2 Hierarchical self-assembly. An illustration of the four-step annealing process used to construct a sixteen tile 4 X 4 square-shaped DNA array from four different sticky-end sequences. [Adapted from reference 115].

the presence of the “correct” DNA strands, the DNAzyme is not properly folded and is inactive, but in the presence of the “incorrect” DNA strands the DNAzyme is folded and proceeds to cleave and remove the errors. Unfortunately, all of these approaches can be somewhat system dependant, and may be difficult to generalize to all DNA assemblies. More approach for the prevention and correction for errors are required.

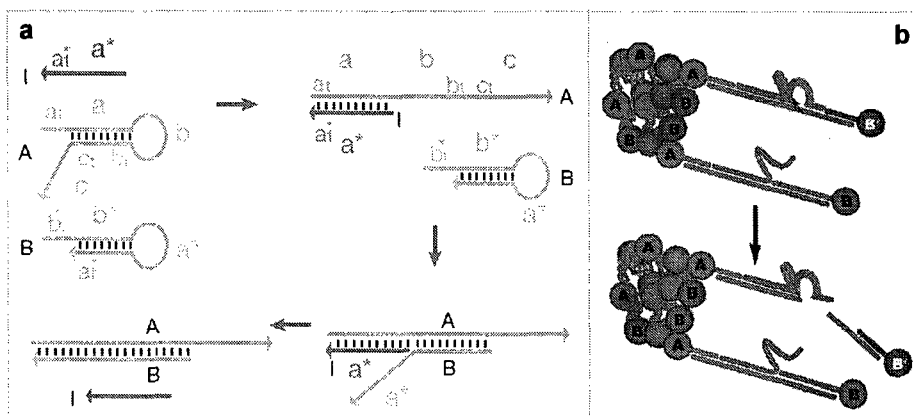
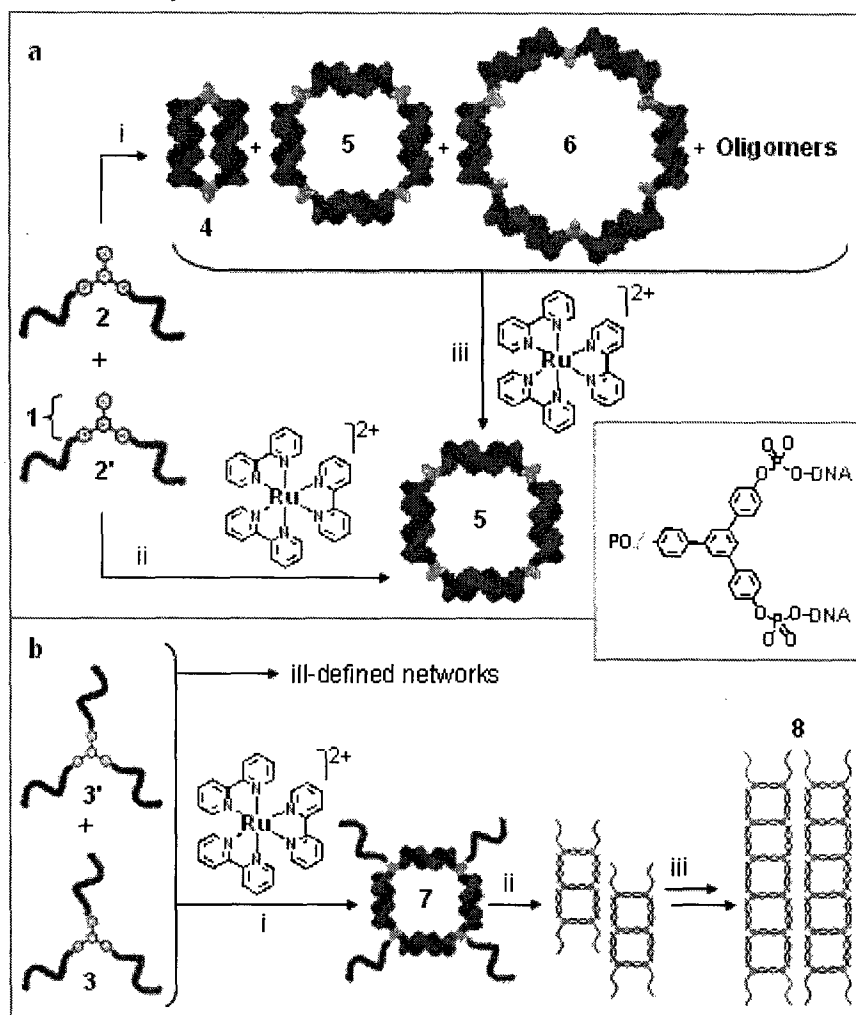


Figure 6.3 Error prevention and correction. (a) In an example of programming biomolecular self-assembly, an initiator promotes assembly of strand A to B, which otherwise would not assemble in their folded states. Initiator I binds part of strand A, unfolding it, and allows it to bind part of strand B, which then displaces the initiator I to fully bind to strand A. (b) Errors within nanoparticle assemblies are cleaved using a DNAzyme (purple) that cleaves DNA when properly folded. Error (blue) allow the enzyme to fold, and are thus cleaved. [Adapted from references 122, 123].

The templated synthesis of a specific molecule from a dynamic library of possible structures has been the recent subject of intense interest.^{124,125} In this approach, a template is added to a mixture of molecules in dynamic equilibrium, which re-equilibrates in favor of the member that best binds this molecule and amplifies it. Although this principle has been used to amplifying the formation of small molecules, supramolecular assemblies, and macromolecules, there are no examples in which this powerful method is used in DNA nanotechnology. Here we construct a set of discrete DNA nanostructures that collectively represent a small dynamic library, from symmetrically branched DNA building blocks **2** and **2'**, and demonstrated the feasibility of applying the rules of host/guest supramolecular chemistry to selectively template the synthesis of a “correct” member from this library of other “incorrect” members, and to convert each already formed “incorrect” member into the same “correct” assembly (Scheme 6.1a). The former is an example of error prevention, while the latter is an approach to error correction. In a direct application, we template the construction of uniform one-dimensional DNA fibers, extending over tens of microns, from the symmetrically branched DNA building blocks **3** and **3'** that would

otherwise assemble into ill-defined oligomeric networks (Scheme 6.1b). Overall, this work provides for a new parameter to prevent and correct for errors, before and after the self-assembly process, and presents for an opportunity to further reduce the number of unique sequences that need to be incorporated when designing larger and more complex DNA systems.

Scheme 6.1 Dynamic DNA assemblies.

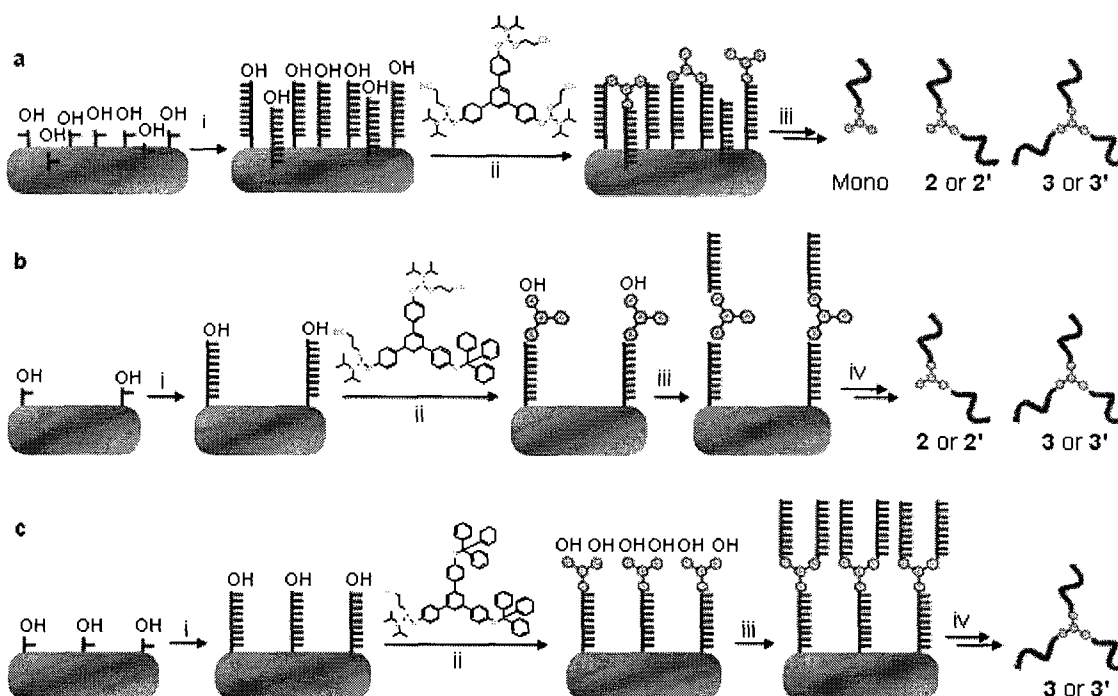


6.1 Synthesis

Initial work is directed towards the synthesis of the branched DNA building blocks **2**, **2'**, **3**, and **3'** in which 17-mer DNA arms radiate from the three-armed rigid organic vertex **1**. To do so, three synthetic approaches were adopted. The first provides access to all three possible branched DNA building blocks – one-armed, two-armed, and three-armed – in relatively equimolar ratios

(Scheme 6.2a). The second provides access to just the two- and the three-armed analogous (Scheme 6.2b). The third approach, however, is used to quantitatively access the three-armed DNA building blocks **3** and **3'** quantitatively (Scheme 6.2c). The method selected is dependant on the amount and type of the building block that needs to be accessed.

Scheme 6.2 Synthetic approaches to accessing symmetrically branched DNA building blocks.



(a) In this approach, (i) DNA of the appropriate sequence is grown on 500Å CPG (high loading density; 85 $\mu\text{mol/g}$), followed by (ii) conjugation of the tris-phosphoramidite derivative of vertex **1** to (iii) yield mono-, bis- and tris-branched DNA building blocks (i.e. mono conjugated, **2** or **2'**, and **3** or **3'**) upon workup and purification. (b) In this approach, (i) DNA is first grown on 2000Å CPG (low loading density; 5 $\mu\text{mol/g}$), followed by (ii) conjugation of the bis-amidite mono-trityl protected derivative of vertex **1**, and the subsequent synthesis of a second DNA arm off of vertex **1** in a 5' to 3' direction to (iii) yield bis- and tris-branched DNA building blocks (i.e. **2** or **2'**, and **3** or **3'**) upon workup and purification. (c) In this final approach, (i) DNA of the appropriate sequence is grown on 1000Å CPG (medium loading density; 35 $\mu\text{mol/g}$), followed by (ii) conjugation of the mono-amidite bis-trityl protected derivative of vertex **1**, and the subsequent synthesis of two DNA arms off of vertex **1** in a 5' to 3' direction to (iii) yield tris-branched DNA building blocks exclusively (i.e. **3** or **3'**) upon workup and purification.

The first synthetic approach is attractive because it provides simultaneous access to all three DNA derivatives (Scheme 6.2a). In this case, it is necessary to carefully select for the loading-density of the CPG used, and the amount of the phosphoramidite derivative of **1** added, to best control the relative ratio of the three building blocks generated. High loading-density CPG increases the probability of accessing the three-armed conjugate, while a ratio of CPG to amidite

of 2:1 insures the production of all three analogues in a relatively equimolar amount. In the second synthetic approach, the first DNA arm is synthesized, the bis-amidite mono-trityl protected derivative of vertex 1 is incorporated, and the second arm is synthesized in a 5' to 3' direction (Scheme 6.2b). In this case, low density CPG is used to produce the two and three-armed DNA building blocks in relatively equimolar ratios; the three-armed building blocks necessarily form as a consequence of both intra and inter-molecular strand couplings. In the third approach, the first DNA arm is synthesized, the mono-amidite bis-trityl protected derivative of vertex 1 is incorporated, and the remaining two arms are synthesized in a 5' to 3' fashion (Scheme 6.2c). In this case, medium loading density CPG is used to prevent overcrowding on the solid-support. The clean isolation of 2, 2', 3 and 3' (along with the mono-conjugated derivatives) is demonstrated denaturing polyacrylamide gel electrophoresis (PAGE; Figure 6.4).

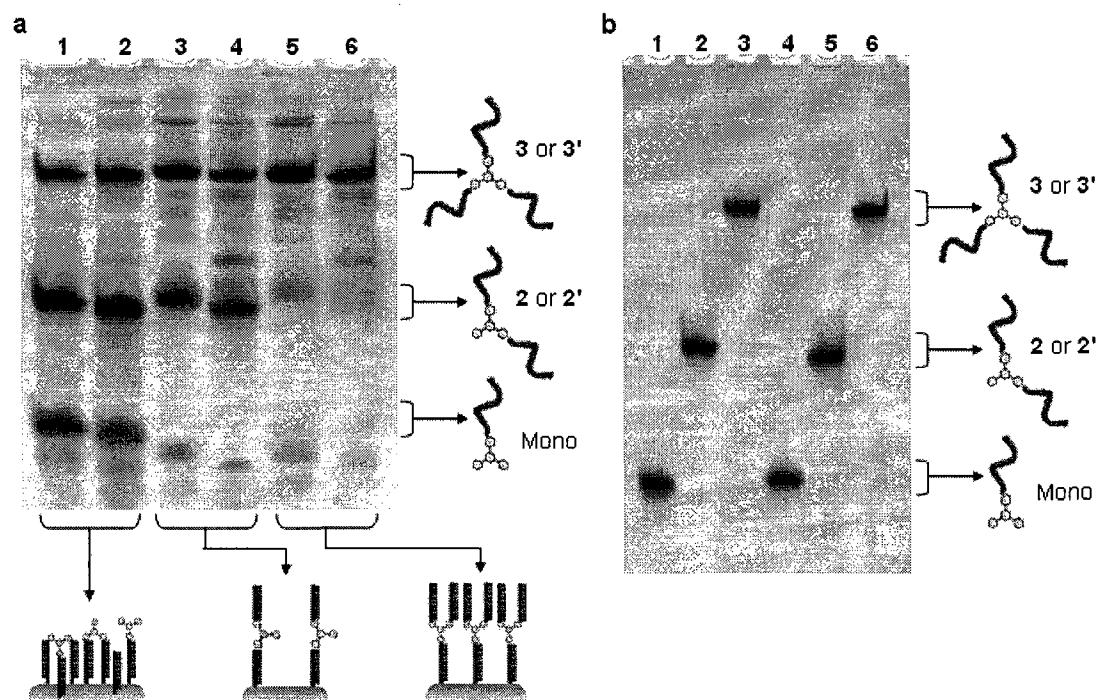


Figure 6.4 Characterization of 2, 2', 3 and 3'. (a) 24% denaturing polyacrylamide gel characterizing the branched DNA conjugates generated using the three synthetic approaches. The first approach provides access to all three DNA conjugates (lane 1 for the sequence of the red DNA strand, lane 2 for the sequence of its complementary blue strand), the second synthetic approach provides access to the bis- and tris-conjugates (lanes 3 for the red strand, lane 4 for the blue strand), while the third approach provides exclusive access to the tris-conjugate (lanes 5 for the red strand, lane 6 for the blue strand). (b) Isolated and purified DNA conjugates are characterized using 24% PAGE. Lanes 1, 2 and 3 correspond to mono-, bis- and tris-branched DNA building blocks, while lanes 4, 5 and 6 correspond to the same set of the complementary conjugates.

6.2 Results and discussion

With the symmetrically branched DNA building blocks in hand, we proceeded to examine their self-assembly behavior. Initial work is directed towards understanding the type of the assemblies constructed using the two-arm branched building blocks **2** and **2'**. Depending on the hybridization protocol used, the two complementary molecules **2** and **2'** can generate a small library of DNA structures. Assemblies are conducted by incubating each building block separately at a given temperature, for a specific period of time, followed by their hybridization and subsequent incubation at a given temperature, for a specific period

of time. The four hybridization protocols used are (pre-assembly, post assembly): (1) 0°C/15 minutes, 0°C/15 minutes, (2) 25°C/15 minutes, 25°C/15 minutes, (3) 95°C/2 minutes, 0°C/15 minutes, and (4) 55°C/10 minutes, 55°C/16 hours. As seen in Figure 6.5, hybridization protocols 1 and 2 result in a single major product of relatively no electrophoretic mobility, assigned to large oligomeric assemblies generated from **2** and **2'** (lanes 2 and 3 respectively), while hybridization protocols 3 and 4 additionally generate a small library of discrete assemblies of relatively faster electrophoretic mobility (lanes 4 and 5, respectively). The three major discrete assemblies **4**, **5**, and **6** are found to move as a 40-, 90- and a 180-mer, when compared to the 20 base pair linear DNA ladder in lane 1, and have since been assigned to dimeric **4**, tetrameric **5** and hexameric **6** cyclic assemblies generated from the hybridization of 2, 4 and 6 units of the two arm branched DNA building blocks **2** and **2'**.

The cyclic nature of **2**, **4**, and **6** is ascertained using Mung Bean nuclease (MBN) digestion assays, which under optimized conditions is selective for the digestion of single-stranded DNA over that of double-stranded DNA.^{92,93} As seen in Figure 6.6, treatment of the self-assembled mixture resulting from the hybridization of **2** to **2'** using protocol 3 (i.e. incubation of each building block at 95°C for 2 minutes followed by their mixing and incubation at 0°C for an

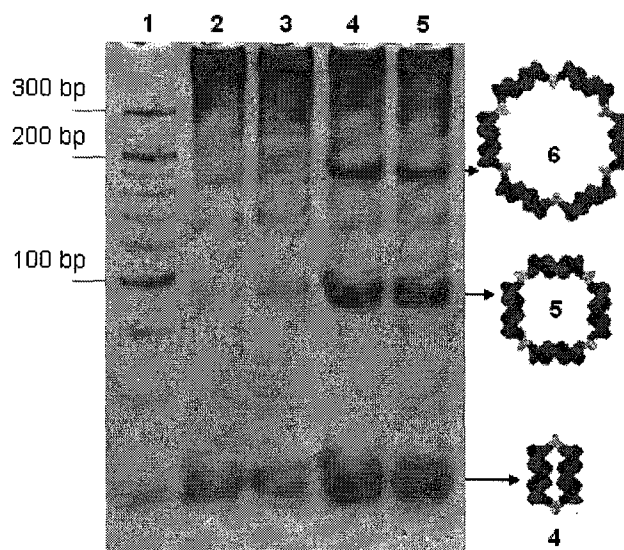


Figure 6.5 Hybridization of **2 to **2'**.** Self-assembly of **2** with **2'**, by their simple addition at 0°C (lane 2), addition at 25°C (lane 3), addition at 95°C followed by incubation at 0°C for 30 minutes (lane 4), and addition at 55°C followed by incubation at 55°C for 16 hours (lane 5). Lane 1 contains the 20 base pair linear molecular weight DNA ladder.

additional 15 minutes) results in no shift in band mobility for either structures **4**, **5**, or **6**; confirming the cyclic nature of these assemblies.

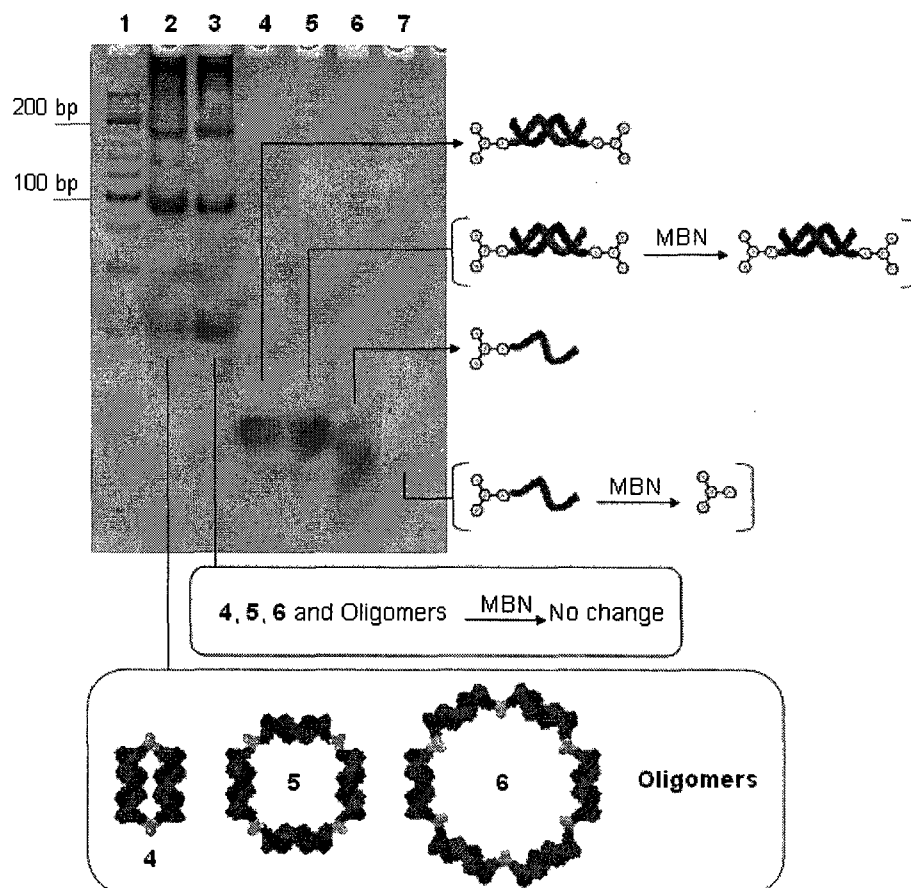


Figure 6.6 Enzymatic digestion of the assemblies generated from **2** and **2'**. MBN enzymatic digestion confirms the double stranded cyclic nature of discrete assemblies **4**, **5** and **6**. Lanes 2 and 3 contain the self-assembled library generated using **2** and **2'** before and after treatment with MBN, respectively, while lanes 4 and 5 contain the single-stranded mono-conjugated building block before and after treatment with MBN, respectively. Lane 1 contains the 20 base pair linear molecular weight DNA ladder.

The dynamic character of this library is then examined. In a first experiment, subjecting either **4**, **6**, or oligomers to incubation at 25°C for 16 hours results in a relative increase in the amount of oligomers for **4** and **6** (lanes 5 and 8, respectively) and in no detectable change for the oligomers, while incubation of the same set of species at 55°C results in re-equilibration into the initial library of assemblies for each of **4**, **6**, and oligomers (Figure 6.7a). This indicates that the library is capable of inter-conversions. In a second experiment, subjecting the initial library to a different number of thermo-cycles between 5°C and 90°C results in the gradual decrease of oligomers remaining, until their essential elimination following 66 such cycles (Figure 6.7b). This indicates that the oligomeric species are kinetic products, while the discrete assemblies are

thermodynamically stable. In a third experiment, the discrete members generated from the same self-assembled library (i.e. dimer **4**, tetramer **5**, or hexamer **6**) are each isolated and subjected to a similar thermocycling study in which each isolated species is cycled between 5°C and 90°C a total of 66 times. As seen in Figure 6.7c, subjecting dimer **4**, tetramer **5**, or hexamer **6** to the same thermocycling experiment results in the regeneration of the initial library of structures **4**, **5**, **6**, and oligomers. This indicates that the individual discrete members formed in this library are dynamic in behavior, and that they should, in principle, be environmentally responsive.

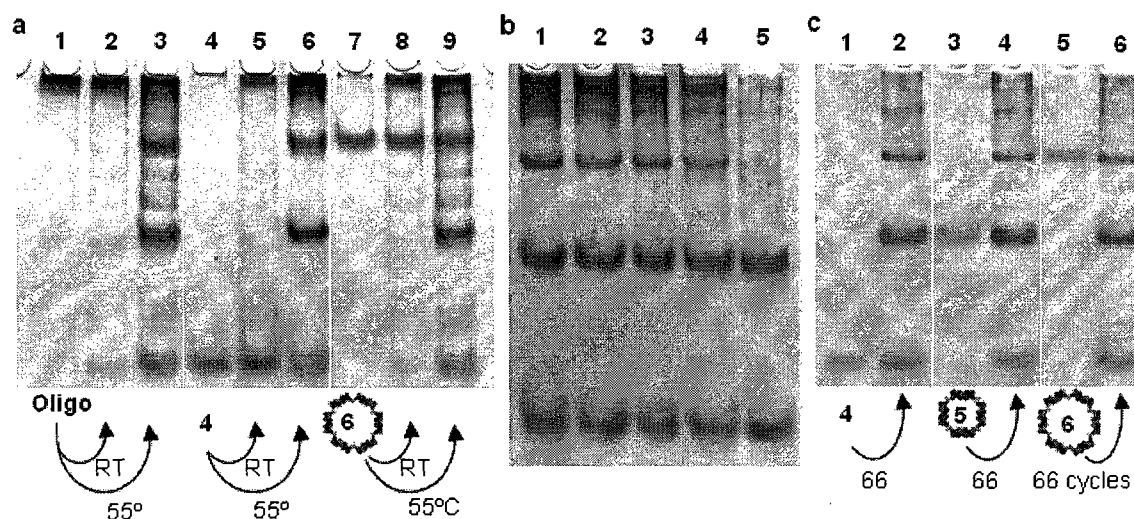


Figure 6.7 Dynamic behavior of the library generated using **2** and **2'**. (a) The oligomers generated using **2** and **2'** (lane 1) were incubated at 25°C and 55°C for 16 hours (lanes 2 and 3, respectively). While, isolated tetramer **4** (lane 4) and hexamer **6** (lane 7) were also incubated at 25°C and 55°C for 16 hours (lanes 2 and 3 for **4**; lanes 8 and 9 for **6**, respectively). (b) The self-assembled mixture generated from the hybridization of **2** to **2'** (addition at 95°C, followed by incubation at 0°C for 30 minutes) (lane 1) was cycled between 90 and 20°C a total of 1, 5, 25 and 55 times (lanes 2, 3, 4 and 5, respectively). (c) Isolated dimer **4** (lane 2), tetramer **5** (lane 4) and hexamer **6** (lane 6) were cycled between 90 and 20°C 66 times (lanes 3, 5, and 7, respectively). Lane 1 contains the 20 base pair linear molecular weight DNA ladder.

With an understanding of the assembly behavior of the symmetrically branched DNA building blocks **2** and **2'**, we proceeded to examine their assembly in the presence of the small molecule template $\text{Ru}(\text{bpy})_3^{2+}$. The self-assembly in the presence of excess $\text{Ru}(\text{bpy})_3^{2+}$ indeed results in dramatically different behavior. Although the hybridization of **2** with **2'** at room temperature exclusively forms oligomers, the same self-assembly in presence of $\text{Ru}(\text{bpy})_3^{2+}$ generates square **5** quantitatively (Figure 6.7a). In addition, when either of the preformed oligomers, dimer **4** or hexamer **6** is isolated and heated with excess $\text{Ru}(\text{bpy})_3^{2+}$ at 55°C for 16 hours, quantitative re-equilibration into square **5** is also observed (Figure 6.7b). Interestingly, the ruthenium template is found to accelerate the equilibration process itself; when added to isolated

4, 6 and oligomers at 25°C for 16 hours, re-equilibration into the library the initial library occurs in contrast to partial re-equilibration into the oligomers in its absence. Heating any of these mixtures (55°C, 16 hrs) in the presence of $\text{Ru}(\text{bpy})_3^{2+}$ produces **5** quantitatively. $\text{Ru}(\text{bpy})_3^{2+}$ essentially has the capacity to quantitatively template the formation of **5** from **2** and **2'**, and to inter-convert each of the already formed member into **5**. The ability of $\text{Ru}(\text{bpy})_3^{2+}$ to provide access to a single structure from sequence degenerate DNA building blocks will allow for the incorporation of symmetry into more complex systems, while its ability to funnel other members into the same single assembly provides a built in mechanism correcting for errors that might be generated during the initial assembly process.

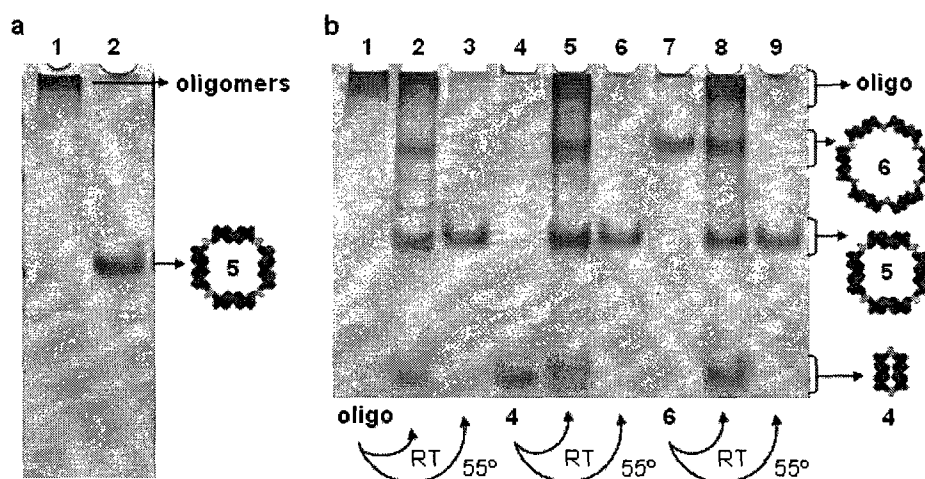


Figure 6.8 Assemblies in the presence of $\text{Ru}(\text{bpy})_3^{2+}$. (a) **2** and **2'** generate cyclic dimer **4**, tetramer **5**, hexamer **6**, and oligomers. (b) Hybridization of **2** to **2'** at room temperature generate polymers (lane 1), while the same assembly in the presence of $\text{Ru}(\text{bpy})_3^{2+}$ results in tetramer **5** quantitatively (lane 2). (c) Oligomers, **4** and **6** (lanes 1, 4 and 7), with $\text{Ru}(\text{bpy})_3^{2+}$, re-equilibrate into all the cyclic structures and oligomers when incubated at 25°C for 16 hours (lanes 2, 5 and 8), and into **5** exclusively when incubated at 55°C for 16 hours (lanes 3, 6 and 9).

In an attempt to better elucidate the reason for the preferential access to tetramer **5** using the small molecule $\text{Ru}(\text{bpy})_3^{2+}$, preliminary structural modeling studies using HyperChem are conducted on dimer **4**, tetramer **5**, and hexamer **6** (Figure 6.9). Prior to the actual self-assembly of **2** to **2'**, it is reasonable to assume that the DNA arms on each building block are fully coated with excess $\text{Ru}(\text{bpy})_3^{2+}$ – $\text{Ru}(\text{bpy})_3^{2+}$ is added to the building block in ~ 1000 fold excess. As seen in Figure 6.9ai, the assembly of dimer **4** generates a small cavity that does not provide enough space for any significant number of $\text{Ru}(\text{bpy})_3^{2+}$ molecules to be packed within. Interestingly, depending on the starting point, the minimization of dimer **4** could also result in an assembly that is not capable of encapsulating any $\text{Ru}(\text{bpy})_3^{2+}$ molecules (Figure 6.8aai). Tetramer **5**, however,

generates a big enough cavity that allows for a considerable amount of $\text{Ru}(\text{bpy})_3^{2+}$ molecules to be incorporated [$\sim 18 \text{ Ru}(\text{bpy})_3^{2+}$], while hexamer **6** allows for an even larger number (Figures 6.9b and 6.9c, respectively). It is thus believed that sterically **4** does not favor encapsulation of $\text{Ru}(\text{bpy})_3^{2+}$, **5** does, and that **6** and higher structures present too much of an entropic cost to be favored over **5**.

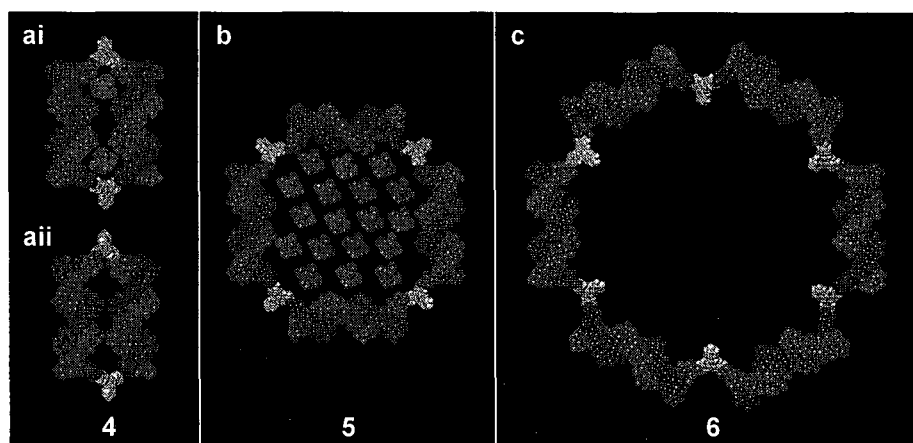


Figure 6.9 HyperChem modeling of **4**, **5** and **6**. Simple HyperChem modeling of the cavities generated from **4**, **5** and **6** reveal that (ai) dimer **4** is barely capable of packing two $\text{Ru}(\text{bpy})_3^{2+}$ molecules (shown in purple), (aai) if any at all, while (b) tetramer **5** possesses a cavity big enough to pack at least 18 ruthenium molecules. (c) Hexamer **6** is found to generate an even bigger cavity, when compared to either dimer **4** or tetramer **5**.

3 and **3'** are the three arm DNA analogues of **2** and **2'**, and are thus expected to generate three-dimensional DNA assemblies. The hybridization of **3** and **3'** conducted using the same four hybridization protocols generates a single band of no electrophoretic mobility, in all cases, and is assigned to high-molecular weight extended assemblies (Figure 6.10). Based on the assembly behavior of **2** to **2'** (i.e. generation of a plethora of different cycles), the networks generated using **3** and **3'** are expected to be ill-defined in composition. This is in fact confirmed using AFM analysis, which reveals the formation of extended random DNA networks (Figure 6.11, *top*). To confirm that these networks are not a consequence of the self-assembly of either **3** to itself, or of **3'** to itself, control experiments are conducted in which **3** and **3'** are individually analyzed using AFM. As

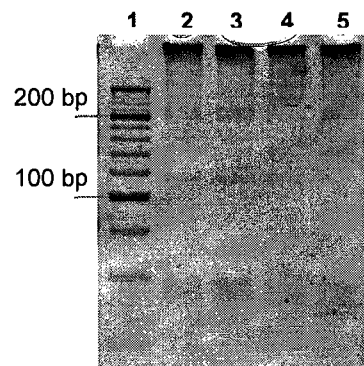


Figure 6.10 Self-assembly of **3** & **3'**. 10% native gel analysis of the products generated from **3** and **3'** at 0°C (lane 2), 25°C (lane 3), 95°C followed by 0°C for 30 minutes (lane 4), and 55°C followed by 55°C for 16 hours (lane 5). Lane 1 contains a 20 bp DNA ladder.

seen in Figure 6.11, *bottom*, neither **3** nor **3'** generate any observable higher-ordered constructs, and certainly none of the extended networks observed in Figure 6.11, *top*.

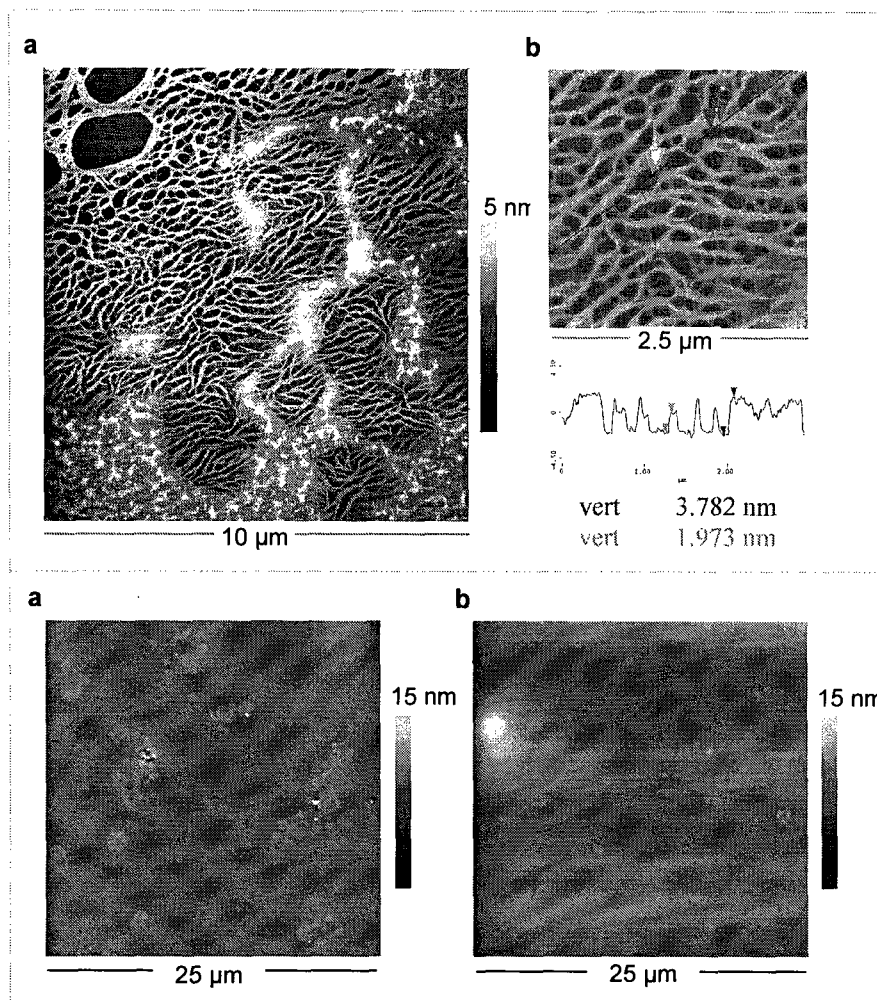


Figure 6.11 AFM analysis of **3** and **3'**. [*Top*] (a) AFM analysis of the structures generated from the self-assembly of **3** and **3'** reveal the formation of ill-defined oligomeric networks. (b) Further cross-sectional analysis of these networks reveal assemblies with a step-height of ~ 2 nm (i.e. diameter of double stranded DNA). [*Bottom*] No assemblies of any type were observed when either of (a) **3** or (b) **3'** are individually analyzed using AFM

In the presence of the structure selective small molecule $\text{Ru}(\text{bpy})_3^{2+}$, the self-assembly of **3** to **3'** generates ordered periodic assemblies. In a manner analogous to that of **2** and **2'** (Scheme 6.1a), the assembly of **3** to **3'** with $\text{Ru}(\text{bpy})_3^{2+}$ is expected to initially result in the formation of a tetrameric construct (Scheme 6.1bi). However, unlike tetramer **5**, the square generated from **3** and **3'** (i.e. tetramer **7**) also contains four single-stranded complementary DNA arms that are capable of further linking the generated squares to each another. In the presence of conditions that continue to contain $\text{Ru}(\text{bpy})_3^{2+}$, these structures are expected to dimerize (Scheme 6.1ii) and

to continue on growing in one-dimension into extended periodic DNA ladders (Scheme 6.1iii).

Although it is difficult to characterize the extended structures resulting from the assembly of **3** and **3'** using PAGE, electrophoresis experiments are conducted to confirm the involvement of $\text{Ru}(\text{bpy})_3^{2+}$ in the self-assembly of **3** and **3'**. The hybridization of **3** to **3'** generates extended networks with no electrophoretic mobility, however, addition of **3** to **3'** in the excess (i.e. molar ratio of 10:1) results in the formation of a single discrete structure of relatively higher electrophoretic mobility (Figure 6.10, lane 2). This assembly has been assigned to a star-like tetrameric construct **10**, made up of a single unit of **3'** and three units of **3**, in which each DNA arm of **3'** is capped with a single unit of **3**. In the presence of $\text{Ru}(\text{bpy})_3^{2+}$, hybridization of **3** to **3'** in the same excess of 10:1 generates a second discrete product assigned to a tetrameric assembly of four building blocks (i.e. two **3** and two **3'**) capped with two units of **3** (i.e. "capped" **7**). As expected, this capped tetrameric assembly is in fact retarded in mobility when compared to tetramer **5**. The fact that a *single other* band is generated in the presence of $\text{Ru}(\text{bpy})_3^{2+}$ confirms its role in re-directing the self-assembly of **3** to **3'** to generate a single construct (i.e. tetramer **7**), in a manner similar to that in which it re-directs the self-assembly of **2** and **2'** to generate a single assembly quantitatively (i.e. tetramer **5**).

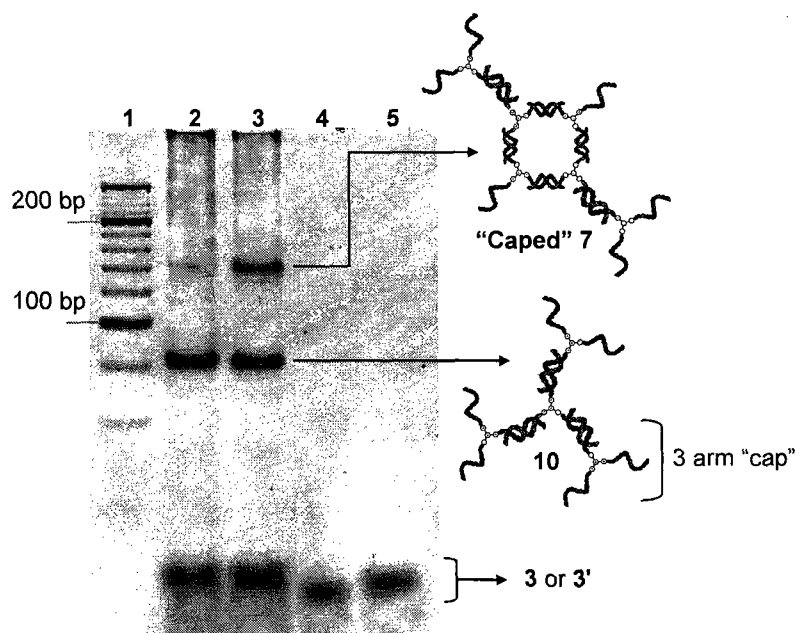


Figure 6.10 Hybridization of excess **3'** to **3**. The addition of **3'** to **3** in a 10 fold excess (at 25°C) results in a single discrete product of relatively high electrophoretic mobility that has been assigned to a star-like tetrameric construct in which each DNA arm of **3** is capped with a single unit of **3'** (lane 2). The same self-assembly in the presence of the small molecule $\text{Ru}(\text{bpy})_3^{2+}$ generates an additional discrete band assigned to a tetrameric square capped with two additional units of **3'** (lane 3). Lanes 4 and 5 contains **3** and **3'**, respectively, while lane 1 contains the 20 base pair linear molecular weight DNA ladder.

AFM analysis of the assemblies generated from **3** and **3'** in the presence of $\text{Ru}(\text{bpy})_3^{2+}$ reveal formation of well-defined structures that are quite different from the ill-defined networks generated from **3** and **3'** alone, and provide conclusive evidence for the formation of the predicted DNA ladder assemblies (Figure 6.13). Highly-extended DNA filaments of relatively large dimensions are observed throughout the entire surface. Unlike the ill-defined networks generated from the assembly of **3** and **3'**, these architectures are almost 100 nm in height (Figure 6.14). These filaments appear to result from the inter-wrapping of the one dimensional DNA ladders that are initially generated from the assembly of **3** to **3'**, in a manner quite similar to the wrapping of multiple fibers to generate a rope. Figure 6.15 contains an AFM image of the smallest structures observed from **3** and **3'**, in the presence of $\text{Ru}(\text{bpy})_3^{2+}$, which are believed to correspond to the initially generated extended DNA ladders. Cross-sectional analysis of these features reveal their height to be around 2 nm (Figure 6.15), while control experiments confirm that these assemblies are simply a consequence of the interaction of $\text{Ru}(\text{bpy})_3^{2+}$ with just **3** or **3'** (Figure 6.17).

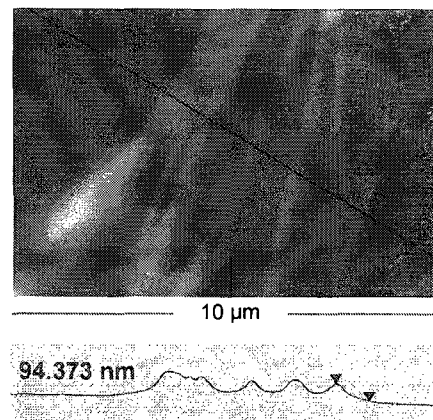


Figure 6.14 Cross sectional analysis of the large fibers generated from **3** and **3'** in the presence of $\text{Ru}(\text{bpy})_3^{2+}$.

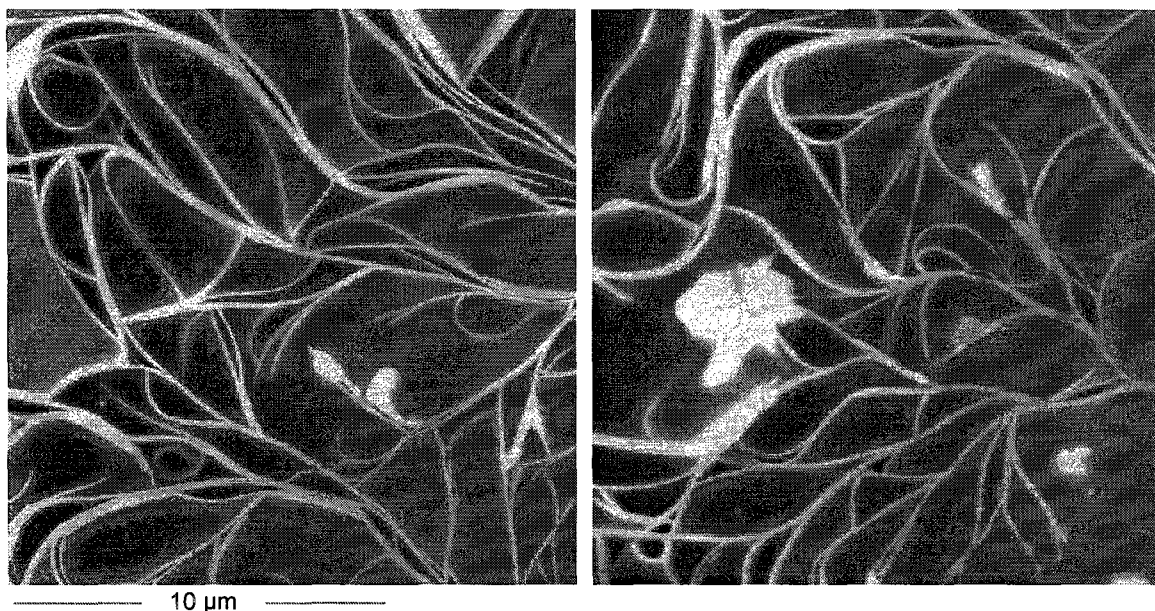


Figure 6.13 AFM analysis of the assemblies generated from **3** and **3'** with $\text{Ru}(\text{bpy})_3^{2+}$. AFM analysis of the assemblies generated from **3** and **3'** using $\text{Ru}(\text{bpy})_3^{2+}$ reveal the formation of one-dimensional DNA fibers.

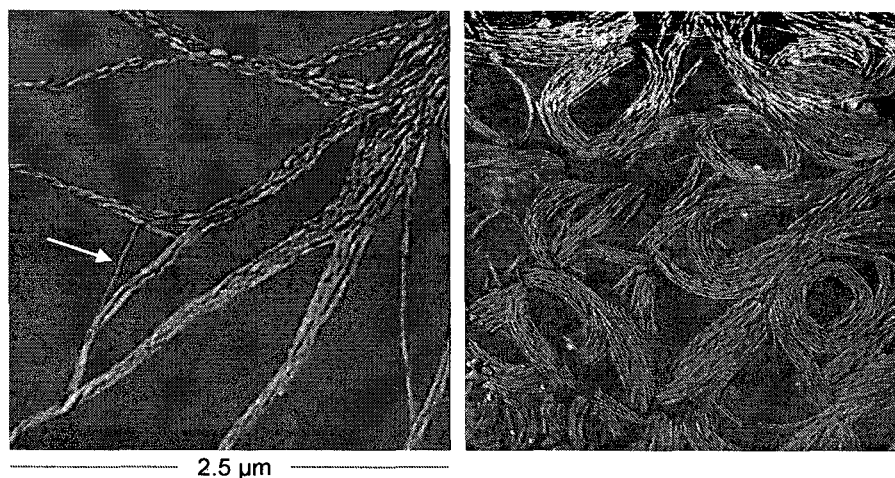


Figure 6.15 Finest structures observed following the hybridization of **3** and **3'** with $\text{Ru}(\text{bpy})_3^{2+}$. In all three examples, the left images correspond to the height, while the right images correspond to their respective phase.

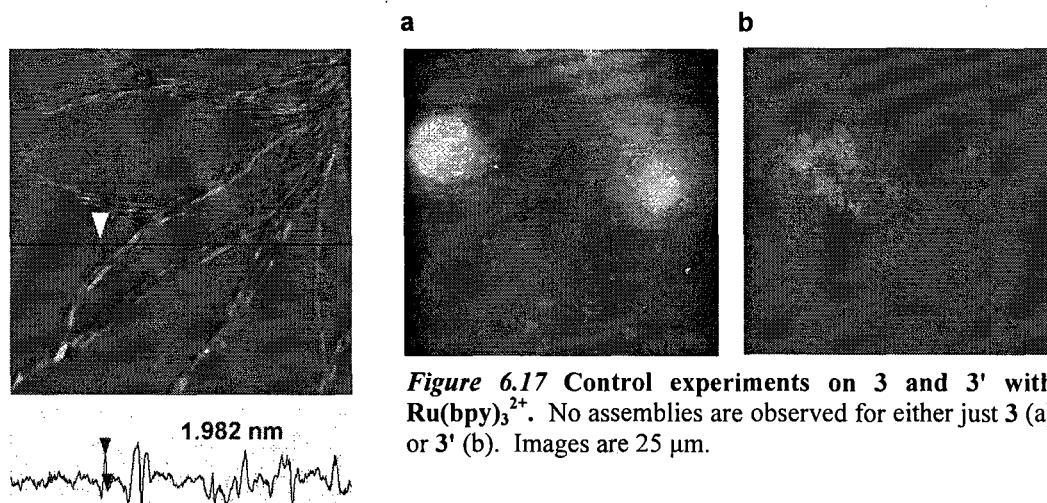


Figure 6.16 Cross sectional analysis of the small fibers generated from **3** and **3'** in the presence of $\text{Ru}(\text{bpy})_3^{2+}$.

Figure 6.17 Control experiments on **3** and **3'** with $\text{Ru}(\text{bpy})_3^{2+}$. No assemblies are observed for either just **3** (a) or **3'** (b). Images are 25 μm .

Assemblies can also be conducted using building blocks **3** and **2'** in the presence of $\text{Ru}(\text{bpy})_3^{2+}$. As seen in Figure 6.18a, in the presence of $\text{Ru}(\text{bpy})_3^{2+}$ these two building blocks assemble into tetramers that contain two single-stranded DNA overhangs that then assemble into diamond-shaped ladders. Unlike the smooth-sided ladders generated from **3** and **3'**, these diamond-shaped ladders are expected to pack into structures that cannot as easily phase shift, and that are thus relatively more rigid. This is indeed observed using AFM analysis (Figure 6.18b).

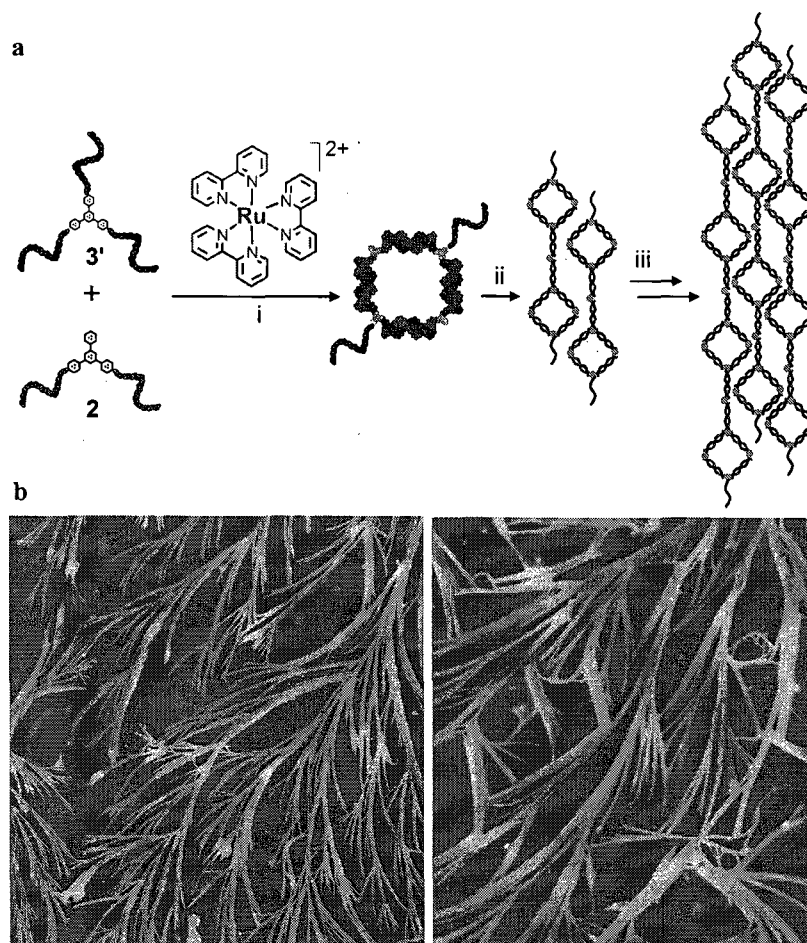


Figure 6.18 Diamond shaped ladders. (a) Assembly of 2 and 3', in the presence of $\text{Ru}(\text{bpy})_3^{2+}$, generates a tetrameric construct (i), which further grows in one dimension (ii) to generate diamond shaped ladders (iii). (b) AFM analysis reveals well-defined, rigid, one-dimensional DNA fibers. Images are 50 μm .

6.3 Conclusions

We have shown that the addition of a small molecule template can be used to quantitatively generate a single DNA nanostructure from a set of building blocks that otherwise results in a library of products. This approach allows for the incorporation of symmetry to construct more complex systems, and presents the immediate advantage of autocorrecting errors that may form during the self-assembly process. We applied this concept to predictably generate well-defined DNA fibers that periodically extend over tens of micrometers. The ability to access a single assembly from a library of possible combinations through the simple use of a small molecule introduces an additional level of control in DNA construction. Considering the wealth of DNA-binding molecules which can tune, modify, and correct the assembly of DNA structures, this approach promises to lead to significant advances in the field of DNA nanotechnology.

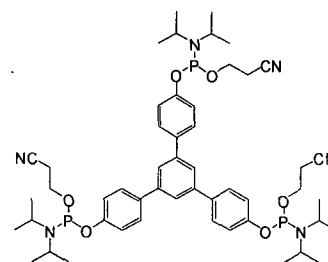
6.4 Experimental

General. Tris(2,2'-bipyridyl)dichlororuthenium(II) hexahydrate, 1,3,5-tris(4-hydroxyphenyl)benzene **1**, tris(hydroxymethyl)aminomethane (Tris), boric acid, acetic acid, ethylenediaminetetraacetic acid, NaCl, $\text{MgCl}_2 \cdot 6\text{H}_2\text{O}$, StainsAll[®], and formamide are used as purchased from Aldrich. 500Å LCAA-CPG solid support with a loading density of 85 $\mu\text{mol/g}$, 1000Å LCAA-CPG solid support with a loading density of 30 $\mu\text{mol/g}$, 2000Å LCAA-CPG solid support with a loading density of 5 $\mu\text{mol/g}$, and reagents used for automated DNA synthesis are purchased from ChemGenes. Sephadex G-25 (super fine DNA grade), and Mung Bean Nuclease (source: Mung Bean Sprouts) are purchased from Amersham Biosciences. O'Range Ruler[™] 20 base-pair molecular weight DNA ladder (0.1 $\mu\text{g}/\mu\text{L}$) is purchased from Fermentas Life Sciences. Microcon[®] size-exclusion centrifugal filter devices are purchased from Millipore. RubyRed mica sheets for atomic force microscopy are purchased from Electron Microscopy Sciences, while etched silicon cantilevers (OMCL-AC160TS) for imaging are used as purchased from Olympus.

Instrumentation. Standard automated oligonucleotide solid-phase syntheses are performed on a Perspective Biosystems Expedite 8900 DNA synthesizer. UV/vis quantifications are conducted on a Varian Cary 300 biospectrophotometer. Gel electrophoresis experiments are carried out on an acrylamide vertical Hoefer 600 electrophoresis unit. Temperature cycling experiments are performed on a Flexigene Techne 60 well thermocycler. Electroelutions are performed using a Centrilutor[®] electroeluter from Millipore. ¹H-NMR is obtained using a Mercury 400MHz NMR spectrometer. ¹³C-NMR is obtained using a Mercury 300MHz NMR spectrometer. ³¹P-NMR spectra are obtained using a Gemini 200MHz NMR spectrometer. High-resolution electrospray ionization mass spectrometry (ESI-MS) measurements are conducted on an IonSpec 7.0 Tesla FTMS instrument (Lake Forest, CA) equipped with a Zspray source from Waters Corporation. Matrix assisted laser desorption time-of-flight mass spectrometry experiments are performed on a KOMPACT MALDI III mass spectrometer. AFM images are either acquired on a Digital Instruments "Dimension 3100" or on an E-scope microscope (Santa Barbara, CA).

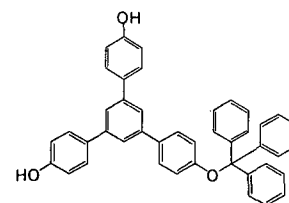
Synthesis of the tris-amidite Derivative of 1. The tris-phosphoramidite derivative of 1,3,5-tris(4-hydroxyphenyl)benzene **1** is prepared in 95% yield according to a procedure reported by Sleiman and co-workers. Briefly, **1** (50 mg, 0.14 mmol) and dimethylaminopyridine (5 mg, 0.042 mmol) are dried under vacuum for 12 hours. 15.0 mL of dry THF, diisopropylethylamine (0.25 mL, 1.4 mmol) and 2-cyanoethyl diisopropylchlorophosphoramidite chloride (0.19 mL, 0.84 mmol) are

added. The mixture is stirred for an additional 30 minutes or until the reaction is complete as monitored by TLC. The THF is removed in vacuo and the yellowish crude precipitate is purified on a silica gel column by elution with dichloromethane:hexanes:triethylamine (30:66:4) (R_f 0.8). ^1H -NMR (CD_2Cl_2 , 400MHz): δ 7.71 (t, 3H, ArH, $J=8.0\text{Hz}$), 7.65 (t, 6H, ArH, $J=8.0\text{Hz}$), 7.17 (t, 6H, ArH, $J=8.0\text{Hz}$), 3.95 (m, 6H, OCH_2), 3.76 (m, 6H, NCH), 2.70 (m, 6H, CH_2CN), 1.10-1.30 (m, 36H, CH_3) ppm; ^{31}P -NMR (CD_2Cl_2 , 200MHz): δ 147.70 ppm; ^{13}C -NMR (CD_2Cl_2 , 300MHz): δ 154.5, 141.9, 135.6, 128.5, 124.2, 20.5, 118.0, 59.3, 44.0, 24.8, 24.5, 20.7 ppm; High-Resolution ESI-MS [m/z]: calculated 955.45465, found 955.45642.

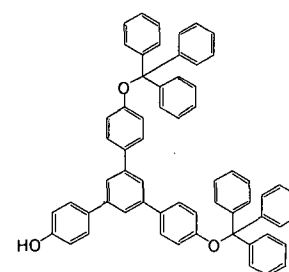


tris-amidite derivative
of 1

Synthesis of mono- and bis-trityl protected derivatives of 1. The mono- and bis-trityl protected derivatives of 1 are simultaneously synthesized. Addition of the protecting group trityl chloride to 1 results in the statistical generation of a mixture of products that contain the tris-, bis-, mono- or un-protected derivatives of 1. The relative amount of each depends on the initial ratio of trityl chloride to 1 used. A ratio of 1.5:1 provides access to the mono- and bis-protected trityl derivatives in an approximate 1:1 molar ratio, and in an overall combined yield of 70%. 1 (50 mg, 0.14 mmol), dimethylaminopyridine (5.1 mg, 0.042 mmol) and trityl chloride (59 mg, 0.21 mmol) are dissolved in 20 mL of dry THF. Diisopropylethylamine (0.25 mL, 1.4 mmol) is then added dropwise, and the mixture is allowed to stir under an atmosphere of argon for an additional hour. After the THF is removed in vacuo, the mono- and bis-protected derivatives are purified from the yellowish crude precipitate on a silica gel column by elution with dichloromethane:triethylamine:methanol (91:4:5) (R_f of the mono-protected derivative is 0.35, R_f of the bis-protected derivative is 0.70). The mono-protected derivative is obtained as a white solid in 32% yield. ^1H -NMR (CD_2Cl_2 , 400MHz): δ 11.70(s, 2H, OH), 7.58 (s, 1H, ArH), 7.42-7.56 (d, 8H, ArH), 7.20-7.40 (m, 15H, TrH), 6.79 (d, 2H, ArH) ppm; ^{13}C -NMR (CD_2Cl_2 , 300MHz): δ 157.8, 156.1, 144.3, 142.2, 141.5, 135.4, 132.3, 129.0, 128.2, 128.0, 127.5, 123.4, 123.2, 121.0, 116.2, 90.4 ppm; High-Resolution ESI-MS [m/z]: calculated 595.22842, found 595.22677. The bis-protected derivative is obtained as an off-white



mono-trityl protected
derivative of 1

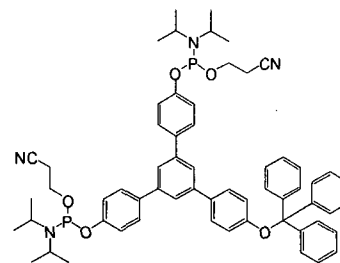


bis-trityl protected
derivative of 1

solid in 39% yield. $^1\text{H-NMR}$ (CD_2Cl_2 , 400MHz): δ 7.42-7.56 (m, 9H, ArH), 7.22-7.38 (m, 30H, TrH), 6.93 (d, 2H, ArH), 6.81 (d, 4H, ArH) ppm; $^{13}\text{C-NMR}$ (CD_2Cl_2 , 300MHz): δ 156.8, 156.2, 144.3, 141.9, 141.6, 134.1, 129.0, 128.9, 128.0, 127.5, 127.3, 127.1, 123.6, 123.5, 121.0, 115.9, 89.2 ppm; High-Resolution ESI-MS $[m/z]$: calculated 837.33867, found 837.33742.

Synthesis of bis-amidite mono-trityl protected derivative of 1. The bis-amidite mono-trityl protected derivative of **1** is synthesized in a 90% yield by converting the hydroxyl groups in the previously synthesized mono-trityl protected derivative of **1** into

an amidite. Mono-trityl derivative of **1** (100 mg, 0.17 mmol) and dimethylaminopyridine (0.61 mg, 0.051 mmol) are dried under vacuum for 12 hours. 15.0 mL of dry THF, diisopropylethylamine (0.29 mL, 1.7 mmol) and 2-cyanoethyl diisopropylchlorophosphoramidite chloride (0.15 mL, 0.68 mmol) are added, and the mixture is left stirring for 30 minutes or until the reaction is complete as monitored by TLC. After the

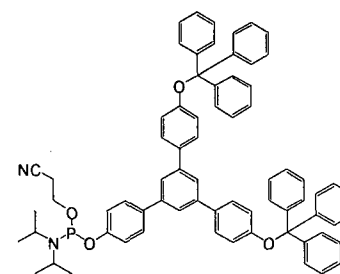


bis-amidite mono-trityl protected derivative of **1**

THF is removed in vacuo, the yellowish crude precipitate is purified on a silica gel column by elution with dichloromethane:hexanes:triethylamine (40:56:4) (R_f 0.8). $^1\text{H-NMR}$ (CD_2Cl_2 , 400MHz): δ 7.46-7.74 (m, 9H, ArH), 7.20-7.40 (m, 15, TrH), 7.15 (d, 4H, ArH, $J=8.4\text{Hz}$), 6.84 (d, 2H, ArH, $J=8.4\text{Hz}$), 3.68-4.48 (m, 8H, OCH_2 and NCH), 2.74-2.84 (m, 4H, CH_2CN), 1.17-1.47 [m, 24H, $\text{NCH}(\text{CH}_3)_2$] ppm; $^{31}\text{P-NMR}$ (CD_2Cl_2 , 200MHz): δ 147.68 ppm; $^{13}\text{C-NMR}$ (CD_2Cl_2 , 300MHz): δ 156.2, 144.3, 141.6, 134.0, 129.0, 128.9, 128.4, 128.2, 128.1, 128.0, 127.5, 127.3, 127.1, 123.8, 120.9, 120.4, 120.3, 90.4, 59.3, 44.0, 24.6, 24.5, 20.6 ppm; High-Resolution ESI-MS $[m/z]$: calculated 1039.45939, found 1039.45982.

Synthesis of Mono-amidite bis-trityl protected derivative of 1.

The mono-amidite bis-trityl protected derivative of **1** is synthesized in 85% yield by converting the hydroxyl group of the bis-trityl protected derivative of **1** into an amidite. bis-trityl derivative of **1** (100 mg, 0.12 mmol) and dimethylaminopyridine (4.4 mg, 0.036 mmol) are dried under vacuum for 12 hours. 15.0 mL of dry THF, diisopropylethylamine (0.21 mL, 1.2 mmol) and 2-cyanoethyl diisopropylchlorophosphoramidite chloride (0.053



mono-amidite bis-trityl protected derivative of **1**

mL, 0.24 mmol) are added, and the mixture is left stirring at room temperature for 30 minutes or until the reaction is complete as monitored by TLC. After the THF is removed in vacuo, the

yellowish crude precipitate is purified on a silica gel column by elution with dichloromethane:hexanes:triethylamine (40:56:4) (R_f 0.75). $^1\text{H-NMR}$ (CD_2Cl_2 , 400MHz): δ 7.40-7.60 (m, 9H, ArH), 7.13 (d, 2H, ArH, $J=7.6\text{Hz}$), 6.80 (d, 4H, ArH, $J=7.6\text{Hz}$), 3.95 (m, 2H, OCH_2), 3.78 (m, 2H, NCH), 2.70 (t, 2H, CH_2CN , $J=6.4\text{Hz}$), 1.22-1.27 [m, 6H, CH_3] ppm; $^{31}\text{P-NMR}$ (CD_2Cl_2 , 200MHz): δ 147.69 ppm; High-Resolution ESI-MS [m/z]: calculated 997.45982, found 997.45812.

Synthesis of 2, 2', 3 and 3'. For the first approach, 500Å LCAA-CPG solid-support with a loading density of 85 $\mu\text{mol/g}$ is used, and the tris-amidite derivative of vertex **1** is added in a 1.5 molar ratio to the CPG (extended coupling 10 mins). For the second approach, 2000Å LCAA-CPG solid support with a loading density of 5 $\mu\text{mol/g}$ is used, and the bis-amidite mono-trityl protected derivative of vertex **1** is added in a 5 molar ratio to the CPG (extended coupling 10 mins). For the third approach, 1000Å LCAA-CPG solid-support with a loading density of 30 $\mu\text{mol/g}$ is used, and the mono-amidite bis-trityl protected derivative of vertex **1** is added in a 10 molar ratio to the CPG (extended coupling 10 mins). DNA synthesis is conducted using standard oligonucleotide synthetic protocols. In all cases, the resulting strands are cleaved and deprotected in concentrated ammonium hydroxide (12 hrs, 55°C). The DNA is purified on 24% polyacrylamide 7M urea gels (up to 20 AU_{260} of crude DNA per gel; 10 mA, 6-7 hrs, pH 8.3). The bands corresponding to the desired products are excised, extracted in 3 mL of sterile water (37°C, 16 hrs), and desalted using Sephadex G-25 size exclusion chromatography. Quantification is carried out by UV/vis analysis, using Beer's law ($A_{\text{total}} = A_{\text{vertex}} + A_{\text{DNA}}$), in which the extinction coefficient of the vertex at 260 nm is calculated to be $2.30 \times 10^5 \text{ L mol}^{-1} \text{ cm}^{-1}$.




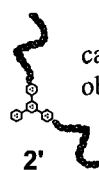
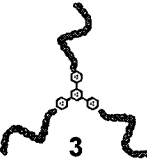
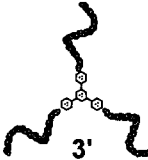
Matrix assisted laser desorption ionization time-of-flight mass spectrometry (MALDI-TOF MS) measurements are used to characterize **2**, **2'**, **3** and **3'** (along with the mono-conjugated derivatives). The matrix is prepared according to a procedure reported by Allison and co-workers. The theoretically calculated and the experimentally obtained molecular weights of **2**, **2'**, **3** and **3'** (along with the mono-conjugated derivatives) are reported in Table 6.1.

Hybridizations in absence of $\text{Ru}(\text{bpy})_3^{2+}$. Generally, initial sample preparation involves the drying down of 0.03 ODs of each building block (i.e. **2** and **2'** separately), and their subsequent dissolution in 10 μL of TAEmg buffer (40 mM Tris, 20 mM acetic acid, 2 mM $\text{EDTA} \cdot 2\text{Na} \cdot 2\text{H}_2\text{O}$, 12.5 mM $\text{MgCl}_2 \cdot 6\text{H}_2\text{O}$). The two solutions are then hybridized using one of the four protocols outlined in section 6.2.

Table 6.1 Sequences and molar masses of branched DNA conjugates.

The 17 base DNA sequence used for building blocks **2** and **3** is 5' – CGATC TTGTGGCATTGG – 3' (i.e. red DNA strand), while its complement 2' and 3' (i.e. blue DNA strand) is 5' – CCAATGCCACAAGATCG – 3'.

Calculated / experimentally obtained molar masses

 <p>cal. 6,077.9 exp. 6,080.7</p> <p>Mono-conjugated</p>	 <p>cal. 5,994.0 exp. 5,998.2</p> <p>Mono-conjugated</p>
 <p>cal. 11,561.9 exp. 11,560.9</p> <p>2</p>	 <p>cal. 11,394.0 obs. 11,433.3 [M+K⁺]</p> <p>2'</p>
 <p>cal. 17,045.9 exp. 17,040.6</p> <p>3</p>	 <p>cal. 16,794.0 obs. 16,792.1</p> <p>3'</p>

Hybridizations in presence of $Ru(bpy)_3^{2+}$. Generally, hybridizations in the presence of $Ru(bpy)_3^{2+}$ are performed by adding 4 μ L of a $Ru(bpy)_3^{2+}$ (10 mM in water) to one of the building blocks, followed by their subsequent hybridization as per the specified hybridization protocol.

Enzymatic digestions. In an attempt to ensure that the enzyme is active on DNA to which our vertex is attached, and to find the optimal conditions under which single-stranded DNA is preferentially digested, the double and single-stranded version of the mono-conjugated building blocks are subjected to varying amounts of MBN. Digestions are performed in 10 μ L of TAE buffer, at 0°C, for 3 hours. In all cases, 1.2×10^{-10} moles of the double and single-stranded DNA building blocks are subjected to 6, 12, 24 and 36 units of the enzyme. The addition of 36 units of MBN results in the selective and complete digestion of the single-stranded species with very little effect to the double stranded analogue (Figure 6.19).

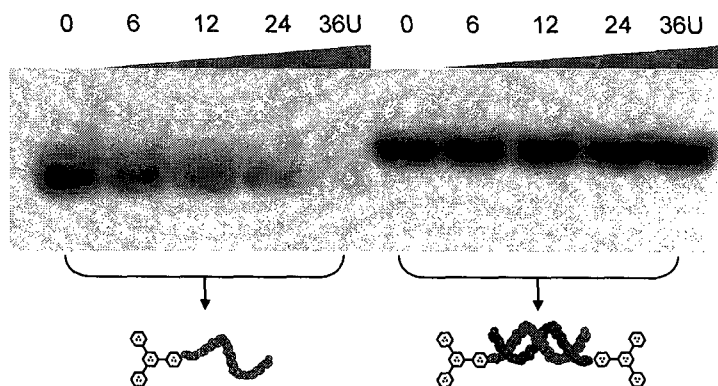


Figure 6.19 Protocol for the selective digestion of single-stranded DNA. Enzymatic digestion study determining that the use of 36 U of MBN, at 0°C and 3 hrs, is selective for single strand digestion.

AFM sample preparation and analysis. AFM sample preparation generally involves the deposition of 10 μ L of the self-assembled mixture (concentration of 10 pM) onto freshly cleaved mica (dimensions of 2.5 X 2.5 cm), followed by adequate evaporation to achieve complete dryness (typically 30 minutes in a fumehood). Whenever possible, imaging is conducted within 24 hours in order to minimize time-dependant sample degradation. AFM images are acquired in air, and at room temperature. “Tapping mode” (i.e. intermittent contact imaging) is performed at a scan rate of 1 Hz using etched silicon cantilevers with a resonance frequency of \sim 300 kHz, a spring constant of \sim 42 N/m, and a tip radius of $<$ 10 nm. All images are acquired with medium tip oscillation damping (20-30%.)

$$\text{N.B. \% oscillation damping} = \frac{(\text{free air amplitude} - \text{imaging setpoint amplitude})}{\text{free air amplitude}} \times 100$$

Guest-mediated reprogramming of the self-assembly outcome of unmodified DNA

Faisal A. Aldaye, Pik Kwan Lo, and Hanadi F. Sleiman, *manuscript in preparation*.

Naturally occurring guanine quadruplexes are found at the ends of telomeres, and are indirectly responsible for decreasing the activity of an enzyme involved in over 80% of all cancers.¹²⁶ Higher-order DNA helices have always been of interest to biologists, but are now attracting the attention of researchers in DNA nanotechnology. For example, Norden and co-workers utilized the naturally occurring triplex forming interaction between DNA strands to construct sequence addressable DNA nanostructures.¹²⁷ If the potential of higher-order DNA assemblies as a new parameter in DNA nanotechnology is to be systematically studied, then access to such DNA helices is going to be a requirement. Typically, access to non-naturally occurring higher-order DNA assemblies involves synthetically reprogramming the DNA bases. Benner and co-workers demonstrated the feasibility of synthetically redesigning the hydrogen-bonding motifs within a DNA duplex.¹²⁸ The group constructed a DNA base-pair with a hydrogen-bonding arrangement different from that of A·T and C·G, and incorporated it using DNA polymerases. Chiba, Inouye and co-workers recently reported the synthesis of a DNA duplex made up of four completely non-naturally occurring hydrogen-bonding bases.¹²⁹ A number of other examples illustrate the feasibility of not just redesigning the hydrogen-bonding motifs within DNA bases, but of completely redesigning the entire structure of the base. The groups of Kool and Schultz replaced

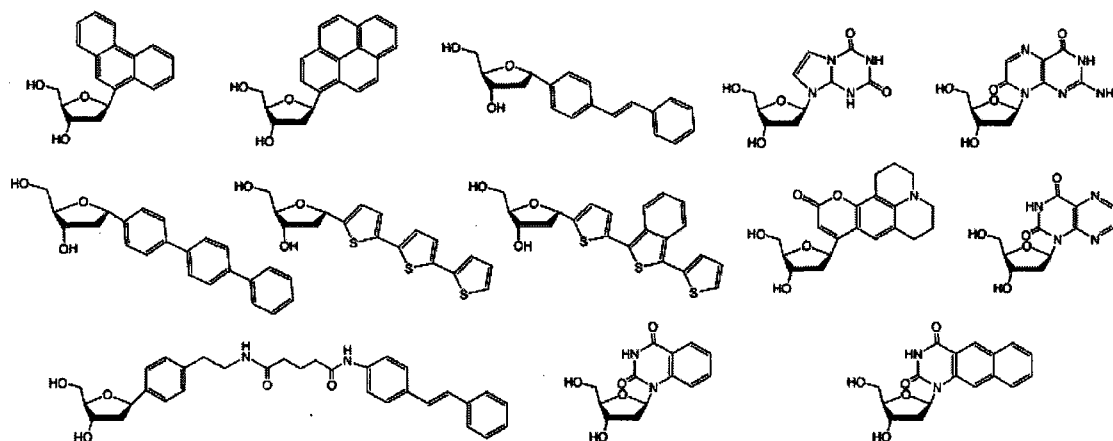


Figure 7.1 Modified DNA bases. This figure provides only a small snapshot of some of the nucleoside modifications/replacements that have been done. [Adapted from reference 131].

DNA bases within the duplexes with shape-mimics of natural bases, simple hydrocarbons, heterocycles, and fluorescent species (Figure 7.1).¹³⁰⁻¹³³ Shionoya, Carell, and co-workers replaced DNA bases with metal binding ligands, and synthesized metallated base-pairs for electrical conductivity and magnetism.^{134,135}

Since higher-order DNA helices will necessarily require for each base to simultaneously interact with more than one strand, bases with more than one bonding face will need to be synthesized and incorporated. The field of supramolecular chemistry extensively studies the assembly behavior of molecules with multiple hydrogen-bonding faces. Whitesides and co-workers assembled cyanuric acid derivatives, containing two hydrogen-bonding faces at a fixed angle of 120° , with the complementary melamine derivative molecules into hexameric rosettes (Figure 7.2a).¹³⁶ Fenniri and co-workers synthesized a class of biphasic molecules that assemble into discrete rosettes, which under the right conditions further π -stack into extended columns.^{137,138} In addition, Sessler and co-workers assembled a self-complementary dinucleotide-type molecule containing guanosine and cytosine into dimers,¹³⁹ Perrin and co-workers assembled a molecule with self-complementary thymine and adenine faces into one-dimensional tapes (Figure 7.2b),¹⁴⁰ while Zimmerman and co-workers assembled a molecule with two self-complementary thymine faces into trimers (Figure 7.2c).¹⁴¹

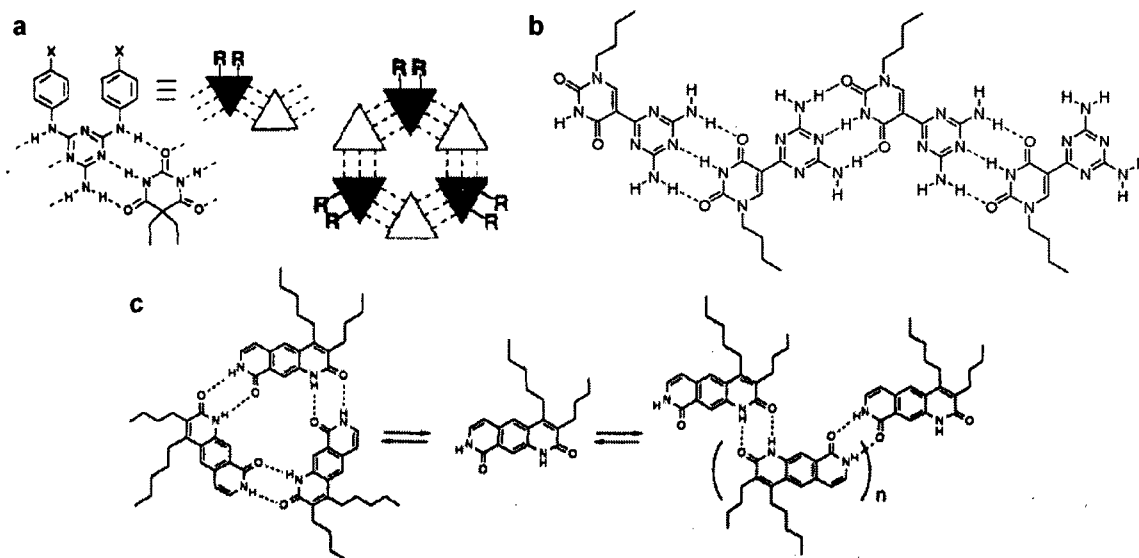


Figure 7.2 Bifacial self-assembling molecules. (a) Cyanuric acid and triaminopyrimidine type molecules assemble into hexameric rosettes. (b) Self-complementary molecule with an adenine type and a thymine type faces assembles into linear tapes. (c) Self-complementary molecule with two thymine type faces assembles into either a trimeric rosette or into linear tapes. [Adapted from references 136, 140, 141].

These selected examples illustrate the feasibility of synthetically modifying DNA bases with molecules to generate higher-order DNA helices. To date, however, only two examples have

emerged. Switzer and co-workers set out to construct a DNA pentaplex.¹⁴² The group used a simple algorithm to predict nucleobase structural requirements within a quintet motif, and synthetically incorporated *iso*-guanine nucleobases into DNA strands that assemble into pentaplexes (Figure 7.3a). Sleiman and co-workers set out to construct a DNA hexaplex.¹⁴³ The group synthesized a triaminopyrimidine-type base with two hydrogen-bonding faces oriented at an angle of 120°, along with the complementary cyanuric acid nucleoside, and assembled them into a discrete hexameric rosette (Figure 7.3b).

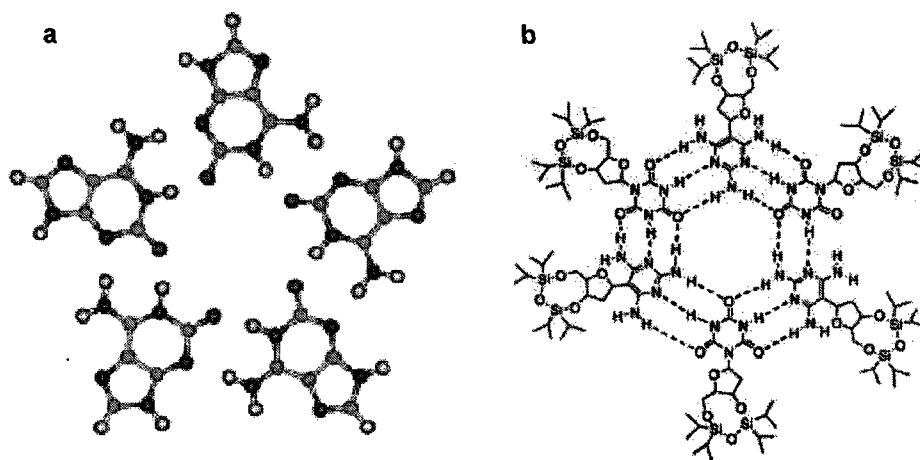
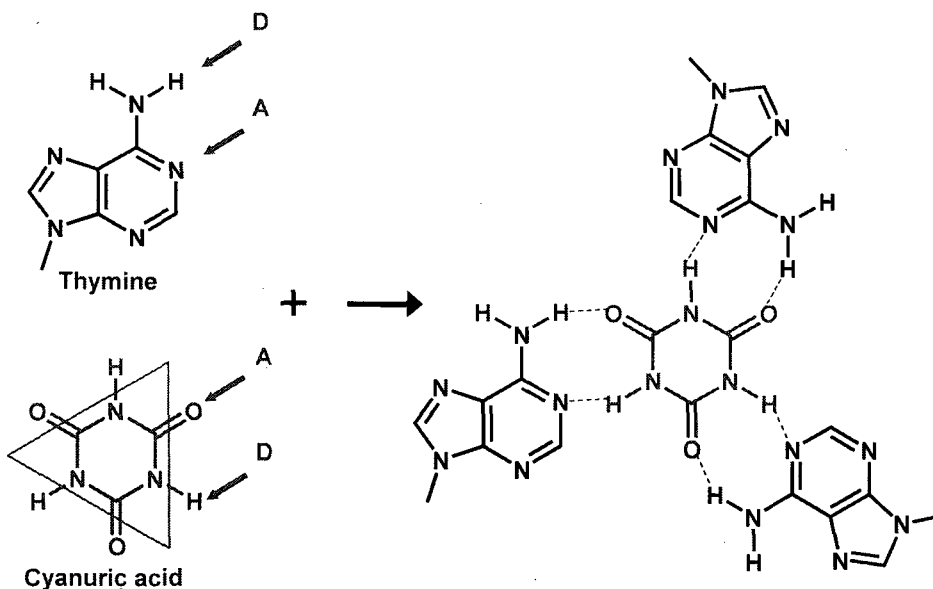


Figure 7.3 Synthetic higher order DNA assemblies. (a) *iso*-Guanines are incorporated into strands that assemble into pentaplexes, (b) while synthetic cyanuric acid and triaminopyrimidine type nucleosides assemble into hexaplexes. [Adapted from references 142, 143].

Higher-order DNA assemblies of more than two DNA strands provide an untapped wealth of potentially unique structural, physical, and chemical properties. Many areas of research will benefit from our ability to easily generate a large number of such higher-order helices, including both materials science and biology. The current difficulty lies in their synthesis; reprogramming the bases to generate a stable DNA strand can be difficult, and in some cases unattainable. In here we solve this problem by developing an approach that rationally reprograms the assembly of unmodified DNA. Instead of resynthesizing DNA bases to redesign their assembly product within DNA, we use small molecules that contain all the necessary structural information to rationally reassemble unmodified DNA into predetermined geometries and number of helices. Specifically, we set out to construct a DNA triplex. Adenine contains a single hydrogen-bonding face with a two-point donor-acceptor motif. In the presence of its complement, thymine, it assembles into a two-stranded helix. We can, in principle, reprogram adenine to assembly into triplexes if instead of using thymine, which has one complementary hydrogen-bonding face, we

use a molecule that contains three complementary thymine-type faces oriented at an angle of 120° . Cyanuric acid contains three well-defined thymine-type faces oriented at an angle of 120° , and indeed reprograms the assembly of unmodified poly-adenine into uniform DNA triple helices (Scheme 7.1). Thus this approach provides a facile and economical method to access higher-order DNA assemblies.

Scheme 7.1 Cyanuric acid mediate construction of adenine triplexes.



7.1 Results and Discussion

The feasibility of constructing a DNA triplex, in which three adenine molecules are assembled around a cyanuric acid (CA) core is initially confirmed using simple molecular modeling experiments with HyperChemTM. In principle, the three poly-adenine strands could be oriented in a parallel-parallel-parallel or a parallel-parallel-antiparallel fashion, and the resulting triplexes could be left- or right-handed. The four possible combinations are, therefore, parallel-parallel-parallel left-handed (**PPP_{left}**), parallel-parallel-parallel right-handed (**PPP_{right}**), parallel-parallel-antiparallel left-handed (**PPA_{left}**), and parallel-parallel-antiparallel right-handed (**PPA_{right}**). AMBER force-field minimizations are conducted on a discrete assembly of four bases, using the Polak-Ribiere (conjugate gradient) algorithm with a termination condition for an RMS gradient of 0.1 kcal/Åmol or 50 cycles. The left-handed parallel-parallel-parallel DNA triplex was found to be the most stable, and is thus the most likely to form. This specific helix is calculated to have a

diameter of 2.35 nm, a base to base distance of 0.51 nm, and a pitch of 16 bases. As seen in Figure 7.4, the **PPP_{left}** assembly appears to be the most uniform, and the best stacked. It is of interest to note, however, that adenine is capable of undergoing a number of different hydrogen-bonding interactions, and is not limited to only Watson-Crick or Hoogsteen bonding motifs; it is therefore conceivable that a number of other helical assemblies do exist, some of which might be even more stable.

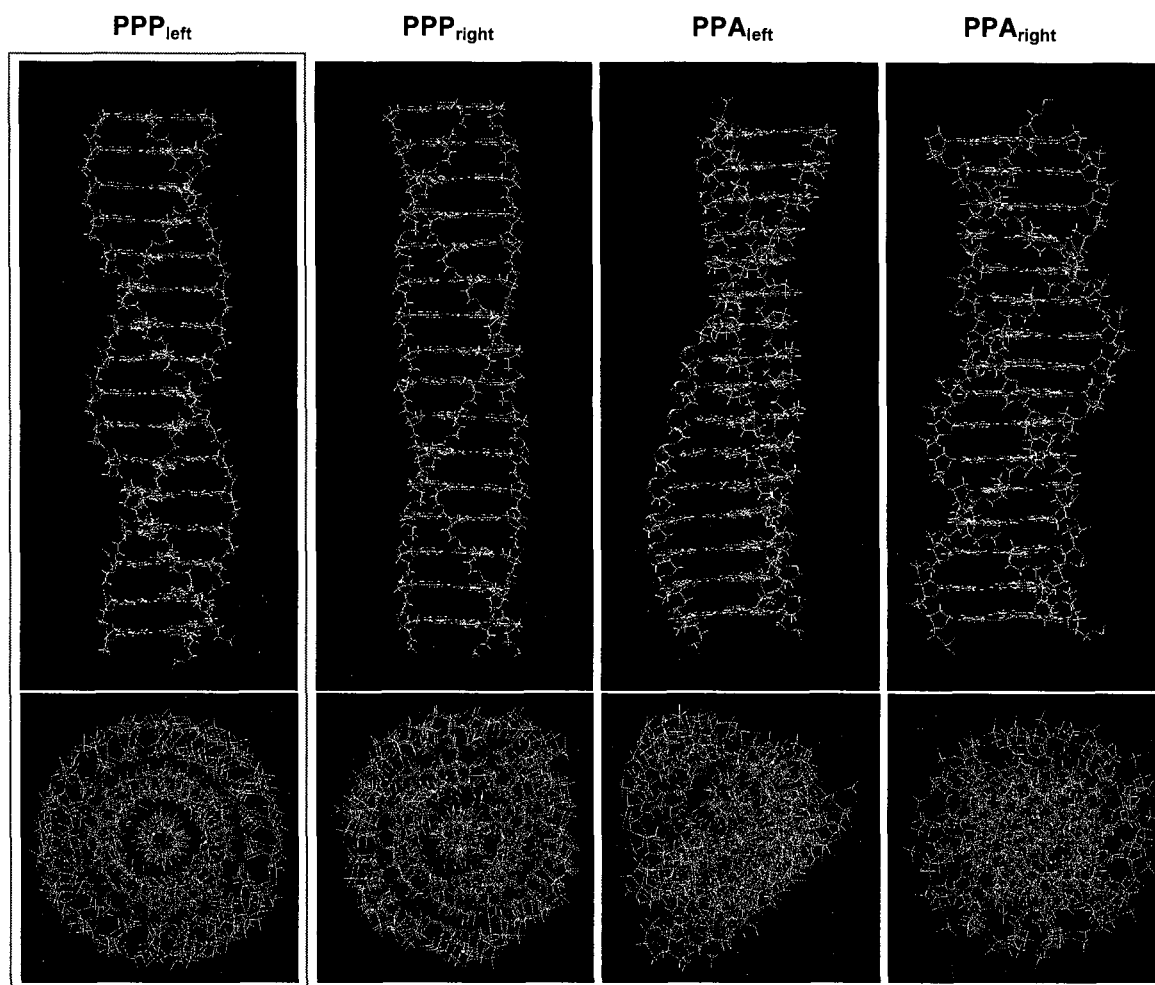


Figure 7.4 Molecular modeling of cyanuric acid mediated assembly of poly-adenine into triple helices. The four different geometries that are analyzed are **PPP_{left}**, **PPP_{right}**, **PPA_{left}** and **PPA_{right}** (left to right). The parallel-parallel-parallel left-assembly appears to be the most uniform, and the best π -stacked. Minimizations conducted on a discrete octamer indeed show **PPP_{left}** to be the most stable.

Studies are then conducted to characterize the interaction between adenines and cyanuric acid at the molecular level. Since homopolymeric poly-adenine strands are expected to phase-shift during the assembly process to produce triple-helices of different lengths, however, a discrete model system with locked poly-adenine regions is constructed to better characterize the

interactions between CA and adenine molecularly. In it, three parallel poly-adenine regions – each of which is twenty bases long – are spatially tethered into position using two double-stranded clipping duplexes (Figure 7.5a). These clipping strands are linked to each of the poly-adenine regions via a triethyloxyglycol pegylated molecule to alleviate any potential structural strain that might occur during the self-assembly process. Thermal denaturation analysis of this system reveals a melting profile with a T_m of 45°C, and a subsequent shift to 55°C upon addition of CA, in a 1:3 molar ratio of CA to adenine molecules (Figure 7.5b). Interestingly, addition of CA to an intermediate assembly containing only two poly-adenine strands (Figure 7.5c *left*), or to an assembly in which one of these strands is in an antiparallel orientation (Figure 7.5c *right*), results in little to no increase in the observed T_m . These findings indicate that the DNA triplex is indeed constructed from three poly-adenine strands oriented in a parallel fashion – as predicted by molecular modeling – which is in agreement with the previously reported synthetic *iso*-guanine DNA pentaplex that was found to also assemble in a fully parallel orientation.¹⁴²

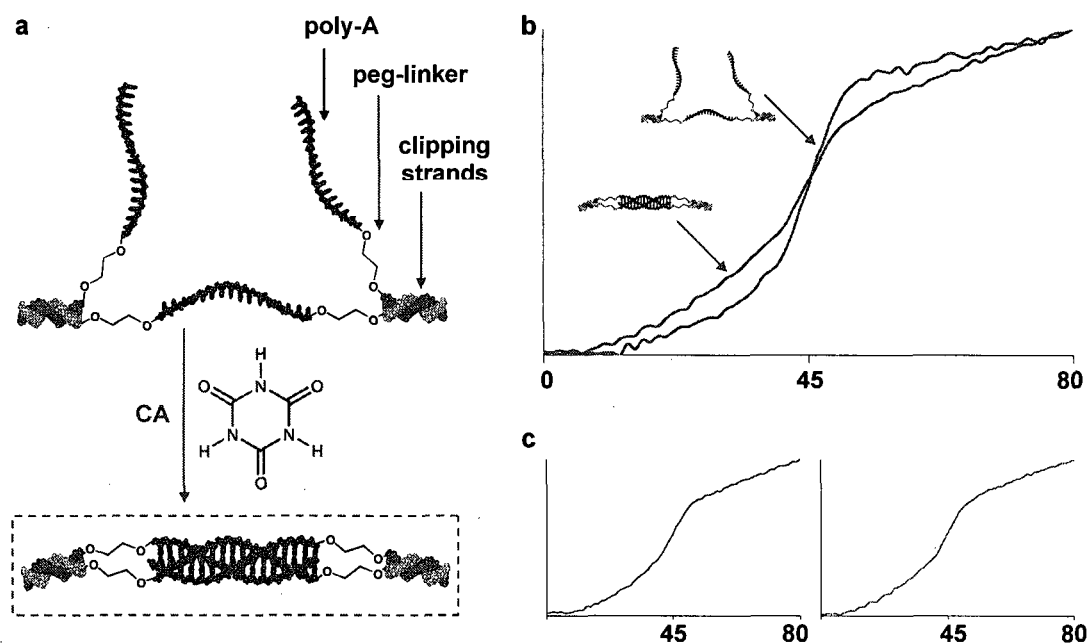


Figure 7.5 Thermal denaturation studies on a discrete poly-adenine model system. (a) Three poly-adenine strands oriented in a parallel-parallel-parallel arrangement are locked into place using two clipping strands. Polyethylene glycol linkers are incorporated to alleviate potential strain. (b) An increase in T_m is observed upon addition cyanuric acid to this model system, indicating their incorporation. (c) A considerably lower increase in T_m is observed when only two strands are titrated with cyanuric acid (*left*), or when a parallel-parallel-antiparallel assembly is used (*right*).

Circular dichroism (CD) titration experiments are conducted to confirm the interaction of each cyanuric acid molecule with three adenine bases. As seen in Figure 7.6a, a marked change

in the CD profile of the three-stranded locked model system is observed upon addition of CA. The titration of this system with increasing amounts of CA results in a gradual decrease in the CD signal at 275 (Figure 7.6b). Addition of CA in 1/9th, 1/6th and 1/3rd the molar ratio of adenines, gradually decrease the CD signal, while the addition of anymore CA results in little to no difference, even when a 50 fold excess is used (Figure 7.6c). This indicates that a single CA molecule interacts with each three adenine bases. This is further confirmed using matrix assisted laser desorption time-of-flight mass spectrometry (MALDI-TOF MS), which confirms the theoretically expected mass of this generated assembly with an experimentally obtained difference of 0.21% (Figure 7.8). Therefore, cyanuric acid is used to template the formation of an adenine triplex with a core of CA molecules.

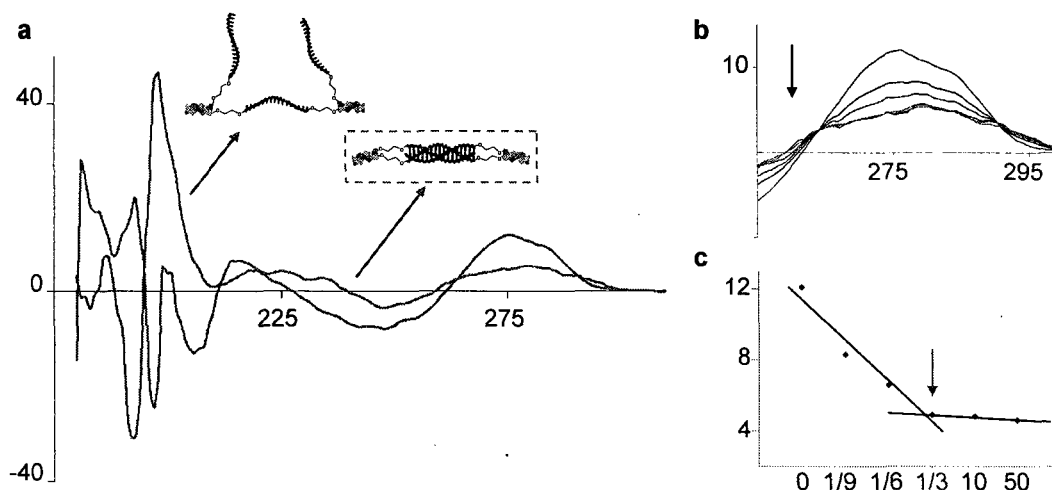


Figure 7.5 Circular dichroism characterization of the adenine triplex formed using CA. (a) A marked difference is observed in the CD profile of the poly-adenine model system upon addition of CA in the right molar ratio. (b) Titration of this system results in a gradual decrease in the observed signal at 275, (c) until a ratio of adenine/CA of 1/3 is used.

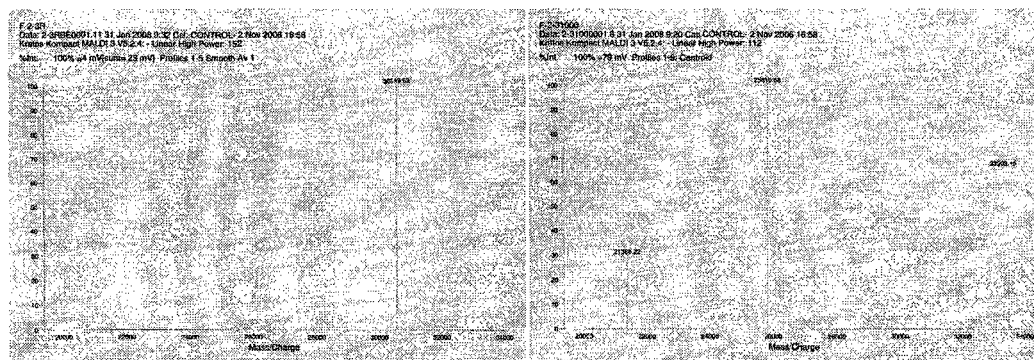


Figure 7.8 MALDI-TOF MS of discrete model system. (left) The calculated/experimental molar masses of the assembled model system are 30,652/30,550, which correspond to an error of 0.33%. (right) While the calculated/experimental values for the assembled triplex with CA molecules are 33,232/33,302, which correspond to an error of 0.21%.

With a good understanding of how CA molecularly interacts with adenine, we proceeded to examine the assembly of a number of unmodified poly-adenine DNA sequences of varying lengths, that is, A_1 - A_6 , A_8 , A_{10} , A_{15} and A_{20} . In the presence of cyanuric acid, the shorter homopolymers A_1 - A_4 assemble into discrete triplexes with a cyanuric acid core (Scheme 7.2a); this is confirmed using MALDI TOF mass spectrometry analysis. Longer homopolymers A_5 - A_{20} are capable of phase-shifting and branching during the assembly process, and are thus expected to result in larger long-range constructs (Scheme 7.2b and 7.2c). Dynamic light scattering experiments on the A_5 system confirm the

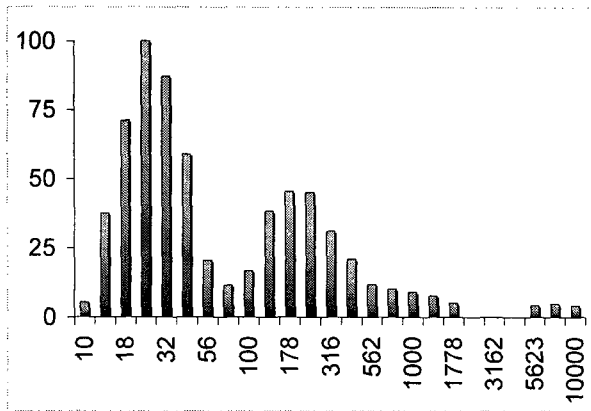
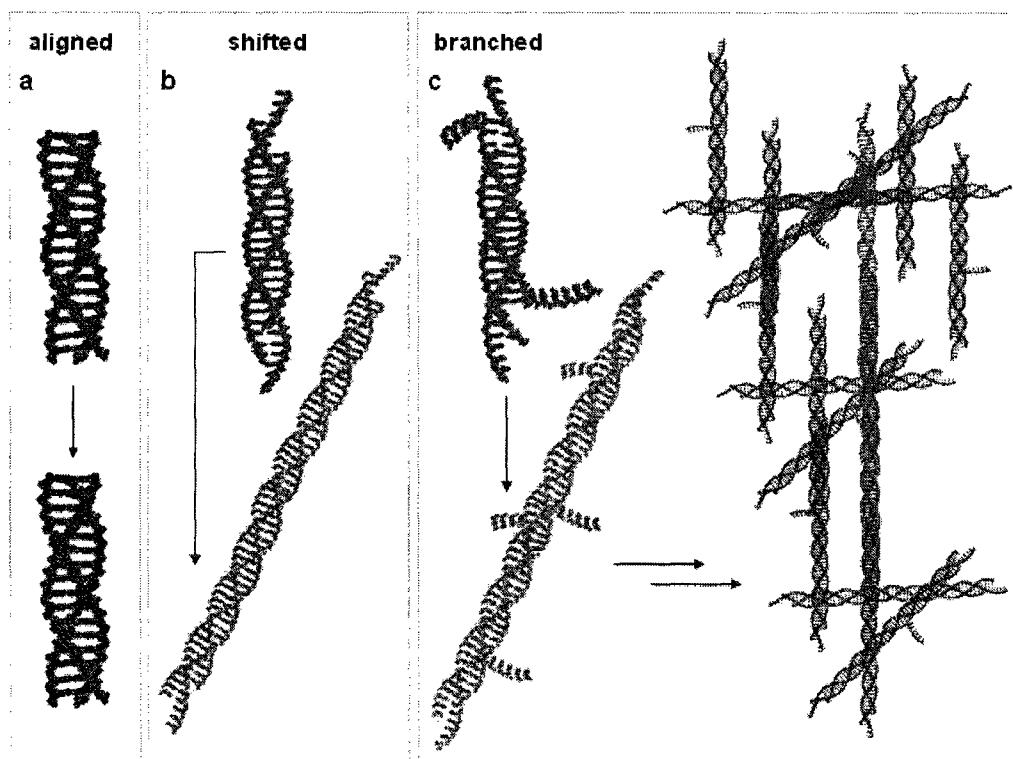


Figure 7.9 DLS analysis of A_5 and CA assemblies.

formation of such higher-order DNA assemblies in solution (Figure 7.9). Interestingly, a different size distribution is obtained when the angle of the light source is modified, indicating that these systems are not spherical. Phase-shifting within these assemblies results in extended

Scheme 7.3 length-dependant assemblies.



one-dimensional triplexes that can now be directly visualized using atomic force microscopy (AFM; Figure 7.10). Analysis of the assembled A_5 system, using AFM, reveals the formation of extended one-dimensional fibers extending over tens of microns. Cross-sectional analysis of these fibers shows them to consistently have a diameter of 2.41 nm, which is in agreement with the theoretically obtained value from our modeling experiments of 2.35 nm. These fibers are thus believed to each correspond to cyanuric acid templated DNA triple helices.

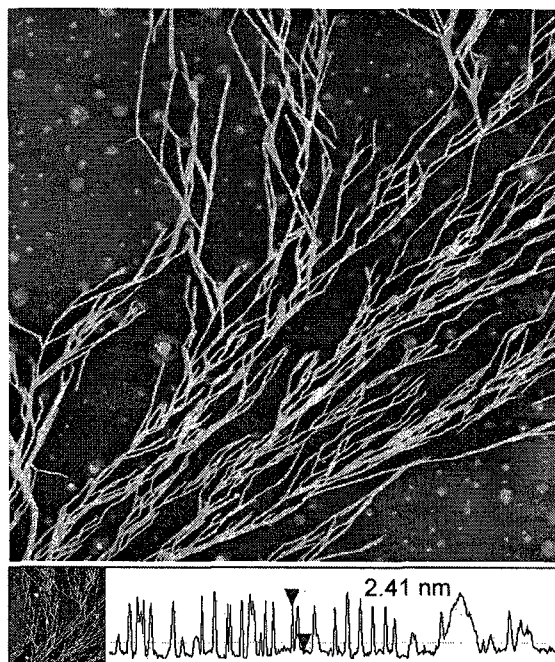


Figure 7.10 AFM analysis of the triple helices generated using A_5 and CA.

A_{1-4} assembles into small discrete triplexes (Scheme 7.3a); A_5 is capable of phase-shifting

and thus assembles into long-range one-dimensional triplexes (Scheme 7.3b; Figure 7.10); strands longer than A_5 , however, are capable of phase-shifting *and branching* and are thus expected to generate hyperbranched triplex assemblies (Scheme 7.3c; Figure 7.11). This is confirmed using a small series of poly-adenine strands that contain a relatively increasing number of bases: A_6 , A_8 , A_{10} , A_{15} , and A_{20} . A_6 indeed generates a random assembly of one-dimensional DNA fibers that are similar to those produced using A_5 , but that are also crosslinked to each other at several positions, which confirms the branching capacity of A_6 (Figure 7.11a). The propensity and degree of branching increases as the length of DNA strands increases. Assemblies using A_8 generate random fibers that crosslink even more (Figure 7.11b), while assemblies using A_{10} generate well-defined ridges in what appears to be a phase transition into an increased level of organization (Figure 7.11c). The use of even longer DNA strands results in a two-dimensional array of ribbon-like fibers in the case of A_{15} poly-adenine DNA (Figure 7.11d), and in even thicker ribbon assemblies in the case of the longer A_{20} DNA strands (Figure 7.11e). As expected, careful analysis of these ribbons using high-resolution AFM reveals them to be constructed of a large number of triplex fibers that are wrapped and inter-woven (Figure 7.12). Thus, modulating the length of the DNA strands used within the construction process provides an additional parameter to fine-tune the structure and topology of the assemblies generated, and can be used to better control the structural outcome of the material being generated.

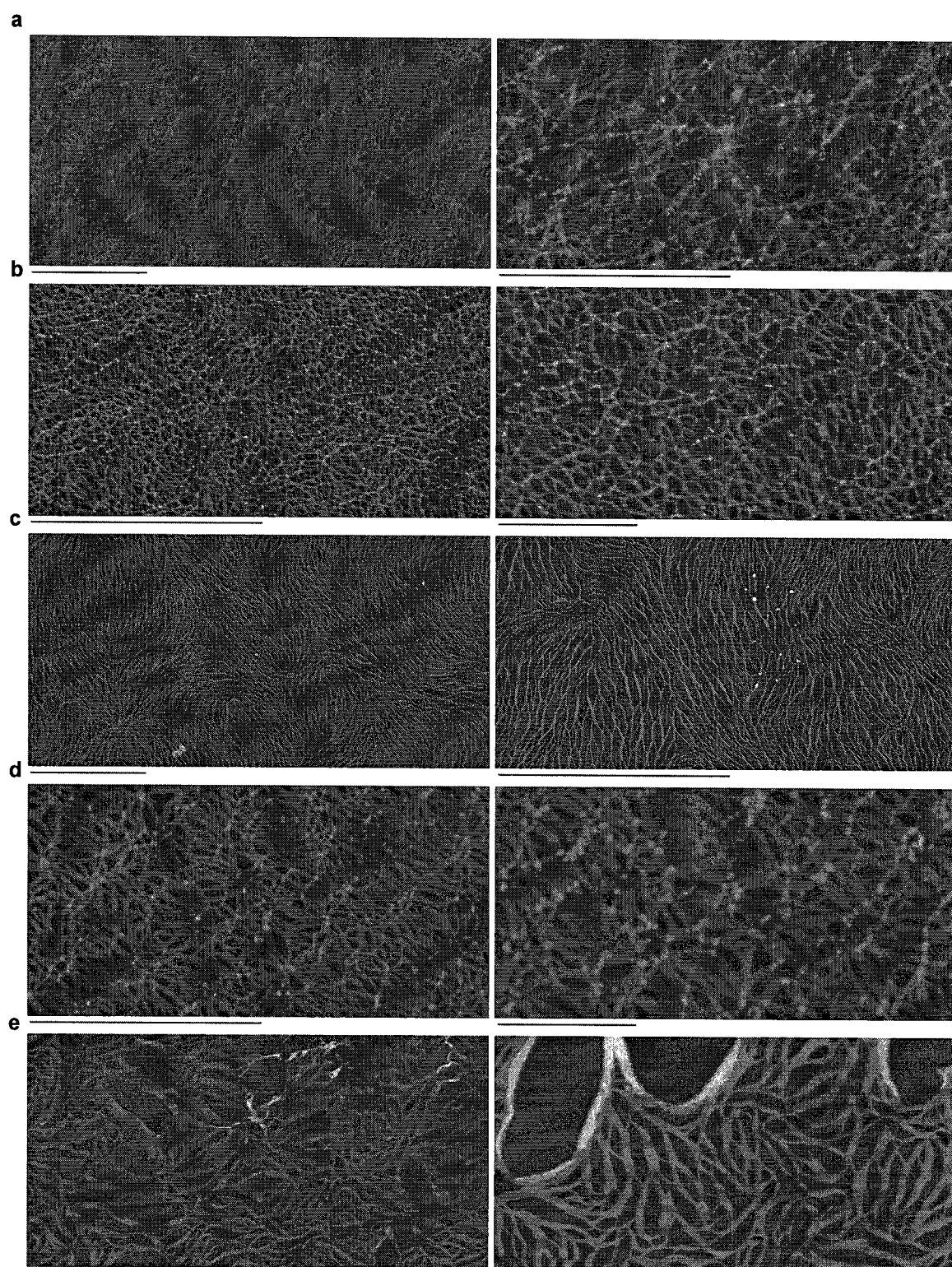


Figure 7.11 AFM analysis of assemblies generated using longer DNA strands. Assemblies are conducted using (a) A_6 , (b) A_8 , (c) A_{10} , (d) A_{15} , and (e) A_{20} . Bar corresponds to $2.5\ \mu\text{m}$.

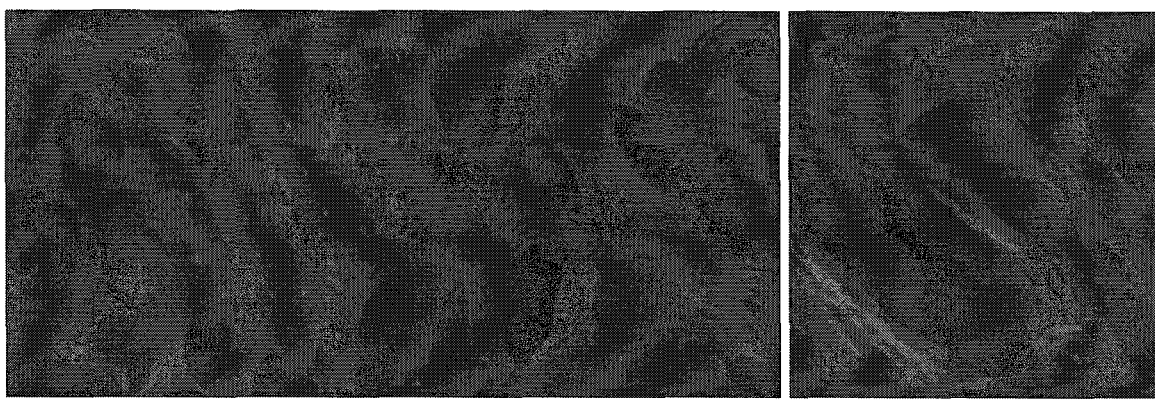


Figure 7.12 High-resolution AFM analysis of the ribbons generated using A_{20} .

To confirm that these structures are not a consequence of the self-assembly of either CA to itself, or of poly-adenine to itself, control experiments are conducted in which CA and A_{20} are individually analyzed using AFM. As seen in Figure 7.13, neither CA nor A_{20} generate any observable higher-ordered constructs, and certainly none of the extended networks observed in Figures 7.10 or 7.11.

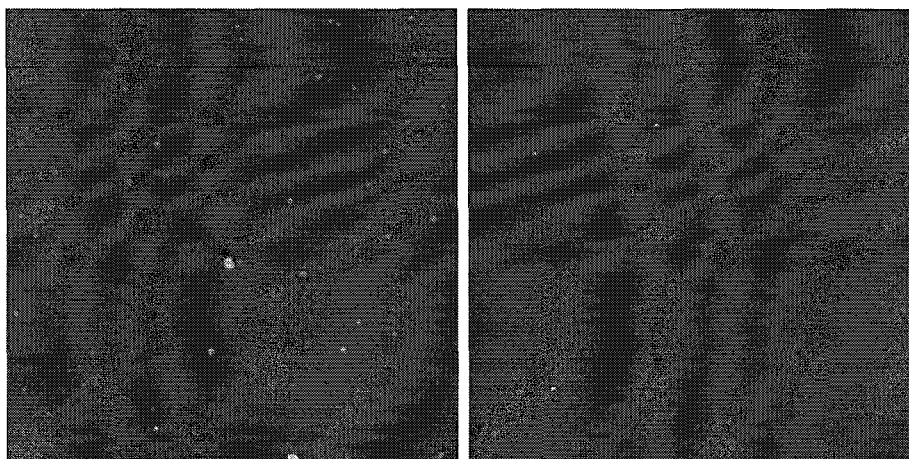


Figure 7.13 AFM analysis of CA (*left*), and A_{20} (*right*).

7.2 Conclusions

We have thus presented a new method that allows for the small molecule templated construction of higher-order DNA helices, and assembled a triple helix from unmodified DNA strands that would otherwise generate a duplex. The approach involves the use of molecule that contain all the necessary structural information to reprogram the assembly outcome of unmodified DNA,

that is, the correct number of complementary hydrogen bonding faces oriented at specific angles. Considering the wealth of molecules containing base-bonding faces, this method promises to allow for the general access to a number of such higher-order DNA assemblies, and will allow for the true structural and functional potential of this class of assemblies to be exploited.

7.3 Experimental

General. Boric acid, cyanuric acid (99%), ethylenediaminetetracetic acid, MgCl_2 , and tris(hydroxymethyl)-aminomethane (Tris) are used as purchased from Aldrich. 1000Å LCAA-CPG solid-support with a loading density of 60 $\mu\text{mol/g}$, DMT-triethyloxy-Glycol phosphoramidite, and reagents used for automated DNA synthesis are purchased from ChemGenes. Sephadex G-25 (super fine DNA grade) is purchased from Amersham Biosciences. RubyRed mica sheets for AFM are purchased from Electron Microscopy Sciences. Etched silicon cantilevers (OMCL-AC160TS) used for AFM imaging are used as purchased from Olympus.

Instrumentation. Standard automated oligonucleotide solid-phase syntheses are performed on a Perspective Biosystems Expedite 8900 DNA synthesizer. UV/vis quantifications are conducted on a Varian Cary 300 biospectrophotometer. Circular dichroism experiments are conducting using a JASCO J-810 spectropolarimeter. Dynamic light scattering measurements are performed on a Brookhaven Instruments Corp. system. Gel electrophoresis experiments are carried out on an acrylamide 20 X 20 cm vertical Hoefer 600 electrophoresis unit. AFM images are either acquired on a Digital Instruments "Dimension 3100" or on an E-scope microscope (Santa Barbara, CA).

Synthesis of the three-stranded locked system, and of strands A_1 - A_6 , A_8 , A_{10} , A_{15} and A_{20} : All syntheses are conducted on 1000Å LCAA-CPG solid-support with a loading density of 60 $\mu\text{mol/g}$ using standard oligonucleotide synthetic approaches. In the case of the three-stranded locked system, incorporation of the pegilated linker is achieved using the DMT-triethyloxy-Glycol phosphoramidite reagent supplied from ChemGenes (coupling 5 mins). Reverse amidite syntheses are conducted using standard synthetic protocols, but with and extended coupling and deprotection times of 5 and 2 minutes, respectively. The resulting strands are cleaved and deprotected in a concentrated solution of ammonium hydroxide (12 hrs, 55°C), purified on 24% polyacrylamide 7M urea gels (up to 20 AU₂₆₀ of crude DNA per gel; 10 mA, 6-7 hrs, pH 8.3),

extracted into 3 mL of sterile water (55°C, 16 hrs), and desalted using Sephadex G-25 size exclusion chromatography. Quantification is carried out using UV/vis analysis. The three strands used in the locked model system are: TCTGCGAGT-peg-(A)₂₀-peg-GAGAGTCCT, (A)₂₀-peg-ACTCGACA, AGGACTCTC-peg-(A)₂₀, while the fourth strand used to generate a parallel-parallel-antiparallel assembly is AGGACTCTC-peg-(A)₂₀. Note, bolded sequences are synthesized using reverse amidites, that is, in a 3' → 5' direction.

Molecular modeling: Modeling experiments are conducted using the HyperChem™ molecular modeling system for windows, version 6.03. The assemblies are geometry optimized using the Polak-Ribiere (conjugate gradient) algorithm, with a termination condition for an RMS gradient of 0.1 kcal/Åmol or a maximum of 50 cycles.

Thermal denaturation experiments on the three-part locked system: A 0.5 μmolar solution of DNA and CA are dissolved in 1 mL of buffer (200 mM NaCl, pH 6.8). Typically, DNA and CA are mixed in the correct molar ratio, and are left incubating at 0°C for a period of 16 hours before analysis. Thermal denaturation experiments are conducted from 5°C to 90°C, at rate of 0.2°C/min. The resulting spectra are normalized using the equation $A_N = (A_1 - A) / (A_1 - A_0)$, in which A_1 is the maximum absorbance, A_0 is the minimum absorbance, and A is the measured absorbance. The actual melting temperature is obtained using a first derivative treatment of the melting profile.

Matrix assisted laser desorption time-of-flight mass spectrometry: MALDI-TOF mass spectrometry was performed using a co-matrix composed of 6-aza-2-thiothymine and fucose, and the additive spermine.

Circular dichroism experiments: Samples are prepared in a manner similar to that of which the sample for the thermal denaturation experiments are prepared. Briefly, a 0.5 μmolar solution of DNA and CA are dissolved in 1 mL of buffer, in the correct molar ratios, and are left incubating at 0°C for a period of 16 hours before analysis. Titrations are conducted such that upon addition of CA, the solution is incubated at 0°C for 1 hour before analysis.

Dynamic light scattering experiments: DLS measurements are performed on an instrument equipped with a BI-200SM goniometer, a BI-9000AT digital correlator, and a Compass 315-150 CW laser light source from Coherent Inc., operating at 532 nm (150 mW). Vials for the

experiments are purchased from Canadawide Scientific. Measurements are obtained on a 1 mL solution of DNA and CA (10 μ molar; 200 mM NaCl in H₂O), filtered through 0.45 μ m PTFE syringe filters purchased from Chromatographic Specialties Inc.

AFM sample preparation and analysis: Samples for AFM imaging are prepared by mixing 0.05 ODs of each respective DNA building block (5 μ L H₂O) with 5 μ L of CA (concentration of 5 mg in 1mL H₂O; 10 mM NaCl, pH 6.8). Sample preparation generally involves the deposition of this self-assembled mixture onto freshly cleaved mica (dimensions 2 X 2 cm), followed by adequate evaporation to achieve complete dryness (typically 15 mins in a fumehood). Whenever possible, imaging is conducted within 24 hours to minimize time-dependant sample degradation. AFM images are acquired in air, and at room temperature. "Tapping mode" (i.e. intermittent contact imaging) is performed at a scan rate of 1 Hz using etched silicon cantilevers with a resonance frequency of \sim 300 kHz, a spring constant of \sim 42 N/m, and a tip radius of \leq 10 nm. All images are acquired with medium tip oscillation damping (20-30%).

$$\text{N.B. \% oscillation damping} = \frac{(\text{free air amplitude} - \text{imaging setpoint amplitude})}{\text{free air amplitude}} \times 100$$

Summary

8.1 Contributions to knowledge

[1] **Facile access to well-defined discrete gold nanoparticle assemblies that can be structurally and functionally addressed in real-time.** One of the central challenges in nanoscience is the ability to organize functional components according to a deliberately designed pattern, and the possibility of addressing and modifying this pattern at will. In particular, gold nanoparticle assemblies have emerged as a promising class of materials with novel optical, electronic, catalytic and sensing applications. To date, however, the assembly of nanoparticles into deliberately designed discrete patterns remains to be a challenge.

In chapter 2, we presented the first example of a well-defined nanoparticle assembly, and organized six gold nanoparticles into a discrete hexagon (Figure 8.1). The approach combines the rules of supramolecular chemistry with those of DNA nanotechnology, and involves labeling each nanoparticle with a DNA molecule that contains rigid organic vertices. This contribution was summarized and published in the journal *Angewandte Chemie International Edition* (F. Aldaye, Prof. H. Sleiman), and was selected by the editors as a *Hot Paper*, and received its own *cover-page*. In chapter 3, we evolved this system to allow for the

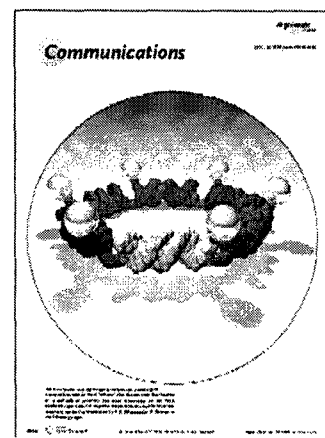


Figure 8.1 Discrete hexamer of six gold nanoparticles.

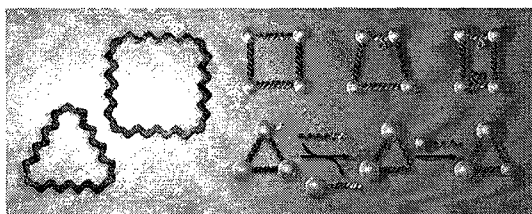


Figure 8.2 Single-stranded DNA templates (left) for the dynamic construction of discrete gold nanoparticle assemblies (right).

facile and economical access to libraries of discrete nanoparticle assemblies that are structurally addressable and switchable, in real-time. This now opens the door to the easy and systematic construction of model discrete nanoparticle assemblies, and allows us to better exploit their electronic, photonic, plasmonic, and catalytic potential. The approach involves the use of single-stranded and cyclic DNA templates, embedded with well-defined synthetic vertices, which are fully functional and independent from the nanoparticles being organized (Figure 8.2). Essentially, this means that a single template can be used to (1) access a large number of nanoparticle assemblies with different *nanoparticle com-*

Nature Nanotechnology**DNA builds bridges***J. Am. Chem. Soc.* **129**, 4130–4131 (2007)

Gold nanoparticle assemblies are of interest for a wide range of applications. Yet the arrangement of the nanoparticles, which greatly influences the electronic and optical properties of the material formed, remains challenging. Now, researchers from McGill University in Montreal, Canada have found a way to systematically organize nanoparticles using DNA templates.

binations, (2) to access nanoparticle assemblies of different geometries, and (3) to generate assemblies that are *addressable* in real-time and in response to external stimuli.

This work provides an unprecedented level of access and control to discrete nanoparticle organization, and as such represents the highest degree over the construction and manipulation of discrete nanoparticle assemblies. This contribution was summarized and published in the *Journal of*

the American Chemical Society (F. Aldaye, Prof. H. Sleiman), and was selected for a research highlight by the editors of *Nature Nanotechnology*: “DNA builds bridges” (inset above). Reviewers’ comments:

[Reviewer 65] “This is really an impressive piece of work. The nanoparticle architectures built by DNA assembly are unparalleled in my opinion... the manuscript should be published as is.”

[Reviewer 66; **complete review**] “A highly attractive and innovative piece of work that opens up a whole new array of possibilities in the nanoparticle world.”

[2] **Modular access to discrete three-dimensional DNA assemblies that are structurally addressable and tunable.** Three-dimensional discrete DNA nanostructures have tremendous potential to encapsulate and release drugs, regulate the folding and activity of encapsulated proteins, selectively encage nanomaterials, and assemble three-dimensional DNA networks for catalysis and biomolecule crystallization. Despite their exciting applications, only five previous reports on this subject have appeared; most of which are low yielding approaches that are non-modular. In chapter 4, we showed how

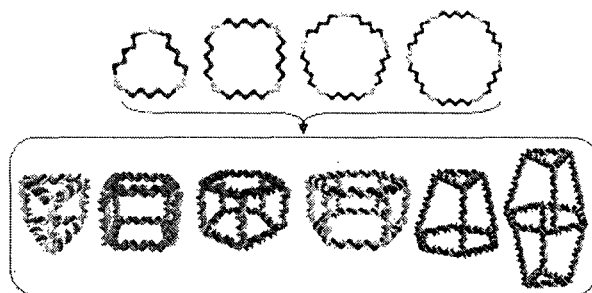


Figure 8.3 Modular access to 3D DNA assemblies from single-stranded and cyclic DNA templates.

single-stranded and cyclic DNA templates of predefined geometry can be used to modularly and quantitatively access a large number of three-dimensional discrete DNA assemblies, and also showed how these assemblies can be structurally oscillated between a number of predefined lengths in real-time, and in response to external stimuli (Figure 8.3). Our approach represents a highly straightforward and economical way to modularly access libraries of discrete and

structurally dynamic three-dimensional DNA assemblies, and as such has made three-dimensional DNA construction accessible and straightforward. This contribution was summarized and published in the *Journal of the American Chemical Society* (F. Aldaye, Prof. H. Sleiman), and was selected for a research highlight by the editors of *Nature*: “Gene boxes”, *Nature Materials*: “Unnatural life”, and *ACS nano*: “Inspiration for nature” (see insets below). A provisional patent entitled “Nucleotide modular assemblies and their use as delivery devices” was filed on the 5th of October, 2007 (F. Aldaye, Prof. H. Sleiman; 50/50).

<i>Nature</i>	<i>Nature Materials</i>	<i>ACS nano</i>
Faisal Aldaye and Hanadi Sleiman of McGill University in Montreal, Canada, have now developed a versatile way to make various DNA polyhedral nanostructures at a stroke. They create prefabricated polygonal rings of single-stranded DNA, which can then be	the symposium. For Hanadi Sleiman (McGill University), DNA is a structural molecule — a building block that, together with rigid organic molecules at the vertices, can be used to make 3D polyhedral cages (Fig. 1) ² . The DNA building blocks and	by Sleiman from McGill University. ¹² These cage-like structures used internal loops in the vertices in the polyhedral structures to create a system where multiple cage geometries and cage size could readily be switched, as demon-

[3] **Geometrically well-defined DNA nanotubes with readily tunable geometry, rigidity, and single- and double-stranded character.** DNA nanotubes are a novel class of materials with many applications; they can be used for the templated growth of metallic nanowires, and for the alignment of transmembrane proteins for NMR their determination, and can also potentially act as stiff interconnects, tracks for molecular motors, and as drug nanocarriers. All current methods for their construction, however, result in symmetrical and cylindrical assemblies that are entirely double-stranded. In chapter 5 we offered a

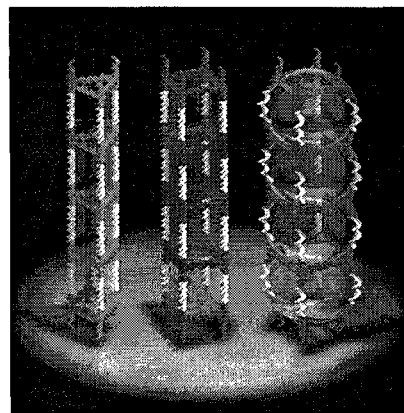


Figure 8.4 Triangular and square DNA nanotubes that can be single- or double-stranded.

modular approach to DNA nanotube synthesis that provided access to geometrically well-defined triangular- and square-shaped DNA nanotubes, which are highly uniform and are 100 times stiffer than double-stranded DNA (Figure 8.4). We also constructed the first example of DNA nanotube assemblies that can exist in both double- or single-stranded forms, with dramatically different stiffness. This is of particular importance because it now opens the door to the possibility of using these nanotubes in their more accessible single-stranded form to allow for the loading of materials, biomolecules or drugs, and subsequently closing them to their double-stranded form to ensure encapsulation. Our approach provides a new parameter to fine tune DNA nanotube construction, and facilitates access to designer nanotubes, with applications ranging from the

growth of nanowires of controlled shape and topology, to the loading and release of cargo, and the real-time modulation of stiffness and persistence length in interconnects. This contribution was summarized and submitted to the journal *Nature Nanotechnology* on the 8th of August, 2008 (F. Aldaye, P. Lo, C. McLaughlin, Prof. H. Sleiman).

[4] Use of transition metal complexes to control and fine-tune the self-assembly of DNA. As it becomes necessary to design larger and more complex DNA assemblies, it inevitably becomes necessary to also incorporate degenerate DNA sequences that may assemble into a number of undesirable products. This is currently a major bottleneck facing researchers in DNA nanotechnology. Because DNA assemblies are hydrogen-bonded, they can in principle be self-healing and error correcting. In chapter 6 we applied the well-established supramolecular rules of host/guest chemistry to DNA nanotechnology, and templated the selective synthesis of a “correct” DNA nanostructure from a library of many other “incorrect” members. We further used this approach to convert each already formed incorrect member into the same correct assembly

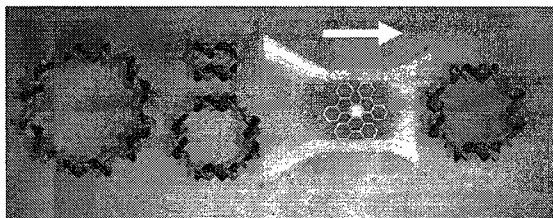


Figure 8.5 A “confused” library of DNA assemblies can be funneled into a single member using the electrostatic binder $\text{Ru}(\text{bpy})_3^{2+}$.

(Figure 8.5). In a direct application, we template the construction of uniform one-dimensional DNA fibers, extending over tens of microns, from symmetrically branched DNA building blocks that otherwise assemble into ill-defined oligomeric networks. This is the first example in which a small molecule is used to dictate the

assembly outcome of DNA nanostructures, and presents a novel solution to a long standing problem, that is, “what do to do when sequences code for more than one structure.” This contribution was summarized and published in the *Journal of the American Chemical Society* (F. Aldaye, Prof. H. Sleiman). Reviewer’s comments:

“This is a terrific work describing equilibrating DNA assemblies that under appropriate conditions equilibrate into a single assembly. Hanadi is to be congratulated for discovering how $\text{Ru}(\text{bpy})_3^{2+}$ can effect this switch... The work itself is so beautiful that it shines alone.”

[5] Small molecule templated synthesis of higher-order DNA helices. Higher-order DNA assemblies with helices composed of more than two DNA strands provide an untapped wealth of potentially unique structural, physical, and chemical properties. Many areas of research will benefit from our ability to easily generate a large number of such higher-order motifs, including

both materials science and biology. To date, however, only two examples have emerged. The current difficulty lies in their synthesis; reprogramming the bases to generate a stable DNA strand can be difficult, and in some cases unattainable. In chapter 7 we developed an approach to rationally reprogram the assembly behavior of unmodified DNA, and constructed a triple helix from DNA strands that would otherwise assemble into a duplex (Figure 8.6). Specifically, we constructed a poly-adenine DNA triplex using the tri-facial complementary molecule cyanuric acid. This approach is both economical and facile. Considering the wealth of molecules that contain base-bonding faces, this method promises to open the door to the facile and economical access to higher-order DNA assemblies, and will allow for the true structural and functional potential of

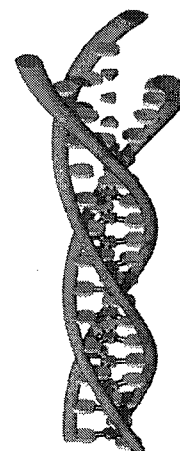


Figure 8.6 Templated construction of a DNA triplex.

this novel class of materials to be systematically studied and exploited. A manuscript summarizing this work is currently being prepared for submission (F. Aldaye, P. Lo, Prof. H. Sleiman).

Overall, the work within this thesis promises to contribute to the areas of nanooptics, photonics, electronics, drug encapsulation and release, protein folding and stability, three-dimensional DNA construction and crystallization, error-correction within DNA construction, and access to higher-order DNA helices. This body of knowledge is summarized in an invited review that appeared in the journal *Science* (F. Aldaye, A. Palmer, Prof. H. Sleiman).

8.2 Future work

[1] The field of well-defined discrete nanoparticle assemblies lacked a method to systematically access model systems that can be structurally and functionally manipulated in real-time. We solved this problem. Future work will now need to be directed towards constructing a number of such model discrete nanoparticle systems, and towards better characterizing their fundamental structural, physical and chemical properties.

[2] The lack of efficient synthetic approaches to construct discrete three-dimensional DNA assemblies was a bottleneck in this field. We solved this problem. Can we now encapsulate cargo into our three-dimensional DNA capsules, such as proteins and nanoparticles, and structurally modulate the resulting assemblies to fine-tune their physical and chemical

parameters? Can we now use these objects to build extended three-dimensional DNA networks with regions that can be structurally modulated to generate stimuli responsive DNA networks?

[3] We provided an approach to DNA nanotube construction that allowed for the complete control over their geometry and surface topology, one rung at a time. Future work will now need to be directed towards exploiting this new method of constructing “designer” DNA nanotubes. Can we construct DNA nanotubes with alternating rungs of different sizes and shapes? Can we use our triangular and square-shaped DNA nanotubes as bioreactors to synthesize triangular and square-shaped metallic wires of dialed in designer properties?

[4] The occurrence of errors during DNA self-assembly is one of the bigger challenges facing researchers in DNA nanotechnology. Our contribution to this field is unique in that it uses a small molecule to select for a single member from a library of multiple DNA nanostructures. What other molecules can be used to select for the remaining members? Future work will thus be directed towards better understating the factors responsible for this selection process – such as charge density, overall size, hydrophobicity – so that the templated synthesis of any arbitrary DNA nanostructure would be feasible.

[5] Higher-order DNA assemblies provide an untapped wealth of potential for materials science and biology. We applied the rules of supramolecular chemistry to address the issue of synthetic access, and reprogrammed the assembly of unmodified polyadenine DNA strands to generate a DNA triplex. Can other molecules now be used to redesign the assembly motif of the remaining three bases, that is, of cytosine, guanine and thymine? And can the same base be made to assemble into a quadruplex, pentaplex, hexaplex, etc, using the appropriate set of different guest molecules?

8.3 Publications

- [1] Aldaye, F. A.; Palmer, A. L.; Sleiman, H. F. “Assembling materials with DNA as the guide.” *Science* **2008**, *321*, 1795-1799.
- [2] Aldaye, F. A.; Sleiman, H. F. “Modular access to structurally switchable 3D discrete DNA assemblies.” *Journal of the American Chemical Society* **2007**, *129*, 13376-13366.

This contribution was highlighted in *Nature* **2007**, 450, 323; *Nature Materials* **2008**, 7, 102; and *ACS nano* **2008**, 2, 4.

- [3] **Aldaye, F. A.**; Sleiman, H. F. "Guest-mediated access to a single DNA nanostructure from a library of multiple assemblies." *Journal of the American Chemical Society* **2007**, 129, 10070-10071.
- [4] **Aldaye, F. A.**; Sleiman, H. F. "Dynamic DNA templates for discrete gold nanoparticle assemblies: control of geometry, modularity, write/erase and structural switching." *Journal of the American Chemical Society* **2007**, 129, 4130-4131.

This contribution was highlighted in *Nature Nanotechnology* **2007**, 2, 264.

- [5] **Aldaye, F. A.**; Sleiman, H. F. "Sequential self-assembly of a DNA hexagon as a template for the organization of gold nanoparticles." *Angewandte Chemie International Edition* **2006**, 45, 2204-2209.

This contribution was selected by the editors as a "Hot Paper", and received its own cover-page.

Other refereed contributions

- [6] **Aldaye, F. A.**; Sleiman, H. F. "DNA-mediated patterning of gold nanoparticles into discrete structures: modularity, write/erase and structural switching." *SPIE Conference Proceedings* **2007**, 6642, 664203/1-664203/8.
- [7] **Aldaye, F. A.**; Yang, H.; Slim, M.; Sleiman, H. F. "Assembling metals and nanoparticles one by one with DNA." *Polymer Preprints* **2007**, 48, 573-574.

Submitted

- [8] **Aldaye, F. A.**; Lo, P. K.; McLaughlin, C. K.; Sleiman, H. F. "Modular construction of DNA nanotubes with readily tunable geometry, rigidity, and single- or double-stranded character." *Nature Nanotechnology* **2008**, submitted August 8, 2008.

In preparation

- [9] **Aldaye, F. A.**; Lo, P. K.; Sleiman, H. F. "Guest-mediated reprogramming of the self-assembly outcome of unmodified DNA."
- [10] Yang, H.; McLaughlin, C. K.; **Aldaye, F. A.**; Sleiman, H. F. "Metallated discrete three-dimensional DNA frameworks."

8.4 Patents

- [1] A provisional patent entitled "Nucleotide modular assemblies and their use as delivery devices" was filed on the 5th of October, 2007. This invention relates to a facile method of accessing a large number of three-dimensional discrete DNA assemblies, and to their use as sensors, bioreactors, and drug delivery vehicles. The two inventors are **F. A. Aldaye** and Prof. H. F. Sleiman (50/50).
- [2] A provisional patent entitled "Dendritic DNA supermolecules" was filed on the 20th of August, 2008. This invention relates to a facile method of attaching branched organic molecules to small single strands of DNA, which assemble into well-defined novel supramolecular DNA nanostructures, and to their use in gene and drug delivery, templated growth of nanowires, biomineralization, and tissue engineering. The three inventors are K. M. M. Carneiro, **F. A. Aldaye** and Prof. H. F. Sleiman (40/20/40).

8.5 Selected conference presentations

- [1] **Aldaye, F. A.**; Sleiman, H. F. *Canadian Chemistry Conference and Exhibition* (Edmonton, Canada) **2008**. [Oral]
- [2] **Aldaye, F. A.**; Sleiman, H. F. *Harvard University - FAS Center for Systems Biology* (Boston, USA) **2008**. [Oral]
- [3] **Aldaye, F. A.**; Sleiman, H. F. *Canadian Institute of Advanced Research* (Vancouver, Canada) **2007**. [Oral/Poster]

- [4] **Aldaye, F. A.**; Sleiman, H. F. *Chemistry and Biochemistry Graduate Research Conference* (Montreal, Canada) **2007**. [Oral]

Received the “**best talk**” award.

- [5] **Aldaye, F. A.**; Sleiman, H. F. *Trends in Nanotechnology 2007* (San Sebastian, Spain) **2007**. [Oral/Poster]

Received the “**best poster**” award.

- [6] **Aldaye, F. A.**; Sleiman, H. F. *American Chemical Society National Meeting* (Chicago, USA) **2007**. [Oral]

- [7] **Aldaye, F. A.**; Sleiman, H. F. *High Polymer Forum* (Gananaque, Canada) **2007**. [Oral]

Award talk: Received the MSSED/LANXESS graduate thesis award for the **best doctoral thesis in Macromolecular Chemistry across Canada**.

- [8] **Aldaye, F. A.**; Sleiman, H. F. *Ludwig Maximilians Universität München* (Munich, Germany) **2006**. [Oral]

- [9] **Aldaye, F. A.**; Sleiman, H. F. *European Center for Nanoscience* (Venice, Italy) **2006**. [Poster]

- [10] **Aldaye, F. A.**; Sleiman, H. F. *International Roundtable on Nucleosides, Nucleotides and Nucleic Acids* (Bern, Switzerland) **2006**. [Poster]

Received the “**best poster**” award.

- [11] **Aldaye, F. A.**; Sleiman, H. F. *Canadian Institute of Advanced Research* (Montreal, Canada) **2006**. [Poster]

- [12] **Aldaye, F. A.**; Sleiman, H. F. *American Chemical Society National Meeting* (Washington, USA) **2005**. [Oral]

- [13] Aldaye, F. A.; Sleiman, H. F. *Center for Self-Assembled Chemical Structures* (Montreal, Canada) **2005**. [Oral]

Received the “**best talk**” award.

- [14] **Aldaye, F. A.**; Sleiman, H. F. *Canadian Institute of Advanced Research* (Santa Barbara, USA) **2005**. [Poster]

- [15] **Aldaye, F. A.**; Sleiman, H. F. *Canadian Society of Chemistry Conference & Exhibition* (Ottawa, Canada) **2004**. [Oral]

References

- 1 English translation: Druery, C.T.; Bateson, W. *J. Roy. Hor. Soc.* **1901**, 26, 1-32.
- 2 Haeckel, E. in *Generelle Morphologie der Organismen*; Reimer, Berlin, pp. 287-288, 1866.
- 3 Simon, U. in *Nanoparticles: From Theory to Application*; Schmid, G. Ed.; Wiley-VCH: Weinheim, 2004.
- 4 Pileni, M. P. *J. Phys. Chem. B* **2001**, 105, 3358-3371.
- 5 Collier, C. P.; Vossmeier, T.; Heath, J. R. *Annu. Rev. Phys. Chem.* **1998**, 49, 371-404.
- 6 Beomseok, K.; Marcelo, C. A.; Tripp, S. L.; Wei, A. *Langmuir* **2004**, 20, 9360-9365.
- 7 Maier, S. A.; Brongersma, M. L.; Kik, P. G.; Meltzer, S.; Requicha, A. A. G.; Atwater, H. A. *Adv. Mater.* **2001**, 13, 1501-1505.
- 8 Erben, C. M.; Goodman, R. P.; Turberfield, A. J. *J. Am. Chem. Soc.* **2007**, 129, 6992-6993.
- 9 Goodman, R. P.; Schaap, I. A. T.; Tarden, C. F.; Erbern, C. M.; Berry, R. M.; Schmidt, C. F.; Turberfield, A. J. *Science* **2005**, 310, 1661-1665.
- 10 Shih, W. M.; Quispe, J. D.; Joyce, G. F. *Nature* **2004**, 427, 618-621.
- 11 Zhang, Y.; Seeman, N. C. *J. Am. Chem. Soc.* **1994**, 116, 1661-1669.
- 12 Chen, J.; Seeman, N. C. *Nature* **1991**, 350, 631-633.
- 13 He, Y.; Tian, Y.; Chen, Y.; Deng, Z.; Ribbe, A. E.; Mao, C. *Angew. Chem. Int. Ed.* **2005**, 44, 6694-6696.
- 14 Chaput, J. C.; Switzer, C. *Proc. Natl. Acad. Sci. USA* **1999**, 96, 10614-10619.
- 15 Rakotondradany, F.; Palmer, A.; Toader, V.; Chen, B.; Whitehead, M. A.; Sleiman, H. F. *Chem. Commun.* **2005**, 5441-5443.
- 16 Tinoco, I. in *Nucleic acids: Structures, properties, and functions*; Bloomfield, V. A., Crothers, D. M., Tinoco, I. Eds; University science books, 2000.
- 17 Braun, E.; Eichen, Y.; Sivan, U.; Ben-Yoseph, G. *Nature* **1998**, 391, 775-778.
- 18 M. Fischler *et al.*, *Small* **2007**, 6, 1049-1055; and reference therein.
- 19 K. Keren *et al.*, *Science* **2002**, 297, 72-75.
- 20 Levina, L.; Sukhovatkin, V.; Musikhin, S.; Cauchi, S.; Nisman, R.; Bazett-Jones, D. P.; Sargent, E. H. *Adv. Mater.* **2005**, 17, 1854-1857.
- 21 Ma, Y.; Zhang, J.; Zhang, G.; He, H. *J. Am. Chem. Soc.* **2004**, 126, 7097-7101.

- 22 Datta, B.; Schuster, G. B. *J. Am. Chem. Soc.* **2008**, *130*, 2965-2973.
- 23 Gugliotti, L. A.; Feldheim, D. L.; Eaton, B. E. *Science* **2004**, *304*, 850-852.
- 24 M. G. Warner, J. E. Hutchinson, *Nat. Mater.* **2003**, *2*, 272-277.
- 25 H. Nakao, H. Shiigi, Y. Yamamoto, S. Tokonami, T. Nagaoka, S. Sugiyama, T. Ohtani, *Nano Lett.* **2003**, *3*, 1391-1394.
- 26 Burley, G. A.; Gierlich, J.; Mofid, M. R.; Nir, H.; Tal, S.; Eichen, Y.; Carell, T. *J. Am. Chem. Soc.* **2006**, *128*, 1398-1399.
- 27 Ford, W. E.; Harnack, O.; Yasuda, A.; Wessels, J. M. *Adv. Mater.* **2001**, *13*, 1793-1797.
- 28 Numata, M.; Sugiyasu, K.; Hasegawa, T.; Shinkai, S. *Angew. Chem. Int. Ed.* **2004**, *43*, 3279-3283.
- 29 Wang, G.; Zhang, J.; Murray, R. W. *Anal. Chem.* **2002**, *74*, 4320-4327.
- 30 Patolsky, F.; Weizmann, Y.; Lioubashevski, O.; Willner, I. *Angew. Chem. Int. Ed.* **2002**, *41*, 2323-2327.
- 31 Slim, M.; Durisic, N.; Grutter, P.; Sleiman, H. F. *ChemBioChem* **2007**, *8*, 804-812.
- 32 Alivisatos, A. P. *et al. Nature* **1996**, *382*, 609-611.
- 33 Loweth, C. J.; Caldwell, W. B.; Peng, X.; Alivisatos, A. P.; Schultz, P. G. *Angew. Chem. Int. Ed.* **1999**, *38*, 1808-1812.
- 34 Deng, Z.; Tian, Y.; Lee, S.-H.; Ribbe, A. E.; Mao, C. *Angew. Chem. Int. Ed.* **2005**, *44*, 3582-3585.
- 35 Niemeyer, C. M. in *Nanotechnology*; Niemeyer, C.; Mirkin, C. Eds; Wiley: Weinheim, 2004, pp. 227-243; and references therein.
- 36 Seeman, N. C. *J. Theor. Biol.* **1982**, *99*, 237-247.
- 37 Winfree, E.; Liu, F.; Wenzler, L. A.; Seeman, N. C. *Nature* **1998**, *394*, 539-544.
- 38 Lin, C. Liu, Y. Rinker, S. Yan, H. *ChemPhysChem* **2006**, *7*, 1641-1647; and references therein.
- 39 Wang, X.; Seeman, N. C. *J. Am. Chem. Soc.* **2007**, *129*, 8169-8176.
- 40 Park, S. H.; Barish, R.; Li, H.; Reif, J. H.; Finkelstein, G.; Yan, H.; LaBean, T. H. *Nano Lett.* **2005**, *5*, 693-696.
- 40 Rothmund, P. W. K. *Nature* **2006**, *440*, 297-302.
- 41 Ke, Y.; Lindsay, S.; Chang, Y.; Liu, Y.; Yan, H. *Science* **2008**, *319*, 180-183.
- 42 Rinker, S.; Ke, Y.; Liu, Y. Chhabra, R.; Yan, H. *Nature Nanotech.* **2008**, *3*, 418-422.
- 43 Douglas, S. M.; Chou, J. J.; Shih, W. M. *Proc. Nat. Acad. Sci. USA* **2007**, *104*, 6644-6648.

- 44 Li, H.; Park, S. H.; Reif, J. H.; LaBean, T. H.; Yan, H. *J. Am. Chem. Soc.* **2004**, *126*, 418-419.
- 45 Liu, Y.; Lin, C.; Li, H.; Yan, H. *Angew. Chem. Int. Ed.* **2005**, *44*, 4333-4338.
- 46 Ellington, A. D.; Szostak, J. W. *Nature* **1990**, *346*, 818-822.
- 47 Tuerk, C.; Gold, L. *Science* **1990**, *249*, 505-510.
- 48 Yan, H.; Park, S. H.; Finkelstein, G.; Reif, G. H.; LaBean, T. H. *Science* **2003**, *301*, 1882-1884.
- 49 Park, S. H.; Yin, P.; Liu, Y.; Reif, J. H.; LaBean, T. H.; Yan, H. *Nano Lett.* **2005**, *5*, 729-733.
- 50 He, Y.; Tian, Y.; Ribbe, A. E.; Mao, C. *J. Am. Chem. Soc.* **2006**, *128*, 12664-12665.
- 51 Williams, B. A. R.; Lund, K.; Liu, Y.; Yan, H.; Chaput, J. C. *Angew. Chem. Int. Ed.* **2007**, *46*, 3051-3054.
- 52 Chhabra, R.; Sharma, J.; Ke, Y.; Liu, Y.; Rinker, S.; Lindsay, S.; Yan, H. *J. Am. Chem. Soc.* **2007**, *129*, 10304-10305.
- 53 Cohen, J. D.; Sadowski, J. P.; Dervan, P. B. *J. Am. Chem. Soc.* **2008**, *130*, 402-403.
- 54 Malo, J. *et al.* *Angew. Chem. Int. Ed.* **2005**, *44*, 3057-3061.
- 55 Le, J. D. *et al.* *Nano Lett.* **2004**, *4*, 2343-2347.
- 56 Pinto, Y. Y. *et al.* *Nano Lett.* **2005**, *5*, 2399-2402.
- 57 Zhang, J.; Liu, Y.; Ke, Y.; Yan, H. *Nano Lett.* **2006**, *6*, 248-251.
- 58 Sharma, J.; Chhabra, R.; Liu, Y.; Ke, Y.; Yan, H. *Angew. Chem. Int. Ed.* **2006**, *45*, 730-735.
- 59 Zheng, J. *et al.* *Nano Lett.* **2006**, *6*, 1502-1504.
- 60 Adleman, L. M. *Science* **1994**, *11*, 1021-1024.
- 61 Benenson, Y.; Gil, B.; Ben-Dor, U.; Adar, R.; Shapiro, E. *Nature* **2004**, *429*, 423-429.
- 62 Winfree, E. *J. Biol. Mol. Struct. Dyn. Conver.* **2000**, *11*, 263-270; and references therein.
- 63 Mao, C.; Sun, W.; Shen, Z.; Seeman, N. C. *Nature* **1999**, *397*, 144-146.
- 64 Yurke, B.; Turberfield, A. J.; Mills, A. P.; Simmel, F. C.; Neumann, J. L. *Nature* **2000**, *406*, 605-608.
- 65 Santoro, S. W.; Joyce, G. F. *Proc. Natl. Acad. Sci. USA* **1997**, *94*, 4262-4266.
- 66 Bath, J.; Turberfield, A. J. *Nature Nanotech.* **2007**, *2*, 275-284.
- 67 Scheffler, M.; Dorenbeck, A.; Jordan, S.; Wüstefeld, M.; von Kiedrowski, G. *Angew. Chem. Int. Ed.* **1999**, *38*, 3312-3315.
- 68 Shchepinov, M. S.; Mir, K. U.; Elder, J. K.; Frank-Kamenetskii, M. D.; Southern, E. M. *Nucleic Acids Res.* **1999**, *27*, 3035-3041.

- 69 Shi, J.; Bergstrom, D. E.; *Angew. Chem. Int. Ed.* **1997**, *36*, 111-113.
- 70 Waybright, S. M.; Singleton, C. P.; Wachter, K.; Murphy, C. J.; Bunz, U. H. F. *J. Am. Chem. Soc.* **2001**, *123*, 1828-1833.
- 71 Vargas-Baca, I.; Mitra, D.; Zulyniak, H. J.; Banerjee, J.; Sleiman, H. F. *Angew. Chem. Int. Ed.* **2001**, *40*, 4629-4632.
- 72 Mitra, D.; Di Cesare, N.; Sleiman, H. F. *Angew. Chem. Int. Ed.* **2004**, *43*, 5804-5808.
- 73 Stewart, K. M.; McLaughlin, L. W. *Chem. Commun.* **2003**, 2934-2935.
- 74 Stewart, K. M.; McLaughlin, L. W. *J. Am. Chem. Soc.* **2004**, *126*, 2050-2057.
- 75 Stewart, K. M.; Rojo, J.; McLaughlin, L. W. *Angew. Chem. Int. Ed.* **2004**, *43*, 5808-5811.
- 76 Yang, H.; Sleiman, H. F. *Angew. Chem. Int. Ed.* **2008**, *47*, 2443-2446.
- 77 Goritz, M.; Kramer, R. *J. Am. Chem. Soc.* **2005**, *127*, 18016-18017.
- 78 Wang, W.; Wan, W.; Zhou, H.-H.; Niu, S.; Li, A. D. Q. *J. Am. Chem. Soc.* **2003**, *125*, 5248-5249.
- 79 Ding, K.; Alemdaroglu, F. E.; Borsch, M.; Berger, R.; Herrmann, A. *Angew. Chem. Int. Ed.* **2007**, *46*, 1172-1175.
- 90 Ackerson, C. J.; Sykes, M. T.; Kornberg, R. D. *Proc. Natl. Acad. Sci. USA* **2005**, *102*, 13383-13385.
- 81 Fu, A.; Micheel, C. M.; Cha, J.; Chang, H.; Yang, H.; Alivisatos, A. P. *J. Am. Chem. Soc.* **2004**, *126*, 10832-10833.
- 82 Claridge, S. A. *et al. Chem. Mater.* **2005**, *17*, 1628-1635.
- 83 Claridge, S. A. *et al. J. Am. Chem. Soc.* **2008**, *130*, 9598-9605.
- 84 Lee, J. H. *et al. Angew. Chem. Int. Ed.* **2007**, *46*, 9006-9010.
- 85 Heuer, D. M.; Saha, S.; Archer, L. A. *Biopolymers* **2003**, *70*, 471-481; and references therein.
- 86 Kroeker, W. D.; Kowalski, D.; Laskowski, M. *Biochemistry* **1976**, *15*, 4463-4467.
- 87 Johnson, P. H.; Laskowski, M. *J. Biol. Chem.* **1970**, *245*, 891-898.
- 88 Nye, S. A.; Swint, S. A. *J. Polym. Sci. Part A* **1994**, *32*, 721-727.
- 89 Rele, S.; Nayale, S. *Syn. Comm.* **2002**, *32*, 3533-3540.
- 90 Damha, M. J.; Ogilvie, K. K. *J. Org. Chem.* **1988**, *53*, 3710-3722.
- 91 Distler, A. M.; Allison, J. *Anal. Chem.* **2001**, *73*, 5000-5003.
- 92 Engler, M.J.; Richardson, C.C. in *The Enzymes*; Boyer, P. D., Ed.; San Diego: Academic Press, 1982.
- 93 Sambrook, J.; Fritsch, E.F.; Maniatis, T. in *Molecular Cloning: A Laboratory Manual*; 1.53-1.73, 1989.

- 94 Zanchet, D.; Micheel, C. M.; Parak, W. J.; Gerion, D.; Alivisatos, A. P. *Nano Lett.* **2001**, *1*, 32-35.
- 95 Schlenoff, J. B.; Li, M.; Ly, H. *J. Am. Chem. Soc.* **1998**, *117*, 12528-12536.
- 96 Kassam, A.; Bremner, G.; Clark, B.; Ulibarri, G.; Lennox, R. B. *J. Am. Chem. Soc.* **2006**, *128*, 3476-3477.
- 97 Aldaye, F. A.; Sleiman, H. F. *Angew. Chem. Int. Ed.* **2006**, *45*, 2204-2209.
- 98 Erben, C. M.; Goodman, R. P.; Turberfield, A. J. *Angew. Chem. Int. Ed.* **2006**, *45*, 7414-7417; and references therein.
- 99 Chen, J.; Seeman, N. C. *Nature* **1991**, *350*, 631-633.
- 100 Zhang, Y.; Seeman, N. C. *J. Am. Chem. Soc.* **1994**, *116*, 1661-1669.
- 101 Goodman, R. P. *et al. Science* **2005**, *310*, 1661-1665.
- 102 Erben, C. M.; Goodman, R. P.; Turberfield, A. J. *J. Am. Chem. Soc.* **2007**, *129*, 6992-6993.
- 103 Shih, W. M.; Quispe, J.; Joyce, G. F. *Nature* **2004**, *427*, 618-6211.
- 104 Carriero, S.; Damha, M. J.; *Org. Lett.* **2003**, *5*, 273-276.
- 105 He, Y. *et al. Nature* **2008**, *452*, 198-202.
- 106 Zimmermann, J.; Cebulla, M. P. J.; Monninghoff, S.; von Kiedrowski, G. *Angew. Chem. Int. Ed.* **2008**, *47*, 3626-3630.
- 107 Aldaye, F. A.; Sleiman, H. F. *J. Am. Chem. Soc.* **2007**, *129*, 4130-4131.
- 108 Geng, Y. *et al. Nature Nanotech.* **2007**, *2*, 249-255.
- 109 Rothmund, P. W. K. *et al. J. Am. Chem. Soc.* **2004**, *126*, 16344-16352.
- 110 Mitchell, J. C.; Harris, J. R.; Malo, J.; Bath, J.; Turberfield, A. J. *J. Am. Chem. Soc.* **2004**, *126*, 16342-16343.
- 111 Sherman, W. B.; Seeman, N. C. *Biophys. J.* **2006**, *90*, 4546-4557.
- 112 Mathieu, F. *et al. Nano Lett.* **2005**, *5*, 661-665.
- 113 Kuzuya, A.; Wang, R.; Sha, R.; Seeman, N. C. *Nano Lett.* **2007**, *7*, 1757-1763.
- 114 Aldaye, F. A.; Sleiman, H. F. *J. Am. Chem. Soc.* **2007**, *129*, 13376-13366.
- 115 Park, S. H. *et al. Angew. Chem. Int. Ed.* **2006**, *45*, 735-739.
- 116 He, Y.; Chen, Y.; Liu, H.; Ribbe, A. E.; Mao, C. *J. Am. Chem. Soc.* **2005**, *127*, 12202-12203.
- 117 He, Y. *et al. Angew. Chem. Int. Ed.* **2005**, *44*, 6694-6696.
- 118 Liu, H.; He, Y.; Ribbe, A. E.; Mao, C. *Biomacromole.* **2005**, *6*, 2943-2945.
- 119 Liu, H.; Chen, Y.; He, Y.; Ribbe, A. E.; Mao, C. *Angew. Chem. Int. Ed.* **2006**, *45*, 1942-1945.

- 120 Liu, Y.; Ke, Y.; Yan, H. *J. Am. Chem. Soc.* **2005**, *127*, 17140-17141.
- 121 Winfree, E.; Bekbolatov, R. *DNA Computing* **2004**, *2943*, 126-144.
- 122 Yin, P.; Choi, H. M. T.; Calvert, C. R.; Pierce, N. A. *Nature* **2008**, *451*, 318-323.
- 123 Liu, J.; Wernette, D. P.; Lu, Y. *Angew. Chem. Int. Ed.* **2005**, *44*, 7290-7293.
- 124 Corbett, P. T. *et al. Chem. Rev.* **2006**, *106*, 3652-3711.
- 125 Lehn, J.-M. *Chem. Soc. Rev.* **2007**, *36*, 151-160.
- 126 Patel, D. J.; Phan, A. T.; Kuryavvi, V. *Nucleic Acids Res.* **2007**, *35*, 7429-7455.
- 127 Tumpene, J. *et al. Nano Lett.* **2007**, *7*, 3832-3839.
- 128 Piccirilli, J. A.; Krauch, T.; Moroney, S. E.; Benner, S. A. *Nature* **1990**, *343*, 33-37.
- 129 Doi, Y.; Chiba, J.; Morikawa, T.; Inouye, M. *J. Am. Chem. Soc.* **2008**, *130*, 8762-8768.
- 130 Krueger, A. T.; Lu, H.; Lee, A. H. F.; Kool, E. T. *Acc. Chem. Res.* **2007**, *40*, 141-150.
- 131 Kool, E. T. *Acc. Chem. Res.* **2002**, *35*, 936-943.
- 132 Ogawa, A. K.; Wu, Y.; Berger, M.; Schultz, P. G.; Romesberg, F. E. *J. Am. Chem. Soc.* **2000**, *122*, 8803-8804.
- 133 Tae, E. L.; Wu, Y.; Xia, G.; Schultz, P. G.; Romesberg, F. E. *J. Am. Chem. Soc.* **2001**, *123*, 7439-7440.
- 134 Tanaka, K.; Tengeiji, A.; Kato, T.; Toyama, N.; Shionoya, M. *Science* **2003**, *299*, 1212-1213.
- 135 Tanaka, K. *et al. Nature Nanotech.* **2006**, *1*, 190-194.
- 136 Zerkowski, J. A.; Seto, C. T.; Whitesides, G. M. *J. Am. Chem. Soc.* **1992**, *114*, 5473-5475.
- 137 Fenniri, H.; Deng, B.-L.; Ribbe, A. E.; Hallenga, K.; Jacob, J.; Thiyagarajan, P. *Proc. Nat. Acad. Sci. USA* **2002**, *99*, 6487-6492.
- 138 Morales, J. G.; Ruez, J.; Yamazaki, T.; Motkuri, K.; Kovalenko, A.; Fenniri, H. *J. Am. Chem. Soc.* **2005**, *127*, 8307-8309.
- 139 Sessler, J. L.; Jayawickramarajah, J.; Sathiosatham, M.; Sherman, C. L.; Brodbelt, J. S. *Org. Lett.* **2003**, *5*, 2627-2630.
- 140 Asadi, A.; Patrick, B. O.; Perrin, D. M. *J. Org. Chem.* **2007**, *72*, 466-475.
- 141 Zimmerman, S. C.; Duerr, B. F. *J. Org. Chem.* **1992**, *57*, 2215-2217.
- 142 Chaput, J. C.; Switzer, C. *Proc. Natl. Acad. Sci. USA* **1999**, *96*, 10614-10619.
- 143 Rakotondradany, F. *et al. Chem. Commun.* **2005**, 5441-5443.

Wow, you made it all the way to the end; thanks!

F.A.